THÈSE DE DOCTORAT ÈS MATHÉMATIQUES

Spécialité : Mathématiques Appliquées

UNIVERSITÉ PARIS-SACLAY

École doctorale de mathématiques Hadamard (EDMH, ED 574)

Établissement d'inscription : ENSTA ParisTech
Laboratoire d'accueil : POEMS (UMR 7231 CNRS - Inria - ENSTA ParisTech)

NNT : 2016SACLY012

&

DOCTOR OF PHILOSOPHY THESIS

Major : Civil Engineering

UNIVERSITY OF MINNESOTA

Department of Civil, Environmental and Geo-Engineering

Développement et utilisation de méthodes asymptotiques d'ordre élevé pour la résolution de problèmes de diffraction inverse

Development and use of higher-order asymptotics to solve inverse scattering problems

Rémi CORNAGGIA

Soutenue le 29 septembre 2016 *après avis des rapporteurs, devant le jury :*

Marc BONNET	(CNRS)	directeur
Josselin GARNIER	(École Polytechnique)	président
Drossos GINTIDES	(National Technical University of Athens)	rapporteur
Stefano GONELLA	(University of Minnesota)	examinateur
Bojan GUZINA	(University of Minnesota)	directeur
Dominique LEGUILLON	(Université Pierre et Marie Curie)	rapporteur
Vaughan VOLLER	(University of Minnesota)	examinateur

À mes parents,
et au souvenir d'un rock dansé lors des 50 ans de Tonton Alain.

Remerciements / Acknowledgements

C'est un mois après avoir soutenu que j'entame ces remerciements. Que j'essaie de me souvenir de ce que vous vous avez fait, pendant ces quatre années de thèse, que je pourrais évoquer en souriant, et qui, j'espère, vous fasse sourire aussi.

My first thanks are of course due to Marc Bonnet and Bojan Guzina, for accepting to supervise this thesis in between mechanics and mathematics and for maintaining the joint PhD program I had the luck to follow. Marc, thanks also for encouraging me to pursue despite my initial doubts, thanks for your availability, your patience and pedagogy when explaining a difficult concept or working on a new idea. Bojan, thanks for welcoming me in the US and in your research group, thanks for all the deep and interesting topics you brought to my attention and for the contagious enthusiasm you have for these researches.

I am also grateful to Drossos Gintides and Dominique Leguillon for accepting to review my dissertation and for their kind and useful remarks from two different but equally enlightening perspectives. Stefano Gonella and Vaughan Voller accepted to be part of the committees of my final defense but also of my preliminary oral defense on behalf of the University of Minnesota, and have my deepest thanks for their comments and questions on these two occasions. Finally, I owe all my gratitude to Josselin Garnier for accepting to be the chairman of the committee of my defense.

I was also lucky to benefit from the great working environments of UMA at ENSTA Paristech and CEGE at University of Minnesota. Beside the great research atmosphere, I would like to thank all the people who ensure the daily operation of these departments. My thoughts go especially to Corinne Chen and Tiffany Ralston for their priceless help with administrative duties, and Christophe Mathulik for his efficiency to fix any computer issue without loosing his smile for a second. I also would like to thank the people from graduate schools on both side on the Atlantic, and those in various institutions who helped to deal with the subtleties of the joint PhD program.

Avant d'être doctorant, j'ai eu la chance, comme chacun, d'être guidé par de nombreux excellents enseignants, tant par leur pédagogie que par leurs qualités humaines. Que soient donc remerciés ici la quasi-totalité de mes professeurs (on ne peux pas aimer tout le monde ...) et en particulier Mme Gilles, M. Lafforgue, M. De Bouard, Blaise Bourdin, David Néron, Eric Florentin et Laurent Champaney.

En arrivant à l'UMA après une formation de mécanique, je craignais un peu d'être perdu parmi tous ces "matheux". Cette crainte s'est vite dissipée, et j'ai trouvé dans ce département

une grande qualité d'accueil, humaine comme scientifique, que ce soit de la part des enseignants chercheurs où des doctorants et post-doctorants, et indifféremment de l'équipe de rattachement de chacun. En conséquence, je remercie profondément Eric Lunéville, Pierre Carpentier, Patrick Joly et Anne-Sophie Bonnet-BenDhia qui ont dirigé tout ou partie de l'UMA durant mon séjour pour m'y avoir accueilli et y avoir préservé cette atmosphère exceptionnelle. Je remercie bien entendu également tous les chercheurs avec qui les échanges furent agréables et enrichissants. Mes premièrs remerciements vont à Stéphanie, pour son aide patiente avec COFFEE et nos fructueuses discussions sur les équations intégrales. Merci également, Laurent, pour la sollicitude aimable avec laquelle tu m'interrogeais sur l'avancée de la thèse et les discussions qui suivaient, Anne-Sophie (encore !) pour l'attention que tu apportes à chacun, Bérengère pour avoir cohabité avec bonne humeur pendant quelques mois, Eliane pour les articles fort intéressants que tu nous envoyais, Frédéric pour ton aide précieuse, doctorale comme logistico-caféinée, Sonia, Christophe, Jean-François, Patrick et Patrick, Marie-Christine, Jérôme ... et tous les autres, pour tous les bons moments passés au coin café et parfois en conf', à parler de maths-mais-pas-que.

Il me faut aussi bien sûr remercier les doctorants, post-doctorants et stagiaires qui ont accompagné cette aventure pendant tout ou partie des quatre années qu'elle a duré, pour leur soutien sans faille et tous les bons moments passés autour d'un tableau noir, d'un goûter à 16h ou d'une bière un peu plus tard. Sans pouvoir tous vous citer, j'aimerais commencer par remercier Aliénor, pour son accueil dans cette communauté, nos échanges de bouquins et la découverte du Magellan. Merci à Maryna et Christian, nos ainés en recherche mais nos amis au quotidien. Merci aussi à tous ceux qui ont partagé mon bureau et supporté mes questions et tentatives de divertissement : Athéna, Anne-Claire, Aurore, Vasileos, Antoine qui détient le record de cohabitation et à qui je souhaite la fin de thèse brillante qu'il mérite (si, si !). Merci à tous ceux, arrivés en cours de route, qui se sont pliés de bonne grâce à mes appels à la "paaaause" pour m'éviter de tourner en rond plus longtemps, et qui ont montré une patience à toute épreuve devant mes tentatives de persuasion que "vous êtes bien trop sérieux". Merci donc Laure, Arnaud, Léandre, Marc ; merci Zouhair, pour ce qui précède mais aussi pour nos discussions et ton aide avec COFFEE.

Je ne peux bien sûr clore ce paragraphe sans remercier la "promo 2012" qui forma ma "garde rapprochée" pendant quatre ans. Merci donc, Goeffrey, pour Angoulême, la poésie et le grain de folie. Merci, Simon, pour les échecs, l'humour grinçant et ton amitié bourrue. Merci, Camille, pour les conseils avisés (en maths comme ailleurs), ton aura d'énergie et de prévenance, et les couleurs dans les diapositives. Merci, Valentin, pour tous les "Toi qui es matheux/physicien ..." qui amorçaient nos échanges, les discussions tout feu tout flammes qui s'ensuivaient ("Elle est régulière ta fonction ?"-"Tu sais, en physique ..."), parfois jusque sur le chemin du retour ("Et donc, le terme d'ordre 2 ... tu vois ?" - "Non, je conduis"), et toutes les autres discussions. Vous avez été -et êtes toujours- fantastiques.

I also was warmly welcomed and supported by the graduate students of the geomechanics group and of SIAM chapter at the UoM, who therefore have all my thanks. In particular, thanks, Egor, for your help when I was moving in at the very beginning, and the pleasant lunches we shared at the 7th floor of CEGE. Thanks also, Roman, for sharing your office and answering patiently to some of my questions. Finally, thanks a lot, Fatemeh, for your good mood, your clever advice and your precious help and support when I had scientific or administrative questions.

J'ai eu la chance de bénéficier d'un financement d'ATER à l'Université Pierre et Marie Curie pour finir cette thèse dans les meilleures conditions. Beaucoup plus qu'un passage obligé et "alimentaire", cette année à la faculté d'ingénierie restera un excellent souvenir et une source d'inspiration précieuse pour les futurs enseignements que j'espère donner. Merci donc à toute l'équipe pédagogique de la licence et du master de mécanique pour m'avoir accueilli comme enseignant et pour la confiance que vous m'avez témoigné, et aux étudiants pour leur enthousiasme (fluctuant selon l'horaire et la matière, mais bien présent !). En particulier, je voudrais exprimer toute ma gratitude à Hélène Dumontet pour la gestion sans faille et toujours humaine de ces formations, et tout le personnel administratif pour leur soutien indispensable et leur réactivité aux inévitables imprévus.

Je voudrais inclure dans ces remerciements tous mes amis et ma famille, qui sans toujours avoir accès aux rebondissements scientifiques de cette thèse, en ont constaté les effets sur mon humeur, les ont supportés (ou partagés quand "ça marchait") et accompagnés. La liste serait un peu fastidieuse, mais pour que chacun puisse se reconnatre un peu, je remercie mes "vieux" amis, les cachanais, et les drôles de zèbres qui constituèrent une bonne partie des nouveaux arrivants dans mes cercles amicaux ces dernières années.

Pour finir, je l'ai dit après la soutenance, et je le maintiens : merci, Papa. Cette thèse aurait été très différente sans ton soutien de chaque instant.

Contents

List of Figures

Introduction générale

La première partie de cette introduction, qui se veut accessible au plus grand nombre, présente les domaines de la physique et des mathématiques auxquels nous rattachons nos travaux, qui sont la *diffraction inverse* et l'*analyse asymptotique*. La deuxième partie, un peu plus technique, s'attache à décrire nos problématiques et les méthodes utilisées pour les résoudre. Un aperçu de la bibliographie pertinente y est fourni. Nous précisons également le contenu des deux parties et cinq chapitres qui constituent ce manuscrit.

I - Contexte de nos travaux et domaines d'étude associés

Diffraction directe et inverse

Dans cette introduction, nous utilisons le terme "diffraction" pour désigner l'altération d'une onde due à une perturbation de son milieu de propagation [1]. Pour restreindre un peu le champ immense de cette définition, on se concentrera sur des exemples concernant les ondes mécaniques, qui se propagent en mettant localement en mouvement la matière constituant leur milieu de propagation. Dans les milieux fluides, on parle alors souvent d'ondes acoustiques. Dans les milieux solides, les ondes sismiques sont un exemple connus de telles ondes. Dans ce cadre, la perturbation du milieu matériel peut être un obstacle rigide ou pénétrable, une fissure dans le cas d'un milieu solide, une interface entre deux matériaux ... Par souci de simplification, on utilisera fréquemment dans cette introduction le terme d'*obstacle* pour désigner une telle perturbation.

En étudiant un phénomène de diffraction, et de façon très générale, on peut s'intéresser à deux grands types de problème. Dans les problèmes *directs*, le milieu de propagation est entièrement connu, ce qui inclut la présence d'éventuels obstacles et leurs caractéristiques. L'onde incidente (non encore perturbée) ou les sollicitations mécaniques qui vont l'engendrer sont également supposés connus. La résolution du problème a alors pour but de déterminer la façon dont cette onde incidente est diffractée, ou plus généralement de déterminer l'état du milieu et les différentes ondes qui s'y propagent pendant le processus de propagation et diffraction. La résolution de tels problèmes, qu'elle soit exacte ou approchée, a de nombreuses applications dans divers domaines de la physique. Par exemple, déterminer les propriétés acoustiques d'une salle de concert dont on connaît toutes les caractéristiques (géométrie de la salle, position des sources sonores ...), c'est-à-dire déterminer les multiples réflexions et diffractions possibles des ondes acoustiques qui s'y propageront, est un problème direct complexe. Pour les ondes sismiques, un autre exemple de problème direct est l'étude de la diffraction d'une onde se propageant dans la croûte terrestre quand elle atteint la

[1] Ce sens assez large est celui du terme anglais *scattering*, qu'on traduit parfois également par "diffusion" selon le contexte.

surface, en fonction de la topologie et des matériaux qui constituent le sous-sol, afin ensuite de prévoir les conséquences d'une telle interaction onde-surface.

Pour les problèmes *inverses*, au contraire, la connaissance des paramètres de la diffraction (onde incidente, milieu de propagation, obstacle(s)) est incomplète. Ces problèmes s'appuient alors sur une connaissance totale ou partielle de l'onde diffractée pour essayer de déterminer les paramètres manquants. L'écholocalisation des chauves-souris et des dauphins, et sa contrepartie artificielle, le sonar, sont certainement l'exemple le plus connus d'une utilisation "inverse" des ondes acoustiques pour déterminer la position des obstacles les plus proches dans une direction donnée. En plus de la position de telles obstacles, on peut aussi imaginer obtenir quelques-unes de leurs caractéristiques comme leur forme et leur caractère rigide ou pénétrable. Ces problèmes inverses ont bien sûr eux aussi de nombreuses applications dans des domaines très différents, on parle ainsi parfois d'*imagerie* (médicale, par exemple), ou de *contrôle non-destructif* quand on cherche à détecter des défauts dans des structures sans les endommager. C'est cette problématique d'identification qui a motivé nos travaux.

La figure 1 illustre ainsi la diffraction d'une onde par un obstacle, et deux problèmes, direct et inverse, qui peuvent y être associés.

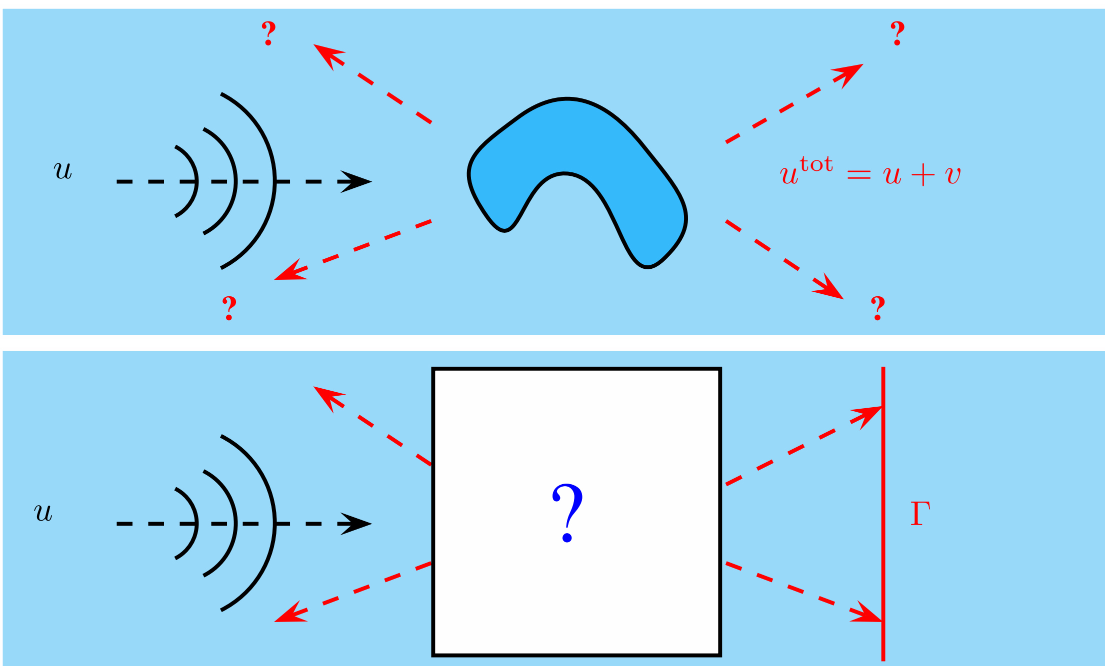

Figure 1: Illustration de problèmes de diffraction (i) *direct* (en haut), pour lequel une onde incidente u et un obstacle sont connus et où l'on veut déterminer le champ total après diffraction u^{tot}, somme de u et du champ diffracté v, et (ii) *inverse* (en bas) pour lequel une observation partielle de u^{tot} sur une surface S^{obs} est disponible mais la cause de la diffraction est inconnue.

Quelques types de méthodes existantes pour la résolution de problèmes inverses

Les problèmes de diffraction inverse appartiennent à la famille des problèmes inverses, qui peuvent concerner bien d'autres domaines que celui -déjà vaste- de la propagation des ondes. Nous renvoyons le lecteur intéressé à la préface et aux deux premiers articles du compte-rendu de conférence [Anger et al., 1993] et à l'introduction de l'ouvrage [Kirsch, 2011] pour une présentation générale de ces problèmes et de certains formalismes mathématiques associés, accompagnée de nombreux exemples dans différents cadres. Pour le cas particulier de la diffraction inverse, l'introduction du célèbre ouvrage [Colton & Kress, 1998] présente un exemple canonique pour l'acoustique et comporte de nombreuses références.

De très nombreuses méthodes existent pour la résolution de tels problèmes. Sans rentrer dans le détail ni espérer être représentatif de cette variété, nous présentons ci-dessous quelques grandes classes de méthodes. Le cas le plus simple se présente quand la relation entre les paramètres inconnus et les données disponibles, établie en résolvant le problème direct, est suffisamment simple pour être inversée et exprimer les inconnues directement en fonction des données. Un exemple canonique est celui de la triangulation : supposons qu'on connaisse l'instant où a été émise une onde se propageant dans toutes les directions d'un plan (par exemple des ondes à la surface plane d'une mare) et sa vitesse de propagation, mais pas l'origine de cette émission ("l'endroit où le caillou est tombé dans l'eau"). Si l'on mesure son temps d'arrivée en trois points différents $(\boldsymbol{x}_1, \boldsymbol{x}_2, \boldsymbol{x}_3)$, on peut calculer directement les trois distances (d_1, d_2, d_3) parcourues depuis le point d'émission et ce point est uniquement déterminé comme l'intersection des trois cercles de centres $\boldsymbol{x}_j$ et de rayons d_j. Souvent, cependant, la relation liant paramètres inconnus et données observables n'est pas si explicite : elle est par exemple définie comme étant la solution d'un système d'équations aux dérivées partielles, non connue analytiquement. On se repose alors fréquemment sur des méthodes approchées.

Les méthodes dites *itératives* s'appuient sur une estimation *a priori* des paramètres à déterminer, qui est utilisée pour simuler un problème direct et comparer les résultats obtenus à des résultats de référence. Par exemple, on se donne un obstacle "test" (défini par son emplacement, sa forme, ses caractéristiques matérielles ...) et on compare les résultats d'une simulation numérique de diffraction par cet obstacle test à des mesures expérimentales du champ diffracté par un obstacle inconnu. Cette comparaison est utilisée pour modifier l'estimation des inconnues, et on itère le processus de simulation-comparaison-mise à jour jusqu'à obtenir une approximation satisfaisante des données de référence. La difficulté de cette approche réside souvent dans la le choix de la méthode de mise à jour des estimations à partir de l'écart aux données de référence observé. L'efficacité de cette étape conditionne en effet la convergence de la méthode vers les paramètres à identifier, et, tout aussi important, la rapidité de cette convergence. En effet, chaque itération nécessite la résolution d'un *nouveau* problème direct, ce qui peut rapidement faire exploser les temps de calcul. Enfin, ces méthodes sont souvent sensibles à la distance de l'estimation initiale aux vrais paramètres. On renvoie encore à l'ouvrage [Kirsch, 2011] et les références qu'il contient pour des exemples de telles méthodes, et à l'article [Bonnet & Guzina, 2009] pour un exemple de reconstruction itérative d'obstacles pénétrables en élasticité.

Une autre classe de méthodes, dites *d'échantillonnage*[2], auxquelles l'ouvrage [Cakoni & Colton, 2006] est consacré, vise à produire une fonction indicatrice calculée en un échantillon de différents points du domaine "testé", dont les valeurs extrémales indiquent la présence d'obstacles (ou parfois, de leurs frontières). La *linear sampling method* est en particulier détaillée dans l'ouvrage [Cakoni et al., 2011]. La *sensibilité topologique* d'une fonction-coût à la nucléation d'un petit obstacle-test, détaillée dans la partie qui suit, est un autre exemple d'une telle fonction indicatrice. Un des avantages de ces méthodes est souvent qu'elles nécessitent peu de calculs de problèmes directs pour

[2] *sampling methods* en anglais

obtenir la “carte” évoquée ci-dessus, contrairement aux méthodes itératives. En revanche, elles sont souvent moins précises, mais peuvent par exemple fournir une bonne estimation pour initialiser une méthode itérative.

Finalement, on peut évoquer des méthodes qui, pour contourner le caractère implicite de la “vraie” relation qui lie paramètres inconnus et données disponibles, commencent par établir une approximation du problème direct et/ou de sa solution. Cette approximation est choisie pour fournir une relation plus explicite qu'on utilise pour mener l'inversion, en gardant bien sûr en tête que l'approximation initiale faite sur le problème direct impactera la qualité de cette inversion. C'est ce dernier type de méthodes dont ce travail de thèse traite, et l'approximation désirée y est obtenue au moyen d' *analyses asymptotiques* des problèmes considérés. Nous décrivons donc à présent ce type d'approche.

Méthodes asymptotiques

L'analyse asymptotique d'un modèle étudie son comportement quand les valeurs d'un ou plusieurs des paramètres qui le définissent, ou les rapports de telles valeurs, s'approchent de valeurs spécifiques. Par exemple, une longueur caractéristique du problème peut tendre à s'annuler, devenir beaucoup plus grande qu'une autre longueur considérée, ou s'approcher d'une longueur *critique* particulièrement digne d'intérêt. La motivation d'une telle étude est par exemple que des valeurs spécifiques peuvent correspondre à différents *régimes* du phénomène physique modélisé. L'écoulement d'un fluide peut ainsi être qualifié de *laminaire* ou *turbulent*, et ces deux régimes correspondent respectivement à des valeurs “petites” et “grandes” du *nombre de Reynolds*. Ce nombre est lui-même défini comme une combinaison de différents paramètres physiques qui interviennent dans les équations *de Navier-Stokes* qui décrivent un tel écoulement.

De façon similaire, un même type d'onde peut adopter des comportements très différents en fonction des valeurs de la fréquence étudiée (ou de sa contrepartie spatiale, la longueur d'onde). Pour les ondes électromagnétiques, le spectre des couleurs visibles constitue par exemple la seule bande de longueurs d'onde perceptible par l'œil humain. Dans le cas de la diffraction d'une onde par un obstacle, le rapport entre la longueur d'onde et une taille caractéristique de l'obstacle (par exemple le rayon d'un obstacle sphérique) a souvent une importance cruciale. Si bien qu'on distingue fréquemment les régimes de *basses fréquences* (et donc de grandes longueurs d'ondes par rapport à une longueur donnée) et de *haute fréquences* et qu'on s'efforce de comprendre le comportement des modèles étudiés dans ces cas limites.

Les méthodes asymptotiques sont toutes les méthodes qui tirent parti de de l'hypothèse l'existence d'un petit paramètre (ou d'un petit rapport de paramètres) pour obtenir une simplification du modèle étudié, valable dans le régime sous-entendu par cette hypothèse. Par exemple, l'influence d'un tel petit paramètre, souvent noté ε, peut parfois être étudiée comme une perturbation d'un modèle de référence plus simple. Ce point de vue, et diverses méthodes et applications associées, sont décrits dans [Holmes, 1995].

Une approche systématique couramment utilisée et que nous suivons dans nos travaux est celle du *développement asymptotique* d'une quantité d'intérêt, ici notée u, qui est recherchée sous la forme[3]:

$$u \approx u_0 + \varepsilon u_1 + \varepsilon^2 u_2 + \dots \tag{1}$$

[3] De façon plus générale, on peut aussi rechercher des développements de la forme $\varepsilon^{\alpha_1} u_1 + \varepsilon^{\alpha_2} u_2 + ...$ sans présupposer de la valeur des exposants $(\alpha_1, \alpha_2 ...)$.

Injecter cette forme de solution dans le modèle considéré, qui lui aussi dépend de ε, permet ensuite de dégager successivement des problèmes satisfaits par le terme dominant u_0, puis ceux d'ordres supérieurs u_1, u_2 ... Comme ε est supposé petit, l'influence de chacun de ces termes diminue avec leur ordre dans la série (1), et le but est de ne calculer qu'un petit nombre d'entre eux et de *tronquer* la série, c'est à dire considérer que les suivants sont négligeables pour obtenir une approximation de u. Typiquement, dans certains cas où l'influence fine de ε n'est pas l'information recherchée, on peut considérer que u_0 ou $u_0 + \varepsilon u_1$ sont des approximations satisfaisantes de u. Cependant, dans d'autres cas il est intéressant de "pousser" le développement, c'est à dire de calculer aussi les termes suivants (du moins, quelques-uns d'entre eux) pour obtenir une meilleure approximation et mieux rendre compte de l'influence de ε. On parle alors de *développements d'ordre élevé*.

C'est précisément à l'aide de tels développements d'ordre élevé que nous proposons par la suite des méthodes approchées d'identification d'obstacles. Les deux problèmes que nous étudions, et l'organisation des parties correspondantes dans la suite du manuscrit, sont à présent détaillés.

II - Problèmes étudiés

Ce manuscrit comprend deux parties pouvant être lues indépendamment l'une de l'autre, correspondant approximativement aux travaux menés au sein de l'équipe POEMS (UMR CNRS-INRIA-ENSTA) sous la direction de Marc Bonnet, et à ceux conduits sous la direction de Bojan Guzina au *Civil, Environmental and Geo-Engineering Department* de l'Université du Minnesota.

Dérivées topologiques et identification de défauts

La première partie de notre travail, réalisé sous la supervision de Marc Bonnet, prend place dans un domaine de recherche né au début des années 2000 : le calcul des *dérivées topologiques* d'une fonction-coût et leur utilisation pour l'identification de défauts enfouis.

Histoire et quelques développements de la dérivée topologique. Le concept de *dérivée* (ou *gradient*) *topologique* $\mathcal{T}$ d'une fonction-coût $\mathbb{J}$ dépendant d'un domaine Ω a été introduit par [Eschenauer et al., 1994; Schumacher, 1996] puis formalisé par [Sokolowski & Zochowski, 1999] où elle est définie par:

$$\mathcal{T}(\boldsymbol{z}) = \lim_{a\to 0} \frac{\mathbb{J}(B_a(\boldsymbol{z})) - \mathbb{J}(\emptyset)}{|B_a(\boldsymbol{z})|}, \tag{2}$$

où $\mathbb{J}(\emptyset)$ et $\mathbb{J}(B_a(\boldsymbol{z}))$ désignent respectivement les valeurs de $\mathbb{J}$ prises quand le domaine Ω de référence est intact et quand une perturbation topologique $B_a(\boldsymbol{z})$ du domaine Ω, de taille a, est introduite autour du point $\boldsymbol{z}$ (typiquement, un trou, mais aussi une fissure, un obstacle pénétrable ...) [4]. $\mathcal{T}$ fournit donc une information sur la variation infinitésimale de $\mathbb{J}$ quand une telle perturbation est effectuée. Son calcul pratique a été rapidement facilité par l'utilisation de la méthode de *l'état adjoint*, par exemple introduite dans le cadre de l'élasticité par [Garreau et al., 2001].

De concert avec la *dérivée de forme*, son analogue pour les perturbations des frontières de Ω, la dérivée topologique $\mathcal{T}$ a tout d'abord été exploitée dans des méthodes d'optimisation [Céa et al., 2000; Novotny et al., 2003]. Cette direction de recherches est encore très active aujourd'hui,

[4] [Sokolowski & Zochowski, 1999], qui considère uniquement des trous, utilise plutôt les notations $\mathbb{J}(\Omega)$ et $\mathbb{J}(\Omega \setminus B_a(\boldsymbol{z}))$, moins adaptées quand B_a désigne un obstacle pénétrable.

par exemple de façon couplée avec l'homogénéisation pour la conception de structures périodiques [Giusti et al., 2010; Toader, 2011].

Son potentiel pour l'identification de défauts qui nous intéresse ici est également vite remarqué et fait l'objet de nombreux travaux. En effet, dans ce domaine, des fonctions-coût $\mathbb{J}$ quantifiant l'écart d'un domaine "test" à un domaine réel Ω^{true} comportant un (ou un ensemble de) défaut(s) B^{true} sont souvent utilisées. Si $\mathcal{T}(\boldsymbol{z})$ est alors calculée pour une modification topologique B_a du domaine test de même nature que B^{true}, ses valeurs les plus négatives correspondent aux "meilleurs" emplacements $\boldsymbol{z}$ (où l'inclusion de B_a ferait diminuer le plus la valeur de $\mathbb{J}(B_a)$) dont on peut supposer qu'ils désignent la (ou les) position(s) du ou des défauts réels B^{true}. Tracer $\mathcal{T}(\boldsymbol{z})$ fournirait donc une "carte" de Ω indiquant l'emplacement de possible défauts.

Dans le cadre de l'élasticité étudié dans ce manuscrit, [Bonnet & Guzina, 2004; Guzina & Bonnet, 2004] ont calculé cette dérivée topologique et ont étudié son potentiel pour l'identification de cavités dans des solides élastiques isotropes soumis à des sollicitations dynamiques dans le régime harmonique. Les fonction-coûts considérées dépendent de B_a implicitement au travers du champ de déplacement défini dans un solide de référence perturbé par B_a et soumis aux mêmes sollicitations. [Bonnet, 2006] étend ces résultats au régime temporel transitoire, toujours pour des cavités, puis [Guzina & Chikichev, 2007] traite le cas d'obstacles pénétrables. [Guzina & Yuan, 2009] traite le cas de solides hétérogènes et visco-élastiques. [Bellis & Bonnet, 2009] aborde l'identification de fissures plutôt que de défauts volumiques. Plus récemment, [Bonnet & Delgado, 2013; Schneider & Andr, 2014] abordent de cas de solides possiblement anisotropes, et [Delgado & Bonnet, 2015] celui de fonctions-coût pouvant dépendre de l'état de contrainte du solide étudié.

Parallèlement à ces développements dans des cas de plus en plus complexes, des travaux se sont attachés à prouver l'heuristique initiale que les valeurs minimales de $\mathcal{T}$ étaient atteintes à l'emplacement des défauts réels. C'est effectivement démontrable dans des cas particuliers, comme le montrent les travaux [Ammari et al., 2012] pour de petits obstacles et [Bellis et al., 2013] pour des obstacles faiblement diffractant (pour lesquels l'approximation de Born peut être utilisée) ou pour des obstacles plus généraux mais dans le cas où on dispose de mesures complètes autour de l'obstacle. Le cas particulier des hautes fréquences, pour lequel la dérivée topologique tend à souligner les frontières des obstacles plutôt que leur support, est étudié dans [Guzina & Pourahmadian, 2015]. Dans un autre registre de validation, [Tokmashev et al., 2013] fournit une des rares études s'appuyant sur des mesures expérimentales (et non pas simulées) pour le calcul de $\mathcal{T}$ et l'imagerie d'une plaque trouée.

Dérivées topologiques d'ordre élevé. De façon générale, et ce sera l'objet de la première partie de ce manuscrit, on peut également définir et calculer *les* dérivées topologiques $\mathcal{T}_j$ d'une fonctionnelle $\mathbb{J}$ comme les termes de son développement asymptotique en a que l'on écrit alors:

$$\mathbb{J}(B_a(\boldsymbol{z})) = \mathbb{J}(\emptyset) + \sum_{j=j_{\min}}^{j_{\max}} a^j \mathcal{T}_j(\boldsymbol{z}) + o(a^{j_{\max}}). \tag{3}$$

L'indice $j_{\min}$ désigne l'ordre dominant de ce développement (généralement égal à la dimension du problème), de sorte que $\mathcal{T}_{j_{\min}} = \mathcal{T}$, et $j_{\max}$ est l'ordre auquel on choisit d'arrêter le développement. En négligeant le résidu $o(a^{j_{\max}})$ pour a suffisamment petit, le développement (3) fournit une *approximation polynomiale* de $\mathbb{J}$, de laquelle certaines informations quantitatives peuvent être extraites, par opposition à l'information uniquement qualitative donnée par la seule connaissance de la première dérivée topologique $\mathcal{T}$. Ainsi, de tels développement sont calculés et exploités pour l'identification par [Bonnet, 2008] dans un cadre acoustique pour des obstacles impénétrables, par [Rocha de Faria & Novotny, 2009; Bonnet, 2009, 2011] pour des problèmes potentiels (de type conductivité), et pour des obstacles pénétrables ou des fissures, et par [Silva et al., 2010] pour un domaine élastique 2D perforé par un petit trou. L'article [Hintermüller et al., 2012] insiste sur le fait que dans ces termes d'ordre élevé interviennent les interactions entre plusieurs obstacles tests que l'on choisirait d'introduire simultanément (contrairement à la première dérivée topologique qui ne prend pas en compte de telles interactions).

C'est dans la poursuite de ces avancées que se situent nos travaux. Nous nous plaçons en effet dans le cadre plus général de l'élasticité tridimensionnelle, et considérons des obstacles pénétrables. De plus, les matériaux constituant le domaine étudié Ω et l'obstacle test B_a sont homogènes mais peuvent être anisotropes.

Organisation de la première partie. Le chapitre 1 présente tout d'abord les notations et définitions des termes et objets utilisés dans cette première partie. Il rappelle ensuite en détail des résultats sur les *problèmes de transmission en milieu infini* dont les solutions seront au cœur des développements asymptotiques présentés dans les chapitres suivants. Le résultat original de ce chapitre est le théorème 1.3 qui porte sur l'opérateur intégral associé à ces problèmes, et étend un résultat d'inversibilité récent prouvé par [Gintides & Kiriaki, 2015] au cas des matériaux anisotropes.

Le chapitre 2 s'intéresse à des fonctions-coûts dépendantes d'un obstacle test B_a implicitement au travers de la perturbation des déplacements induite par la présence de cet obstacle dans un domaine Ω soumis à des sollicitations *statiques*. Un développement asymptotique de cette perturbation en la taille a de l'obstacle est donc calculé dans un premier temps, au moyen d'une formulation par équations intégrales volumiques. Ce développement est ensuite injecté dans l'expression de la fonction-coût pour obtenir un développement de la forme (3) à l'ordre 6 , qui fait l'objet du théorème 2.4. Une nouveauté de ce travail est la justification de ce développement par une estimation de l'ordre du résidu.

Les résultats de ces deux premiers chapitres ont fait l'objet d'un article soumis [Bonnet & Cornaggia, a].

Finalement, le chapitre 3 reprend la démarche du chapitre 2 dans le cas de sollicitations dynamiques dans le régime harmonique, et détaille le calcul des termes inertiels qui viennent s'ajouter tant dans le développement de la perturbation du déplacement (on parle plutôt dans ce chapitre de *champ diffracté* par l'obstacle) que dans celui de la fonction-coût. Ce dernier est précisé par le théorème 3.3. De plus, l'objectif initial d'identification est réalisé par la proposition d'une méthode s'appuyant sur l'approximation polynomiale de $\mathbb{J}$ ainsi obtenue pour déterminer position et taille d'un obstacle pénétrable. Cette méthode est illustrée par quelques exemples numériques dans des cas simples (milieu infini, obstacle sphérique et matériaux isotropes). Ce chapitre est destiné à être remanié sous la forme d'un article [Bonnet & Cornaggia, b] constituant la suite immédiate de [Bonnet & Cornaggia, a].

Pour ces trois chapitres, le cas particulier des matériaux isotropes et des obstacles de forme ellipsodale, pour lesquels de nombreux résultats sont disponibles, en particulier dans l'ouvrage [Mura, 1982], est traité analytiquement. Les calculs sont complètement détaillés pour le cas d'une inclusion sphérique et tous les éléments nécessaires aux calculs finaux sont fournis dans les autres cas. Pour plus de lisibilité du corps du texte, le détail de ces calculs est souvent relégué aux annexes.

Homogénéisation d'un problème de transmission intérieur pour l'identification d'un obstacle périodique

La seconde partie du manuscrit rend compte d'un travail réalisé en collaboration avec Cédric Bellis et sous la supervision de Bojan Guzina. Le but de ce travail est de proposer une méthode d'identification d'une inclusion périodique monodimensionnelle (typiquement, une portion de barre crénelée) à partir de la connaissance des *fréquences propres de transmission* de cette barre, définies ci-dessous. Cette méthode se repose *l'homogénéisation* d'une telle barre pour prendre en compte sa structure périodique. Cette approche asymptotique est également brièvement présentée ci-dessous.

Fréquences propres de transmission. Pour définir les fréquences propres de transmission, considérons un problème simple de diffraction acoustique en régime fréquentiel et en espace libre $\mathbb{R}^3$. On note u^{i} une onde incidente de pulsation ω et de vitesse c uniforme dans le milieu ambiant, c'est-à-dire une solution de l'équation de Helmholtz $\Delta u^{\mathrm{i}} + k^2 u^{\mathrm{i}} = 0$ dans $\mathbb{R}^3$ tout entier, où $k = \omega/c$ désigne le nombre d'onde associé à ω. Cette onde est diffractée par un obstacle de support D et d'indice de réfraction n. On recherche alors le champ diffracté u^{s} et le champ total interne à l'obstacle u, comme les solutions du problème:

$$\left| \begin{array}{ll} \Delta u^{\mathrm{s}} + k^2 u^{\mathrm{s}} = 0 & \text{dans } \mathbb{R}^3 \setminus \overline{D} \\ \Delta u + n k^2 u = 0 & \text{dans } D \\ u = u^{\mathrm{i}} + u^{\mathrm{s}} \text{ et } \dfrac{\partial u}{\partial \nu} = \dfrac{\partial (u^{\mathrm{i}} + u^{\mathrm{s}})}{\partial \nu} & \text{sur } \partial D \\ \lim\limits_{r \to +\infty} r \left(\dfrac{\partial u^{\mathrm{s}}}{\partial r} - \mathrm{i} k u^{\mathrm{s}} \right) = 0 & \end{array} \right. \tag{4}$$

où, sans rentrer dans le détail, la troisième ligne traduit la continuité du champ total et de sa dérivée normale au passage de la frontière de l'obstacle, et la dernière ligne, appelée la condition de rayonnement de Sommerfeld, assure que u^{s} représente des ondes "sortantes" (et où r désigne la coordonnée radiale).

Pour certaines formes et caractéristiques d'obstacles, il existe des pulsations ω (ou de façon équivalente, des nombres d'ondes k) et des champs incidents u^{i} spécifiques qui ne sont pas diffractées par l'obstacle, c'est-à-dire pour lesquels $u^{\mathrm{s}} = 0$. Vu d'un observateur extérieur à D, l'obstacle est "invisible" à ces ondes. Ces fréquences sont appelées fréquences propres de transmission, et les nombres d'onde associés, qui sont valeurs propres du problème (4) pour $u^{\mathrm{s}} = 0$, les valeurs propres de transmission.

L'étude de ces fréquences propres de transmission a débuté à la fin des années 80 avec l'article [Kirsch, 1986], au début parce qu'elles constituaient des "points durs" de certaines méthodes d'identifications telle que la *linear sampling method* citée ci-dessus. Ces méthodes reposent en effet sur l'injectivité de l'application $u^{\mathrm{i}} \mapsto u^{\mathrm{s}}$, qui n'est plus vraie à ces fréquences. Pour une étude plus facile des possibles valeurs propres de transmission, il a été montré qu'on pouvait se ramener à un problème dit de *transmission intérieur* posé uniquement sur D. Pour ce problème, on cherche un couple de fonctions (v, w) telles que

$$\left| \begin{array}{ll} \Delta v + k^2 v = 0 & \text{dans } D \\ \Delta w + n k^2 w = 0 & \text{dans } D \\ w = v \text{ et } \dfrac{\partial w}{\partial \nu} = \dfrac{\partial v}{\partial \nu} & \text{sur } \partial D. \end{array} \right. \tag{5}$$

Les valeurs propres de transmission *intérieures* sont les nombres d'onde k telles qu'il existe une solution (v, w) non triviale à ce problème (5). On voit facilement que toute valeur propre de transmission est également valeur propre de transmission intérieure. En effet, supposons que (u^{i}, u) soient un couple solution du problème de diffraction (4) avec $u^{\mathrm{s}} = 0$ pour un nombre d'onde k donné, alors $(v, w) = (u^{\mathrm{i}}_{|D}, u)$ est une solution du problème de transmission intérieur pour le même nombre d'onde. L'implication inverse est plus subtile, et nous renvoyons le lecteur à l'article de revue [Colton et al., 2007] pour plus de détails.

Plus récemment, le potentiel de ces fréquences propres comme données utilisables pour identifier les caractéristiques de l'obstacle a commencé à être exploité. En effet, elles peuvent d'une part être déterminées grâce à des mesures de champs diffractés à différentes fréquences [Cakoni et al., 2010], et d'autre part leur dépendance à la géométrie et aux caractéristiques de l'obstacle peut être étudiée - et inversée - au travers du problème de transmission intérieur (5). Cette nouvelle orientation a donné lieu à de nombreux travaux, détaillés en partie dans l'article de revue [Cakoni & Haddar, 2013].

Problème étudié. Dans nos travaux, on se propose de considérer le cas d'un "obstacle" unidimensionnel, qui peut modéliser par exemple une longueur de barre sur laquelle la section varie. Les fréquences de transmission sont donc les fréquences pour lesquelles certaines ondes longitudinales en régime établi ne sembleraient pas affectées par l'existence de cet obstacle pour un observateur n'ayant accès qu'aux parties "saines" (à section constante) de la barre.

La difficulté supplémentaire que nous introduisons est la nature de cet obstacle : comme dit ci-dessus, on s'intéresse à des variations de section *périodiques* au sein de l'inclusion, ou de façon équivalente pour la propagation d'ondes longitudinales à des variations de paramètres matériaux. Une telle inclusion est représentée figure par la figure 2.On imagine que cet obstacle est "sondé" par une onde incidente u^{i} pour une gamme de fréquence et que des relevés de champ de déplacement sont effectués plus loin dans la barre (capteurs représentés en rouges), de façon à obtenir les valeurs propres de transmission sur lesquelles nous travaillons pour finalement reconstruire les paramères (longeur, contraste, période) de l'inhomogénéité.

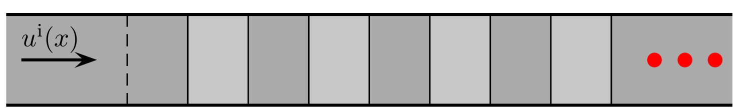

Figure 2: Barre dont une partie est constitué de deux matériaux periodiquement alternés.

On verra dans le détail de nos travaux que l'étude analytique des fréquences propres d'une telle structure est peu aisée, ce qui rend difficile la détermination d'une procédure d'inversion. C'est pourquoi on se repose sur la méthode de l'homogénéisation, décrite ci-après, pour produire un modèle approché que l'on cherchera ensuite à inverser.

Homogénéisation d'ordre élevée. L'homogénéisation est un outil de modélisation de matériaux complexes, généralement dans le sens que les coefficients caractérisant ces matériaux varient rapidement dans l'espace. On peut penser par exemple à une suspension de particules dans un fluide, une plaque trouée, ou les matériaux composites constitués de fibres de verre ou de carbone liées par une matrice de résine. La variation des coefficients peut aussi être provoquée par des variations géométriques de la structure étudiée.

La prise en compte de ces variations est rarement analytiquement possible, et peut être très coûteuse numériquement. C'est pourquoi les méthodes d'homogénéisation visent à produire un modèle correspondant à un *matériau fictif homogène*, ayant des caractéristiques semblables à celles du matériau complexe pour tout ou partie de sa gamme d'utilisation : il existe par exemple des techniques d'homogénéisation spécifiques aux régimes de hautes fréquences. En particulier, on s'intéressera à l'homogénéisation *périodique*, utilisée quand les variations considérées sont périodiques en espace, et plus précisément à la méthode d'homogénéisation dite *double-échelle* introduite dans les années 70. On renvoie aux ouvrages precurseurs [Bensoussan et al., 1978; Sanchez-Palencia, 1980] pour le détail de ces premiers travaux et à [Cioranescu & Donato, 1999] pour une présentation plus récente.

Pour exposer rapidement les principes de cette méthode, considérons l'exemple canonique d'un barreau élastique modélisé en une dimension dont la section S est périodique de période ε. Sa rigidité axiale est donc donné par une fonction périodique a de période 1 telle que $ES(x) = a(x/\varepsilon)$ (E étant le module d'Young du matériau constituant le barreau). L'équation d'équilibre statique dans un tel barreau soumis à des forces linéiques axiales notées f s'écrit :

$$\frac{d}{dx}\left(a(x/\varepsilon)\frac{du}{dx}(x)\right) + f(x) = 0, \tag{6}$$

où $u(x)$ est le déplacement longitudinal d'une section située en x. L'idée de l'homogénéisation double-échelle est de supposer que u est soumis à deux régimes de variation : un régime "lent" correspondant aux variations dans un barreau homogène "équivalent" qu'on va chercher à déterminer, et un régime "rapide" de période ε concrétisé par des oscillations autour du régime lent. On introduit donc une variable rapide $y = x/\varepsilon$ et on cherche à approcher u à l'aide d'une fonction $\hat{u}(x, y)$ des deux variables lentes et rapides telle que $u(x) = \hat{u}(x, x/\varepsilon)$.

Pour obtenir un modèle homogène équivalent, on suppose ensuite que la période ε est "petite" (devant une dimension caractéristique du problème, typiquement une longueur d'onde pour les problèmes ondulatoires) et on regarde ce qui se passe à la limite $\varepsilon \to 0$. En particulier, on cherche la fonction $\hat{u}$ sous la forme d'un développement asymptotique:

$$\hat{u}(x, y) = u_0(x, y) + \varepsilon u_1(x, y) + \varepsilon^2 u_2(x, y) + \dots, \tag{7}$$

chaque terme du développement étant formellement négligeable devant les précédents quand ε tend vers 0. Typiquement, et sans détailler les calculs qui suivent, on trouve ensuite que u_0 ne dépend que de x et satisfait une équation d'équilibre:

$$a_0 \frac{d^2 u_0}{dx^2}(x) + f(x) = 0, \tag{8}$$

où le coefficient a_0, constant, caractérise le matériau fictif dit *homogénéisé* qui était recherché.

Pour à présent revenir à la problématique qui nous intéresse, on remarque que nous ne pouvons pas espérer produire une méthode d'identification de la période ε d'une barre périodique en nous limitant à l'ordre dominant, puisque le modèle associé, similaire à l'équation (8), ne dépend plus de cette période. Dans ce but d'identification, et plus généralement pour rendre compte finement des phénomènes liées à la microstructure du barreau, il faut nécessairement étudier les termes suivants de la série (7). Sans pouvoir rendre compte de l'abondante littérature sur le sujet, on se contentera de citer ici les travaux récents [Fish et al., 2002; Andrianov et al., 2008; Wautier & Guzina, 2015] pour le cas de l'homogénéisation de l'équation des ondes en une dimension sur lequel nous travaillons.

Organisation de la seconde partie. Nous commençons dans le chapitre 4 par établir les résultats utile pour la suite de l'étude. Nous y rappelons les récents résultats cités ci-dessus pour l'homogénéisation d'ordre élevée des domaines unidimensionnels non bornés. Nous proposons ensuite des conditions aux limites adaptées, en expliquant en particulier comment nous pouvons éviter d'étudier des problèmes de couche limite grâce aux particularités du cas unidimensionnel. La pertinence de notre proposition est justifiée par une analyse de convergence pour l'homogénéisation d'un problème aux frontières simple modélisant une poutre encastrée soumise à des efforts axiaux. Nous étudions ensuite en détails ce problème dans le cas d'un matériau biphasique, pour lequel un traitement analytique est possible.

Le chapitre 5 est ensuite consacré au problème de transmission intérieur unidimensionnel pour une inclusion de longueur L. Nous commençons par discuter brièvement du cas de l'inclusion homogène. Nous montrons ensuite que pour une inclusion périodique, modélisant une longueur de poutre de section constante par morceaux, l'étude du problème homogénéisé classique (d'ordre 0) permet d'identifier les paramètres macroscopiques (L et rapport des sections) de l'inclusion. Dans le but de fournir un modèle dépendant de la période de la structure et convenant à une inversion conduisant à une identification de cette période, nous présentons finalement les problèmes homogénéisés d'ordre supérieur obtenus par applications des résultats présentés dans le chapitre 4.

Ce travail devrait également après sa complétion faire l'objet d'un article [Cornaggia et al., a].

Context and overview of the thesis

The purpose of this PhD work was to develop new methods to address *inverse problems* in elasticity. Generally speaking, such methods aim to recover some of the missing parameters of a model from the knowledge of some of their outputs for given inputs. They are the counterpart to *direct problems*, in which the model is fully known and one wants to determine its output. For a more complete presentation of general inverse problems, associated mathematical formalism and numerous examples from various physical situations, we refer to the first articles of the proceeding [Anger et al., 1993] and the introduction of the book [Kirsch, 2011]. In the specific case of inverse problems in elasticity, the paper [Bonnet & Constantinescu, 2005] and the references therein provides a good overview of existing methods.

More specifically, we focus on *inverse scattering*. Supposing we have some information about the scattering of a probing elastic wave by an obstacle (such information may be e.g. measurements of the scattered field, or the knowledge of specific frequencies which entails remarkable properties), we aim at recovering (some of) the properties of this obstacle. We refer to the introduction of the celebrated book [Colton & Kress, 1998] for relevant literature on these problems and for an example of inverse acoustic scattering problem. Such problems cover many useful applications, from medical imaging to non-destructive testing.

Since the direct problems we consider are not easily invertible, we will rely on *higher-order asymptotic expansions* to obtain approximations of the corresponding models. These problems indeed feature a small parameter, e.g. the ratio between a characteristic length of the obstacle and the wavelength of a probing wave. Therefore, based on previous results addressing mostly the leading order of relevant asymptotic expansions, we aim to show the improvements and possibilities brought by pushing these expansions to higher orders.

The two main problems we addressed are (i) the identification of a penetrable inhomogeneity in a 3D elastic domain using a higher-order expansion of a misfit function, which constitutes the natural expansion of the concept of *topological derivative*, and (ii) the identification of a 1D periodic scatterer from the knowledge of the associated *transmission eigenvalues*. They correspond roughly to the periods of the joint program spent in (i) team POEMS, at ENSTA Paristech and under the supervision of Marc Bonnet, and (ii) the Civil, Environmental and Geo-Engineering department of the University of Minnesota, under the supervision of Bojan Guzina. They are now described in further detail.

Identification of buried obstacles using higher-order expansion of a misfit cost functional

This first part is dedicated to the localization and size identification of a inhomogeneity B^{true} buried in an elastic solid occupying a domain Ω. In this goal, we focus on the study of functionals $\mathbb{J}(B_a)$

quantifying the misfit between (i) measurements of the displacement in the real solid embedding B^{true} and/or at its surface, when it is submitted to some static or time-harmonic excitations (ii) the displacement that would lie in a reference solid occupying Ω, perturbed by a *trial* inhomogeneity B_a, and submitted to the same excitations. Such functional is classically expected to be minimized with respect to some or all the characteristics (location, size, mechanical properties ...) of the trial inclusion B_a to find the best agreement with B^{true}.

In the case of small obstacles (e.g. compared to a reference wavelength), instead of computing $\mathbb{J}$ explicitly, we propose to build a *polynomial approximation* of $\mathbb{J}(B_a)$ for small trial inhomogeneities B_a, obtained by asymptotic expansion with respect to the size a of B_a, whose terms will depend in particular on the location $\boldsymbol{z}$ of the inhomogeneity. The leading-order term of such expansion, the *topological derivative* $\mathcal{T}(\boldsymbol{z})$ of $\mathbb{J}$, was the subject of thorough studies in the last decade. As it is the basis of the upcoming higher-order expansion, we provide below a short review of some of these works.

A short story of the topological derivative. The well-known topological derivative $\mathcal{T}(\boldsymbol{z})$ was introduced for general cost functional $\mathbb{J}$ by [Eschenauer et al., 1994; Schumacher, 1996] and [Sokolowski & Zochowski, 1999]. It was at first defined as:

$$\mathcal{T}(\boldsymbol{z}) = \lim_{a\to 0} \frac{\mathbb{J}(B_a(\boldsymbol{z})) - \mathbb{J}(\emptyset)}{|\overline{B_a(\boldsymbol{z})}|}, \tag{9}$$

where $\mathbb{J}(\emptyset)$ is the value taken by $\mathbb{J}$ for no inhomogeneity in Ω. Roughly speaking, this derivative provides an information on how an infinitesimal perturbation B_a of Ω placed at location $\boldsymbol{z}$ would perturb the considered functional $\mathbb{J}$.

A convenient way to effectively compute $\mathcal{T}$ was rapidly provided by the *adjoint state method* that is explained by [Garreau et al., 2001] for the elasticity system. The topological derivative was at first used in optimization methods, e.g. in [Céa et al., 2000; Novotny et al., 2003], along with the *shape derivative*, its analogous for the perturbations of the boundaries of Ω. This research direction is still very active, for instance when the optimization of periodic structures is sought. In this goal, and one has to look for the "best" perturbation of the periodicity cell to reach interesting effective material properties, which is done in [Giusti et al., 2010; Toader, 2011].

The potential of the topological derivative for defect localization and identification was also quickly remarked. Indeed, if $\mathbb{J}(B_a)$ is a misfit cost functional as described above and B_a is of the same topological nature than the obstacle B^{true}, then the most negative values of $\mathcal{T}$ indicate the best location(s) where the introduction of an infinitesimal obstacle would reduce the misfit. One can therefore hope that plotting $\mathcal{T}(\boldsymbol{z})$ over a sampling grid Ω^{test} will provide a "map" where the most negative values indicate the position of real defects.

For the elasticity context addressed in this dissertation [Bonnet & Guzina, 2004; Guzina & Bonnet, 2004] computed the topological derivative and used it to localize cavities in isotropic elastic solids submitted to time-harmonic excitations. These results were extended to the time domain by [Bonnet, 2006]. The resulting localization method was rapidly extended to other type of defects e.g. to penetrable obstacles by [Guzina & Chikichev, 2007] and cracks by [Bellis & Bonnet, 2009], and was shown to be easily adaptable to classical computational frameworks, e.g. by [Bellis & Guzina, 2010]. It is also studied for more and more complex materials: [Guzina & Yuan, 2009] consider visco-elastic heterogeneous solids and more recently [Bonnet & Delgado, 2013; Schneider & Andr, 2014] consider anisotropic solids. Finally, recent works [Delgado & Bonnet, 2015] address the difficulties of computing the topological derivatives of cost functionals that depend on the stress state (and not only on the displacements) inside the domain Ω.

In the meantime, some works aimed at showing the reliability of this approach for identification, hence investigated the original heuristic which supposed that the most negative values of $\mathcal{T}(\boldsymbol{z})$ are reached at the position of the real defect. It was indeed proven for small obstacles in [Ammari et al., 2012], and for "weak" scatterers (for which Born's approximation holds) and/or full aperture measurements around the defect to be identified in [Bellis et al., 2013]. In high-frequency regime, the topological derivative was shown to emphasize boundaries of obstacles in [Guzina & Pourahmadian, 2015], as already observed in previous studies. Another kind of validation was provided by [Tokmashev et al., 2013], one of the few studies relying on experimental measurements (rather than simulated ones) to compute the topological derivative and to localize holes in a thin aluminum plate.

Moreover, it is to be noted that $\mathcal{T}$ only provides *qualitative* information on "relevant" positions $\boldsymbol{z}$. Pushing the expansion to higher-order terms, on the other hand, provides a polynomial approximation of $\mathbb{J}$ that can be minimized to obtain *quantitative* informations such as the "best" size a of B_a for a given trial shape $\mathcal{B}$. Previous works in this direction include [Bonnet, 2008] for acoustics and a sound-hard scatterer, [Rocha de Faria & Novotny, 2009; Bonnet, 2009, 2011] for potential (conductivity-like) problems and penetrable obstacles or cracks, and [Silva et al., 2010] for holes in a two-dimensional elastic solid. It was emphasized by [Hintermüller et al., 2012] that such higher-order expansion includes terms accounting for the interactions between several trial obstacles that one would choose to introduce simultaneously inside Ω. Indeed, when using the (first) topological derivative, which accounts only for the leading-order contribution of each obstacles, one could just sum up the contributions of several obstacles.

Contents of the first part. Our results are a natural continuation of the works above. They lie in a 3D elastic setting, for both static and time-harmonic excitations, and for possibly anisotropic materials. In these cases, under certain assumptions on the cost-functional $\mathbb{J}$ specified thereafter, we derived sixth-order expansions of the kind:

$$\mathbb{J}(B_a) = \mathbb{J}(\emptyset) + a^3\mathcal{T}_3(\boldsymbol{z}) + a^4\mathcal{T}_4(\boldsymbol{z}) + a^5\mathcal{T}_5(\boldsymbol{z}) + a^6\mathcal{T}_6(\boldsymbol{z}) + o(a^6). \tag{10}$$

where $\mathcal{T}_3 = \mathcal{T}$ and we call the other $\mathcal{T}_j$ higher-order topological derivatives.

Chapter 1 is dedicated to (i) the definitions and notations used throughout the first part of this dissertation and (ii) the collection of required results on elastostatic *free-space transmission problems* (FSTPs), whose solutions will play a key role in the ensuing asymptotic expansions. The main new result of this chapter is Theorem 1.3, that focuses on the integral operator associated with these FSTPs and extends the recent invertibility result proven by [Gintides & Kiriaki, 2015] for isotropic materials to any anisotropic material.

Chapter 2 addresses the expansion of a cost-functional depending on the displacement in an elastic solid submitted to static excitations and perturbed by an inhomogeneity B_a. In a volume integral equation framework, we first derive the expansion for the perturbation of the displacement due the presence of this inhomogeneity. We then produce and justify an expansion such as (10) for cost-functionals depending on B_a implicitly through this displacement perturbation. One original result to be noted is the rigorous estimate of the remainder of such expansion (which is proven to be of order $o(a^6)$ as expected).

The main results of these two chapters are gathered in a submitted journal paper [Bonnet & Cornaggia, a].

We then pursue by addressing solids submitted to time-harmonic excitations and displacements in Chapter 3. Most of the steps of Chapter 2 are repeated, with emphasis on the new inertial terms. We also propose an identification procedure based on the minimization of the sixth-order approximation (10) of $\mathbb{J}$, supported by numerical illustrations for simple obstacles in full-space $\mathbb{R}^3$. This chapter provides the basis for another paper under preparation [Bonnet & Cornaggia, b], which would be a natural follow-up to [Bonnet & Cornaggia, a].

Identification of a one-dimensional micro-structured inclusion using homogenized interior transmission problems

The main purpose of the second part is to propose an identification procedure of a two-phase layered 1D inclusion of length L (typically, a rod whose cross-section periodically varies on $[0, L]$ and is constant elsewhere), supposing we already know its low-frequency *transmission eigenvalues* (TEs). Such eigenvalues are defined as the frequencies for which there exists an incident wave (the associated eigenfunction) that is completely transmitted through the inclusion, i.e. that produces no reflected wave. On the other hand, they can be computed as the eigenvalues of an equivalent *interior transmission problem* (ITP) posed only on the support $[0, L]$ of the inclusion. A short introduction on the interior transmission problems is accordingly provided below.

The main difficulty of this study is to provide a model simple enough to be inverted, while accounting for the microstructure effects. In this goal, we relied on *homogenized* approximations of the exact ITP for the periodic inclusion. To support such decision, a recent work [Cakoni et al., 2015] showed that the TEs of the leading-order homogenized ITP converge to these of the exact periodic ITP. Homogenization methods, and in particular the *two-scale homogenization method* that we will use, are discussed afterwards.

Transmission eigenvalues. To define the transmission eigenvalues, consider the simple example of an acoustic scattering problem in time-harmonic domain and in full space $\mathbb{R}^3$. An incident wave u^{i} propagates at circular frequency ω and uniform wavespeed c in the background medium. It is a solution to Helmholtz equation $\Delta u^{\mathrm{i}} + k^2 u^{\mathrm{i}} = 0$ in full-space $\mathbb{R}^3$, where $k = \omega/c$ is the background wavenumber. This wave is scattered by an obstacle occupying a domain D and characterized by the refraction index n. We then look for the scattered field u^{s} and the internal field u inside the obstacle as the solutions of the problem:

$$\left|\begin{array}{ll} \Delta u^{\mathrm{s}} + k^2 u^{\mathrm{s}} = 0 & \text{in } \mathbb{R}^3 \setminus \overline{D} \\ \Delta u + n k^2 u = 0 & \text{in } D \\ u = u^{\mathrm{i}} + u^{\mathrm{s}} \text{ and } \dfrac{\partial u}{\partial \nu} = \dfrac{\partial (u^{\mathrm{i}} + u^{\mathrm{s}})}{\partial \nu} & \text{on } \partial D \\ \displaystyle\lim_{r \to +\infty} r \left(\frac{\partial u^{\mathrm{s}}}{\partial r} - \mathrm{i} k u^{\mathrm{s}} \right) = 0. & \end{array}\right. \tag{11}$$

Without going into detail, the third line stands for the continuity of the total field and its normal derivative across the boundary ∂D of the obstacle, and the last line, called the Sommerfeld radiation condition, ensures that u^{s} corresponds to "outgoing" waves.

For certain shapes and characteristics of the obstacle, there exist circular frequencies ω (or, equivalently, wavenumbers k) and specific corresponding incident fields u^{i} that are not scattered by the obstacle, i.e. for which $u^{\mathrm{s}} = 0$. The obstacle is somewhat "invisible" to an observer located outside D in the sense that these specific incident fields u^{i} are not perturbed. Those values of the wavenumber k are called scattering eigenvalues.

The study of such eigenvalues began in the late eighties with the work [Kirsch, 1986]. In the beginning, they were studied because they indicate "blind spots" of existing identification methods such as the *linear sampling method* explained in the book [Cakoni et al., 2011]. Indeed, roughly speaking, these methods require the mapping $u^{\mathrm{i}} \mapsto u^{\mathrm{s}}$ to be one-to-one, which does not hold for these wavenumbers. For an easier study of the the scattering eigenvalues, it was shown that, instead of investigating the full-space scattering problem, one could look at an *interior transmission problem* (ITP) posed only on the obstacle's support D. For this problem, we look for a couple of functions (v, w) such that:

$$\left| \begin{array}{ll} \Delta v + k^2 v = 0 & \text{in } D, \\ \Delta w + n k^2 w = 0 & \text{in } D, \\ w = v \text{ and } \dfrac{\partial w}{\partial \nu} = \dfrac{\partial v}{\partial \nu} & \text{on } \partial D. \end{array} \right. \tag{12}$$

The *interior transmission eigenvalues* (ITEs or TEs) are the wavenumbers k such that there exists a non-trivial solution (v, w) to this problem. It is easily observed that any scattering eigenvalue is a transmission eigenvalue. Indeed, suppose that k is a scattering eigenvalue with associated incident field u^{i} (i.e. $u^{\mathrm{s}} = 0$ in problem (11)), then the couple $(v, w) = (u^{\mathrm{i}}_{|D}, u)$ is a non-trivial solution of the ITP (12). The reverse implication is more subtle, and we refer to the review paper [Colton et al., 2007] for further details.

More recently, the possibility to consider these TEs as available data to identity the obstacle began to be investigated. Indeed, they can be determined from scattered field measurements over a range of sampling frequencies as shown by [Cakoni et al., 2010]. On the other hand, the way they depend on the obstacle can be studied thanks to the interior transmission problem. This whole new branch of research lead to numerous works, partly covered by the recent review article [Cakoni & Haddar, 2013].

We now describe the homogenization method, that we will use as explained before to investigate interior transmission problems for *periodic* scatterers.

Homogenization. Homogenization is a modeling tool of complex materials, generally in the sense that the coefficients that describe these materials vary within space. One can think e.g. to a particle suspension in some fluid, a perforated plate, concrete, or fiber-reinforced composite materials.

Taking these variations into account is rarely analytically possible, and can be very costly in numerical computations. It is why homogenization methods aim at determining a model corresponding to a *fictitious homogeneous material*, such that this model reproduces the behavior of the original material for the range of use that is of interest. It exists for instance homogenization methods dedicated to high-frequency behaviors to such material. In particular, we are interested in *periodic* homogenization, used when the original variations are periodic in space. More precisely, we will use the *two-scale homogenization method* whose original ideas appeared in the seventies. We refer to the celebrated books [Bensoussan et al., 1978; Sanchez-Palencia, 1980] for these early works, and to [Cioranescu & Donato, 1999] for a more recent review.

To introduce this method, let us consider the canonical example of a unidimensional problem modeling an elastic rod whose section S varies periodically along x with period ε. Its axial stiffness is therefore expressed thanks to a 1-periodic function a such that $ES(x) = a(x/\varepsilon)$, where E is the

Young's modulus of the material the rod is made of. The static equilibrium equation for such a rod submitted to longitudinal force density f writes:

$$\frac{d}{dx}\left(a(x/\varepsilon)\frac{du}{dx}(x)\right) + f(x) = 0, \tag{13}$$

where $u(x)$ is the longitudinal displacement of the neutral axis of the rod at point x. The idea of the double-scale homogenization is to assume that u is submitted to two variation regimes: a "slow" regime corresponding to the "macroscopic" response of the rod to the loading, and a "fast" regime of period ε accounting for the microstructure. One therefore introduce a fast variable $y = x/\varepsilon$ and look for u as a function $\hat{u}(x, y)$ of both variables so that $u(x) = \hat{u}(x, x/\varepsilon)$.

To obtain an equivalent homogenized model, one then suppose that the period ε is small in front of a characteristic length of the problem, typically a wavelength for scattering problems. The asymptotic behavior of the original problem as $\varepsilon \to 0$ is therefore investigated. In particular, the functions $\hat{u}$ is sought as the asymptotic expansion:

$$\hat{u}(x, y) = u_0(x, y) + \varepsilon u_1(x, y) + \varepsilon^2 u_2(x, y) + \dots. \tag{14}$$

Each term of such expansion is formally negligible in front of the previous ones as ε becomes smaller. Typically, without addressing the computations which occur from such assumptions, one then finds that u_0 depends only on the slow variable x and is the solution of an equilibrium equation:

$$a_0 \frac{d^2 u_0}{dx^2}(x) + f(x) = 0, \tag{15}$$

where the constant coefficient a_0 characterizes a fictitious *homogenized* material.

Coming back to our final goal, i.e. the identification of a periodic 1D scatterer, we observe that one cannot expect to derive a method able to recover the period ε while considering only the leading-order homogenized model since this model does not depend on ε anymore. More generally, to account accurately for the microstucture effects, one has to study the higher-order terms of the expansion (14). On the corresponding *higher-order homogenization* methods, we do not give here an overview of the wide existing literature, but refer to Chapter 4 where some of it is provided.

Contents of the second part Chapter 4 indeed collects notations and recall recent results obtained for the higher-order homogenization of 1D wave equation by [Andrianov et al., 2008; Wautier & Guzina, 2015] among other. An effort is made to provide relevant high-order boundary conditions, exploiting the pecularities of the one-dimensional modeling to avoid dealing with the well-known boundary layers that appear in higher dimensions. The need for such conditions and the efficiency of our proposition are illustrated by the homogenization of a simple 1D boundary-value problem and for a two-phase layered material for which analytical treatment is possible.

Chapter 5 then focuses on interior transmission problems associated with 1D elastic inclusions. We first present some preliminary results on the transmission eigenvalues of homogeneous inclusions. We then address the case of a periodic inclusion made of the two-phase layered material studied in Chapter 4. The analysis of the leading-order homogenization of the ITP shows that the length of such inclusion and the contrast between the two phases can be recovered easily from the two lowest-frequency TE, under reasonable low-contrast assumption. We finally define the higher-order homogenized ITP featuring the boundary conditions defined in Chapter 4 and discuss their relevance.

This work is conducted in collaboration with Cédric Bellis and under the supervision of Bojan Guzina. A journal paper [Cornaggia et al., a] is under preparation.

Part I

High-order topological derivatives in anisotropic elasticity; application to the identification of penetrable obstacles

Chapter 1

Free-space transmission problem

Contents

This chapter is dedicated to the introduction of notations and results (most of them already existing) that will be of wide use in the following chapters. Section 1.1 introduces our notations for tensor calculus, along with the needed basics of linearized elasticity. We then address in detail the *free-space transmission problem* (FSTP) that describes the perturbations of the displacement field due to the presence of a perfectly-bounded inhomogeneity embedded in an otherwise homogeneous infinite elastic solid. Indeed, this problem will play a key role in the upcoming asymptotic expansions. We firstly recall in Section 1.2 the corresponding local and integral formulations. These formulations are shown to be equivalent, and the well-posedness of the problem is proven for both of them. On this basis, the invertibility of the integro-differential operator associated to the transmission problem is shown, which is the main new result in this chapter. Finally, Section 1.3 addresses the specific case of FSTPs featuring polynomial background displacements, whose solution relies on Eshelby's equivalent inclusion method for ellipsoidal inhomogeneities. We notably recall the definition of the so-called *elastic moment tensors*, we introduce the *inertial polarization tensors*, and we provide the expressions of these tensors for such ellipsoids.

1.1 General notations in linearized elasticity

This section is devoted to the introduction of the notations used all along our work. It has no pretension of completeness, and for a complete presentation of linearized elasticity the interested reader is invited to refer to the textbook [Gonzalez & Stuart, 2008] and the numerous references therein; see in particular the very enlightening bibliographic notes that conclude each chapter.

1.1.1 Vectors and tensors

The spatial domain we will consider will either be the whole three-dimensional space $\mathbb{R}^3$ or a subset of it. A fixed Cartesian coordinate system with orthonormal basis $(\boldsymbol{e}_i)_{1\leq i\leq 3}$ is adopted. Most of the *vectors* will be denoted by boldface lowercases (e.g. $\boldsymbol{x}$, $\boldsymbol{u}$) and represented by 3-by-1 component arrays (e.g. x_i, u_i) in this basis. As a consequence, the space of vectors is identified to $\mathbb{R}^3$ thereafter.

We more generally use p-th order *tensors*, defined here as p-linear forms on $(\mathbb{R}^3)^p$ and represented by p-dimensional arrays. Vectors are thus identified to first-order tensors. Most second-order tensors will be denoted by uppercase letters (e.g. $\boldsymbol{E}$, $\boldsymbol{A}$), except for stress $\boldsymbol{\sigma}$ and strain $\boldsymbol{\varepsilon}$, and represented by 3-by-3 matrices (with components E_{ij}, A_{ij}, σ_{ij}). Higher-order tensors, denoted by calligraphic uppercase letters for some of them (e.g. $\boldsymbol{\mathcal{C}}$, $\boldsymbol{\mathcal{A}}$) are similarly represented by multi-dimensional arrays.

The classical tensor product $\otimes$ between two tensors $\boldsymbol{T}$ and $\boldsymbol{R}$ of orders p and q is defined so that $\boldsymbol{T}\otimes\boldsymbol{R}$ is the $(p+q)$-th order tensor acting on $(\mathbb{R}^3)^p\times(\mathbb{R}^3)^q$ which corresponds to the multiplication of the p and q-linear forms associated with $\boldsymbol{T}$ and $\boldsymbol{R}$.

For $\boldsymbol{u}$ a vector, $\boldsymbol{E}$ a second-order tensor and $\boldsymbol{\mathcal{C}}$ a fourth-order tensor, we therefore note:

$$\boldsymbol{u} = u_i\,\boldsymbol{e}_i, \quad \boldsymbol{E} = E_{ij}(\boldsymbol{e}_i\otimes\boldsymbol{e}_j), \quad \boldsymbol{\mathcal{C}} = \mathcal{C}_{ijkl}(\boldsymbol{e}_i\otimes\boldsymbol{e}_j\otimes\boldsymbol{e}_k\otimes\boldsymbol{e}_l), \tag{1.1}$$

where Einstein's convention of summation over repeated indices is implicitly used here and throughout this dissertation, so that:

$$u_i\,\boldsymbol{e}_i = \sum_{i=1}^{3} u_i\,\boldsymbol{e}_i, \quad E_{ij}(\boldsymbol{e}_i\otimes\boldsymbol{e}_j) = \sum_{i=1}^{3}\sum_{j=1}^{3} E_{ij}(\boldsymbol{e}_i\otimes\boldsymbol{e}_j). \tag{1.2}$$

1.1.1.1 Inner products, norm and trace

Considering two tensors $\boldsymbol{T}$ and $\boldsymbol{R}$ of orders p and q, we note $\boldsymbol{T}\overset{j}{\bullet}\boldsymbol{R}$ the *j-th order inner product* of $\boldsymbol{T}$ and $\boldsymbol{R}$ defined for any integer $j\leq\min(p,q)$. This product is a tensor of order $(p+q-2j)$ resulting from the *contraction* of j indices of each tensor, i.e. the sum over the j last indices of $\boldsymbol{T}$

and the j first indices of $\boldsymbol{R}$. In other words, noting γ a sequence of j indices,

$$(\boldsymbol{T} \overset{j}{\bullet} \boldsymbol{R})_{\alpha\beta} = T_{\alpha\gamma} R_{\gamma\beta}, \tag{1.3}$$

where summation is implicit on each of the j indices of the sequence γ, and α and β design respectively the sequences of remaining indices in $\boldsymbol{T}$ and $\boldsymbol{R}$.

The most frequently used of these inner products are the *single* and *double inner products* $\overset{1}{\bullet}$ and $\overset{2}{\bullet}$ that will be noted as usual "$\cdot$" and ":". For instance, with the same notations as in (1.1),

$$\boldsymbol{u} \cdot \boldsymbol{v} = u_i v_i, \quad \boldsymbol{E} \cdot \boldsymbol{u} = E_{ij} u_j \, \boldsymbol{e}_i, \quad \boldsymbol{E} : \boldsymbol{F} = E_{ij} F_{ij}, \quad \boldsymbol{\mathcal{C}} : \boldsymbol{E} = \mathcal{C}_{ijkl} E_{kl} (\boldsymbol{e}_i \otimes \boldsymbol{e}_j). \tag{1.4}$$

We also introduce a "maximal" inner product noted $\bullet$ that contracts the maximum number of indices available, i.e.

$$\boldsymbol{T} \bullet \boldsymbol{R} := \boldsymbol{T} \overset{\min(p,q)}{\bullet} \boldsymbol{R} \tag{1.5}$$

with the notations above. For example:

$$\boldsymbol{u} \bullet \boldsymbol{v} = \boldsymbol{u} \cdot \boldsymbol{v}, \quad \boldsymbol{\mathcal{C}} \bullet \boldsymbol{E} = \boldsymbol{\mathcal{C}} : \boldsymbol{E}, \quad \boldsymbol{\mathcal{C}} \bullet \boldsymbol{\mathcal{C}} = \boldsymbol{\mathcal{C}} \overset{4}{\bullet} \boldsymbol{\mathcal{C}} = \mathcal{C}_{ijkl} \mathcal{C}_{ijkl} \tag{1.6}$$

We then define the norm of a tensor by $|\boldsymbol{T}| := \sqrt{\boldsymbol{T} \bullet \boldsymbol{T}}$. In particular, it coincides with classical Euclidean and Frobenius norms of vectors and second order tensors:

$$|\boldsymbol{u}| = \sqrt{u_i u_i} \quad \text{and} \quad |\boldsymbol{E}| = \sqrt{E_{ij} E_{ij}}. \tag{1.7}$$

Finally the *trace* of a second-order tensor $\boldsymbol{E}$ designs the sum of its diagonal components: $\mathrm{Tr}(\boldsymbol{E}) := E_{ii}$.

1.1.1.2 Special tensors

We now define some particular tensors used widely thereafter.

Identities First of all, we note $\boldsymbol{I}$ the *second-order identity* represented by the 3-by-3 identity matrix in any orthonormal basis, whose components are given in index notation by *Kronecker's delta* δ_{ij}:

$$\boldsymbol{I} = \delta_{ij} (\boldsymbol{e}_i \otimes \boldsymbol{e}_j). \tag{1.8}$$

Among other uses of the identity, remark that $\boldsymbol{I} : \boldsymbol{T}$ (resp $\boldsymbol{T} : \boldsymbol{I}$) denotes the contraction of the two first (resp. last) indices of any tensor $\boldsymbol{T}$. Similarly, $\boldsymbol{I}^{(4)}$ and $\boldsymbol{I}^{(6)}$ are the fourth-order and sixth-order identities for second and third-order tensors:

$$I^{(4)}_{ijab} = \delta_{ia} \delta_{jb} \quad \text{and} \quad I^{(6)}_{ijkabc} = \delta_{ia} \delta_{jb} \delta_{kc}. \tag{1.9}$$

The calligraphic $\boldsymbol{\mathcal{I}}$ will denote the fourth-order identity for symmetric second-order tensors, or symmetrization operator for the two first indices of any tensor:

$$\mathcal{I}_{ijkl} = \frac{1}{2} (\delta_{ik} \delta_{jl} + \delta_{il} \delta_{jk}) \quad \text{so that} \quad \boldsymbol{\mathcal{I}} : \boldsymbol{T} = \boldsymbol{T}^{\mathrm{s}} \qquad \text{with} \quad T^{\mathrm{s}}_{ij\ldots} := \frac{1}{2} (T_{ij\ldots} + T_{ji\ldots}). \tag{1.10}$$

Similarly, $\boldsymbol{\mathcal{I}}^{(6)}$ will denote the sixth-order identity for third-order tensors symmetric on indices 1-2.

Projectors The fourth-order tensors $\boldsymbol{\mathcal{J}}, \boldsymbol{\mathcal{K}}$, defined by

$$\boldsymbol{\mathcal{J}} := (1/3)\boldsymbol{I} \otimes \boldsymbol{I} \qquad \text{and} \qquad \boldsymbol{\mathcal{K}} := \boldsymbol{\mathcal{I}} - \boldsymbol{\mathcal{J}}, \tag{1.11}$$

are the projectors onto the spherical and deviatoric components of a symmetric second-order tensor:

$$\boldsymbol{\mathcal{J}} : \boldsymbol{E} = \frac{1}{3}\mathrm{Tr}(\boldsymbol{E})\boldsymbol{I} \quad \text{and} \quad \boldsymbol{\mathcal{K}} : \boldsymbol{E} = \boldsymbol{E}^{\mathrm{D}} := \boldsymbol{E} - \frac{1}{3}\mathrm{Tr}(\boldsymbol{E})\boldsymbol{I}. \tag{1.12}$$

Remark that $\boldsymbol{\mathcal{J}}$ and $\boldsymbol{\mathcal{K}}$ are orthogonal projectors and thus:

$$\boldsymbol{\mathcal{J}} : \boldsymbol{\mathcal{J}} = \boldsymbol{\mathcal{J}}, \quad \boldsymbol{\mathcal{K}} : \boldsymbol{\mathcal{K}} = \boldsymbol{\mathcal{K}} \quad \text{and} \quad \boldsymbol{\mathcal{J}} : \boldsymbol{\mathcal{K}} = \boldsymbol{\mathcal{K}} : \boldsymbol{\mathcal{J}} = \boldsymbol{0}. \tag{1.13}$$

In particular, that implies that any tensor $\boldsymbol{T}$ of the form $\boldsymbol{T} = A\boldsymbol{\mathcal{J}} + B\boldsymbol{\mathcal{K}}$ is invertible if $A \neq 0$ and $B \neq 0$, with $\boldsymbol{T}^{-1} = A^{-1}\boldsymbol{\mathcal{J}} + B^{-1}\boldsymbol{\mathcal{K}}$.

Polynomial tensors in $\boldsymbol{r}$ Finally, homogeneous polynomials of a position vector (in the tensor product sense) will be used in this dissertation. The simplest of such polynomial is the k-th order tensor product of $\boldsymbol{r}$ by itself, noted $\boldsymbol{r}^{\otimes k}$ (e.g. $\boldsymbol{r}^{\otimes 3} = \boldsymbol{r} \otimes \boldsymbol{r} \otimes \boldsymbol{r}$). For any even integer p and any integer q, we also introduce the $(p+q)$-th order tensor $\boldsymbol{k}^{p,q}(\boldsymbol{r})$, invariant by any permutation of its indices, such that p indices are accounted into Kronecker's deltas, and the remaining q as $\boldsymbol{r}$'s components (so that $\boldsymbol{k}^{p,q}$ is a q-th order polynomial in $\boldsymbol{r}$). For instance, the first ones of these tensors are:

$$\begin{aligned}
p+q=1: \quad & k^{0,1}_{k}(\boldsymbol{r}) = r_k \\
p+q=2: \quad & k^{2,0}_{kl}(\boldsymbol{r}) = \delta_{kl}, \\
& k^{0,2}_{kl}(\boldsymbol{r}) = r_k r_l \\
p+q=3: \quad & k^{2,1}_{klm}(\boldsymbol{r}) = \delta_{kl} r_m + \delta_{km} r_l + \delta_{lm} r_k \\
& k^{0,3}_{klm}(\boldsymbol{r}) = r_k r_l r_m
\end{aligned} \tag{1.14}$$

Such notations may seem unnecessary, especially for smallest $(p+q)$ (e.g $\boldsymbol{k}^{2,0}(\boldsymbol{r}) = \boldsymbol{I}$ and $\boldsymbol{k}^{0,q}(\boldsymbol{r}) = \boldsymbol{r}^{\otimes q}$ for any q). However, their usefulness will appear when dealing with (i) high-order tensors defined through combinations of Kronecker's deltas (e.g. in Appendix 1.A.4) and (ii) high-order gradients of functions of $r = |\boldsymbol{r}|$, (e.g. in Appendix 3.B). In particular, the tensor $\boldsymbol{k}^{2,1}(\boldsymbol{r})$ will be used multiple times, and we can provide the alternative expression:

$$\boldsymbol{k}^{2,1}(\boldsymbol{r}) = (3\boldsymbol{\mathcal{J}} + 2\boldsymbol{\mathcal{I}}) \cdot \boldsymbol{r} = (5\boldsymbol{\mathcal{J}} + 2\boldsymbol{\mathcal{K}}) \cdot \boldsymbol{r}. \tag{1.15}$$

1.1.1.3 Differential operators on tensors

Tensor-valued functions of the space variable $\boldsymbol{x}$ (including vector-valued functions) that will be considered are generally regular enough to be differentiated once or several times. Within our Cartesian framework, we call the q-th order *gradient* of a p-th order tensor-valued function[1] $\boldsymbol{T}$ the

[1] Note that for compactness, we will often call "vectors" and "tensors" vector-valued functions and tensors-valued functions.

$(p+q)$-th order tensor whose components are defined as the q-th order partial derivatives of the components of $\boldsymbol{T}$ w.r.t. $\boldsymbol{x}$'s components and we note:

$$\begin{aligned}\boldsymbol{\nabla}^q \boldsymbol{T} &= \frac{\partial T_{ij\ldots}}{\partial x_m \partial x_n \ldots}(\underbrace{\boldsymbol{e}_i \otimes \boldsymbol{e}_j \otimes \ldots}_{p \text{ indices}} \otimes \underbrace{\boldsymbol{e}_m \otimes \boldsymbol{e}_n \otimes \ldots}_{q \text{ indices}}) \\ &= T_{ij\ldots,mn\ldots}(\boldsymbol{e}_i \otimes \boldsymbol{e}_j \otimes \ldots \otimes \boldsymbol{e}_m \otimes \boldsymbol{e}_n \otimes \ldots),\end{aligned} \tag{1.16}$$

where the comma serves to distinguish between component indices of $\boldsymbol{T}$ and differentiation indices in the last term. Among the most used particular case is the (first) gradient of a vector function:

$$\boldsymbol{\nabla u} = u_{i,j}(\boldsymbol{e}_i \otimes \boldsymbol{e}_j). \tag{1.17}$$

The *divergence* of a p-th order tensor $\boldsymbol{T}$ (for $p \geq 1$) is the $(p-1)$-th order tensor defined intrinsically by div $\boldsymbol{T} := \boldsymbol{\nabla T} : \boldsymbol{I}$. In particular this definition implies for vectors and second-order tensors the classical formulae:

$$\text{div } \boldsymbol{u} = u_{i,i} \quad \text{and} \quad \text{div } \boldsymbol{E} = E_{ij,j}\, \boldsymbol{e}_i. \tag{1.18}$$

Finally, the *Laplacian* of a tensor is a tensor of the same order computed as:

$$\boldsymbol{\Delta T} := \text{div}(\boldsymbol{\nabla T}) = (\boldsymbol{\nabla}^2 \boldsymbol{T}) : \boldsymbol{I} = \boldsymbol{T}_{,ii}. \tag{1.19}$$

1.1.1.4 Taylor's expansion of a vector

Eventually, the Taylor's expansion of a smooth vector function $\boldsymbol{u}$ w.r.t. the sapce variable $\boldsymbol{x}$, which makes use of many of the notations defined above, will be widely used in the upcoming asymptotic expansions. About $\boldsymbol{x} = \boldsymbol{0}$, and for $|\boldsymbol{x}|$ small enough so that the infinite expansion is defined, it is written:

$$\boldsymbol{u}(\boldsymbol{x}) = \boldsymbol{u}(\boldsymbol{0}) + \boldsymbol{\nabla u}(\boldsymbol{0}) \cdot \boldsymbol{x} + \frac{1}{2}\boldsymbol{\nabla}^2 \boldsymbol{u}(\boldsymbol{0}) : (\boldsymbol{x} \otimes \boldsymbol{x}) + \frac{1}{6}\boldsymbol{\nabla}^3 \boldsymbol{u}(\boldsymbol{0}) \overset{3}{\bullet} (\boldsymbol{x} \otimes \boldsymbol{x} \otimes \boldsymbol{x}) \ldots, \tag{1.20}$$

which can be written in compact form:

$$\boldsymbol{u}(\boldsymbol{x}) = \boldsymbol{u}(\boldsymbol{0}) + \sum_{k \geq 1} \frac{1}{k!} \boldsymbol{\nabla}^k \boldsymbol{u}(\boldsymbol{0}) \bullet \boldsymbol{x}^{\otimes k}. \tag{1.21}$$

1.1.1.5 Functional spaces of vector and tensor-valued functions

Throughout this dissertation, we will use the boldface $\boldsymbol{L}^2$, $\boldsymbol{H}^1$ ... to design classic Sobolev spaces of vector or tensor-valued functions, the order of the considered tensors being specified when necessary. When addressing symmetric tensor-valued function, it will be explicitly mentioned in the suitable functional space, e.g. $L^2(\mathbb{R}^3; \mathbb{R}^{3\times3}_{\text{sym}})$ for symmetric second-order tensor-valued L^2 functions of the space variable.

Finally, the subscripts $_{\text{comp}}$ and $_{\text{loc}}$ have their usual meaning, e.g. L^2_{comp} and L^2_{loc} mean compactly supported L^2 functions and locally L^2 functions.

1.1.2 Displacement, strain and stress

Studying now the behavior of an elastic body occupying the domain $\Omega \subset \mathbb{R}^3$ ($\Omega = \mathbb{R}^3$ being possible), we note $\boldsymbol{u}(\boldsymbol{x})$ the displacement vector at point $\boldsymbol{x}$. In this introductory part, $\boldsymbol{u}$ is supposed regular enough so that all the introduced quantities are well-defined. More precise regularity will be specified when needed in the following.

The assumption of *small perturbations*, underpinning all this work, postulates that $|\boldsymbol{\nabla u}| \ll 1$ in Ω, and, if the considered problem features a characteristic length L, that $|\boldsymbol{u}| \ll L$ in Ω. Under this assumption, $\boldsymbol{x}$ designs both the positions in initial and deformed configurations, and the *strain* of the material is approximated by the linearized strain $\boldsymbol{\varepsilon}[\boldsymbol{u}]$ defined as the symmetric part of the gradient of $\boldsymbol{u}$:

$$\boldsymbol{\varepsilon}[\boldsymbol{u}] = \frac{1}{2}\left(\boldsymbol{\nabla u} + \boldsymbol{\nabla}^T\boldsymbol{u}\right). \tag{1.22}$$

To define internal stress of the material, consider now an infinitesimal surface $\mathrm{d}S$ around a point $\boldsymbol{x}$, oriented by unit normal vector $\boldsymbol{n}$. Then the infinitesimal force $\mathrm{d}\boldsymbol{f}$ applied on $\mathrm{d}S$ by the side to which $\boldsymbol{n}$ is pointing is computed as $\mathrm{d}\boldsymbol{f} = \boldsymbol{t}(\boldsymbol{x};\boldsymbol{n})\,\mathrm{d}S$ where the surface force density $\boldsymbol{t}$ will be called the *traction vector*. This traction vector is easily shown to linearly depend on $\boldsymbol{n}$, and is therefore represented by the second order *Cauchy stress tensor* $\boldsymbol{\sigma}$ such that:

$$\boldsymbol{t}(\boldsymbol{x};\boldsymbol{n}) = \boldsymbol{\sigma}(\boldsymbol{x}) \cdot \boldsymbol{n}. \tag{1.23}$$

When these internal stresses are the only strain source, the relation between stress $\boldsymbol{\sigma}$ and strain $\boldsymbol{\varepsilon}$ for linear elasticity is given by Hooke's law:

$$\boldsymbol{\sigma} = \boldsymbol{\mathcal{C}} : \boldsymbol{\varepsilon}[\boldsymbol{u}], \tag{1.24}$$

where *Hooke's tensor* $\boldsymbol{\mathcal{C}}$ is a fourth-order tensor endowed with the minor and major symmetries $\mathcal{C}_{ijkl} = \mathcal{C}_{jikl} = \mathcal{C}_{ijlk} = \mathcal{C}_{klij}$. Equivalently, (1.24) combined with (1.22) can be written:

$$\sigma_{ij} = \mathcal{C}_{ijkl}\,\varepsilon_{kl} = \frac{1}{2}\mathcal{C}_{ijkl}(u_{k,l} + u_{l,k}) = \mathcal{C}_{ijkl}\,u_{k,l}. \tag{1.25}$$

The last equality, corresponding to $\boldsymbol{\sigma} = \boldsymbol{\mathcal{C}} : \boldsymbol{\nabla u}$, results from the minor symmetry of $\boldsymbol{\mathcal{C}}$ given above.

1.1.3 Equilibrium equations and fundamental solution

The static equilibrium of an infinitesimal volume of the material submitted to volume force density $\boldsymbol{f}$ implies the equilibrium of (i) forces and (ii) momentum. It translates into (i) a system of equations for Cauchy stress tensor components:

$$\operatorname{div} \boldsymbol{\sigma} + \boldsymbol{f} = \boldsymbol{0}, \tag{1.26}$$

and (ii) the symmetry of $\boldsymbol{\sigma}$, i.e. $\sigma_{ij} = \sigma_{ji}$. This last condition was taken in account into Hooke's law by imposing the minor symmetry of $\boldsymbol{\mathcal{C}}$.

Introducing Hooke's law (1.24) into these equations leads to the displacement formulation of the equilibrium:

$$\operatorname{div}(\boldsymbol{\mathcal{C}} : \boldsymbol{\nabla u}) + \boldsymbol{f} = \boldsymbol{0}. \tag{1.27}$$

We then define the *fundamental solution* (or full-space Green's tensor) $\boldsymbol{G}_\infty$ associated to this system of equations as the solution of:

$$\operatorname{div}(\boldsymbol{\mathcal{C}} : \boldsymbol{\nabla} \boldsymbol{G}_\infty(\boldsymbol{r})) + \delta(\boldsymbol{r})\boldsymbol{I} = 0 \quad \text{in } \mathbb{R}^3, \qquad |\boldsymbol{G}_\infty(\boldsymbol{r})| \to 0 \quad \text{as } |\boldsymbol{r}| \to \infty, \tag{1.28}$$

where $\boldsymbol{r}$ was preferred to $\boldsymbol{x}$ to denote positions in full space, and δ is the Dirac distribution. $\boldsymbol{G}_\infty$ is thus a second-order tensor-valued generalized function. One of its components $[\boldsymbol{G}_\infty(\boldsymbol{r})]_{ij} = G_{ij}(\boldsymbol{r})$ may be seen as the i-th component of the displacement at $\boldsymbol{r}$ resulting from a unitary force imposed at $\boldsymbol{x} = \boldsymbol{0}$ in the j-th direction. The inner products will be applied accordingly on the "displacement" index e.g. $[\boldsymbol{v} \cdot \boldsymbol{G}_\infty]_j = v_i G_{ij}$ and $[\boldsymbol{\mathcal{C}} : \boldsymbol{\nabla} \boldsymbol{G}_\infty]_{mnj} = \mathcal{C}_{mnik} G_{ij,k}$.

Referring to [Mura, 1982, Chap. I, part 5] for details, $\boldsymbol{G}_\infty$ can be expressed as an inverse Fourier integral:

$$\boldsymbol{G}_\infty(\boldsymbol{r}) = \frac{1}{(2\pi)^3} \int_{\mathbb{R}^3} \boldsymbol{K}^{-1}(\boldsymbol{\xi}) \exp(\mathrm{i}\boldsymbol{\xi} \cdot \boldsymbol{r}) \, \mathrm{d}V_\xi \quad (\boldsymbol{r} \in \mathbb{R}^3 \backslash \{\boldsymbol{0}\}) \tag{1.29}$$

where the second-order *acoustic tensor* $\boldsymbol{K}(\boldsymbol{\xi})$ is defined by $K_{ik}(\boldsymbol{\xi}) = \mathcal{C}_{ijkl} \xi_j \xi_l$ and is invertible for any $\boldsymbol{\xi} \neq \boldsymbol{0}$ and positive definite $\boldsymbol{\mathcal{C}}$. In particular, $\boldsymbol{K}$ is symmetric, and so are $\boldsymbol{K}^{-1}$ and $\boldsymbol{G}_\infty$. From the expression (1.29), we can also assert that for any $\boldsymbol{r} \in \mathbb{R}^3 \setminus \{\boldsymbol{0}\}$ and $\alpha \in \mathbb{R} \setminus \{0\}$, one has

$$\begin{aligned} &\text{(i)} \quad \boldsymbol{G}_\infty(\alpha \boldsymbol{r}) = |\alpha|^{-1} \boldsymbol{G}_\infty(\boldsymbol{r}) \\ &\text{(ii)} \quad \boldsymbol{\nabla} \boldsymbol{G}_\infty(\alpha \boldsymbol{r}) = |\alpha|^{-3} \alpha \boldsymbol{\nabla} \boldsymbol{G}_\infty(\boldsymbol{r}) = |\alpha|^{-2} \operatorname{sgn}(\alpha) \boldsymbol{\nabla} \boldsymbol{G}_\infty(\boldsymbol{r}), \end{aligned} \tag{1.30}$$

the second relation meaning that $\boldsymbol{\nabla} \boldsymbol{G}_\infty$ is a homogeneous tensor-valued function of degree -2.

Remark 1.1. *For a homogeneous material, by translational invariance of $\mathbb{R}^3$, the displacements at point $\boldsymbol{\xi}$ due to point forces applied at another point $\boldsymbol{x}$ are given by $\boldsymbol{G}_\infty(\boldsymbol{\xi} - \boldsymbol{x})$.*

1.1.4 Isotropic homogeneous materials

For isotropic materials, many simple expressions of the quantities and functions defined above are available. First of all, the Hooke's tensor $\boldsymbol{\mathcal{C}}$ depends only on two independent coefficients, and can be expressed in several ways, e.g. using the identity tensors $\boldsymbol{I}$ and $\boldsymbol{\mathcal{I}}$:

$$\boldsymbol{\mathcal{C}} = \lambda \boldsymbol{I} \otimes \boldsymbol{I} + 2\mu \boldsymbol{\mathcal{I}} = 2\mu \left(\frac{\nu}{1 - 2\nu} \boldsymbol{I} \otimes \boldsymbol{I} + \boldsymbol{\mathcal{I}} \right), \tag{1.31}$$

or, using the projectors $\boldsymbol{\mathcal{J}}$ and $\boldsymbol{\mathcal{K}}$ defined by (1.12):

$$\boldsymbol{\mathcal{C}} = 3\kappa \boldsymbol{\mathcal{J}} + 2\mu \boldsymbol{\mathcal{K}} = 2\mu \left(\frac{1 + \nu}{1 - 2\nu} \boldsymbol{\mathcal{J}} + \boldsymbol{\mathcal{K}} \right), \tag{1.32}$$

where λ is the first Lamé parameter, κ and μ are the bulk and shear moduli, and ν is Poisson's ratio. Although only two of these parameters suffice to define $\boldsymbol{\mathcal{C}}$, we'll use alternatively one couple or another depending on the simplest expression available.

Hooke's law is then expressed in closed-form, e.g. using Lamé parameters (λ, μ):

$$\boldsymbol{\sigma} = 2\mu \, \boldsymbol{\varepsilon}[\boldsymbol{u}] + \lambda \operatorname{Tr}(\boldsymbol{\varepsilon}[\boldsymbol{u}]) \boldsymbol{I} = 2\mu \, \boldsymbol{\varepsilon}[\boldsymbol{u}] + \lambda \operatorname{div}(\boldsymbol{u}) \boldsymbol{I}, \tag{1.33}$$

and the inverse relation is, using Young's modulus $E = 2\mu(1 + \nu)$ and Poisson's ratio ν:

$$\boldsymbol{\varepsilon}[\boldsymbol{u}] = \frac{1}{E} \left((1 + \nu) \boldsymbol{\sigma} - \nu \operatorname{Tr}(\boldsymbol{\sigma}) \boldsymbol{I} \right) \tag{1.34}$$

Injecting (1.33) into equilibrium equation (1.27) leads to the *Navier equations* for the displacement $\boldsymbol{u}$:

$$(\lambda+\mu)\boldsymbol{\nabla}(\operatorname{div}\,\boldsymbol{u})+\mu\boldsymbol{\Delta}\boldsymbol{u}+\boldsymbol{f}=\boldsymbol{0} \tag{1.35}$$

The associated fundamental solution, called the *Kelvin solution* after Lord Kelvin who firstly derived its expression, is given by:

$$\boldsymbol{G}_{\infty}(\boldsymbol{r})=\frac{1}{16\pi\mu(1-\nu)r}\left[(3-4\nu)\boldsymbol{I}+\hat{\boldsymbol{r}}\otimes\hat{\boldsymbol{r}}\right],\ r=|\boldsymbol{r}| \text{ and } \hat{\boldsymbol{r}}=\frac{\boldsymbol{r}}{r}, \tag{1.36}$$

as showed e.g. in [Mura, 1982, Chap. I Part 5]. Its gradient is::

$$\boldsymbol{\nabla}\boldsymbol{G}_{\infty}(\boldsymbol{r})=\frac{-1}{16\pi\mu(1-\nu)r^2}\left[4(1-\nu)\boldsymbol{I}\otimes\hat{\boldsymbol{r}}-\boldsymbol{k}^{2,1}(\hat{\boldsymbol{r}})+3\,\hat{\boldsymbol{r}}\otimes\hat{\boldsymbol{r}}\otimes\hat{\boldsymbol{r}}\right], \tag{1.37}$$

with $k^{2,1}_{ijk}(\boldsymbol{x})=x_i\delta_{ij}+\delta_{ik}x_j+\delta_{ij}x_k$.

1.2 Free-space transmission problem

This section is dedicated on the free-space transmission problem (FSTP), whose goal is to determine the perturbation of the displacement field due to the presence of an inhomogeneity having domain $\mathcal{B}$ in an otherwise homogeneous elastic medium occupying $\mathbb{R}^3$. Its purpose is (i) to establish the needed local and integral equation framework, and (ii) to rigorously prove the invertibility of the integral operator associated to the transmission problem. Since both background and inhomogeneity materials are allowed to be anisotropic, this result completes the recent work [Gintides & Kiriaki, 2015] which focused on isotropic materials.

1.2.1 Setting of the problem

Consider an homogeneous elastic medium occupying the whole space $\mathbb{R}^3$, characterized by the elasticity tensor $\boldsymbol{\mathcal{C}}$ and submitted to a body force density $\boldsymbol{f}$. We define the *background displacement* $\boldsymbol{u}$ as the solution of the static equilibrium equation in the homogeneous medium, which reads:

$$\operatorname{div}(\boldsymbol{\mathcal{C}}:\boldsymbol{\nabla}\boldsymbol{u}(\boldsymbol{x}))+\boldsymbol{f}(\boldsymbol{x})=\boldsymbol{0}\quad\forall\boldsymbol{x}\in\mathbb{R}^3. \tag{1.38}$$

Assume now the presence of a bounded inhomogeneity of support $\mathcal{B}$ with smooth boundary, and made of a material characterized by another (constant) elasticity tensor $\boldsymbol{\mathcal{C}}^{\star}=\boldsymbol{\mathcal{C}}+\Delta\boldsymbol{\mathcal{C}}$. Accordingly, we define the piecewise-constant elastic tensors $\Delta\boldsymbol{\mathcal{C}}_{\mathcal{B}}$ and $\boldsymbol{\mathcal{C}}_{\mathcal{B}}$ by:

$$\Delta\boldsymbol{\mathcal{C}}_{\mathcal{B}}(\boldsymbol{x}):=\chi_{\mathcal{B}}(\boldsymbol{x})\Delta\boldsymbol{\mathcal{C}},\qquad\boldsymbol{\mathcal{C}}_{\mathcal{B}}(\boldsymbol{x}):=(1-\chi_{\mathcal{B}}(\boldsymbol{x}))\boldsymbol{\mathcal{C}}+\chi_{\mathcal{B}}(\boldsymbol{x})\boldsymbol{\mathcal{C}}^{\star}=\boldsymbol{\mathcal{C}}+\Delta\boldsymbol{\mathcal{C}}_{\mathcal{B}}(\boldsymbol{x}), \tag{1.39}$$

where $\chi_{\mathcal{B}}$ is the characteristic function of $\mathcal{B}$.

The total displacement field $\boldsymbol{u}_{\mathcal{B}}$ accounting for the presence of the inhomogeneity $(\mathcal{B},\boldsymbol{\mathcal{C}}^{\star})$ therefore satisfies:

$$\left|\begin{array}{ll}\operatorname{div}(\boldsymbol{\mathcal{C}}_{\mathcal{B}}(\boldsymbol{x}):\boldsymbol{\nabla}\boldsymbol{u}_{\mathcal{B}}(\boldsymbol{x}))+\boldsymbol{f}(\boldsymbol{x})=\boldsymbol{0} & \boldsymbol{x}\in\mathbb{R}^3\\ \boldsymbol{u}^{+}_{\mathcal{B}}(\boldsymbol{x})=\boldsymbol{u}^{-}_{\mathcal{B}}(\boldsymbol{x}) & \boldsymbol{x}\in\partial\mathcal{B}\\ \boldsymbol{t}^{+}[\boldsymbol{u}_{\mathcal{B}}](\boldsymbol{x})=\boldsymbol{t}^{\star-}[\boldsymbol{u}_{\mathcal{B}}](\boldsymbol{x}) & \boldsymbol{x}\in\partial\mathcal{B},\end{array}\right. \tag{1.40}$$

where we used the following notations:

$$\boldsymbol{u}_{\mathcal{B}}^{\pm}(\boldsymbol{x}) = \lim_{h\searrow 0} \boldsymbol{u}_{\mathcal{B}}(\boldsymbol{x} \pm h\boldsymbol{n}), \qquad \begin{aligned} \boldsymbol{t}^{\pm}[\boldsymbol{u}_{\mathcal{B}}](\boldsymbol{x}) &= \lim_{h\searrow 0} (\boldsymbol{\mathcal{C}} : \boldsymbol{\nabla}\boldsymbol{u}_{\mathcal{B}}(\boldsymbol{x} \pm h\boldsymbol{n})) \cdot \boldsymbol{n}, \\ \boldsymbol{t}^{\star\pm}[\boldsymbol{u}_{\mathcal{B}}](\boldsymbol{x}) &= \lim_{h\searrow 0} (\boldsymbol{\mathcal{C}}^{\star} : \boldsymbol{\nabla}\boldsymbol{u}_{\mathcal{B}}(\boldsymbol{x} \pm h\boldsymbol{n})) \cdot \boldsymbol{n}, \end{aligned} \tag{1.41}$$

and $\boldsymbol{n} = \boldsymbol{n}(\boldsymbol{x})$ is defined as the outward normal to $\partial\mathcal{B}$ at point $\boldsymbol{x}$. The two last equations in (1.40) express the continuity of displacements and tractions across $\partial\mathcal{B}$.

Remark 1.2. *The limit case $\Delta\boldsymbol{\mathcal{C}} = \boldsymbol{0}$, which corresponds to no elasticity contrast between background and inhomogeneity materials, results in no perturbation ($\boldsymbol{u}_{\mathcal{B}} = \boldsymbol{u}$) for the static excitations which are assumed in this chapter and the following one. Moreover, the analysis of Chapter 3 for time-harmonic excitations remains valid, and is in fact much simpler when canceling all terms depending on $\Delta\boldsymbol{\mathcal{C}}$.*

As said of the introduction, our primary interest will be to study the *perturbation* of the displacement field that is noted $\boldsymbol{v}_{\mathcal{B}}$ and defined by:

$$\boldsymbol{v}_{\mathcal{B}} := \boldsymbol{u}_{\mathcal{B}} - \boldsymbol{u}. \tag{1.42}$$

The background field $\boldsymbol{u}$ being assumed to be known from now, the problem (1.40) can be written in terms of $\boldsymbol{v}_{\mathcal{B}}$ and reads in this case:

$$\left| \begin{array}{ll} \operatorname{div}(\boldsymbol{\mathcal{C}}_{\mathcal{B}}(\boldsymbol{x}) : \boldsymbol{\nabla}\boldsymbol{v}_{\mathcal{B}}(\boldsymbol{x})) = -\operatorname{div}(\Delta\boldsymbol{\mathcal{C}}_{\mathcal{B}}(\boldsymbol{x}) : \boldsymbol{\nabla}\boldsymbol{u}(\boldsymbol{x})) & \boldsymbol{x} \in \mathbb{R}^3 \\ \boldsymbol{v}_{\mathcal{B}}^{+}(\boldsymbol{x}) - \boldsymbol{v}_{\mathcal{B}}^{-}(\boldsymbol{x}) = \boldsymbol{0} & \boldsymbol{x} \in \partial\mathcal{B} \\ (\boldsymbol{t}^{+} - \boldsymbol{t}^{\star -})[\boldsymbol{v}_{\mathcal{B}}](\boldsymbol{x}) = (\boldsymbol{t}^{\star -} - \boldsymbol{t}^{+})[\boldsymbol{u}](\boldsymbol{x}) & \boldsymbol{x} \in \partial\mathcal{B} \end{array} \right. \tag{1.43}$$

Remark that the source terms of this problem can be seen as (i) pre-stress $\Delta\boldsymbol{\mathcal{C}} : \boldsymbol{\nabla}\boldsymbol{u}$ on $\mathcal{B}$ and (ii) surface forces $(\boldsymbol{t}^{\star -} - \boldsymbol{t}^{+})[\boldsymbol{u}]$ on $\partial\mathcal{B}$, both defined by contrast $\Delta\boldsymbol{\mathcal{C}}$ and background field $\boldsymbol{u}$. For the problems (1.43) and therefore (1.40) to be well-posed, we finally need to prescribe the asymptotic behavior of $\boldsymbol{v}_{\mathcal{B}}$:

$$\boldsymbol{v}_{\mathcal{B}}(\boldsymbol{x}) = o(1) \text{ as } |\boldsymbol{x}| \to \infty. \tag{1.44}$$

Remark 1.3. *This very relaxed condition* (1.44) *is proposed by [Gurtin & Sternberg, 1961] who shows (Thm. 5.1) that it implies $\boldsymbol{v}_{\mathcal{B}}(\boldsymbol{x}) = O(|\boldsymbol{x}|^{-1})$ as $|\boldsymbol{x}| \to \infty$ for isotropic background material. This last condition is thus often used instead, e.g. in [Gintides & Kiriaki, 2015]. One can also refer to the discussion for exterior problems in [Knops & Payne, 1971, Sect. 4.2].*

Multiplying the first equation of (1.43) by a test function $\boldsymbol{w}$ and integrating by part over $\mathbb{R}^3$, $\boldsymbol{v}_{\mathcal{B}}$ is found to satisfy the integral identity:

$$\langle \boldsymbol{v}_{\mathcal{B}}, \boldsymbol{w} \rangle_{\mathbb{R}^3}^{\mathcal{C}_{\mathcal{B}}} = - \langle \boldsymbol{u}, \boldsymbol{w} \rangle_{\mathcal{B}}^{\Delta\mathcal{C}}, \quad \forall \boldsymbol{w} \in \boldsymbol{W}_{\infty}, \tag{1.45}$$

where $\langle \boldsymbol{u}, \boldsymbol{w} \rangle_D^{\mathcal{C}}$ denotes the bilinear elastic energy form associated with a given domain $D \subset \mathbb{R}^3$ and elasticity tensor $\boldsymbol{\mathcal{C}}$, i.e.:

$$\langle \boldsymbol{u}, \boldsymbol{w} \rangle_D^{\mathcal{C}} := \int_D \boldsymbol{\varepsilon}[\boldsymbol{u}] : \boldsymbol{\mathcal{C}} : \boldsymbol{\varepsilon}[\boldsymbol{w}] \, \mathrm{d}V = \int_D \boldsymbol{\nabla}\boldsymbol{u} : \boldsymbol{\mathcal{C}} : \boldsymbol{\nabla}\boldsymbol{w} \, \mathrm{d}V, \tag{1.46}$$

and the function space $\boldsymbol{W}_{\infty}$ is defined by

$$\boldsymbol{W}_{\infty} = \left\{ \, \boldsymbol{w} \in \boldsymbol{L}^2_{\mathrm{loc}}(\mathbb{R}^3), \; \boldsymbol{\nabla}\boldsymbol{w} \in \boldsymbol{L}^2(\mathbb{R}^3) \right\} \tag{1.47}$$

and can be seen as the space of displacements having finite strain energy over all $\mathbb{R}^3$.

Remark 1.4. *Note that the decay condition* (1.44) *also implies* $\boldsymbol{\nabla} \boldsymbol{v}_{\mathcal{B}}(\boldsymbol{x}) = O(|\boldsymbol{x}|^{-2})$ *for isotropic materials as shown in [Gurtin & Sternberg, 1961], which is sufficient to guarantee that* $\boldsymbol{v}_{\mathcal{B}} \in \boldsymbol{W}_\infty$*. In this case, we can justify the integral over* $\mathbb{R}^3$ *that appears in* (1.45)*, by e.g. (i) writing the weak formulation on a sphere* B_R *of radius* R *containing* $\mathcal{B}$ *and (ii) showing that the boundary terms on* ∂B_R *cancel as* $R \to \infty$ *and that the remaining integral is well-defined for* $\boldsymbol{w} \in \boldsymbol{W}_\infty$*. For more general cases, we refer to [Bonnet, 2016b].*

Using the identity (1.45), some major properties of the solution $\boldsymbol{u}_{\mathcal{B}}$ of the FSTP (1.40) are now addressed. We begin by a classical uniqueness result:

Lemma 1.1. *(Uniqueness) Provided that* $\boldsymbol{\mathcal{C}}$ *and* $\boldsymbol{\mathcal{C}}^\star$ *are both positive definite, the FSTP* (1.43) *completed with condition* (1.44) *admits a unique solution for any background displacement* $\boldsymbol{u}$ *defined up to a rigid-body displacement.*

Proof. Let us consider the homogeneous problem in static elasticity, i.e. the case where the background displacement is of rigid-body type: $\boldsymbol{\varepsilon}[\boldsymbol{u}] = \boldsymbol{0}$. We then show that the perturbation $\boldsymbol{v}_{\mathcal{B}}$ vanishes. Setting $\boldsymbol{w} = \boldsymbol{v}_{\mathcal{B}}$ in (1.45), we obtain:

$$\langle \boldsymbol{v}_{\mathcal{B}}, \boldsymbol{v}_{\mathcal{B}} \rangle_{\mathbb{R}^3}^{\mathcal{C}_{\mathcal{B}}} = 0. \tag{1.48}$$

Since $\boldsymbol{\mathcal{C}}_{\mathcal{B}}$ is positive everywhere by assumption, it implies that $\boldsymbol{\varepsilon}[\boldsymbol{v}_{\mathcal{B}}](\boldsymbol{x}) = \boldsymbol{0}$ for all $\boldsymbol{x} \in \mathbb{R}^3$. That means that $\boldsymbol{v}_{\mathcal{B}}$ is a rigid-body displacement. We conclude using the decreasing condition at infinity (1.44) that $\boldsymbol{v}_{\mathcal{B}}$ is zero everywhere. □

Remark 1.5. *The lack of uniqueness when the inhomogeneity is a cavity (i.e.* $\boldsymbol{\mathcal{C}}^\star = \boldsymbol{0}$*) was demonstrated in [Furuhashi & Mura, 1979] (with explicit counter-example for spherical shape* $\mathcal{B}$*).*

We also assert:

Lemma 1.2. *(Reciprocity identity) Let* $\boldsymbol{u}_{\mathcal{B}}$*,* $\boldsymbol{u}'_{\mathcal{B}}$ *solve the FSTP* (1.40) *with respective background displacements* $\boldsymbol{u}$*,* $\boldsymbol{u}'$*. Then we have:*

$$\left\langle \boldsymbol{u}_{\mathcal{B}}, \boldsymbol{u}' \right\rangle_{\mathcal{B}}^{\Delta\mathcal{C}} = \left\langle \boldsymbol{u}, \boldsymbol{u}'_{\mathcal{B}} \right\rangle_{\mathcal{B}}^{\Delta\mathcal{C}}. \tag{1.49}$$

Proof. We invoke the integral identity (1.45) satisfied by $\boldsymbol{v}_{\mathcal{B}}$ with $\boldsymbol{w} = \boldsymbol{v}'_{\mathcal{B}} \in \boldsymbol{W}_\infty$ (see Remark 1.4) and obtain:

$$\left\langle \boldsymbol{v}_{\mathcal{B}}, \boldsymbol{v}'_{\mathcal{B}} \right\rangle_{\mathbb{R}^3}^{\mathcal{C}} + \left\langle \boldsymbol{v}_{\mathcal{B}}, \boldsymbol{v}'_{\mathcal{B}} \right\rangle_{\mathcal{B}}^{\Delta\mathcal{C}} = -\left\langle \boldsymbol{u}, \boldsymbol{v}'_{\mathcal{B}} \right\rangle_{\mathcal{B}}^{\Delta\mathcal{C}}. \tag{1.50}$$

We then write the similar identity satisfied by $\boldsymbol{v}'_{\mathcal{B}}$ with $\boldsymbol{w} = \boldsymbol{v}_{\mathcal{B}}$ and, thanks to symmetry of $\langle \cdot, \cdot \rangle$, obtain:

$$\left\langle \boldsymbol{u}', \boldsymbol{v}_{\mathcal{B}} \right\rangle_{\mathcal{B}}^{\Delta\mathcal{C}} = \left\langle \boldsymbol{u}, \boldsymbol{v}'_{\mathcal{B}} \right\rangle_{\mathcal{B}}^{\Delta\mathcal{C}}, \tag{1.51}$$

the equivalent identity (1.49) being finally obtained by adding $\langle \boldsymbol{u}, \boldsymbol{u}' \rangle_{\mathcal{B}}^{\Delta\mathcal{C}}$ to both sides. □

1.2.2 Integral equation and equivalence with local formulation

Applying equation (1.28) in the sense of distributions to a trial displacement $\boldsymbol{w}$, and using Remark 1.1, the fundamental solution $\boldsymbol{G}_\infty$ defined in Section 1.1.3 is found to verify the identity:

$$\langle \boldsymbol{G}_\infty(\cdot - \boldsymbol{x}), \boldsymbol{w} \rangle_{\mathbb{R}^3}^{\mathcal{C}} = \boldsymbol{w}(\boldsymbol{x}) \quad \forall \boldsymbol{w} \in \boldsymbol{W}_\infty \cap C^1(\omega_{\boldsymbol{x}}), \tag{1.52}$$

where $\omega_{\boldsymbol{x}}$ is a neighborhood of $\boldsymbol{x}$.

Setting $\boldsymbol{w} = \boldsymbol{G}_\infty(\cdot - \boldsymbol{x})$ in (1.45) (the resulting integral remaining well-defined despite the fact that $\boldsymbol{G}_\infty \notin \boldsymbol{W}_\infty$ due to sufficient interior regularity of $\boldsymbol{v}_{\mathcal{B}}$ in $\mathcal{B}$) and using (1.52), we obtain the integral formulation:

$$\mathcal{L}[\boldsymbol{v}_{\mathcal{B}}](\boldsymbol{x}) = -\left\langle \boldsymbol{u}, \boldsymbol{G}_\infty(\cdot - \boldsymbol{x})\right\rangle_{\mathcal{B}}^{\Delta\mathcal{C}} \quad \forall \boldsymbol{x} \in \mathcal{B} \cup \mathbb{R}^3 \backslash \overline{\mathcal{B}}, \tag{1.53}$$

where the linear integral operator $\mathcal{L}$ is defined by

$$\mathcal{L}[\boldsymbol{v}](\boldsymbol{x}) := \boldsymbol{v}(\boldsymbol{x}) + \left\langle \boldsymbol{v}, \boldsymbol{G}_\infty(\cdot - \boldsymbol{x})\right\rangle_{\mathcal{B}}^{\Delta\mathcal{C}} = \boldsymbol{v}(\boldsymbol{x}) + \int_{\mathcal{B}} \boldsymbol{\nabla}\boldsymbol{v}(\boldsymbol{\xi}) : \Delta\boldsymbol{\mathcal{C}} : \boldsymbol{\nabla}\boldsymbol{G}_\infty(\boldsymbol{\xi} - \boldsymbol{x}) \,\mathrm{d}V_\xi. \tag{1.54}$$

For $\boldsymbol{x} \in \mathcal{B}$, the identity (1.53) is an integral equation to solve in order to obtain $\boldsymbol{v}_{\mathcal{B}}$ (and $\boldsymbol{\nabla}\boldsymbol{v}_{\mathcal{B}}$) in the inhomogeneity. Once these are known, it becomes an integral representation for $\boldsymbol{x} \notin \overline{\mathcal{B}}$:

$$\boldsymbol{v}_{\mathcal{B}}(\boldsymbol{x}) = -\left\langle \boldsymbol{u}_{\mathcal{B}}, \boldsymbol{G}_\infty(\cdot - \boldsymbol{x})\right\rangle_{\mathcal{B}}^{\Delta\mathcal{C}}, \quad \boldsymbol{x} \in \mathbb{R}^3 \backslash \overline{\mathcal{B}}. \tag{1.55}$$

Remark 1.6. *From the homogeneity property of $\boldsymbol{\nabla}\boldsymbol{G}_\infty$ given by* (1.30)*, the representation* (1.55) *implies $\boldsymbol{v}_{\mathcal{B}}(\boldsymbol{x}) = O(|\boldsymbol{x}|^{-2})$ as $|\boldsymbol{x}| \to \infty$, so the condition* (1.44) *is verified.*

From the local formulation of the problem (1.40), we just established the integral equation (1.53) satisfied by $\boldsymbol{v}_{\mathcal{B}}$. We now want to show the converse implication, i.e. that the solution of the integral equation is solution to (1.40). For this, consider a displacement density $\boldsymbol{h} \in \boldsymbol{H}^1(\mathcal{B})$, and define $\boldsymbol{V}_{\mathcal{B}}[\boldsymbol{h}]$ as in (1.55) by:

$$\boldsymbol{V}_{\mathcal{B}}[\boldsymbol{h}](\boldsymbol{x}) = -\int_{\mathcal{B}} \boldsymbol{\nabla}\boldsymbol{h}(\boldsymbol{\xi}) : \Delta\boldsymbol{\mathcal{C}} : \boldsymbol{\nabla}\boldsymbol{G}_\infty(\boldsymbol{\xi} - \boldsymbol{x}) \,\mathrm{d}V_\xi. \tag{1.56}$$

Defining $\tilde{\boldsymbol{v}}_{\mathcal{B}}$ as the solution of (1.53), the goal is then to prove that setting $\boldsymbol{h} = (\boldsymbol{u} + \tilde{\boldsymbol{v}}_{\mathcal{B}})_{|\mathcal{B}} = \tilde{\boldsymbol{u}}_{\mathcal{B}|\mathcal{B}}$, and extending outside $\mathcal{B}$ by $\tilde{\boldsymbol{u}}_{\mathcal{B}} = \boldsymbol{u} + \boldsymbol{V}_{\mathcal{B}}[\tilde{\boldsymbol{u}}_{\mathcal{B}}]$, we obtain a field satisfying the local volume equation and transmission conditions (1.40).

To facilitate the ensuing computations, let's define the local differential operators L and $L^\star$ as:

$$L[\boldsymbol{v}](\boldsymbol{x}) := \operatorname{div}(\boldsymbol{\mathcal{C}} : \boldsymbol{\nabla}\boldsymbol{v}(\boldsymbol{x})) \quad \text{and} \quad L^\star[\boldsymbol{v}](\boldsymbol{x}) = \operatorname{div}(\boldsymbol{\mathcal{C}}^\star : \boldsymbol{\nabla}\boldsymbol{v}(\boldsymbol{x})). \tag{1.57}$$

We also introduce the single-layer potential $\mathcal{S}$ and the Newtonian potential $\mathcal{V}$ associated to $\mathcal{B}$ and background medium as integral operators acting on surface and volume vector-valued densities $\boldsymbol{q}$ and $\boldsymbol{\varphi}$, and defined as:

$$\mathcal{S}[\boldsymbol{q}](\boldsymbol{x}) := \int_{\partial\mathcal{B}} \boldsymbol{G}_\infty(\boldsymbol{\xi} - \boldsymbol{x}) \cdot \boldsymbol{q}(\boldsymbol{\xi}) \,\mathrm{d}S_\xi \quad \text{and} \quad \mathcal{V}[\boldsymbol{\varphi}](\boldsymbol{x}) := \int_{\mathcal{B}} \boldsymbol{G}_\infty(\boldsymbol{\xi} - \boldsymbol{x}) \cdot \boldsymbol{\varphi}(\boldsymbol{\xi}) \,\mathrm{d}V_\xi. \tag{1.58}$$

Then, for $\boldsymbol{x} \notin \partial\Omega$, integrating (1.56) by parts gives:

$$\begin{aligned}\boldsymbol{V}_{\mathcal{B}}[\boldsymbol{h}](\boldsymbol{x}) &= \int_{\partial\mathcal{B}} \boldsymbol{G}_\infty(\boldsymbol{\xi} - \boldsymbol{x}) \cdot (\boldsymbol{t}^- - \boldsymbol{t}^{\star -})[\boldsymbol{h}](\boldsymbol{\xi}) \,\mathrm{d}S_\xi + \int_{\mathcal{B}} \boldsymbol{G}_\infty(\boldsymbol{\xi} - \boldsymbol{x}) \cdot (L^\star - L)[\boldsymbol{h}](\boldsymbol{\xi}) \,\mathrm{d}V_\xi \\ &= \mathcal{S}[(\boldsymbol{t}^- - \boldsymbol{t}^{\star -})[\boldsymbol{h}]](\boldsymbol{x}) + \mathcal{V}[(L^\star - L)[\boldsymbol{h}]](\boldsymbol{x})\end{aligned} \tag{1.59}$$

Remark 1.7. *One can note that the expression* (1.59) *is the one directly proposed in [Knops, 1964] where it is shown that applying the surface and volume forces $(\boldsymbol{t}^- - \boldsymbol{t}^{\star -})[\boldsymbol{h}]$ and $(L^\star - L)[\boldsymbol{h}]$, on $\partial\mathcal{B}$ and $\mathcal{B}$ and to the homogeneous medium, would induce the same perturbation than introducing an inhomogeneity $(\mathcal{B}, \boldsymbol{\mathcal{C}}^\star)$.*

Still for $\boldsymbol{x} \notin \partial\mathcal{B}$, in which case the potentials have regular (for $\mathcal{S}$) and weakly singular (for $\mathcal{V}$) kernels, we can then compute the local equation for $\boldsymbol{V}_{\mathcal{B}}[\boldsymbol{h}]$:

$$\begin{aligned} L\left[\boldsymbol{V}_{\mathcal{B}}[\boldsymbol{h}]\right](\boldsymbol{x}) &= \int_{\partial\mathcal{B}} -L[\boldsymbol{G}_\infty](\boldsymbol{\xi}-\boldsymbol{x})\cdot(\boldsymbol{t}^- - \boldsymbol{t}^{\star -})[\boldsymbol{h}](\boldsymbol{\xi})\,\mathrm{d}S_\xi \\ &\qquad + \int_{\mathcal{B}} -L[\boldsymbol{G}_\infty](\boldsymbol{\xi}-\boldsymbol{x})\cdot(L^\star - L)[\boldsymbol{h}](\boldsymbol{\xi})\,\mathrm{d}V_\xi \\ &= -\int_{\partial\mathcal{B}} \delta(\boldsymbol{\xi}-\boldsymbol{x})(\boldsymbol{t}^- - \boldsymbol{t}^{\star -})[\boldsymbol{h}](\boldsymbol{\xi})\,\mathrm{d}S_\xi - \int_{\mathcal{B}} \delta(\boldsymbol{\xi}-\boldsymbol{x})(L^\star - L)[\boldsymbol{h}](\boldsymbol{\xi})\,\mathrm{d}V_\xi \\ &= \chi_{\mathcal{B}}(\boldsymbol{x})(L-L^\star)[\boldsymbol{h}](\boldsymbol{x}), \end{aligned} \tag{1.60}$$

We abused a bit the notations by differentiating twice the weakly singular kernel of $\mathcal{V}$ under the integral in the first line. The above identity holds, however, and can be justified e.g. by writing $\mathcal{V}$ as the convolution of distributions:

$$\mathcal{V}[\boldsymbol{\varphi}] = \boldsymbol{G}_\infty \star (\chi_{\mathcal{B}}\boldsymbol{\varphi}), \tag{1.61}$$

Then, we conclude invoking [Rudin, 1991, Thm. 6.37] which states that the derivatives of a convolution such as (1.61) in the distributional sense can be computed as in the classical sense provided that one of the involved distributions has compact support (which is indeed the case here owing to the presence of $\chi_{\mathcal{B}}$).

We still have to estimate the jump of (i) the displacement $\boldsymbol{V}_{\mathcal{B}}[\boldsymbol{h}]$ and (ii) the associated dtraction vector $\boldsymbol{t}\left[\boldsymbol{V}_{\mathcal{B}}[\boldsymbol{h}]\right]$ across $\partial\mathcal{B}$. (i) Both $\mathcal{S}$ and $\mathcal{V}$ are known (see e.g. [Kress, 1989]) to be continuous across the boundary $\partial\mathcal{B}$, so the displacement $\boldsymbol{V}_{\mathcal{B}}[\boldsymbol{h}](\boldsymbol{x})$ is continuous across $\partial\mathcal{B}$:

$$\boldsymbol{V}^+_{\mathcal{B}}[\boldsymbol{h}](\boldsymbol{x}) = \boldsymbol{V}^-_{\mathcal{B}}[\boldsymbol{h}](\boldsymbol{x}). \tag{1.62}$$

(ii) The associated traction vectors are defined by:

$$\boldsymbol{t}^\pm\left[\boldsymbol{V}_{\mathcal{B}}[\boldsymbol{h}]\right](\boldsymbol{x}) = \boldsymbol{t}^\pm\left[\mathcal{S}[(\boldsymbol{t}^- - \boldsymbol{t}^{\star -})[\boldsymbol{h}]]\right](\boldsymbol{x}) + \boldsymbol{t}^\pm\left[\mathcal{V}[(L^\star - L)[\boldsymbol{h}]]\right](\boldsymbol{x}). \tag{1.63}$$

The traction vector associated to the Newtonian volume potential $\mathcal{V}$ is continuous across $\partial\mathcal{B}$, while this of the single-layer potential $\mathcal{S}$ is discontinuous and the jump is equal to the opposite of the considered density ([Kupradze, 1979, eq. V.5.9] [2], [Dahlberg et al., 1988] [3]) :

$$\left(\boldsymbol{t}^+ - \boldsymbol{t}^-\right)\left[\mathcal{V}[\boldsymbol{\varphi}]\right](\boldsymbol{x}) = \boldsymbol{0}, \qquad \left(\boldsymbol{t}^+ - \boldsymbol{t}^-\right)\left[\mathcal{S}[\boldsymbol{q}]\right](\boldsymbol{x}) = -\boldsymbol{q}(\boldsymbol{x}). \tag{1.64}$$

So the jump of $\boldsymbol{t}\left[\boldsymbol{V}_{\mathcal{B}}[\boldsymbol{h}]\right]$ is:

$$\left(\boldsymbol{t}^+ - \boldsymbol{t}^-\right)\left[\boldsymbol{V}_{\mathcal{B}}[\boldsymbol{h}]\right](\boldsymbol{x}) = -(\boldsymbol{t}^- - \boldsymbol{t}^{\star -})[\boldsymbol{h}]. \tag{1.65}$$

Finally setting $\boldsymbol{h} = \tilde{\boldsymbol{u}}_{\mathcal{B}|\mathcal{B}}$ inside $\mathcal{B}$ and $\tilde{\boldsymbol{u}_{\mathcal{B}}} = \boldsymbol{u} + \boldsymbol{V}_{\mathcal{B}}[\tilde{\boldsymbol{u}_{\mathcal{B}}}]$ outside reads:

$$\left|\begin{array}{ll} L[\tilde{\boldsymbol{u}_{\mathcal{B}}}](\boldsymbol{x}) + \boldsymbol{f}(\boldsymbol{x}) = \boldsymbol{0} & \boldsymbol{x} \in \mathbb{R}^3\backslash\bar{\mathcal{B}} \\ L^\star[\tilde{\boldsymbol{u}_{\mathcal{B}}}](\boldsymbol{x}) + \boldsymbol{f}(\boldsymbol{x}) = \boldsymbol{0} & \boldsymbol{x} \in \mathcal{B} \\ \tilde{\boldsymbol{u}_{\mathcal{B}}}^+(\boldsymbol{x}) = \tilde{\boldsymbol{u}_{\mathcal{B}}}^-(\boldsymbol{x}) & \boldsymbol{x} \in \partial\mathcal{B} \\ \boldsymbol{t}^+[\tilde{\boldsymbol{u}_{\mathcal{B}}}](\boldsymbol{x}) = \boldsymbol{t}^{\star -}[\tilde{\boldsymbol{u}_{\mathcal{B}}}](\boldsymbol{x}) & \boldsymbol{x} \in \partial\mathcal{B}, \end{array}\right. \tag{1.66}$$

[2] Note that Kupradze uses opposite sign notations for the limits (1.41) (see Chap. V, §1) and a fundamental solution $\boldsymbol{\Gamma} = 2\boldsymbol{G}_\infty$ (see Chap. II, §1) .

[3] In the papers by Ammari and colleagues (e.g. [Ammari & Kang, 2007], [Kang & Milton, 2008]), we find opposite sign for this jump, perhaps due to a notational mistake when referring to the original source [Dahlberg et al., 1988] which also uses opposite sign notations.

which is exactly the initial local formulation (1.40).

1.2.3 Invertibility of the integro-differential operator

We now state the main result of this chapter, which extends Theorem 1 of [Gintides & Kiriaki, 2015] to anisotropic materials:

Theorem 1.3. *Consider the free-space transmission problem featuring an inhomogeneity* $(\mathcal{B}, \boldsymbol{\mathcal{C}}^\star = \boldsymbol{\mathcal{C}} + \Delta\boldsymbol{\mathcal{C}})$*. Under the assumptions that both* $\boldsymbol{\mathcal{C}}$ *and* $\boldsymbol{\mathcal{C}}^\star$ *are positive and bounded, the associated operator* $\mathcal{L}$ *defined by:*

$$\mathcal{L}[\boldsymbol{v}](\boldsymbol{x}) := \boldsymbol{v}(\boldsymbol{x}) + \int_{\mathcal{B}} \boldsymbol{\nabla}\boldsymbol{v} : \Delta\boldsymbol{\mathcal{C}} : \boldsymbol{\nabla}\boldsymbol{G}_\infty(\cdot - \boldsymbol{x}) \, \mathrm{d}V \tag{1.67}$$

is invertible with bounded inverse from $\boldsymbol{H}^1(\mathcal{B})$ *to itself.*

Proof. Consider the integral equation satisfied by the total field $\boldsymbol{u}_{\mathcal{B}} = \boldsymbol{u} + \boldsymbol{v}_{\mathcal{B}}$:

$$\mathcal{L}[\boldsymbol{u}_{\mathcal{B}}](\boldsymbol{x}) = \boldsymbol{u}(\boldsymbol{x}), \quad \boldsymbol{x} \in \mathcal{B}. \tag{1.68}$$

It is then useful to reformulate this problem introducing the additional unknown $\boldsymbol{\sigma}^\star = \Delta\boldsymbol{\mathcal{C}}_{\mathcal{B}} : \boldsymbol{\nabla}\boldsymbol{u}_{\mathcal{B}}$. Note that this unknown $\boldsymbol{\sigma}^\star$, having the meaning of a pre-stress, is called the *equivalent stress* in Eshelby's equivalent inclusion method as it will be explained in Section 1.3.1. Applying the operator $\Delta\boldsymbol{\mathcal{C}}_{\mathcal{B}} : \boldsymbol{\varepsilon} = \Delta\boldsymbol{\mathcal{C}}_{\mathcal{B}} : \boldsymbol{\nabla}$ to (1.68) provides the equivalent system:

$$\begin{cases} \mathcal{G}[\boldsymbol{\sigma}^\star] = \Delta\boldsymbol{\mathcal{C}}_{\mathcal{B}} : \boldsymbol{\varepsilon}[\boldsymbol{u}] \\ \boldsymbol{u}_{\mathcal{B}} = \boldsymbol{u} + \mathcal{M}[\boldsymbol{\sigma}^\star] \ \text{ i.e. } \ \boldsymbol{v}_{\mathcal{B}} = \mathcal{M}[\boldsymbol{\sigma}^\star], \end{cases} \tag{1.69}$$

where the volume potential $\mathcal{M}$ acting on second-order symmetric tensor-values functions $\boldsymbol{\sigma}^\star \in L^2(\mathbb{R}^3; \mathbb{R}^{3\times 3}_{\mathrm{sym}})$ is defined by:

$$\mathcal{M}[\boldsymbol{\sigma}^\star](\boldsymbol{x}) := \int_{\mathbb{R}^3} \boldsymbol{\nabla}\boldsymbol{G}_\infty(\boldsymbol{x} - \boldsymbol{\xi}) : \boldsymbol{\sigma}^\star(\boldsymbol{\xi}) \, \mathrm{d}V_\xi, \tag{1.70}$$

and where we used $\boldsymbol{\nabla}\boldsymbol{G}_\infty(\boldsymbol{\xi} - \boldsymbol{x}) = -\boldsymbol{\nabla}\boldsymbol{G}_\infty(\boldsymbol{x} - \boldsymbol{\xi})$ to write $\mathcal{M}$ as a convolution operator. Since $\boldsymbol{\nabla}\boldsymbol{G}_\infty \in L^1_{\mathrm{loc}}(\mathbb{R}^3; \mathbb{R}^{3\times 3\times 3})$, $\mathcal{M}$ is well-defined as a $L^2_{\mathrm{comp}}(\mathbb{R}^3; \mathbb{R}^{3\times 3}_{\mathrm{sym}}) \to \boldsymbol{L}^2_{\mathrm{loc}}(\mathbb{R}^3)$ operator by virtue of Young's convolution theorem [Brezis, 2011, Thm 4.15]. The singular integral operator $\mathcal{G}$ is then defined in terms of $\mathcal{M}$ by:

$$\mathcal{G} := \boldsymbol{\mathcal{I}} - \Delta\boldsymbol{\mathcal{C}}_{\mathcal{B}} : \boldsymbol{\varepsilon}\left[\mathcal{M}\right]. \tag{1.71}$$

The operator $\boldsymbol{\sigma}^\star \mapsto \boldsymbol{\varepsilon}\left[\mathcal{M}[\boldsymbol{\sigma}^\star]\right]$ can be given a representation in terms of a singular integral operator involving the kernel $\boldsymbol{H}_\infty$, defined as the symmetrized version of $\boldsymbol{\nabla}^2\boldsymbol{G}_\infty$:

$$[\boldsymbol{H}_\infty]_{ijkl} = \frac{1}{4}\left(G_{ik,jl} + G_{il,jk} + G_{jk,il} + G_{jl,ik}\right), \tag{1.72}$$

and whose singularity at the origin is not integrable; see e.g. [Gintides & Kiriaki, 2015, Sec. 4]. This definition is consistent with the symmetry of $\boldsymbol{\sigma}^\star$ (by assumption) and of $\boldsymbol{\varepsilon}\left[\mathcal{M}[\boldsymbol{\sigma}^\star]\right]$. The precise singular integral operator form of $\boldsymbol{\sigma}^\star \mapsto \boldsymbol{\varepsilon}\left[\mathcal{M}[\boldsymbol{\sigma}^\star]\right]$, that requires a limiting process described in [Kupradze, 1979; Gintides & Kiriaki, 2015] to handle the singularity, will not be needed here.

The mapping from the initial data $\boldsymbol{u}$ to the sought perturbation $\boldsymbol{v}_{\mathcal{B}}$ is then formally given by:

$$\boldsymbol{u} \xrightarrow{\Delta\mathcal{C}:\frac{1}{2}(\boldsymbol{\nabla}+\boldsymbol{\nabla}^T)} \Delta\boldsymbol{\mathcal{C}} : \boldsymbol{\varepsilon}[\boldsymbol{u}] \xrightarrow{\mathcal{G}^{-1}} \boldsymbol{\sigma}^\star \xrightarrow{\mathcal{M}} \boldsymbol{v}_{\mathcal{B}}, \tag{1.73}$$

where we emphasized that the solution depends only on $\boldsymbol{\varepsilon}[\boldsymbol{u}]$. The inverse of $\mathcal{L}$ (whose existence is to be proved) would be decomposed as:

$$\boldsymbol{u}_{\mathcal{B}} = \mathcal{L}^{-1}[\boldsymbol{u}] := \left(\boldsymbol{I} + \mathcal{M}\mathcal{G}^{-1}\Delta\boldsymbol{\mathcal{C}}_{\mathcal{B}} : \boldsymbol{\varepsilon}\right)[\boldsymbol{u}]. \tag{1.74}$$

Since $\boldsymbol{u} \mapsto \Delta\boldsymbol{\mathcal{C}}_{\mathcal{B}} : \boldsymbol{\varepsilon}[\boldsymbol{u}]$ is a continuous $\boldsymbol{H}^1(\mathcal{B}) \to \boldsymbol{L}^2(\mathcal{B})$ mapping, proving the existence and continuity of the mapping $\mathcal{L}^{-1} : \boldsymbol{H}^1(\mathcal{B}) \to \boldsymbol{H}^1(\mathcal{B})$ above requires proving that (i) $\mathcal{M} : \boldsymbol{L}^2(\mathcal{B}) \to \boldsymbol{H}^1(\mathcal{B})$ is bounded and (ii) $\mathcal{G} : \boldsymbol{L}^2(\mathcal{B}) \to \boldsymbol{L}^2(\mathcal{B})$ is invertible with bounded inverse. Step (i) is a known result on elastic volume potentials that can be obtained by the theory of pseudo-differential operators, see e.g. [Hsiao & Wendland, 2008, Thm. 6.1.12]. We nevertheless give a proof as some of its ingredients will be used in step (ii).

Step (i): Boundedness of $\mathcal{M} : \boldsymbol{L}^2(\mathcal{B}) \to \boldsymbol{H}^1(\mathcal{B})$ In fact, it is possible to state the more general result:

Lemma 1.4. *Provided that the background elasticity tensor $\boldsymbol{\mathcal{C}}$ is definite, positive and bounded, the integral operator $\mathcal{M}$ defined by (1.70) is continuous as a $L^2_{\mathrm{comp}}(\mathbb{R}^3; \mathbb{R}^{3\times 3}_{\mathrm{sym}}) \to \boldsymbol{H}^1_{\mathrm{loc}}(\mathbb{R}^3)$ operator.*

Proof. We already know that $\mathcal{M} : L^2_{\mathrm{comp}}(\mathbb{R}^3; \mathbb{R}^{3\times 3}_{\mathrm{sym}}) \to \boldsymbol{L}^2_{\mathrm{loc}}(\mathbb{R}^3)$ is bounded, so we only have to prove the boundedness of $\boldsymbol{\varepsilon}[\mathcal{M}] : L^2_{\mathrm{comp}}(\mathbb{R}^3; \mathbb{R}^{3\times 3}_{\mathrm{sym}}) \to \boldsymbol{L}^2_{\mathrm{loc}}(\mathbb{R}^3)$.

The kernel $\boldsymbol{\nabla}\boldsymbol{G}_\infty$ defines a tempered distribution (since $\boldsymbol{\nabla}\boldsymbol{G}_\infty$ is locally summable and belongs to the class of slowly growing functions), making the convolution $\mathcal{M}[\boldsymbol{\sigma}^\star] = (\boldsymbol{\varepsilon}[\boldsymbol{G}_\infty]) \star \boldsymbol{\sigma}^\star$ well-defined for any $\boldsymbol{\sigma}^\star \in L^2_{\mathrm{comp}}(\mathbb{R}^3; \mathbb{R}^{3\times 3}_{\mathrm{sym}})$. Therefore, $\boldsymbol{\varepsilon}[\mathcal{M}[\boldsymbol{\sigma}^\star]] = \boldsymbol{H}_\infty \star \boldsymbol{\sigma}^\star$ also holds in the sense of distributions. Under the present conditions, the distributional version of the Fourier convolution theorem applies:

$$\mathcal{F}\left[\boldsymbol{\varepsilon}[\mathcal{M}[\boldsymbol{\sigma}^\star]]\right] = \mathcal{F}\left[\boldsymbol{H}_\infty \star \boldsymbol{\sigma}^\star\right] = \mathcal{F}\left[\boldsymbol{H}_\infty\right] : \mathcal{F}\left[\boldsymbol{\sigma}^\star\right], \tag{1.75}$$

with the Fourier transform defined for any $f \in L^1(\mathbb{R}^3)$ such that:

$$\mathcal{F}\left[f\right](\boldsymbol{\rho}) = \int_{\mathbb{R}^3} \mathrm{e}^{\mathrm{i}2\pi \boldsymbol{x}\cdot\boldsymbol{\rho}} f(\boldsymbol{x}) \,\mathrm{d}V_x. \tag{1.76}$$

Moreover, referring to expression (1.29) of $\boldsymbol{G}_\infty$, $\hat{\boldsymbol{H}}(\boldsymbol{\rho}) = \mathcal{F}[\boldsymbol{H}_\infty](\boldsymbol{\rho})$ is given for $\boldsymbol{\rho} \neq \boldsymbol{0}$ by the expression:

$$[\hat{\boldsymbol{H}}]_{ijkl} = -\frac{1}{4}\Big(Q_{ik}(\boldsymbol{\rho})\rho_j\rho_l + Q_{il}(\boldsymbol{\rho})\rho_j\rho_k + Q_{jk}(\boldsymbol{\rho})\rho_i\rho_l + Q_{jl}(\boldsymbol{\rho})\rho_i\rho_k\Big), \tag{1.77}$$

where $\boldsymbol{Q}(\boldsymbol{\rho}) = \boldsymbol{K}^{-1}(\boldsymbol{\rho})$ and $\boldsymbol{K}$ is the acoustic tensor already seen in Section 1.1.3 and defined by $K_{ik}(\boldsymbol{\rho}) = \mathcal{C}_{ijk\ell}\rho_j\rho_\ell$. $\boldsymbol{Q}$ is well-defined and bounded under the assumptions on $\boldsymbol{\mathcal{C}}$ we made. In particular, $\hat{\boldsymbol{H}}(\boldsymbol{\rho})$ is $C^\infty(\mathbb{R}^3\backslash\boldsymbol{0})$ and homogeneous with degree 0, i.e. $\hat{\boldsymbol{H}}(\boldsymbol{\rho}) = \hat{\boldsymbol{H}}(\hat{\boldsymbol{\rho}})$ with $\hat{\boldsymbol{\rho}} = \boldsymbol{\rho}/|\boldsymbol{\rho}|$. It is therefore bounded in $\mathbb{R}^3$, and the boundedness of $\boldsymbol{\varepsilon}[\mathcal{M}] : L^2_{\mathrm{comp}}(\mathbb{R}^3; \mathbb{R}^{3\times 3}_{\mathrm{sym}}) \to \boldsymbol{L}^2_{\mathrm{loc}}(\mathbb{R}^3)$ follows with the help of Plancherel's theorem:

$$\begin{aligned}\|\boldsymbol{\varepsilon}[\mathcal{M}[\boldsymbol{\sigma}^\star]]\|_{L^2(\mathbb{R})} = \|\mathcal{F}(\boldsymbol{\varepsilon}[\mathcal{M}[\boldsymbol{\sigma}^\star]])\|_{L^2(\mathbb{R})} = \|\hat{\boldsymbol{H}} : \mathcal{F}[\boldsymbol{\sigma}^\star]\|_{L^2(\mathbb{R})} \\ \leq C\|\mathcal{F}[\boldsymbol{\sigma}^\star]\|_{L^2(\mathbb{R})} = C\|\boldsymbol{\sigma}^\star\|_{L^2(\mathbb{R})}.\end{aligned} \tag{1.78}$$

□

Remark 1.8. *The representation* $\boldsymbol{h} \mapsto \mathcal{M}[\Delta\boldsymbol{\mathcal{C}}_{\mathcal{B}} : \boldsymbol{\nabla h}]$ *used in* (1.56) *is therefore seen to be continuous from* $\boldsymbol{H}^1(\mathcal{B})$ *to itself.*

Step (ii): bounded invertibility of $\mathcal{G}: \ \boldsymbol{L}^2(\mathcal{B}) \to \boldsymbol{L}^2(\mathcal{B})$

To prove the invertibility of the tensorial operator $\mathcal{G}$, we pass by the study of its (tensor-valued) symbol $\boldsymbol{\Psi}(\boldsymbol{x}, \hat{\boldsymbol{\rho}})$ as defined by [Mikhlin & Prössdorf, 1986, Sec. 11.1]. Since $\mathcal{G} = \boldsymbol{\mathcal{I}} - \Delta\boldsymbol{\mathcal{C}}_{\mathcal{B}} : \boldsymbol{\varepsilon}\,[\mathcal{M}]$, $\boldsymbol{\Psi}$ is given in terms of $\hat{\boldsymbol{H}} = \mathcal{F}[\boldsymbol{H}_\infty]$ as:

$$\boldsymbol{\Psi}(\boldsymbol{x}, \hat{\boldsymbol{\rho}}) = \boldsymbol{\mathcal{I}} - \Delta\boldsymbol{\mathcal{C}}_{\mathcal{B}}(\boldsymbol{x}) : \hat{\boldsymbol{H}}(\hat{\boldsymbol{\rho}}), \tag{1.79}$$

and can be given a 6×6 matrix representation $[\boldsymbol{\Psi}(\boldsymbol{x}, \hat{\boldsymbol{\rho}})]_{6\times 6}$ corresponding e.g. to the Mandel vector representation of symmetric second-order tensors [Helnwein, 2001]. Moreover, the identity:

$$[\boldsymbol{\mathcal{I}} + \Delta\boldsymbol{\mathcal{C}}_{\mathcal{B}}(\boldsymbol{x}) : \hat{\boldsymbol{H}}^\star] : [\boldsymbol{\mathcal{I}} - \Delta\boldsymbol{\mathcal{C}}_{\mathcal{B}}(\boldsymbol{x}) : \hat{\boldsymbol{H}}] = \boldsymbol{\mathcal{I}} \tag{1.80}$$

holds as shown by [Freidin & Kucher, 2016], where $\hat{\boldsymbol{H}}^\star$ is defined by (1.72) with $\boldsymbol{\mathcal{C}}$ replaced by $\boldsymbol{\mathcal{C}}^\star$ as a consequence of:

$$\hat{\boldsymbol{H}}^\star : \Delta\boldsymbol{\mathcal{C}} : \hat{\boldsymbol{H}} = \Delta\boldsymbol{\mathcal{C}} : (\hat{\boldsymbol{H}}^\star - \hat{\boldsymbol{H}}) \tag{1.81}$$

which can be checked using (1.72). This identity shows that the symbol tensor $\boldsymbol{\Psi}(\boldsymbol{x}, \hat{\boldsymbol{\rho}})$ is invertible with its inverse given by $\boldsymbol{\Psi}^{-1}(\boldsymbol{x}, \hat{\boldsymbol{\rho}}) = \boldsymbol{\mathcal{I}} + \Delta\boldsymbol{\mathcal{C}}_{\mathcal{B}}(\boldsymbol{x}) : \hat{\boldsymbol{H}}^\star$. A corresponding invertibility result of course holds for the symbol matrix $[\boldsymbol{\Psi}(\boldsymbol{x}, \hat{\boldsymbol{\rho}})]_{6\times 6}$. We can then rely on the following result from Mikhlin's theory for singular integral equations:

Lemma 1.5. *([Mikhlin & Prössdorf, 1986, Chap. 14, Thm 5.2]): Let* $\boldsymbol{A}$ *be a singular matrix operator with pole* $\boldsymbol{x}$ *and* $[\boldsymbol{\Psi}(\boldsymbol{x}, \hat{\boldsymbol{\rho}})]_{n\times n}$ *its* $n \times n$ *symbol matrix. Then if the moduli of the minors:*

$$D_1 := \Psi_{11}(\boldsymbol{x}, \hat{\boldsymbol{\rho}}), \quad D_2 := \begin{vmatrix} \Psi_{11}(\boldsymbol{x}, \hat{\boldsymbol{\rho}}) & \Psi_{12}(\boldsymbol{x}, \hat{\boldsymbol{\rho}}) \\ \Psi_{21}(\boldsymbol{x}, \hat{\boldsymbol{\rho}}) & \Psi_{22}(\boldsymbol{x}, \hat{\boldsymbol{\rho}}) \end{vmatrix}, \ldots, \quad D_n := \det\big([\boldsymbol{\Psi}(\boldsymbol{x}, \hat{\boldsymbol{\rho}})]_{n\times n}\big)$$

are bounded below by a positive constant almost everywhere for $(\boldsymbol{x}, \hat{\boldsymbol{\rho}}) \in \mathbb{R}^3 \times \hat{S}$*,* $\boldsymbol{A}$ *is Fredholm with index 0*[4]*.*

Since (i) $\hat{\boldsymbol{\rho}} \mapsto [\boldsymbol{\Psi}(\boldsymbol{x}, \hat{\boldsymbol{\rho}})]_{6\times 6}$ is (together with all its minors) continuous on the (compact) unit sphere and (ii) $\boldsymbol{x} \mapsto [\boldsymbol{\Psi}(\boldsymbol{x}, \hat{\boldsymbol{\rho}})]_{6\times 6}$ is piecewise-constant, the invertibility of $[\boldsymbol{\Psi}(\boldsymbol{x}, \hat{\boldsymbol{\rho}})]_{6\times 6}$ for each $(\boldsymbol{x}, \hat{\boldsymbol{\rho}})$ guarantees that all minors involved in Lemma 1.5 are nonzero and bounded away from zero (possibly after applying a suitable column permutation to $[\boldsymbol{\Psi}(\boldsymbol{x}, \hat{\boldsymbol{\rho}})]_{6\times 6}$). The condition of Lemma 1.5 being fulfilled, the operator $\mathcal{G}$ is bounded and Fredholm with index 0.

The solution $\boldsymbol{u}_{\mathcal{B}}$ to the FSTP (1.40) was shown by Lemma 1.1 to be unique, and we showed in Section 1.2.2 the equivalence between local and integral formulations. Equation (1.68) therefore has at most one solution. Concluding, as a Fredholm operator with index 0, $\mathcal{G}: \ L^2(\mathcal{B}; \mathbb{R}^{3\times 3}_{\text{sym}}) \to L^2(\mathcal{B}; \mathbb{R}^{3\times 3}_{\text{sym}})$ is invertible with bounded inverse (by virtue of e.g. [McLean, 2000, Thm. 2.1 and Corollary 2.2]).

[4] Fredholm operators with index zero are defined in [Mikhlin & Prössdorf, 1986, Chap. 1]; one can also refer to the presentations of [McLean, 2000],[Ramm, 2001].

Conclusion on $\mathcal{L}$

The mapping from the background displacement $\boldsymbol{u} \in \boldsymbol{H}^1(\mathcal{B})$ to the total field $\boldsymbol{u}_{\mathcal{B}} \in \boldsymbol{H}^1(\mathcal{B})$ due to an inhomogeneity $\mathcal{B}$ embedded in an infinite medium and corresponding to the integral equation $\mathcal{L}[\boldsymbol{u}_{\mathcal{B}}] = \boldsymbol{u}$ is given by:

$$\boldsymbol{u}_{\mathcal{B}} = \mathcal{L}^{-1}[\boldsymbol{u}] = \boldsymbol{u} + \boldsymbol{v}_{\mathcal{B}} = (\boldsymbol{I} + \mathcal{M}\mathcal{G}^{-1}\Delta\boldsymbol{\mathcal{C}}_{\mathcal{B}} : \boldsymbol{\varepsilon})[\boldsymbol{u}] \tag{1.82}$$

and is continuous as the sum and composition of continuous operators. □

As a immediate corollary of we can assert the continuity of the mapping between the gradients of $\boldsymbol{u}$ and $\boldsymbol{u}_{\mathcal{B}}$:

Lemma 1.6. *The mapping*

$$\boldsymbol{\nabla u} \mapsto \boldsymbol{\nabla u}_{\mathcal{B}} = \boldsymbol{\nabla}\mathcal{L}^{-1}[\boldsymbol{u}] = (\boldsymbol{I}^{(4)} + \boldsymbol{\nabla}\mathcal{M}\mathcal{G}^{-1}\Delta\boldsymbol{\mathcal{C}}_{\mathcal{B}} : \boldsymbol{\mathcal{I}})[\boldsymbol{\nabla u}] \tag{1.83}$$

is continuous from $\boldsymbol{L}^2(\mathcal{B})$ to itself.

Remark 1.9. *In the case addressed by [Gintides & Kiriaki, 2015] for which both materials are isotropic and characterized by the couples (μ, ν) and $(\mu^\star, \nu^\star)$, the matrix representation of the symbol* (1.79) *can be computed explicitly, and in particular we find:*

$$\det\left([\boldsymbol{\Psi}(\boldsymbol{x}, \hat{\boldsymbol{\rho}})]_{6\times 6}\right) = \frac{(1-\nu^\star)(1-2\nu)}{(1-2\nu^\star)(1-\nu)}\left(\frac{\mu^\star}{\mu}\right)^3, \tag{1.84}$$

which, along with the expression of the other minors required by Lemma 1.5 (not provided here for brevity), ensures that the only forbidden values of the material parameters are $\nu = 0.5$, $\nu^\star = 0.5$ (which correspond to incompressible materials), and $\mu = 0$, $\mu^\star = 0$. As expected, these are the transpositions of assumptions made in Theorem 1.3 to isotropic materials.

1.2.4 Centrally symmetric inhomogeneities

To end this section, we provide an important auxiliary result that will permit significant subsequent simplifications:

Lemma 1.7. *Let $\mathcal{B}$ be centrally symmetric, i.e. $\boldsymbol{x} \in \mathcal{B} \Rightarrow -\boldsymbol{x} \in \mathcal{B}$. Let the symmetry operator $\boldsymbol{S}$ be defined by $\boldsymbol{Sw}(\boldsymbol{x}) = -\boldsymbol{w}(-\boldsymbol{x})$ for any vector function $\boldsymbol{w} \in \boldsymbol{H}^1(\mathcal{B})$. Then if $\boldsymbol{u}_{\mathcal{B}}$ is the solution of the FSTP* (1.43) *with background field $\boldsymbol{u}$ (i.e. $\mathcal{L}[\boldsymbol{u}_{\mathcal{B}}] = \boldsymbol{u}$ holds), $\boldsymbol{Su}_{\mathcal{B}}$ is the solution of the FSTP with background field $\boldsymbol{Su}$ (i.e. $\mathcal{L}[\boldsymbol{Su}_{\mathcal{B}}] = \boldsymbol{Su}$ holds).*

Proof. We write the integral equation $\mathcal{L}[\boldsymbol{u}_{\mathcal{B}}] = \boldsymbol{u}$ at collocation point $-\boldsymbol{x}$ ($-\boldsymbol{x} \in \mathcal{B}$ by symmetry assumption):

$$\boldsymbol{u}_{\mathcal{B}}(-\boldsymbol{x}) + \int_{\mathcal{B}} \boldsymbol{\nabla u}_{\mathcal{B}}(\boldsymbol{\xi}) : \Delta\boldsymbol{\mathcal{C}} : \boldsymbol{\nabla G}_\infty(\boldsymbol{\xi} + \boldsymbol{x}) \, \mathrm{d}V_\xi = \boldsymbol{u}(-\boldsymbol{x}) \tag{1.85}$$

Then, using $\boldsymbol{\nabla G}_\infty(\boldsymbol{\xi} + \boldsymbol{x}) = -\boldsymbol{\nabla G}_\infty(-\boldsymbol{\xi} - \boldsymbol{x})$ and introducing the integration variable $\boldsymbol{y} = -\boldsymbol{\xi}$ (so that $\boldsymbol{\nabla}_y = -\boldsymbol{\nabla}_\xi$),

$$\boldsymbol{u}_{\mathcal{B}}(-\boldsymbol{x}) - \int_{\mathcal{B}} \boldsymbol{\nabla u}_{\mathcal{B}}(-\boldsymbol{y}) : \Delta\boldsymbol{\mathcal{C}} : \boldsymbol{\nabla G}_\infty(\boldsymbol{y} - \boldsymbol{x}) \, \mathrm{d}V_y = \boldsymbol{u}(-\boldsymbol{x}) \tag{1.86}$$

Finally, noting that $\boldsymbol{\nabla}(\boldsymbol{Su}_{\mathcal{B}})(\boldsymbol{x}) = \boldsymbol{\nabla}(\boldsymbol{u}_{\mathcal{B}})(-\boldsymbol{x})$ arise from the definition of $\boldsymbol{S}$ directly yields the desired equation $\mathcal{L}[\boldsymbol{Su}_{\mathcal{B}}] = \boldsymbol{Su}$. □

As a consequence of Theorem 1.3 and this lemma, the following corollary immediately holds:

Lemma 1.8. *Let $\mathcal{B}$ be centrally symmetric. Then if the considered background field $\boldsymbol{u}$ is an even function of $\boldsymbol{x}$, the solution $\boldsymbol{u}_\mathcal{B}$ of the FSTP is also an even function of $\boldsymbol{x}$. Likewise for odd functions $\boldsymbol{u}$.*

Proof. $\boldsymbol{u}$ is an even function means $\boldsymbol{u}(-\boldsymbol{x}) = \boldsymbol{u}(\boldsymbol{x})$, i.e. $\boldsymbol{S}\boldsymbol{u} = -\boldsymbol{u}$ with $\boldsymbol{S}$ the symmetry operator defined in Lemma 1.7. Invoking this lemma and the invertibility of $\mathcal{L}$ given by Theorem 1.3 directly yields $\boldsymbol{S}\boldsymbol{u}_\mathcal{B} = \mathcal{L}^{-1}[\boldsymbol{S}\boldsymbol{u}] = -\mathcal{L}^{-1}[\boldsymbol{u}] = -\boldsymbol{u}_\mathcal{B}$, i.e. $\boldsymbol{u}_\mathcal{B}$ is also even. Likewise when $\boldsymbol{u}$ is odd, i.e. $\boldsymbol{S}\boldsymbol{u} = \boldsymbol{u}$. $\square$

1.3 Transmission of polynomial background displacement

This part addresses the particular case where the background displacement is polynomial. A polynomial displacement of order n is noted:

$$\boldsymbol{u} = \boldsymbol{E}_0 + \sum_{j=1}^{n} \boldsymbol{\varphi}_j[\boldsymbol{E}_j] \quad \text{with:} \quad \boldsymbol{\varphi}_j[\boldsymbol{E}_j](\boldsymbol{x}) = \frac{1}{j}\boldsymbol{E}_j \bullet \boldsymbol{x}^{\otimes j}, \tag{1.87}$$

and where $\boldsymbol{E}_j$ are constant tensors of order $j+1$. Owing to the linearity of the FSTP, we will specifically address the FSTPs featuring the homogeneous polynomial displacements $\boldsymbol{\varphi}_j[\boldsymbol{E}_j]$ as background fields. The solutions to these particular FSTPs will be denoted $\boldsymbol{u}_\mathcal{B}^{(j)}[\boldsymbol{E}_j]$. The perturbation $\boldsymbol{u}_\mathcal{B}^{(j)}[\boldsymbol{E}_j] - \boldsymbol{\varphi}_j[\boldsymbol{E}_j]$ is accordingly denoted $\boldsymbol{v}_\mathcal{B}^{(j)}[\boldsymbol{E}_j]$. Setting $\boldsymbol{u} = \boldsymbol{\varphi}_j[\boldsymbol{E}_j]$ into the general integral equation (1.53), these perturbations $\boldsymbol{v}_\mathcal{B}^{(j)}[\boldsymbol{E}_j]$ are found to be solutions of the equations:

$$\mathcal{L}\left[\boldsymbol{v}_\mathcal{B}^{(j)}[\boldsymbol{E}_j]\right](\boldsymbol{x}) = -\int_\mathcal{B} \left(\boldsymbol{E}_j \overset{j-1}{\bullet} \boldsymbol{\xi}^{\otimes j-1}\right) : \Delta\boldsymbol{\mathcal{C}} : \boldsymbol{\nabla}\boldsymbol{G}_\infty(\boldsymbol{\xi} - \boldsymbol{x}) \,\mathrm{d}V_\xi. \tag{1.88}$$

1.3.1 Eshelby's equivalent inclusion method for ellipsoidal inhomogeneities

When $\mathcal{B}$ is an *ellipsoid*, Eshelby proposed a method to solve the transmission problem, expressed in terms of strains rather than displacements. His landmark paper [Eshelby, 1957] initially dealt with uniform strains (corresponding to linear displacements) and isotropic materials. His original idea then inspired many works, and some of his conjectures where proved only recently, as related in the historical introductions of [Kang & Milton, 2008; Gintides & Kiriaki, 2015] and in the recent review [Parnell, 2016]. Of particular interest for us is the extension of his method to polynomial strains, as explained in [Mura, 1982, Chap. 4].

Eshelby first had the idea of following imaginary process : (i) remove the inhomogeneity from the matrix, which results in transformation of the border $\partial\mathcal{B}$ of the new hole, (ii) apply surface tractions to this border to recover the original shape $\mathcal{B}$, (iii) fill the hole with background material and (iv) relax the surface tractions so that the matrix is in its original state, which results in an additional stress and strain state of the material occupying $\mathcal{B}$, now called the *inclusion*. This original thought experiment lead him to formulate the assumption that the perturbation field $\boldsymbol{v}_\mathcal{B}$ generated by any inhomogeneity $(\mathcal{B}, \boldsymbol{\mathcal{C}}^\star)$ could be generated by an inclusion of support $\mathcal{B}$ having the same properties $\boldsymbol{\mathcal{C}}$ than the outside medium but supporting an additional *eigenstrain* $\boldsymbol{\varepsilon}^\star$. The problem is therefore described using three different strains defined inside $\mathcal{B}$:

- the known polynomial background strain associated with the polynomial displacement (1.87), given by:

$$\boldsymbol{\varepsilon}[\boldsymbol{u}](\boldsymbol{x}) = \boldsymbol{E}_1^{\mathrm{s}} + \boldsymbol{E}_2^{\mathrm{s}} \cdot \boldsymbol{x} + \boldsymbol{E}_3^{\mathrm{s}} : (\boldsymbol{x} \otimes \boldsymbol{x}) \dots \tag{1.89}$$

where the superscript $\cdot^{\mathrm{s}}$ means symmetrization w.r.t. the two first indices of the tensors $\boldsymbol{E}_j$,

- the sought equivalent eigenstrain, also polynomial and defined by the tensors $\boldsymbol{B}_j$, symmetric on indices $1-2$ (i.e. $\boldsymbol{B}_j^{\mathrm{s}} = \boldsymbol{B}_j$):

$$\boldsymbol{\varepsilon}^\star(\boldsymbol{x}) = \boldsymbol{B}_1 + \boldsymbol{B}_2 \cdot \boldsymbol{x} + \boldsymbol{B}_3 : (\boldsymbol{x} \otimes \boldsymbol{x}) \dots \tag{1.90}$$

- the sought perturbation strain $\boldsymbol{\varepsilon}(\boldsymbol{x}) = \boldsymbol{\varepsilon}[\boldsymbol{v}_{\mathcal{B}}](\boldsymbol{x})$, which is linked to the eigenstrain through the *Eshelby tensors* $\boldsymbol{\mathcal{D}}_j$ as:

$$\boldsymbol{\varepsilon}(\boldsymbol{x}) = \boldsymbol{\mathcal{D}}_1(\boldsymbol{x}) : \boldsymbol{B}_1 + \boldsymbol{\mathcal{D}}_2(\boldsymbol{x}) \overset{3}{\bullet} \boldsymbol{B}_2 + \boldsymbol{\mathcal{D}}_3(\boldsymbol{x}) \overset{4}{\bullet} \boldsymbol{B}_3 \dots \tag{1.91}$$

The method then relies on two steps. Firstly, one needs to compute the tensors $\boldsymbol{\mathcal{D}}_j$ (i.e. to solve the inclusion problem for polynomial eigenstrains). This step is developed in [Mura, 1982, Part 12] for isotropic media. It relies on the well-known integral representation of the solution of the inclusion problem:

$$\begin{aligned} \boldsymbol{v}_{\mathcal{B}} = \mathcal{M}[\boldsymbol{\mathcal{C}} : \boldsymbol{\varepsilon}^\star] &= \int_{\mathcal{B}} \boldsymbol{\nabla} \boldsymbol{G}_\infty(\boldsymbol{x} - \boldsymbol{\xi}) : (\boldsymbol{\mathcal{C}} : \boldsymbol{\varepsilon}^\star(\boldsymbol{\xi}))\ \mathrm{d}V_\xi \\ &= -\int_{\mathcal{B}} \boldsymbol{\nabla}_{\boldsymbol{\xi}} \boldsymbol{G}_\infty(\boldsymbol{\xi} - \boldsymbol{x}) : (\boldsymbol{\mathcal{C}} : \boldsymbol{\varepsilon}^\star(\boldsymbol{\xi}))\ \mathrm{d}V_\xi \end{aligned} \tag{1.92}$$

that is analytically computable for polynomial $\boldsymbol{\varepsilon}^\star$ and isotropic material. These computations and the results for the first and second Eshelby tensors are reproduced for convenience in Appendix 1.A.4. It is also found that inside the inclusion, these tensors are polynomial in $\boldsymbol{x}$ with terms having the same parity, i.e. $\boldsymbol{\mathcal{D}}_j(\boldsymbol{x})$ is a polynomial of $\boldsymbol{x}$ with terms of degrees $j-1$, $j-3$, $j-5\dots$.

Remark 1.10. *This property was firstly highlighted in [Eshelby, 1961] under the form: if $\boldsymbol{\varepsilon}^\star(\boldsymbol{x})$ is a homogeneous polynomial of $\boldsymbol{x}$ with degree n, then $\boldsymbol{\varepsilon}(\boldsymbol{x})$ will be an inhomogeneous polynomial whose terms are of degrees n, $n-2$, $n-4\dots$*

Secondly, the equivalent inclusion method states the *equality of stresses in $\mathcal{B}$ for the inhomogeneity and the inclusion problems* that we write:

$$\begin{aligned} &\boldsymbol{\mathcal{C}}^\star : (\boldsymbol{\varepsilon}[\boldsymbol{u}] + \boldsymbol{\varepsilon}) = \boldsymbol{\mathcal{C}} : (\boldsymbol{\varepsilon}[\boldsymbol{u}] + \boldsymbol{\varepsilon} - \boldsymbol{\varepsilon}^\star) \quad \forall \boldsymbol{x} \in \mathcal{B}, \\ \text{i.e.}\quad &\Delta\boldsymbol{\mathcal{C}} : \boldsymbol{\varepsilon} + \boldsymbol{\mathcal{C}} : \boldsymbol{\varepsilon}^\star = -\Delta\boldsymbol{\mathcal{C}} : \boldsymbol{\varepsilon}[\boldsymbol{u}] \qquad\qquad \forall \boldsymbol{x} \in \mathcal{B}. \end{aligned} \tag{1.93}$$

Inserting the expressions (1.89-1.91) of the strains $\boldsymbol{\varepsilon}[\boldsymbol{u}]$, $\boldsymbol{\varepsilon}^\star$ and $\boldsymbol{\varepsilon}$, and from the property of Eshelby's tensors described above, this equation is found to be an equality between two polynomials. Writing it and its gradients for $\boldsymbol{x} = \boldsymbol{0}$ then leads to the following tensorial equations satisfied by the unknown tensors $\boldsymbol{B}_n$:

$$\Delta\boldsymbol{\mathcal{C}} : \boldsymbol{d}_n \bullet \boldsymbol{B}_n + \boldsymbol{\mathcal{C}} : \boldsymbol{B}_n = -\Delta\boldsymbol{\mathcal{C}} : \boldsymbol{E}_n, \tag{1.94}$$

where the constant tensors $\boldsymbol{d}_n$ are defined such that $\boldsymbol{d}_n \bullet \boldsymbol{B}_n = \boldsymbol{\nabla}^{n-1}\left(\boldsymbol{\mathcal{D}}_n(\boldsymbol{x}) \bullet \boldsymbol{B}_n\right)$. Solving these equations, one finally obtains the $\boldsymbol{B}_n$ and therefore the sought perturbation strain $\boldsymbol{\varepsilon}[\boldsymbol{v}_{\mathcal{B}}]$ given by expression (1.91).

The particular cases $n = 1$ and $n = 2$, which correspond to constant and linear background strains and that we call *first* and *second Eshelby problems*, are now specified.

1.3.2 Transmission problems for constant and linear background strains

1.3.2.1 First Eshelby problem

The first Eshelby problem is the particular transmission problem considering a *linear background displacement* $\boldsymbol{u}(\boldsymbol{x}) = \boldsymbol{E}_1 \cdot \boldsymbol{x}$. Equivalently, it was firstly described in [Eshelby, 1957] for a constant background strain $\boldsymbol{\varepsilon}[\boldsymbol{u}] = \boldsymbol{E}_1^{\mathrm{s}}$. Writing the stress equality (1.93) for this particular case lies the original equation given by Eshelby:

$$\Delta\boldsymbol{\mathcal{C}} : \boldsymbol{\mathcal{D}}_1 : \boldsymbol{B}_1 + \boldsymbol{\mathcal{C}} : \boldsymbol{B}_1 = -\Delta\boldsymbol{\mathcal{C}} : \boldsymbol{E}_1. \tag{1.95}$$

This equation is a tensorial system to solve to recover $\boldsymbol{B}_1$, and its solvability, well-known for isotropic materials, was definitely established very recently for any anisotropic material by [Freidin & Kucher, 2016]. It involves the first Eshelby tensor $\boldsymbol{\mathcal{D}}_1$, which is computed for any ellipsoid in Appendix 1.A.4 for isotropic materials. Once solving this equation is done, the perturbation strain can be written as:

$$\boldsymbol{\varepsilon}\left[\boldsymbol{v}_{\mathcal{B}}^{(1)}[\boldsymbol{E}_1]\right] = \boldsymbol{A}_1 : \boldsymbol{E}_1, \tag{1.96}$$

with the fourth-order tensor $\boldsymbol{A}_1$ given by:

$$\boldsymbol{A}_1 = -\boldsymbol{\mathcal{D}}_1 : (\boldsymbol{\mathcal{C}} + \Delta\boldsymbol{\mathcal{C}} : \boldsymbol{\mathcal{D}}_1)^{-1} : \Delta\boldsymbol{\mathcal{C}}, \tag{1.97}$$

and the total strain is $\boldsymbol{\varepsilon}[\boldsymbol{u}_{\mathcal{B}}^{(1)}[\boldsymbol{E}_1]] = (\boldsymbol{\mathcal{I}} + \boldsymbol{A}_1) : \boldsymbol{E}_1$. The resulting displacement $\boldsymbol{u}_{\mathcal{B}}^{(1)}[\boldsymbol{E}_1] = (\boldsymbol{\varphi}_1 + \boldsymbol{v}_{\mathcal{B}}^{(1)})[\boldsymbol{E}_1]$ is obtained by integrating (1.96) as:

$$\boldsymbol{u}_{\mathcal{B}}^{(1)}[\boldsymbol{E}_1](\boldsymbol{x}) = \boldsymbol{E}_1 \cdot \boldsymbol{x} + (\boldsymbol{A}_1 : \boldsymbol{E}_1) \cdot \boldsymbol{x} = \Big((\boldsymbol{I}^{(4)} + \boldsymbol{A}_1) : \boldsymbol{E}_1\Big) \cdot \boldsymbol{x} \tag{1.98}$$

For the simplest case of ball in an isotropic material, we note $\boldsymbol{\mathcal{S}} = \boldsymbol{\mathcal{D}}_1$ the first Eshelby tensor, which is given by [Mura, 1982, eq. 17.19] as:

$$\boldsymbol{\mathcal{S}} = S_1 \boldsymbol{\mathcal{J}} + S_2 \boldsymbol{\mathcal{K}}, \qquad \text{with} \quad S_1 := \frac{1+\nu}{3(1-\nu)}, \quad S_2 = \frac{8-10\nu}{15(1-\nu)}. \tag{1.99}$$

Moreover, inserting (1.99), $\boldsymbol{\mathcal{C}}$'s decomposition (1.32) and its analogous for $\Delta\boldsymbol{\mathcal{C}}$ into (1.97), and using the properties of the projectors $\boldsymbol{\mathcal{J}}$ and $\boldsymbol{\mathcal{K}}$ detailed by (1.13), one easily computes $\boldsymbol{A}_1$:

$$\boldsymbol{A}_1 = -\frac{S_1(\gamma_\kappa - 1)}{1 + S_1(\gamma_\kappa - 1)} \boldsymbol{\mathcal{J}} - \frac{S_2(\gamma_\mu - 1)}{1 + S_2(\gamma_\mu - 1)} \boldsymbol{\mathcal{K}}, \tag{1.100}$$

with $\gamma_\kappa = \kappa^\star/\kappa$ and $\gamma_\mu = \mu^\star/\mu$.

1.3.2.2 Second Eshelby problem

Similarly, the second Eshelby problem is the particular transmission problem considering a *quadratic* background displacement $\boldsymbol{u}(\boldsymbol{x}) = (\boldsymbol{E}_2 : (\boldsymbol{x} \otimes \boldsymbol{x}))/2$, or, equivalently, a linear background strain $\boldsymbol{\varepsilon}[\boldsymbol{u}](\boldsymbol{x}) = \boldsymbol{E}_2^{\mathrm{s}} \cdot \boldsymbol{x}$.

For an ellipsoidal inhomogeneity $\mathcal{B}$, as seen above, the perturbation strain is given as the product of the second (5th-order) Eshelby tensor $\boldsymbol{\mathcal{D}}_2$ and the 3d-order tensor $\boldsymbol{B}_2$:

$$\boldsymbol{\varepsilon}\left[\boldsymbol{v}_{\mathcal{B}}^{(2)}[\boldsymbol{E}_2]\right](\boldsymbol{x}) = \boldsymbol{\mathcal{D}}_2(\boldsymbol{x}) \overset{3}{\bullet} \boldsymbol{B}_2 = (\boldsymbol{\nabla}\boldsymbol{\mathcal{D}}_2 \cdot \boldsymbol{x}) \overset{3}{\bullet} \boldsymbol{B}_2, \tag{1.101}$$

the second equality arising because $\boldsymbol{\mathcal{D}}_2$ is a linear function of $\boldsymbol{x}$ as explained above, so that $\boldsymbol{\nabla}\boldsymbol{\mathcal{D}}_2$ is a constant 6th-order tensor. Note also that, since $\boldsymbol{\varepsilon}$ and $\boldsymbol{B}_2$ are symmetric on their two first indices, $\boldsymbol{\mathcal{D}}_2$ and $\boldsymbol{\nabla}\boldsymbol{\mathcal{D}}_2$ are uniquely defined as symmetric tensors for the couples of indices 1-2 and 3-4. $\boldsymbol{\nabla}\boldsymbol{\mathcal{D}}_2$ is given in Appendix 1.A.4 for a general ellipsoid and isotropic materials. When $\mathcal{B}$ is the unit sphere, it becomes:

$$\begin{aligned}70(1-\nu)\mathcal{D}_{ijklq,p} = &-2k^{6,0}_{ijklqp} + 14\nu k^{4,0}_{ijqp}\delta_{kl} \\ &+ 7(1-\nu)\left(\delta_{il}k^{4,0}_{jkqp} + \delta_{jl}k^{4,0}_{ikqp} + \delta_{ik}k^{4,0}_{jlqp} + \delta_{jk}k^{4,0}_{ilqp}\right)\end{aligned} \tag{1.102}$$

in terms of the tensors $\boldsymbol{k}^{6,0}$ and $\boldsymbol{k}^{4,0}$ defined in Section 1.1.1.

The third-order-tensorial equation allowing to compute $\boldsymbol{B}_2$ from $\boldsymbol{E}_2$ is then obtained setting $n = 2$ in (1.94):

$$\begin{aligned} &\Delta\boldsymbol{\mathcal{C}} : \boldsymbol{\nabla}(\boldsymbol{\mathcal{D}}_2 \overset{3}{\bullet} \boldsymbol{B}_2) + \boldsymbol{\mathcal{C}} : \boldsymbol{B}_2 = -\Delta\boldsymbol{\mathcal{C}} : \boldsymbol{E}_2, \\ \text{i.e.}\quad &\Delta\mathcal{C}_{mnij}\mathcal{D}_{ijklq,p}B_{klq} + \mathcal{C}_{mnkl}B_{klp} = -\Delta\mathcal{C}_{mnkl}E_{klp} \\ \text{or}\quad &(\Delta\mathcal{C}_{mnij}\mathcal{D}_{ijklq,p} + \mathcal{C}_{mnkl}\delta_{pq})B_{klq} = -\Delta\mathcal{C}_{mnkl}E_{klp}. \end{aligned} \tag{1.103}$$

This system is thus written in compact form as:

$$\boldsymbol{\mathcal{T}} \overset{3}{\bullet} \boldsymbol{B}_2 = \Delta\boldsymbol{\mathcal{C}} : \boldsymbol{E}_2 \qquad \text{with} \quad \boldsymbol{\mathcal{T}} := P_{126345}\left[-\Delta\boldsymbol{\mathcal{C}} : \boldsymbol{\nabla}\boldsymbol{\mathcal{D}}_2 - \boldsymbol{\mathcal{C}} \otimes \boldsymbol{I}_2\right], \tag{1.104}$$

where P_{126345} designs the index permutation: $P_{126345}(\boldsymbol{A})_{mnklpq} = A_{mnpklq}$. Remark that the 6-th order tensor $\boldsymbol{\mathcal{T}}$ is therefore symmetric on the couples of indices 1-2 and 4-5. To solve the system (1.104), so far and unlike for the first Eshelby problem, we did not find any analytical formula. Therefore, for any given isotropic materials defined by (μ, ν) and contrasts $(\Delta\kappa, \Delta\mu)$, we numerically solve the equivalent matrix system - whose size is 18×18 due to $\boldsymbol{\mathcal{T}}$'s symmetries.

Once this inversion has been performed, we can write:

$$\boldsymbol{B}_2 = \boldsymbol{\mathcal{T}}^{\text{inv}} \overset{3}{\bullet} \boldsymbol{E}_2 \quad \text{with} \quad \mathcal{T}^{\text{inv}}_{klqmnp} = (\boldsymbol{\mathcal{T}}^{-1})_{klqijp}\Delta\mathcal{C}_{ijmn} \tag{1.105}$$

Inserting this expression into the strain expression (1.101), using $\boldsymbol{\mathcal{D}}_2(\boldsymbol{x}) = \boldsymbol{\nabla}\boldsymbol{\mathcal{D}}_2 \cdot \boldsymbol{x}$, and upon some indices reorganizations, the linear background and perturbation strains are finally found to be linked by a 6-th order tensor $\boldsymbol{A}_2$ such that:

$$\boldsymbol{\varepsilon}\left[\boldsymbol{v}^{(2)}_{\mathcal{B}}[\boldsymbol{E}_2]\right](\boldsymbol{x}) = (\boldsymbol{A}_2 \overset{3}{\bullet} \boldsymbol{E}_2) \cdot \boldsymbol{x}, \tag{1.106}$$

$\boldsymbol{A}_2$ being defined by:

$$\boldsymbol{A}_2 = P_{126345}(\boldsymbol{\nabla}\boldsymbol{\mathcal{D}}_2) \overset{3}{\bullet} \boldsymbol{\mathcal{T}}^{\text{inv}}, \tag{1.107}$$

and the total strain is:

$$\boldsymbol{\varepsilon}[\boldsymbol{u}^{(2)}_{\mathcal{B}}[\boldsymbol{E}_2]](\boldsymbol{x}) = \boldsymbol{E}^{\text{s}}_2 \cdot \boldsymbol{x} + (\boldsymbol{A}_2 \overset{3}{\bullet} \boldsymbol{E}_2) \cdot \boldsymbol{x} = ((\boldsymbol{\mathcal{I}}^{(6)} + \boldsymbol{A}_2) \overset{3}{\bullet} \boldsymbol{E}_2) \cdot \boldsymbol{x}, \tag{1.108}$$

where $\boldsymbol{\mathcal{I}}^{(6)}$ is the sixth-order identity for third-order symmetric tensors on indices 1-2.

To obtain the resulting displacement $\boldsymbol{u}^{(2)}_{\mathcal{B}}[\boldsymbol{E}_2] = (\boldsymbol{\varphi}_2 + \boldsymbol{v}^{(2)}_{\mathcal{B}})[\boldsymbol{E}_2]$, one must integrate the linear strain (1.106). To this end, consider the general case of a symmetric third-order tensor $\boldsymbol{E}$ and of a linear strain written:

$$\boldsymbol{\varepsilon} = \boldsymbol{E} \cdot \boldsymbol{x} \text{ i.e. } \varepsilon_{ij} = E_{ijk}x_k, \text{ with } E_{ijk} = E_{jik}. \tag{1.109}$$

To compute the associated displacement that we note $\boldsymbol{q}[\boldsymbol{E}]$, we need the skew-symmetric part of its gradient $\boldsymbol{\omega}$ defined as $\omega_{ij} = (q_{i,j} - q_{j,i})/2$ and such that $\boldsymbol{\nabla q}[\boldsymbol{E}] = \boldsymbol{\varepsilon} + \boldsymbol{\omega}$. Classically, the partial derivatives of $\boldsymbol{\omega}$ are given as combinations of those of $\boldsymbol{\varepsilon}$:

$$\omega_{ij,k} = \frac{1}{2}(q_{i,jk} - q_{j,ik}) = \varepsilon_{ik,j} - \varepsilon_{jk,i} = E_{ikj} - E_{jki}. \tag{1.110}$$

Integrating these equations (and canceling the arising constants that correspond to rigid-body rotations) gives:

$$\omega_{ij} = (E_{ikj} - E_{jki})x_k \qquad \text{and} \qquad q_{i,j} = \varepsilon_{ij} + \omega_{ij} = (E_{ijk} + E_{ikj} - E_{jki})x_k. \tag{1.111}$$

Integrating once more, and again canceling integration constants that this time correspond to rigid-body translations,

$$\boldsymbol{q}[\boldsymbol{E}](\boldsymbol{x}) = \frac{1}{2}\boldsymbol{F} : (\boldsymbol{x} \otimes \boldsymbol{x}) \quad \text{with} \quad F_{ijk} = E_{ijk} + E_{ikj} - E_{jki}. \tag{1.112}$$

To keep an explicit tensor formulation in $\boldsymbol{E}$, we furthermore introduce the sixth-order tensor $\boldsymbol{\mathcal{F}}$ as:

$$\mathcal{F}_{ijkabc} = \delta_{ia}\delta_{jb}\delta_{kc} + \delta_{ia}\delta_{jc}\delta_{kb} - \delta_{ic}\delta_{ja}\delta_{kb} \tag{1.113}$$

so that $\boldsymbol{F} = \boldsymbol{\mathcal{F}} \bullet \boldsymbol{E}$ and $\boldsymbol{q}[\boldsymbol{E}](\boldsymbol{x}) = (\boldsymbol{\mathcal{F}} \bullet \boldsymbol{E}) : (\boldsymbol{x} \otimes \boldsymbol{x})/2$. The displacement solution of the second Eshelby problem is then given by:

$$\boldsymbol{u}_{\mathcal{B}}^{(2)}[\boldsymbol{E}_2](\boldsymbol{x}) = \left(\boldsymbol{\varphi}_2 + \boldsymbol{v}_{\mathcal{B}}^{(2)}\right)[\boldsymbol{E}_2](\boldsymbol{x}) = \frac{1}{2}\left((\boldsymbol{I}^{(6)} + \boldsymbol{\mathcal{F}} \bullet \boldsymbol{A}_2) \bullet \boldsymbol{E}_2\right) : (\boldsymbol{x} \otimes \boldsymbol{x}). \tag{1.114}$$

1.3.3 Elastic Moment tensors

For a given couple of tensors $(\boldsymbol{E}_p, \boldsymbol{E}_q)$, the "stiffness product" $\left\langle \boldsymbol{u}_{\mathcal{B}}^{(p)}[\boldsymbol{E}_p], \boldsymbol{\varphi}_q[\boldsymbol{E}_q]\right\rangle_{\mathcal{B}}^{\Delta\mathcal{C}}$ will be widely used in the upcoming chapters. It involves (i) the solution $\boldsymbol{u}_{\mathcal{B}}^{(p)}[\boldsymbol{E}_p]$ to a transmission problem with polynomial background displacement defined by $\boldsymbol{E}_p$ and (ii) another polynomial displacement $\boldsymbol{\varphi}_q[\boldsymbol{E}_q]$. It can be compacted introducing the $(p+q+2)$-th order *elastic moment tensor* $\boldsymbol{\mathcal{A}}_{pq}$ such that:

$$\int_{\mathcal{B}} \boldsymbol{\nabla u}_{\mathcal{B}}^{(p)}[\boldsymbol{E}_p](\boldsymbol{\xi}) : \Delta\boldsymbol{\mathcal{C}} : \left(\boldsymbol{E}_q \overset{q-1}{\bullet} \boldsymbol{\xi}^{\otimes q-1}\right) \, \mathrm{d}V_\xi = \boldsymbol{E}_p \bullet \boldsymbol{\mathcal{A}}_{pq} \bullet \boldsymbol{E}_q. \tag{1.115}$$

$\boldsymbol{\mathcal{A}}_{pq}$ accounts for the transmission problem solved by $\boldsymbol{u}_{\mathcal{B}}^{(p)}[\boldsymbol{E}_p]$, and the integral on $\mathcal{B}$. Its thus depends on $\mathcal{B}$, $\boldsymbol{\mathcal{C}}$ and $\Delta\boldsymbol{\mathcal{C}}$. Noting that the left-hand side of (1.115) only depends on the partially-symmetrized versions $\boldsymbol{E}_p^{\mathrm{s}}$, $\boldsymbol{E}_q^{\mathrm{s}}$ of $\boldsymbol{E}_p$ and $\boldsymbol{E}_q$, $\boldsymbol{\mathcal{A}}_{pq}$ is uniquely defined by upon enforcing minor symmetries mirroring those of $\boldsymbol{E}_p$, $\boldsymbol{E}_q$, e.g. $[\boldsymbol{\mathcal{A}}_{22}]_{ijkmnp} = [\boldsymbol{\mathcal{A}}_{22}]_{jikmnp} = [\boldsymbol{\mathcal{A}}_{22}]_{ijknmp}$. Moreover, note that the reciprocity identity (1.49) applied to two solutions $\boldsymbol{u}_{\mathcal{B}}^{(p)}[\boldsymbol{E}_p]$ and $\boldsymbol{u}_{\mathcal{B}}^{(q)}[\boldsymbol{E}_q]$ ensures:

$$\boldsymbol{E}_p \bullet \boldsymbol{\mathcal{A}}_{pq} \bullet \boldsymbol{E}_q = \boldsymbol{E}_q \bullet \boldsymbol{\mathcal{A}}_{qp} \bullet \boldsymbol{E}_p \quad \forall(\boldsymbol{E}_p, \boldsymbol{E}_q), \tag{1.116}$$

so that the practical evaluation of $\boldsymbol{\mathcal{A}}_{pq}$ requires only this of the solution $\boldsymbol{u}_{\mathcal{B}}^{(m)}[\boldsymbol{E}_m]$ with $m = \min(p, q)$.

Remark 1.11. *These elastic moment tensors, introduced in [Ammari et al., 2002] with different formalism, are the analogous for elasticity to the widely studied* polarization tensors *for acoustics, see e.g. [Ammari & Kang, 2007].*

From the symmetry properties of transmission solutions in the case of a centrally symmetric $\mathcal{B}$, given by Lemmas 1.7 and 1.8, the following property holds:

Lemma 1.9. *For any centrally symmetric inclusion $\mathcal{B}$, $\boldsymbol{\mathcal{A}}_{pq} = \mathbf{0}$ whenever $p+q$ is odd.*

Proof. Lemma 1.8 applied to $\boldsymbol{u} = \boldsymbol{\varphi}_p[\boldsymbol{E}_p]$ states that $\boldsymbol{u}^{(p)}_{\mathcal{B}}[\boldsymbol{E}_p]$ has the same parity than p for centrally symmetric inclusions. Then, one finds that the integrand in (1.115) has the same parity than $p+q$, thus the above result. □

Thereafter, we concentrate on (i) the fourth-order tensor $\boldsymbol{\mathcal{A}}_{11}$ that we call the *first elastic moment tensor* and note $\boldsymbol{\mathcal{A}} := \boldsymbol{\mathcal{A}}_{11}$ for compactness and consistency with previous works [Bonnet & Delgado, 2013] and (ii) the sixth-order tensors $\boldsymbol{\mathcal{A}}_{13}$ and $\boldsymbol{\mathcal{A}}_{22}$. These are computed for ellipsoidal shapes thanks to the resolutions of first and second Eshelby problems that we addressed in the previous section.

1.3.3.1 First elastic moment tensor

The *first elastic moment tensor* $\boldsymbol{\mathcal{A}}$ is defined for an inhomogeneity $\mathcal{B}$, elasticity tensors $\boldsymbol{\mathcal{C}}$ and $\Delta\boldsymbol{\mathcal{C}}$ and for any second-order tensor $\boldsymbol{E}_1$ by:

$$\boldsymbol{\mathcal{A}} : \boldsymbol{E}_1 = \int_{\mathcal{B}} \Delta\boldsymbol{\mathcal{C}} : \boldsymbol{\nabla}\boldsymbol{u}^{(1)}_{\mathcal{B}}[\boldsymbol{E}_1](\boldsymbol{\xi}) \, \mathrm{d}V_{\xi} = \int_{\mathcal{B}} \Delta\boldsymbol{\mathcal{C}} : \Big(\boldsymbol{E}_1 + \boldsymbol{\nabla}\boldsymbol{v}^{(1)}_{\mathcal{B}}[\boldsymbol{E}_1](\boldsymbol{\xi})\Big) \, \mathrm{d}V_{\xi}. \tag{1.117}$$

Its properties are extensively explained in [Bonnet & Delgado, 2013, Sect. 5]. In particular, it is easily shown from (1.96) and (1.97) that $\boldsymbol{\mathcal{A}}$ is given by $\boldsymbol{\mathcal{A}} = |\mathcal{B}|\Delta\boldsymbol{\mathcal{C}} : (\boldsymbol{\mathcal{I}} + \boldsymbol{A}_1)$ for ellipsoidal inclusions, and that it results in the expression:

$$\boldsymbol{\mathcal{A}} = |\mathcal{B}|\boldsymbol{\mathcal{C}} : (\boldsymbol{\mathcal{C}} + \Delta\boldsymbol{\mathcal{C}} : \boldsymbol{\mathcal{D}}_1)^{-1} : \Delta\boldsymbol{\mathcal{C}} \tag{1.118}$$

featuring the first Eshelby tensor $\boldsymbol{\mathcal{D}}_1$. From this expression, the special case of a spherical inclusion in an isotropic material results in:

$$\boldsymbol{\mathcal{A}} = \frac{4\pi}{3}\left[3\kappa\frac{\gamma_\kappa - 1}{1 + S_1(\gamma_\kappa - 1)}\boldsymbol{\mathcal{J}} + 2\mu\frac{\gamma_\mu - 1}{1 + S_2(\gamma_\mu - 1)}\boldsymbol{\mathcal{K}}\right], \tag{1.119}$$

with (S_1, S_2) defined by (1.99), $\gamma_\kappa = \kappa^\star/\kappa$ and $\gamma_\mu = \mu^\star/\mu$.

1.3.3.2 Sixth-order elastic moment tensors

$\boldsymbol{\mathcal{A}}_{13}$ is defined for any second-order tensor $\boldsymbol{E}_1$ and fourth-order tensor $\boldsymbol{E}_3$ such that:

$$\boldsymbol{E}_1 : \boldsymbol{\mathcal{A}}_{13} \bullet \boldsymbol{E}_3 = \int_{\mathcal{B}} \boldsymbol{\nabla}\boldsymbol{u}^{(1)}_{\mathcal{B}}[\boldsymbol{E}_1](\boldsymbol{\xi}) : \Delta\boldsymbol{\mathcal{C}} : \big(\boldsymbol{E}_3 : \boldsymbol{\xi}^{\otimes 2}\big) \, \mathrm{d}V_{\xi}. \tag{1.120}$$

When $\mathcal{B}$ is an ellipsoid, this product becomes:

$$\boldsymbol{E}_1 : \boldsymbol{\mathcal{A}}_{13} \bullet \boldsymbol{E}_3 = (\boldsymbol{E}_1 : (\boldsymbol{\mathcal{I}} + \boldsymbol{A}_1)) : \Delta\boldsymbol{\mathcal{C}} : \left(\boldsymbol{E}_3 : \int_{\mathcal{B}} \boldsymbol{\xi} \otimes \boldsymbol{\xi} \, \mathrm{d}V_{\xi}\right), \tag{1.121}$$

from which we can write:

$$\boldsymbol{\mathcal{A}}_{13} = ((\boldsymbol{\mathcal{I}} + \boldsymbol{A}_1) : \Delta\boldsymbol{\mathcal{C}}) \otimes \boldsymbol{M}^{(2)} = \frac{1}{|\mathcal{B}|}\boldsymbol{\mathcal{A}} \otimes \boldsymbol{M}^{(2)} \qquad \text{with} \qquad \boldsymbol{M}^{(2)} = \int_{\mathcal{B}} \boldsymbol{\xi} \otimes \boldsymbol{\xi} \, \mathrm{d}V_{\xi}. \tag{1.122}$$

$\boldsymbol{M}^{(2)}$ is the geometrical inertia tensor of $\mathcal{B}$ and is given for an ellipsoid with semi-principal axes a_j and principal directions $\boldsymbol{\eta}_j$ as:

$$\boldsymbol{M}^{(2)} = \int_{\mathcal{B}} \boldsymbol{\xi} \otimes \boldsymbol{\xi} \, \mathrm{d}V_\xi = \frac{4\pi}{15} a_1 a_2 a_3 \sum_{j=1}^{3} a_j^2 \boldsymbol{\eta}_j \otimes \boldsymbol{\eta}_j. \tag{1.123}$$

In particular, $\boldsymbol{M}^{(2)} = (4\pi a^5/15)\boldsymbol{I}$ for a sphere of radius a.

Remark 1.12. *Using property* (1.116)*, we thus define* $\boldsymbol{\mathcal{A}}_{31}$ *without computing it by:*

$$\boldsymbol{E}_3 \bullet \boldsymbol{\mathcal{A}}_{31} : \boldsymbol{E}_1 = \boldsymbol{E}_1 : \boldsymbol{\mathcal{A}}_{13} \bullet \boldsymbol{E}_3 \quad \forall(\boldsymbol{E}_1, \boldsymbol{E}_3). \tag{1.124}$$

Similarly, $\boldsymbol{\mathcal{A}}_{22}$ is defined so that for any couple of third order tensors $(\boldsymbol{E}_2, \boldsymbol{E}_2')$,

$$\boldsymbol{E}_2' \overset{3}{\bullet} \boldsymbol{\mathcal{A}}_{22} \overset{3}{\bullet} \boldsymbol{E}_2 = \int_{\mathcal{B}} \left(\boldsymbol{E}_2' \cdot \boldsymbol{\xi}\right) : \Delta\boldsymbol{\mathcal{C}} : \boldsymbol{\nabla} \boldsymbol{u}_{\mathcal{B}}^{(2)}[\boldsymbol{E}_2](\boldsymbol{\xi}) \, \mathrm{d}V_\xi. \tag{1.125}$$

Let the 6th order tensor $\boldsymbol{M}^{(6)}$ be defined as:

$$\boldsymbol{M}^{(6)} = \int_{\mathcal{B}} \boldsymbol{\xi} \otimes \Delta\boldsymbol{\mathcal{C}} \otimes \boldsymbol{\xi} \, \mathrm{d}V_\xi \quad \text{i.e.} \quad M_{aijklb}^{(6)} = \int_{\mathcal{B}} \xi_a \, \Delta\mathcal{C}_{ijkl} \, \xi_b \, \mathrm{d}V_\xi. \tag{1.126}$$

Then, for ellipsoids, knowing the tensor $\boldsymbol{A}_2$ and inserting expression (1.108) for the second Eshelby solution in (1.125), $\boldsymbol{\mathcal{A}}_{22}$ is computed as:

$$[\boldsymbol{\mathcal{A}}_{22}]_{abcijk} = M_{cabmnp}^{(6)} [\boldsymbol{\mathcal{I}}^{(6)} + \boldsymbol{A}_2]_{mnpijk}. \tag{1.127}$$

As for $\boldsymbol{M}^{(2)}$, when $\mathcal{B}$ is an ellipsoid with semi-principal axes a_j and principal directions $\boldsymbol{\eta}_j$, $\boldsymbol{M}^{(6)}$ is given by:

$$\boldsymbol{M}^{(6)} = \frac{4\pi}{15} a_1 a_2 a_3 \sum_{j=1}^{3} a_j^2 (\boldsymbol{\eta}_j \otimes \Delta\boldsymbol{\mathcal{C}} \otimes \boldsymbol{\eta}_j). \tag{1.128}$$

In particular, if $\mathcal{B}$ is a sphere of radius a, $M_{aijklb}^{(6)} = (4\pi a^5/15)\delta_{ab}\Delta\mathcal{C}_{ijkl}$.

1.3.4 Inertial polarization tensors

Similarly to the elastic moment tensors, we define for (i) the couple of tensors $(\boldsymbol{E}_p, \boldsymbol{E}_q)$ and (ii) a scalar weight function ρ (typically, a material density) defined on $\mathcal{B}$ the $(p+q+2)$-th order tensors $\boldsymbol{\mathcal{Q}}_{pq}^{\rho}$ such that, for $p = 0$ or $q = 0$:

$$\int_{\mathcal{B}} \rho(\boldsymbol{\xi}) \, \boldsymbol{u}_{\mathcal{B}}^{(p)}[\boldsymbol{E}_p](\boldsymbol{\xi}) \, \mathrm{d}V_\xi = \boldsymbol{E}_p \bullet \boldsymbol{\mathcal{Q}}_{p0}^{\rho} = \boldsymbol{\mathcal{Q}}_{0p}^{\rho} \bullet \boldsymbol{E}_p, \tag{1.129}$$

and, for $p \neq 0$ and $q \neq 0$,

$$\int_{\mathcal{B}} \rho(\boldsymbol{\xi}) \, \boldsymbol{u}_{\mathcal{B}}^{(p)}[\boldsymbol{E}_p](\boldsymbol{\xi}) \cdot \boldsymbol{u}_{\mathcal{B}}^{(q)}[\boldsymbol{E}_q](\boldsymbol{\xi}) \, \mathrm{d}V_\xi = \boldsymbol{E}_p \bullet \boldsymbol{\mathcal{Q}}_{pq}^{\rho} \bullet \boldsymbol{E}_q. \tag{1.130}$$

Whenever ρ is a mass density, the left-hand-side of (1.130) corresponds to a "mass product" (the inertial counterpart of the "stiffness product" computed thanks to the EMTs defined above) between two FSTP solutions and will intervene in time-harmonic contexts. Thus the choice of the name "inertial polarization tensors".

From definition (1.130), it is straightforward that $\boldsymbol{E}_p \bullet \boldsymbol{\mathcal{Q}}^{\rho}_{pq} \bullet \boldsymbol{E}_q = \boldsymbol{E}_q \bullet \boldsymbol{\mathcal{Q}}^{\rho}_{qp} \bullet \boldsymbol{E}_p$. Moreover, in the upcoming works, the considered density ρ will be constant, and we therefore focus on the particular tensors $\boldsymbol{\mathcal{Q}}_{pq} := \boldsymbol{\mathcal{Q}}^{1}_{pq}$ (so that $\boldsymbol{\mathcal{Q}}^{\rho}_{pq} = \rho \boldsymbol{\mathcal{Q}}_{pq}$ for constant ρ). For these $\boldsymbol{\mathcal{Q}}_{pq}$, from the symmetry properties of Eshelby's solutions and similarly to the EMTs, the analog of Lemma 1.9 holds:

Lemma 1.10. *For any centrally-symmetric inclusion $\mathcal{B}$, $\boldsymbol{\mathcal{Q}}_{pq} = \boldsymbol{0}$ whenever $p+q$ is odd.*

However, unlike for the EMTs, both Eshelby solutions of order p and q are required to evaluate $\boldsymbol{\mathcal{Q}}_{pq}$.

Expressions for ellipsoids When $\mathcal{B}$ is an ellipsoid, the first non-zero of these polarization tensors are the fourth-order tensors $\boldsymbol{\mathcal{Q}}_{02}$ and $\boldsymbol{\mathcal{Q}}_{11}$. From the second Eshelby solution (1.114), we can compute for any third-order tensor $\boldsymbol{E}_2$:

$$\int_{\mathcal{B}} \boldsymbol{u}^{(2)}_{\mathcal{B}}[\boldsymbol{E}_2](\boldsymbol{\xi}) \, \mathrm{d}V_\xi = \int_{\mathcal{B}} \frac{1}{2} \Big((\boldsymbol{I}^{(6)} + \boldsymbol{\mathcal{F}} \bullet \boldsymbol{A}_2) \bullet \boldsymbol{E}_2 \Big) : \boldsymbol{\xi}^{\otimes 2} \, \mathrm{d}V_\xi, \tag{1.131}$$

and $\boldsymbol{\mathcal{Q}}_{02}$ is therefore defined by:

$$\boldsymbol{\mathcal{Q}}_{02} \bullet \boldsymbol{E}_2 = \frac{1}{2} \Big((\boldsymbol{I}^{(6)} + \boldsymbol{\mathcal{F}} \bullet \boldsymbol{A}_2) \bullet \boldsymbol{E}_2 \Big) : \boldsymbol{M}^{(2)}. \tag{1.132}$$

After suitable permutation of the indices, $\boldsymbol{\mathcal{Q}}_{02}$ is given in index notations by:

$$[\boldsymbol{\mathcal{Q}}_{02}]_{iabc} = \frac{1}{2} \Big[\boldsymbol{I}^{(6)} + \boldsymbol{\mathcal{F}} \bullet \boldsymbol{A}_2 \Big]_{ijkabc} M^{(2)}_{jk}. \tag{1.133}$$

Similarly, for two second-order tensors $\boldsymbol{E}_1$ and $\boldsymbol{E}'_1$ and using the first Eshelby solution (1.98), one obtains

$$\boldsymbol{E}_1 : \boldsymbol{\mathcal{Q}}_{11} : \boldsymbol{E}'_1 = \int_{\mathcal{B}} \Big[\Big((\boldsymbol{I}^{(4)} + \boldsymbol{A}_1) : \boldsymbol{E}_1 \Big) \cdot \boldsymbol{\xi} \Big] \cdot \Big[\Big((\boldsymbol{I}^{(4)} + \boldsymbol{A}_1) : \boldsymbol{E}'_1 \Big) \cdot \boldsymbol{\xi} \Big] \, \mathrm{d}V_\xi, \tag{1.134}$$

which provides the expression of $\boldsymbol{\mathcal{Q}}_{11}$ as:

$$[\boldsymbol{\mathcal{Q}}_{11}]_{ijab} = \Big[\boldsymbol{I}^{(4)} + \boldsymbol{A}_1 \Big]_{klij} M^{(2)}_{lc} \Big[\boldsymbol{I}^{(4)} + \boldsymbol{A}_1 \Big]_{kcab}. \tag{1.135}$$

1.4 Conclusions

In this introductory chapter concerning the free-space transmission problem, most of the accessory tools needed thereafter were provided, with explicit expressions whenever available. An important invertibility result was first stated by Theorem 1.3, which will permit upcoming estimates of expansion residuals. Free-space transmission problems with polynomial background displacements were then addressed, and some of their solutions that we called the *Eshelby solutions* were specified for ellipsoidal inhomogeneities. Finally, "stiffness" and "mass" bilinear forms (corresponding to elastic and kinetic energy) involving one or two of these solutions were expressed in closed-form thanks to the introduction of elastic moment tensors and inertial polarization tensors.

1.A (Bi)harmonic potentials and Eshelby tensors

The n-th order tensor-valued harmonic and biharmonic potentials $\boldsymbol{\phi}^{(n)}$ and $\boldsymbol{\psi}^{(n)}$ associated to a shape $\mathcal{B}$ are defined by:

$$\boldsymbol{\phi}^{(n)}(\boldsymbol{x}) = \int_{\mathcal{B}} \frac{\boldsymbol{\xi}^{\otimes n}}{|\boldsymbol{\xi} - \boldsymbol{x}|} \, \mathrm{d}V_{\xi}, \qquad \boldsymbol{\psi}^{(n)}(\boldsymbol{x}) = \int_{\mathcal{B}} \boldsymbol{\xi}^{\otimes n} |\boldsymbol{\xi} - \boldsymbol{x}| \, \mathrm{d}V_{\xi}, \tag{1.136}$$

or in index notation (in which case the order of the potential is indicated by the number of indices) by:

$$\phi_{ab\ldots m}(\boldsymbol{x}) = \int_{\mathcal{B}} \frac{\xi_a \xi_b \ldots \xi_m}{|\boldsymbol{\xi} - \boldsymbol{x}|} \, \mathrm{d}V_{\xi}, \qquad \psi_{ab\ldots m}(\boldsymbol{x}) = \int_{\mathcal{B}} \xi_a \xi_b \ldots \xi_m |\boldsymbol{\xi} - \boldsymbol{x}| \, \mathrm{d}V_{\xi}. \tag{1.137}$$

Since they are the elementary bricks to compute many of the integrals involved in our study in the isotropic case, a compilation of the expressions we need is given in this section. It includes some of these potentials and their derivatives when $\mathcal{B}$ is an ellipsoid whose axis are aligned with the Cartesian basis $(\boldsymbol{e}_i)$ and whose half-lengths are noted (a_1, a_2, a_3).

Remark 1.13. *The following expressions are almost all provided in [Mura, 1982], along with more general results and many particular cases for specific ellipsoids. However, we chose to reproduce them here (with slight simplifications) so that the dissertation is as self-consistent as possible and the interested reader is able to reproduce most of our upcoming numerical experiments without referring extensively to additional material.*

1.A.1 Elliptic integrals

$\boldsymbol{\phi}^{(n)}$ and $\boldsymbol{\psi}^{(n)}$ will be given in the following parts as functions of *elliptic integrals* $I_{i\ldots k}$ whose expressions are therefore recalled here:

$$\begin{aligned} I_{i\ldots k}(\lambda(\boldsymbol{x})) &= 2\pi a_1 a_2 a_3 \int_{\lambda(\boldsymbol{x})}^{\infty} \frac{\mathrm{d}s}{(a_i^2 + s) \ldots (a_k^2 + s)\Delta(s)} \\ \text{with: } \Delta(s) &= \sqrt{(a_1^2 + s)(a_2^2 + s)(a_3^2 + s)}. \end{aligned} \tag{1.138}$$

The lower bound $\lambda(\boldsymbol{x})$ of the integral above is itself defined implicitly by (i) $\lambda(\boldsymbol{x}) = 0$ if $\boldsymbol{x} \in \mathcal{B}$ and (ii) $\lambda(\boldsymbol{x})$ is the largest positive root of $U(s; \boldsymbol{x})$ if $\boldsymbol{x} \notin \mathcal{B}$, U being defined by:

$$U(s; \boldsymbol{x}) = 1 - \left[\frac{x_1^2}{a_1^2 + s} + \frac{x_2^2}{a_2^2 + s} + \frac{x_3^2}{a_3^2 + s} \right] \tag{1.139}$$

In the case of a sphere of ray a, the computation of the elliptic integrals is simpler and results in:

$$I^{(n)}(\lambda) = \frac{4\pi a^3}{(2n+1)(a^2 + \lambda)^{n+\frac{1}{2}}} \tag{1.140}$$

where (n) indicates the order of the integral.

Since we aim to compute the potentials $\boldsymbol{\phi}^{(n)}$ and $\boldsymbol{\psi}^{(n)}$ for $\boldsymbol{x} \in \mathcal{B}$, we actually considered only this case, for which $\lambda = 0$ and the $I_{i\ldots k}$ are constants w.r.t. $\boldsymbol{x}$. The general case $\lambda \neq 0$ is addressed in [Mura, 1982, Chap. 11, from eq. 11.38].

1.A.2 Harmonic potentials

The following expressions are given in index notation, and with Mura's convention: upper case indexes take the same value than the corresponding lower case indexes, and repetition of lower-case indexes still stands for summation. For example, $x_i x_i I_I = \sum_i x_i^2 I_i = x_1^2 I_1 + x_2^2 I_2 + x_3^2 I_3$ and $x_i I_I$ represents the vector with components ($x_1 I_1$,$x_2 I_2$, $x_3 I_3$).

Scalar harmonic potential $\phi^{(0)}$:

$$\begin{aligned} \phi &= \frac{1}{2}(I - x_r x_r I_R) \\ \phi_{,k} &= -x_k I_K \\ \phi_{,kl} &= -\delta_{kl} I_K \end{aligned} \tag{1.141}$$

First-order harmonic potential $\boldsymbol{\phi}^{(1)}$:

$$\begin{aligned} \phi_a =& \frac{a_A^2}{2} x_a (I_A - x_r x_r I_{RA}) \\ \phi_{a,k} =& \frac{a_A^2}{2} (I_A - x_r x_r I_{RA}) \delta_{ak} - a_A^2 x_a x_k I_{AK} \\ \phi_{a,kl} =& - a_A^2 (\delta_{ak} x_l I_{AL} + (\delta_{al} x_k + \delta_{kl} x_a) I_{AK}) \end{aligned} \tag{1.142}$$

Second-order harmonic potential $\boldsymbol{\phi}^{(2)}$:

$$\begin{aligned} \phi_{ab} =& \frac{a_A^2}{2} \Big\{ x_a x_b a_B^2 (I_{AB} - x_r x_r I_{RAB}) \\ & \quad + \frac{1}{4} \delta_{ab} (I - a_A^2 I_A - x_r x_r (I_R - a_A^2 I_{RA}) + x_r x_r x_s x_s (I_{RS} - a_A^2 I_{RSA})) \Big\} \\ \phi_{ab,k} =& a_A^2 \Big\{ \frac{a_B^2}{2} (\delta_{ak} x_b + \delta_{bk} x_a)(I_{AB} - x_r x_r I_{RAB}) - x_a x_b x_k a_B^2 I_{ABK} \\ & - \frac{\delta_{ab}}{2} x_k (I_K - a_A^2 I_{AK} - x_r x_r (I_{RK} - a_A^2 I_{RAK})) \Big\} \\ \phi_{ab,kl} =& a_A^2 \Big\{ \frac{a_B^2}{2} (\delta_{ak}\delta_{bl} + \delta_{bk}\delta_{al})(I_{AB} - x_r x_r I_{RAB}) - a_B^2 (\delta_{ak} x_b + \delta_{bk} x_a) x_l I_{LAB} \\ & - (\delta_{al} x_b x_k + x_a \delta_{bl} x_k + x_a x_b \delta_{kl}) a_B^2 I_{ABK} \\ & - \frac{\delta_{ab}\delta_{kl}}{2} (I_K - a_A^2 I_{AK} - x_r x_r (I_{RK} - a_A^2 I_{RAK})) \\ & + \delta_{ab} x_k x_l (I_{LK} - a_A^2 I_{LAK}) \Big\} \end{aligned} \tag{1.143}$$

1.A.3 Biharmonic potentials

Scalar biharmonic potential $\psi^{(0)}$:

$$\psi = \sum_{i=1}^{3} \frac{a_i^2}{8} (I - a_i^2 I_I) + \frac{1}{4} x_r x_r (I - a_R^2 I_R) - \frac{1}{8} x_r x_r x_s x_s (I_R - a_S^2 I_{RS}) \tag{1.144}$$

Its gradients are thus given by:

$$
\begin{aligned}
\psi_{,p} =& \frac{x_p}{2}(I - a_P^2 I_P - x_r x_r (I_R - a_P^2 I_{RP})) \\
\psi_{,pj} =& \frac{\delta_{pj}}{2}(I - a_P^2 I_P - x_r x_r (I_R - a_P^2 I_{RP})) - x_j x_p (I_J - a_P^2 I_{JP}) \\
\psi_{,pjk} =& -\delta_{pj} x_k (I_K - a_P^2 I_{PK}) + (\delta_{jk} x_p + \delta_{pk} x_j)(I_J - a_P^2 I_{JP}) \\
\psi_{,pjkl} =& -\delta_{pj}\delta_{kl}(I_K - a_P^2 I_{PK}) + (\delta_{jk}\delta_{pl} + \delta_{pk}\delta_{jl})(I_J - a_P^2 I_{JP})
\end{aligned}
\tag{1.145}
$$

First-order biharmonic potential $\boldsymbol{\psi}^{(1)}$: This potential intervenes in e.g. the computation of the second Eshelby tensor $\boldsymbol{\mathcal{D}}_2$, and we provide only its derivatives of second to fourth order:

$$
\begin{aligned}
\psi_{a,pj} =& \frac{a_A^2}{2}\Big\{\delta_{ap} x_j (I_J - a_A^2 I_{AJ} - x_r x_r (I_{RJ} - a_A^2 I_{RAJ})) \\
&+ (\delta_{aj} x_p + x_a \delta_{pj})(I_P - a_A^2 I_{AP} - x_r x_r (I_{RP} - a_A^2 I_{RAP})) \\
&- 2 x_a x_j x_p (I_{PJ} - a_A^2 I_{APJ})\Big\}
\end{aligned}
\tag{1.146}
$$

Third derivative:

$$
\begin{aligned}
\psi_{a,pjk} =& \frac{a_A^2}{2}\Big\{\delta_{ap}\delta_{jk}(I_J - a_A^2 I_{AJ} - x_r x_r (I_{RJ} - a_A^2 I_{RAJ})) \\
&+ (\delta_{aj}\delta_{pk} + \delta_{ak}\delta_{pj})(I_P - a_A^2 I_{AP} - x_r x_r (I_{RP} - a_A^2 I_{RAP})) \\
&- 2(\delta_{aj} x_p + x_a \delta_{pj}) x_k (I_{PK} - a_A^2 I_{APK}) - 2(\delta_{ak} x_p + x_a \delta_{pk}) x_j (I_{PJ} - a_A^2 I_{APJ}) \\
&- 2\delta_{ap} x_j x_k (I_{JK} - a_A^2 I_{AJK}) - 2 x_a x_p \delta_{jk}(I_{PJ} - a_A^2 I_{APJ})
\end{aligned}
\tag{1.147}
$$

Fourth derivative:

$$
\begin{aligned}
\psi_{a,pjkl} =& -a_A^2\Big\{\delta_{ap}\delta_{jk} x_l (I_{LJ} - a_A^2 I_{LAJ}) + (\delta_{aj}\delta_{pk} + \delta_{ak}\delta_{pj}) x_l (I_{LP} - a_A^2 I_{LAP}) \\
&+ \left[(\delta_{aj}\delta_{pl} + \delta_{al}\delta_{pj}) x_k + (\delta_{aj} x_p + x_a \delta_{pj})\delta_{kl}\right](I_{PK} - a_A^2 I_{APK}) \\
&+ \left[(\delta_{ak}\delta_{pl} + \delta_{al}\delta_{pk}) x_j + (\delta_{ak} x_p + x_a \delta_{pk})\delta_{jl}\right](I_{PJ} - a_A^2 I_{APJ}) \\
&+ \delta_{ap}(\delta_{jl} x_k + x_j \delta_{kl})(I_{JK} - a_A^2 I_{AJK}) \\
&+ (\delta_{al} x_p + x_a \delta_{pl})\delta_{jk}(I_{PJ} - a_A^2 I_{APJ})\Big\}
\end{aligned}
\tag{1.148}
$$

Second-order harmonic potential $\boldsymbol{\psi}^{(2)}$: As above, only the second and third order derivatives of $\boldsymbol{\psi}^{(2)}$ are given:

$$\begin{aligned}
\psi_{ab,pj} =& \frac{a_A^2 a_B^2}{8}\Big\{ -(\delta_{ap}\delta_{bj}+\delta_{aj}\delta_{bp})\Big[I_A - a_B^2 I_{AB} - 2x_r x_r(I_{RA} - a_B^2 I_{RAB}) \\
&\qquad\qquad\qquad\qquad\qquad + x_r x_r x_s x_s (I_{RSA} - a_B^2 I_{RSAB}))\Big] \\
&\qquad + 4(\delta_{ap}x_b + x_a\delta_{bp})x_j(I_{AJ} - a_B^2 I_{ABJ} - x_r x_r(I_{RAJ} - a_B^2 I_{RABJ})) \\
&\qquad + 4(x_a x_b \delta_{pj} + x_a\delta_{bj}x_p + \delta_{aj}x_b x_p)(I_{AB} - a_P^2 I_{ABP} - x_r x_r(I_{RAJ} - a_P^2 I_{RABP})) \\
&\qquad - 8x_a x_b x_p x_j (I_{ABJ} - a_P^2 I_{ABPJ})\Big\} \\
&+ \frac{a_A^2}{8}\delta_{ab}\Big\{\delta_{pj}\Big[I - (a_P^2 + a_A^2)I_A + a_P^4 I_{AP} - 2x_r x_r(I_R - (a_P^2 + a_A^2)I_{RA} + a_P^4 I_{RAP}) \\
&\qquad\qquad + x_r x_r x_s x_s (I_{RS} - (a_P^2 + a_A^2)I_{RSA} + a_P^4 I_{RSAP})\Big] \\
&\qquad - 4x_p x_j\Big[I_J - (a_P^2 + a_A^2)I_{AJ} + a_P^4 I_{APJ} \\
&\qquad\qquad - x_r x_r(I_{RJ} - (a_P^2 + a_A^2)I_{RAJ} + a_P^4 I_{RAPJ})\Big]\Big\}
\end{aligned} \tag{1.149}$$

Third derivative:

$$\begin{aligned}
\psi_{ab,pjk} =& \frac{a_A^2 a_B^2}{2}\Big\{(\delta_{ap}\delta_{bj}+\delta_{aj}\delta_{bp})x_k(I_{AK} - a_B^2 I_{ABK} - x_r x_r(I_{RAK} - a_B^2 I_{RABK})) \\
&\quad + (\delta_{ap}\delta_{bk}+\delta_{ak}\delta_{bp})x_j(I_{AJ} - a_B^2 I_{ABJ} - x_r x_r(I_{RAJ} - a_B^2 I_{RABJ})) \\
&\quad + (\delta_{ap}x_b + x_a\delta_{bp})\delta_{jk}(I_{AJ} - a_B^2 I_{ABJ} - x_r x_r(I_{RAJ} - a_B^2 I_{RABJ})) \\
&\quad + [(\delta_{aj}\delta_{bk}+\delta_{ak}\delta_{bj})x_p + (\delta_{aj}\delta_{pk}+\delta_{ak}\delta_{pj})x_b + (\delta_{bj}\delta_{pk}+\delta_{bk}\delta_{pj})x_a] \\
&\qquad (I_{AB} - a_P^2 I_{ABP} - x_r x_r(I_{RAJ} - a_P^2 I_{RABP})) \\
&\quad - 2(\delta_{aj}x_b x_p + x_a\delta_{bj}x_p + x_a x_b\delta_{pj})x_k(I_{ABK} - a_P^2 I_{ABPK}) \\
&\quad - 2(\delta_{ak}x_b x_p + x_a\delta_{bk}x_p + x_a x_b\delta_{pk})x_j(I_{ABJ} - a_P^2 I_{ABPJ}) \\
&\quad - 2(\delta_{ap}x_b + x_a\delta_{bp})x_j x_k(I_{AJK} - a_B^2 I_{ABJK}) \\
&\quad - 2x_a x_b x_p \delta_{jk}(I_{ABJ} - a_P^2 I_{ABPJ})\Big\} \\
&- \frac{a_A^2}{2}\delta_{ab}x_p\Big\{\delta_{jk}(I_J - (a_P^2 + a_A^2)I_{AJ} + a_P^4 I_{APJ}) \\
&\qquad - \delta_{jk}x_r x_r(I_{RJ} - (a_P^2 + a_A^2)I_{RAJ} + a_P^4 I_{RAPJ}) \\
&\qquad - 2x_j x_k(I_{JK} - (a_P^2 + a_A^2)I_{AJK} + a_P^4 I_{APJK})\Big\}
\end{aligned} \tag{1.150}$$

1.A.4 Eshelby tensors

We now are in position to provide explicit expression for the fourth and fifth-order Eshelby tensors $\boldsymbol{\mathcal{D}}_1$ and $\boldsymbol{\mathcal{D}}_2$ for any ellipsoid.

First Eshelby tensor The fourth-order tensor $\boldsymbol{\mathcal{D}}_1$ is given [Mura, 1982, eq. 11.34] with the help of the derivatives of the scalar harmonic and biharmonic potentials $\phi^{(0)}$ and $\psi^{(0)}$:

$$8\pi(1-\nu)\mathcal{D}_{ijkl} = \psi_{,ijkl} - 2\nu\phi_{,ij}\delta_{kl} - (1-\nu)\Big[\phi_{,jk}\delta_{il} + \phi_{,ik}\delta_{jl} + \phi_{,jl}\delta_{ik} + \phi_{,il}\delta_{jk}\Big]. \tag{1.151}$$

For $\boldsymbol{x} \in \mathcal{B}$, we use the above expressions (1.141) and (1.145) for these potentials, which results in [Mura, 1982, eq. 11.42]:

$$\begin{aligned}8\pi(1-\nu)\mathcal{D}_{ijkl} =& \delta_{ij}\delta_{kl}(2\nu I_I - I_K + a_I^2 I_{IK}) \\ &+ (\delta_{ik}\delta_{jl} + \delta_{jk}\delta_{il})\left(a_I^2 I_{IJ} - I_J + (1-\nu)(I_K + I_L)\right)\end{aligned} \tag{1.152}$$

For the unit sphere, the elliptic integrals are given by (1.140) and we obtain the expression (1.99).

Second Eshelby tensor Similarly, the fifth-order tensor $\boldsymbol{\mathcal{D}}_2$ is given by [Mura, 1982, eq 12.11], with the help of the harmonic and biharmonic potentials of first order $\boldsymbol{\phi}^{(1)}$ and $\boldsymbol{\psi}^{(1)}$:

$$8\pi(1-\nu)\mathcal{D}_{ijklq} = \psi_{q,ijkl} - 2\nu\phi_{q,ij}\delta_{kl} - (1-\nu)\Big[\phi_{q,jk}\delta_{il} + \phi_{q,ik}\delta_{jl} + \phi_{q,jl}\delta_{ik} + \phi_{q,il}\delta_{jk}\Big]. \tag{1.153}$$

Inserting the expressions (1.142) and (1.148) into (1.153), we obtain:

$$\begin{aligned}8\pi(1-\nu)\mathcal{D}_{ijklq} =& a_Q^2\Big\{\delta_{il}\delta_{kq}x_j(a_Q^2 I_{JLQ} - I_{JL}) \\ &\quad + (\delta_{jl}\delta_{kq}x_i + \delta_{ij}\delta_{kq}x_l)(a_Q^2 I_{ILQ} - I_{IL}) \\ &\quad + (\delta_{ik}\delta_{lq} + \delta_{iq}\delta_{kl})x_j(a_Q^2 I_{JKQ} - I_{JK}) \\ &\quad + \Big[(\delta_{jk}\delta_{lq} + \delta_{jq}\delta_{kl})x_i + \delta_{ij}\delta_{lq}x_k + \delta_{ij}\delta_{kl}x_q\Big](a_Q^2 I_{IKQ} - I_{IK}) \\ &\quad + \Big[(\delta_{iq}\delta_{jk} + \delta_{ik}\delta_{jq})x_l + (\delta_{iq}\delta_{jl} + \delta_{il}\delta_{jq})x_k + (\delta_{ik}\delta_{jl} + \delta_{il}\delta_{jk})x_q\Big] \\ &\qquad (a_Q^2 I_{LKQ} - I_{LK})\Big\} \\ &+ 2\nu a_Q^2\delta_{kl}(\delta_{iq}x_j I_{JQ} + (\delta_{ij}x_q + \delta_{jq}x_i)I_{IQ}) \\ &+ (1-\nu)a_Q^2\Big\{\delta_{il}(\delta_{kq}x_j I_{JQ} + (\delta_{jk}x_q + \delta_{jq}x_k)I_{KQ}) \\ &\qquad + \delta_{jl}(\delta_{iq}x_k I_{KQ} + (\delta_{ik}x_q + \delta_{kq}x_i)I_{IQ}) \\ &\qquad + \delta_{ik}(\delta_{lq}x_j I_{JQ} + (\delta_{jl}x_q + \delta_{jq}x_l)I_{LQ}) \\ &\qquad + \delta_{jk}(\delta_{iq}x_l I_{LQ} + (\delta_{il}x_q + \delta_{lq}x_i)I_{IQ})\Big\}.\end{aligned} \tag{1.154}$$

As expected, $\boldsymbol{\mathcal{D}}_2(\boldsymbol{x})$ is a linear function of $\boldsymbol{x}$ and we can therefore write $\boldsymbol{\mathcal{D}}_2(\boldsymbol{x}) = \boldsymbol{\nabla}\boldsymbol{\mathcal{D}}_2 \cdot \boldsymbol{x}$, $\boldsymbol{\nabla}\boldsymbol{\mathcal{D}}_2$ being a constant sixth-order tensor. For a sphere ($a_1 = a_2 = a_3 = a$), the elliptic integral expression (1.140) permits to compute:

$$I^{(2)} = \frac{4\pi}{5a^2}, \quad I^{(3)} = \frac{4\pi}{7a^4} \quad \text{and} \quad a^2 I^{(3)} - I^{(2)} = -\frac{8\pi}{35a^2}. \tag{1.155}$$

For the unit sphere ($a = 1$) computing the gradient of (1.154) results in:

$$
\begin{aligned}
70(1-\nu)\mathcal{D}_{ijklq,p} = &- 2\left(\delta_{ij}\delta_{lp} + \delta_{il}\delta_{jp} + \delta_{ip}\delta_{jl}\right)\delta_{kq} \\
&- 2\Big\{(\delta_{ik}\delta_{lq} + \delta_{iq}\delta_{kl})\delta_{jp} + \delta_{ip}(\delta_{jk}\delta_{lq} + \delta_{jq}\delta_{kl}) + \delta_{ij}(\delta_{kp}\delta_{lq} + \delta_{kl}\delta_{qp}) \\
&\quad + (\delta_{iq}\delta_{jk} + \delta_{ik}\delta_{jq})\delta_{lp} + (\delta_{iq}\delta_{jl} + \delta_{il}\delta_{jq})\delta_{kp} + (\delta_{ik}\delta_{jl} + \delta_{il}\delta_{jk})\delta_{qp}\Big\} \\
&+ 14\nu\left(\delta_{iq}\delta_{jp} + \delta_{ij}\delta_{qp} + \delta_{ip}\delta_{jq}\right)\delta_{kl} \\
&+ 7(1-\nu)\Big\{\delta_{il}(\delta_{jp}\delta_{kq} + \delta_{jq}\delta_{kp} + \delta_{jk}\delta_{qp}) + (\delta_{iq}\delta_{kp} + \delta_{ip}\delta_{kq} + \delta_{ik}\delta_{qp})\delta_{jl} \\
&\quad + \delta_{ik}(\delta_{jp}\delta_{lq} + \delta_{jq}\delta_{lp} + \delta_{jl}\delta_{qp}) + (\delta_{iq}\delta_{lp} + \delta_{ip}\delta_{lq} + \delta_{il}\delta_{qp})\delta_{jk}\Big\}.
\end{aligned}
\tag{1.156}
$$

Introducing the tensors $\boldsymbol{k}^{p,0}$ defined in Section 1.1.1 provides a more compact expression:

$$
\begin{aligned}
70(1-\nu)\mathcal{D}_{ijklq,p} = &- 2k^{6,0}_{ijklqp} + 14\nu k^{4,0}_{ijqp}\delta_{kl} \\
&+ 7(1-\nu)\left(\delta_{il}k^{4,0}_{jkqp} + \delta_{jl}k^{4,0}_{ikqp} + \delta_{ik}k^{4,0}_{jlqp} + \delta_{jk}k^{4,0}_{ilqp}\right).
\end{aligned}
\tag{1.157}
$$

Chapter 2

Displacement and misfit function expansions in static elasticity

Contents

This chapter aims to compute and justify a sixth-order expansion for a certain class of cost functionals, w.r.t. the size a of a inhomogeneity B_a nucleating in an elastic solid occupying a bounded domain Ω submitted to *static* excitations.

In Section 2.1, we begin by setting the elastostatic transmission problem featuring an inhomogeneity B_a in Ω. We next specify the hypothesis on the misfit functions that will be considered in this chapter and the next one. In particular, these functional depends on B_a implicitly through the perturbation $\boldsymbol{v}_a$ of the displacement in Ω, and the computation of their expansion is made easier by the use of an *adjoint field*. Consequently, after introducing a convenient volume integral equation framework, we compute in Section 2.2 the *inner* expansion (inside B_a) of $\boldsymbol{v}_a$ up to the fourth order.

Finally, in Section 2.3, using this expansion and the already known leading-order *outer* expansion (sufficient for our needs), we compute the sought sixth-order expansion for the cost functional. This expansion, stated in Theorem 2.4, is justified by an evaluation of the residual.

Appendix 2.A shows how some of the computations on the expansion of $\boldsymbol{v}_a$ presented in a general setting can be addressed in practice, in the case of two concentric isotropic spheres (the smallest being considered as the inclusion).

2.1 Transmission problem and misfit function.

This section is devoted to the presentation of the elastostatic transmission problem and the definition of the cost functional to be expanded.

2.1.1 Background, total and and perturbation displacements

An homogeneous elastic material ocupying the domain $\Omega \subset \mathbb{R}^3$ is considered, fully characterized by Hooke's Tensor $\boldsymbol{\mathcal{C}}$. It is submitted to volumic forces $\boldsymbol{f} \in C^\infty(\Omega)$. Prescribed displacement $\boldsymbol{u}_\text{D}$ and traction $\boldsymbol{t}_\text{N}$ are supported by the surfaces Γ_D and Γ_N such that $\Gamma_\text{D} \cup \Gamma_\text{N} = \partial\Omega$, $\Gamma_\text{D} \cap \Gamma_\text{N} = \emptyset$ and $|\Gamma_\text{D}| \neq 0$. These solicitations give rise to the background displacement $\boldsymbol{u}(\boldsymbol{x})$ satisfying the following problem:

$$\left| \begin{array}{ll} \text{div}(\boldsymbol{\mathcal{C}} : \boldsymbol{\nabla}\boldsymbol{u}(\boldsymbol{x})) + \boldsymbol{f}(\boldsymbol{x}) = \boldsymbol{0} & \text{in } \Omega \\ \boldsymbol{u}(\boldsymbol{x}) = \boldsymbol{u}_\text{D}(\boldsymbol{x}) & \text{on } \Gamma_\text{D} \\ \boldsymbol{t}[\boldsymbol{u}](\boldsymbol{x}) = \boldsymbol{t}_\text{N}(\boldsymbol{x}) & \text{on } \Gamma_\text{N} \end{array} \right. \tag{2.1}$$

where $\boldsymbol{t}[\boldsymbol{u}](\boldsymbol{x}) = \boldsymbol{\sigma}[\boldsymbol{u}](\boldsymbol{x}) \cdot \boldsymbol{n}(\boldsymbol{x}) = (\boldsymbol{\mathcal{C}} : \boldsymbol{\nabla}\boldsymbol{u}(\boldsymbol{x})) \cdot \boldsymbol{n}(\boldsymbol{x})$ is the traction vector associated with $\boldsymbol{u}$, $\boldsymbol{n}$ being the output normal to the surface $\partial\Omega$.

The weak formulation corresponding to problem (2.1) is:

$$\text{Find } \boldsymbol{u} \in \boldsymbol{W}(\boldsymbol{u}_\text{D}), \;\; \langle \boldsymbol{u}, \boldsymbol{w} \rangle_\Omega^{\mathcal{C}} = \int_\Omega \boldsymbol{f} \cdot \boldsymbol{w} + \int_{\Gamma_\text{N}} \boldsymbol{t}_\text{N} \cdot \boldsymbol{w}, \quad \forall \boldsymbol{w} \in \boldsymbol{W}_0, \tag{2.2}$$

and we recall that $\langle \boldsymbol{u}, \boldsymbol{w} \rangle_D^{\mathcal{C}}$ stands for:

$$\langle \boldsymbol{u}, \boldsymbol{w} \rangle_D^{\mathcal{C}} := \int_D \boldsymbol{\varepsilon}[\boldsymbol{u}] : \boldsymbol{\mathcal{C}} : \boldsymbol{\varepsilon}[\boldsymbol{w}] \; \text{d}V = \int_D \boldsymbol{\nabla}\boldsymbol{u} : \boldsymbol{\mathcal{C}} : \boldsymbol{\nabla}\boldsymbol{w} \; \text{d}V, \tag{2.3}$$

(the second equality holding again by virtue of the minor symmetries of $\boldsymbol{\mathcal{C}}$). The function spaces $\boldsymbol{W}$, $\boldsymbol{W}_0$ of admissible displacements are defined by

$$\boldsymbol{W}(\boldsymbol{u}_\text{D}) = \left\{ \; \boldsymbol{w} \in H^1(\Omega); \; \boldsymbol{u} = \boldsymbol{u}_\text{D} \text{ on } \Gamma_\text{D} \right\}, \qquad \boldsymbol{W}_0 = \boldsymbol{W}(\boldsymbol{0}). \tag{2.4}$$

Transmission by a small inhomogeneity. An inhomogeneity B_a of small size a and shape $\mathcal{B}$ is then introduced in the medium, centered at a point $\boldsymbol{z}$, so that we note $B_a = \boldsymbol{z} + a\mathcal{B}$. It is characterized by Hooke's tensor $\boldsymbol{\mathcal{C}}^\star$, defined similarly to (1.31) by two coefficients among $(\lambda^\star, \kappa^\star, \mu^\star, \nu^\star)$ if isotropic. We note the associated contrasts $\Delta\boldsymbol{\mathcal{C}} := \boldsymbol{\mathcal{C}}^\star - \boldsymbol{\mathcal{C}}$, and $(\Delta\lambda, \Delta\kappa, \Delta\mu)$ when applicable. By analogy with (2.2), the displacement $\boldsymbol{u}_a$ for the perturbed solid solves the weak formulation:

$$\text{Find } \boldsymbol{u}_a \in \boldsymbol{W}(\boldsymbol{u}_\text{D}), \;\; \langle \boldsymbol{u}, \boldsymbol{w} \rangle_\Omega^{\mathcal{C}_a} = \int_\Omega \boldsymbol{f} \cdot \boldsymbol{w} + \int_{\Gamma_\text{N}} \boldsymbol{t}_\text{N} \cdot \boldsymbol{w}, \quad \forall \boldsymbol{w} \in \boldsymbol{W}_0, \tag{2.5}$$

$\langle\cdot,\cdot\rangle$ being defined by (2.3), and $\boldsymbol{\mathcal{C}}_a(\boldsymbol{x}) = (1-\chi_{B_a}(\boldsymbol{x}))\boldsymbol{\mathcal{C}} + \chi_{B_a}(\boldsymbol{x})\boldsymbol{\mathcal{C}}^\star = \boldsymbol{\mathcal{C}} + \chi_{B_a}(\boldsymbol{x})\Delta\boldsymbol{\mathcal{C}}$ (where χ_{B_a} is B_a's characteristic function) is the piecewise-constant elasticity tensor of the whole solid. Subtracting (2.2) to (2.5), the perturbation displacement $\boldsymbol{v}_a := \boldsymbol{u}_a - \boldsymbol{u}$ is found to solve the weak formulation:

$$\text{Find } \boldsymbol{v}_a \in \boldsymbol{W}_0, \quad \langle \boldsymbol{v}_a, \boldsymbol{w}\rangle_\Omega^{\mathcal{C}_a} = -\langle \boldsymbol{u}, \boldsymbol{w}\rangle_{B_a}^{\Delta\mathcal{C}}, \quad \forall \boldsymbol{w} \in \boldsymbol{W}_0. \tag{2.6}$$

Remark 2.1. *The condition $\boldsymbol{f} \in C^\infty(\Omega)$ in* (2.1) *is adopted for the sake of simplicity and ensures $\boldsymbol{u} \in C^\infty(\Omega)$. Though it is satisfied in many applications (e.g. when the volumic forces such as weight are neglected in front of boundary tractions), it might may be weakened if needed, provided they allow sufficient regularity of $\boldsymbol{u}$ (C^4, as it will be seen later) at the chosen inhomogeneity location $\boldsymbol{z}$.*

2.1.2 Cost functional and adjoint field

We consider cost functionals $\mathbb{J}(B_a)$ that depend on the inhomogeneity $(B_a, \boldsymbol{\mathcal{C}}^\star)$ implicitly through the perturbed displacement $\boldsymbol{u}_a$ solution of (2.5), of the form:

$$\mathbb{J}(B_a) = J(\boldsymbol{u}_a) \quad \text{with} \quad J(\boldsymbol{w}) = \int_{\Omega^{\mathrm{m}}} \Psi_\Omega(\boldsymbol{x}; \boldsymbol{w}(\boldsymbol{x}))\,\mathrm{d}V_x + \int_{\Gamma^{\mathrm{m}}} \Psi_\Gamma(\boldsymbol{x}; \boldsymbol{w}(\boldsymbol{x}))\,\mathrm{d}S_x, \tag{2.7}$$

with the volume and surface densities $\Psi_\Omega : (\Omega^{\mathrm{m}} \times \mathbb{R}^3) \to \mathbb{R}$ and $\Psi_\Gamma : (\Gamma^{\mathrm{m}} \times \mathbb{R}^3) \to \mathbb{R}$ assumed to be twice differentiable in their second argument. Moreover, the corresponding second-order derivatives of Ψ_Ω and Ψ_Γ are assumed to have $C^{0,\gamma}$ regularity with respect to their second argument for some $\gamma > 0$. The supports Ω^{m} and Γ^{m} are open subsets of Ω and Γ_N, respectively; moreover we assume $\boldsymbol{z} \neq \Omega^{\mathrm{m}}$, which ensures that $B_a \cap \Omega^{\mathrm{m}} = \emptyset$ for a small enough. Using Taylor expansion with integral remainder of Ψ_Ω and Ψ_Γ, $J(\boldsymbol{u}_a)$ can be expanded about the background solution $\boldsymbol{u}$ as:

$$J(\boldsymbol{u}_a) = J(\boldsymbol{u}) + J'(\boldsymbol{u}; \boldsymbol{v}_a) + \frac{1}{2} J''(\boldsymbol{u}; \boldsymbol{v}_a) + R(\boldsymbol{u}; \boldsymbol{v}_a) \tag{2.8}$$

with:

$$\begin{aligned}
J'(\boldsymbol{u}; \boldsymbol{v}_a) &= \int_{\Omega^{\mathrm{m}}} \boldsymbol{\nabla}_2 \Psi_\Omega(\cdot; \boldsymbol{u}) \cdot \boldsymbol{v}_a \,\mathrm{d}V + \int_{\Gamma^{\mathrm{m}}} \boldsymbol{\nabla}_2 \Psi_\Gamma(\cdot; \boldsymbol{u}) \cdot \boldsymbol{v}_a \,\mathrm{d}S, \\
J''(\boldsymbol{u}; \boldsymbol{v}_a) &= \int_{\Omega^{\mathrm{m}}} \boldsymbol{\nabla}_{22} \Psi_\Omega(\cdot; \boldsymbol{u}) : (\boldsymbol{v}_a \otimes \boldsymbol{v}_a) \,\mathrm{d}V + \int_{\Gamma^{\mathrm{m}}} \boldsymbol{\nabla}_{22} \Psi_\Gamma(\cdot; \boldsymbol{u}) : (\boldsymbol{v}_a \otimes \boldsymbol{v}_a) \,\mathrm{d}S, \\
R(\boldsymbol{u}; \boldsymbol{v}_a) &= \int_0^1 (1-t) J''(\boldsymbol{u} + t\boldsymbol{v}_a; \boldsymbol{v}_a) \,\mathrm{d}t - \frac{1}{2} J''(\boldsymbol{u}; \boldsymbol{v}_a),
\end{aligned} \tag{2.9}$$

where, for any function ψ having two arguments, $\boldsymbol{\nabla}_k \psi$ denotes its gradient with respect with its k-th argument, and $\boldsymbol{\nabla}_{k\ell}\psi$ its second gradient w.r.t. k-th and ℓ-th arguments.

To evaluate the directional derivative $J'(\boldsymbol{u}; \boldsymbol{v}_a)$, it is convenient to introduce the *adjoint solution* $\boldsymbol{p}$ defined as the solution of the weak formulation

$$\text{Find } \boldsymbol{p} \in \boldsymbol{W}_0, \qquad \langle \boldsymbol{p}, \boldsymbol{w}\rangle_\Omega^{\mathcal{C}} = J'(\boldsymbol{u}; \boldsymbol{w}), \quad \forall \boldsymbol{w} \in \boldsymbol{W}_0. \tag{2.10}$$

Then, on setting $\boldsymbol{w} = \boldsymbol{p}$ in (2.6) and $\boldsymbol{w} = \boldsymbol{v}_a$ in (2.10), combining the resulting identities and exploiting the symmetry of the energy bilinear form, one obtains

$$J'(\boldsymbol{u}; \boldsymbol{v}_a) = -\langle \boldsymbol{p}, \boldsymbol{u}\rangle_{B_a}^{\Delta\mathcal{C}} - \langle \boldsymbol{p}, \boldsymbol{v}_a\rangle_{B_a}^{\Delta\mathcal{C}} = -\langle \boldsymbol{p}, \boldsymbol{u}_a\rangle_{B_a}^{\Delta\mathcal{C}}. \tag{2.11}$$

Least-squares misfit cost functional. One of the most simple of such cost functional is the one evaluating the misfit between a simulated displacement $\boldsymbol{w}$ and measurements $\boldsymbol{u}^{\mathrm{m}}$ resulting from e.g. experiments on a real configuration to be recovered, on a measurement surface $\Gamma^{\mathrm{m}} \subset \Gamma_N$:

$$J(\boldsymbol{w}) = \frac{1}{2} \int_{\Gamma^{\mathrm{m}}} |\boldsymbol{w} - \boldsymbol{u}^{\mathrm{m}}|^2 \,\mathrm{d}S. \tag{2.12}$$

It corresponds to $\Psi_\Gamma(\boldsymbol{x}, \boldsymbol{w}) = \frac{1}{2}|\boldsymbol{w}(\boldsymbol{x}) - \boldsymbol{u}^{\mathrm{m}}(\boldsymbol{x})|^2$ and $\Psi_\Omega = 0$ in the above formalism. In this case, the expansion (2.8) is exact and reads:

$$J'(\boldsymbol{u}; \boldsymbol{v}_a) = \int_{\Gamma^{\mathrm{m}}} (\boldsymbol{u} - \boldsymbol{u}^{\mathrm{m}}) \cdot \boldsymbol{v}_a \,\mathrm{d}S, \quad J''(\boldsymbol{u}; \boldsymbol{v}_a) = \frac{1}{2} \int_{\Gamma^{\mathrm{m}}} |\boldsymbol{v}_a|^2 \,\mathrm{d}S \quad \text{and} \quad R(\boldsymbol{u}; \boldsymbol{v}_a) = 0, \tag{2.13}$$

and the adjoint solution $\boldsymbol{p}$ is therefore defined by:

$$\text{Find } \boldsymbol{p} \in \boldsymbol{W}_0, \qquad \langle \boldsymbol{p}, \boldsymbol{w} \rangle_\Omega^{\mathcal{C}} = \int_{\Gamma^{\mathrm{m}}} (\boldsymbol{u} - \boldsymbol{u}^{\mathrm{m}}) \cdot \boldsymbol{w} \,\mathrm{d}S, \quad \forall \boldsymbol{w} \in \boldsymbol{W}_0. \tag{2.14}$$

The case of interior measurements of displacements recorded in a region $\Omega^{\mathrm{m}} \subset \Omega$ can be accommodated in a essentially identical fashion, setting $\Psi_\Gamma(\boldsymbol{x}, \boldsymbol{w}) = 0$ and $\Psi_\Omega = \frac{1}{2}|\boldsymbol{w}(\boldsymbol{x}) - \boldsymbol{u}^{\mathrm{m}}(\boldsymbol{x})|^2$, $\boldsymbol{x} \in \Omega^{\mathrm{m}}$.

Eventually, J' and J'' being expressed by (2.11) and (2.9) as linear and quadratic functionals of $\boldsymbol{v}_a$, it is readily seen that we need to know the asymptotic behavior of $\boldsymbol{v}_a$ to determine that of J. As it enables to make the dependency of the transmission problem on a more explicit, the framework of volumic integral equations is adopted for such study. This framework is now presented.

2.1.3 Volume integral equation (VIE) formulation

We first recall the definition of the Green's tensor of the considered problem, which is in the core of any integral equation formulation. We give the integral equation and representation equivalent to the transmission problem (2.5), involving integrals on the support B_a of the inhomogeneity. In order to (i) make use of the results of Chapter 1 and (ii) make the dependency in a explicit for the upcoming expansion, a scaling $B_a \to \mathcal{B}$ is then specified, along with the isomorphism mapping the functions defined in B_a to these defined in $\mathcal{B}$. Finally, the considered integral operator is shown to be invertible with bounded inverse by Theorem 2.1, which is a natural follow-up for bounded domains of Theorem 1.3.

2.1.3.1 Elastostatic Green's tensor

The elastostatic static Green's tensor $\boldsymbol{G}(\boldsymbol{\xi}, \boldsymbol{x})$ associated to the problem (2.1) is defined for any source point $\boldsymbol{x} \in \Omega$ by:

$$\left| \begin{array}{ll} \operatorname{div}(\boldsymbol{\mathcal{C}} : \boldsymbol{\nabla} \boldsymbol{G}(\cdot, \boldsymbol{x})) + \delta(\cdot - \boldsymbol{x}) \boldsymbol{I} = \boldsymbol{0} & \text{in } \Omega \\ \boldsymbol{G}(\cdot, \boldsymbol{x}) = \boldsymbol{0} & \text{on } \Gamma_{\mathrm{D}} \\ \boldsymbol{t}[\boldsymbol{G}(\cdot, \boldsymbol{x})] = \boldsymbol{0} & \text{on } \Gamma_{\mathrm{N}}. \end{array} \right. \tag{2.15}$$

The components $[\boldsymbol{G}(\boldsymbol{\xi}, \boldsymbol{x})]_{ij}$ denote the i-th component of the displacement at $\boldsymbol{\xi}$ resulting from a unitary force imposed at $\boldsymbol{x}$ in the j-th direction. Consequently, the inner products apply first on the "displacement" index of $\boldsymbol{G}$. Green's tensor can be decomposed according to:

$$\boldsymbol{G}(\boldsymbol{\xi}, \boldsymbol{x}) = \boldsymbol{G}_\infty(\boldsymbol{\xi} - \boldsymbol{x}) + \boldsymbol{G}_{\mathrm{C}}(\boldsymbol{\xi}, \boldsymbol{x}) \tag{2.16}$$

where $\boldsymbol{G}_\infty(\boldsymbol{r})$ is the (singular) full-space Green's tensor previously introduced in Section 1.1.3. To account for the homogeneous boundary conditions in (2.15), the complementary part $\boldsymbol{G}_\mathrm{C}(\boldsymbol{\xi},\boldsymbol{x})$ is the solution the elastostatic boundary-value problem:

$$\left|\begin{array}{ll} \operatorname{div}(\boldsymbol{\mathcal{C}}:\boldsymbol{\nabla}\boldsymbol{G}_\mathrm{C}(\cdot,\boldsymbol{x}))=\boldsymbol{0} & \text{in } \Omega \\ \boldsymbol{G}(\cdot,\boldsymbol{x})=-\boldsymbol{G}_\infty(\cdot-\boldsymbol{x}) & \text{on } \Gamma_\mathrm{D} \\ \boldsymbol{t}[\boldsymbol{G}(\cdot,\boldsymbol{x})]=-\boldsymbol{t}[\boldsymbol{G}_\infty(\cdot-\boldsymbol{x})] & \text{on } \Gamma_\mathrm{N}. \end{array}\right. \tag{2.17}$$

Due to the regularity of the boundary data of this problem for any $\boldsymbol{x}\in\Omega$, $\boldsymbol{G}_\mathrm{C}(\cdot,\boldsymbol{x})\in C^\infty(\Omega;\mathbb{R}^{3,3})$ and in particular is bounded at $\boldsymbol{\xi}=\boldsymbol{x}$. Eventually, on applying the first equation of (2.15) to a test function $\boldsymbol{w}\in\boldsymbol{W}_0\cap C^0(\omega_{\boldsymbol{x}})$ (where $\omega_{\boldsymbol{x}}$ is a neighborhood of $\boldsymbol{x}$) and integrating by part the first term over Ω, Green's tensor is seen to verify:

$$\langle\boldsymbol{G}(\cdot,\boldsymbol{x}),\boldsymbol{w}\rangle_\Omega^{\mathcal{C}}=\boldsymbol{x}(\boldsymbol{x})\quad\forall\boldsymbol{w}\in\boldsymbol{W}_0\cap C^0(\omega_{\boldsymbol{x}}), \tag{2.18}$$

where $\omega_{\boldsymbol{x}}$ is a neighborhood of $\boldsymbol{x}$.

2.1.3.2 Integral equation and representation for perturbation

Setting (i) $\boldsymbol{w}=\boldsymbol{G}(\cdot,\boldsymbol{x})$ in (2.6), (ii) $\boldsymbol{w}=\boldsymbol{v}_a$ in (2.18) and (iii) subtracting the two resulting equalities, we obtain the governing volume integral equation (VIE) for $\boldsymbol{v}_a$:

$$\mathcal{L}_a[\boldsymbol{v}_a](\boldsymbol{x})=-\langle\boldsymbol{u},\boldsymbol{G}(\cdot,\boldsymbol{x})\rangle_{B_a}^{\Delta\mathcal{C}},\quad\forall\boldsymbol{x}\in B_a\cup\Omega\setminus\overline{B_a}, \tag{2.19}$$

where the linear integral operator $\mathcal{L}_a$ is defined by

$$\mathcal{L}_a[\boldsymbol{v}](\boldsymbol{x}):=\boldsymbol{v}(\boldsymbol{x})+\langle\boldsymbol{v},\boldsymbol{G}(\cdot,\boldsymbol{x})\rangle_{B_a}^{\Delta\mathcal{C}}. \tag{2.20}$$

Note that the integral arising from steps (i) and (ii) above are well-defined for $\boldsymbol{x}\in B_a\cup\Omega\setminus\overline{B_a}$ due to interior elliptic regularity of $\boldsymbol{v}_a$ and the fact that $\boldsymbol{\nabla}\boldsymbol{G}(\cdot,\boldsymbol{x})\in L^1(\Omega)$. The equality (2.19) can be understood differently whether or not $\boldsymbol{x}\in B_a$. If $\boldsymbol{x}\in B_a$, (2.19) is an integro-differential equation of the Lippman-Schwinger type to be solved to compute the restrictions $\boldsymbol{v}_{a|B_a}$ and $\boldsymbol{\nabla}\boldsymbol{v}_{a|B_a}$. Once this step is performed, $\boldsymbol{v}_a$ is given outside B_a by (2.19), this time written as the integral representation:

$$\boldsymbol{v}_a(\boldsymbol{x})=-\langle\boldsymbol{u}_a,\boldsymbol{G}(\cdot,\boldsymbol{x})\rangle_{B_a}^{\Delta\mathcal{C}},\quad\forall\boldsymbol{x}\notin\overline{B_a}. \tag{2.21}$$

2.1.3.3 Scaling on the reference shape

For easier reference to the previously studied FSTPs (Sections 1.2 and 1.3), and to take into account the dependency w.r.t. a of the integrals over the small inhomogeneity B_a, it will be convenient to rescale the integrals intervening in (2.20) onto the fixed reference domain $\mathcal{B}$. We consequently define the scaled counterparts $(\bar{\boldsymbol{\xi}},\bar{\boldsymbol{x}},\ \mathrm{d}V_{\bar{\xi}})$ to the position vectors $\boldsymbol{\xi},\boldsymbol{x}\in B_a$ and the differential volume element $\mathrm{d}V_\xi$ according to:

$$\text{(a) } (\boldsymbol{\xi},\boldsymbol{x})=\boldsymbol{z}+a(\bar{\boldsymbol{\xi}},\bar{\boldsymbol{x}}),\qquad\text{(b) } \mathrm{d}V_\xi=a^3\,\mathrm{d}V_{\bar{\xi}}\qquad\qquad(\boldsymbol{\xi}\in B_a,\ \bar{\boldsymbol{\xi}}\in\mathcal{B}). \tag{2.22}$$

Then, we define the isomorphism $\mathcal{P}_a:\boldsymbol{H}^1(B_a)\to\boldsymbol{H}^1(\mathcal{B})$ associated with this scaling, and its inverse $\mathcal{P}_a^{-1}$, by:

$$\mathcal{P}_a[\boldsymbol{v}](\bar{\boldsymbol{x}}):=\boldsymbol{v}(\boldsymbol{z}+a\bar{\boldsymbol{x}})\quad\text{and:}\quad\mathcal{P}_a^{-1}[\boldsymbol{V}](\boldsymbol{x}):=\boldsymbol{V}\left(\frac{\boldsymbol{x}-\boldsymbol{z}}{a}\right). \tag{2.23}$$

The following properties are then verified by $\mathcal{P}_a$ when considering the gradients of scaled functions:

$$\boldsymbol{\nabla}(\mathcal{P}_a[\boldsymbol{v}])(\bar{\boldsymbol{x}}) = a\mathcal{P}_a[\boldsymbol{\nabla v}](\bar{\boldsymbol{x}}), \qquad \boldsymbol{\nabla}(\mathcal{P}_a^{-1}[\boldsymbol{V}])(\boldsymbol{x}) = a^{-1}\mathcal{P}_a^{-1}[\boldsymbol{\nabla V}](\boldsymbol{x}). \tag{2.24}$$

Furthermore, computing the norms of such scaled functions leads to:

$$\|\boldsymbol{v}\|_{L^2(B_a)} = a^{3/2}\|\mathcal{P}_a[\boldsymbol{v}]\|_{L^2(\mathcal{B})}, \qquad \|\boldsymbol{\nabla v}\|_{L^2(B_a)} = a^{1/2}\|\boldsymbol{\nabla}(\mathcal{P}_a[\boldsymbol{v}])\|_{L^2(\mathcal{B})}. \tag{2.25}$$

2.1.3.4 Solvability of the VIE

In order to prove that (2.19) is uniquely solvable, let us work a little further on the operator $\mathcal{L}_a$. The decomposition of Green's tensor $\boldsymbol{G} = \boldsymbol{G}_\infty + \boldsymbol{G}_\mathrm{C}$ leads to a natural decomposition of $\mathcal{L}_a$:

$$\mathcal{L}_a = \mathcal{K}_\infty + \mathcal{K}_\mathrm{C} \tag{2.26}$$

with:

$$\mathcal{K}_\infty[\boldsymbol{v}](\boldsymbol{x}) := \boldsymbol{v}(\boldsymbol{x}) + \langle \boldsymbol{v}, \boldsymbol{G}_\infty(\cdot - \boldsymbol{x})\rangle_{B_a}^{\Delta\mathcal{C}} \quad \text{and} \quad \mathcal{K}_\mathrm{C}[\boldsymbol{v}](\boldsymbol{x}) := \langle \boldsymbol{v}, \boldsymbol{G}_\mathrm{C}(\cdot, \boldsymbol{x})\rangle_{B_a}^{\Delta\mathcal{C}}. \tag{2.27}$$

Remark that the operator $\mathcal{K}_\infty$ corresponds to the transmission by B_a when it is embedded in an infinite medium rather than in Ω, as studied in the previous chapter. To come back to the reference shape $\mathcal{B}$, recall that $\boldsymbol{\nabla G}_\infty$ is homogeneous of degree -2 as explained in Section 1.1.3, which writes with the notations of (2.22):

$$\boldsymbol{\nabla G}_\infty(\boldsymbol{\xi} - \boldsymbol{x}) = a^{-2}\boldsymbol{\nabla G}_\infty(\bar{\boldsymbol{\xi}} - \bar{\boldsymbol{x}}). \tag{2.28}$$

Then, in terms of the scaling operator $\mathcal{P}_a$ defined by (2.23), one shows:

$$\mathcal{K}_\infty = \mathcal{P}_a^{-1}\mathcal{L}\mathcal{P}_a. \tag{2.29}$$

where $\mathcal{L}$ denotes the operator associated with the transmission by $\mathcal{B}$, i.e.:

$$\mathcal{L}[\boldsymbol{V}](\bar{\boldsymbol{x}}) := \boldsymbol{V}(\bar{\boldsymbol{x}}) + \langle \boldsymbol{V}, \boldsymbol{G}_\infty(\cdot - \bar{\boldsymbol{x}})\rangle_{\mathcal{B}}^{\Delta\mathcal{C}} \tag{2.30}$$

The decomposition (2.26) eventually writes:

$$\mathcal{L}_a = \mathcal{P}_a^{-1}\mathcal{L}\mathcal{P}_a + \mathcal{K}_\mathrm{C} \tag{2.31}$$

and we are now in position to assert:

Theorem 2.1. *Consider the transmission problem featuring an inhomogeneity $(B_a, \boldsymbol{\mathcal{C}}^\star)$ embedded in a finite elastic domain Ω characterized by $\boldsymbol{\mathcal{C}}$. Under the assumptions of Theorem 1.3 on $\boldsymbol{\mathcal{C}}$ and $\boldsymbol{\mathcal{C}}^\star$, the corresponding integro-differential operator $\mathcal{L}_a : \boldsymbol{H}^1(B_a) \to \boldsymbol{H}^1(B_a)$ defined by* (2.20) *and decomposition* (2.31) *is invertible. Moreover, there exists $a_1 > 0$ such that $\mathcal{L}_a^{-1}$ is bounded uniformly in a, for all $a < a_1$.*

A first step is to prove the following Lemma:

Lemma 2.2. *Under the same assumptions than for Theorem 1.3, the operator $\mathcal{K}_\infty := \mathcal{P}_a^{-1}\mathcal{L}\mathcal{P}_a : \boldsymbol{H}^1(B_a) \to \boldsymbol{H}^1(B_a)$ is invertible and its inverse is bounded uniformly in a for sufficiently small a.*

Proof. The invertibility is given by that of $\mathcal{L}$, stated by Theorem 1.3, and definition $\mathcal{K}_\infty := \mathcal{P}_a^{-1}\mathcal{L}\mathcal{P}_a$. To estimate the norm of $(\mathcal{K}_\infty)^{-1}$, we consider the equation $\mathcal{P}_a^{-1}\mathcal{L}\mathcal{P}_a[\boldsymbol{v}] = \boldsymbol{u}$, equivalent to $\mathcal{L}\mathcal{P}_a[\boldsymbol{v}] = \mathcal{P}_a[\boldsymbol{u}]$ for some given background displacement $\boldsymbol{u} \in \boldsymbol{H}^1(B_a)$, and use the representation (1.74) of its solution, introduced in the proof of Theorem 1.3:

$$\mathcal{P}_a\boldsymbol{v} = \mathcal{L}^{-1}[\mathcal{P}_a\boldsymbol{u}] = \left(\boldsymbol{I} + \mathcal{M}\mathcal{G}^{-1}\Delta\boldsymbol{\mathcal{C}}_{\mathcal{B}} : \boldsymbol{\varepsilon}\right)[\mathcal{P}_a\boldsymbol{u}]. \tag{2.32}$$

By virtue of the continuity of $\mathcal{G}^{-1} : \boldsymbol{L}^2(\mathcal{B}) \to \boldsymbol{L}^2(\mathcal{B})$ and $\mathcal{M} : \boldsymbol{L}^2(\mathcal{B}) \to \boldsymbol{H}^1(\mathcal{B})$, there exists $C > 0$ independent of a such that:

$$\|\mathcal{P}_a\boldsymbol{v}\|_{L^2(\mathcal{B})} \leq \|\mathcal{P}_a\boldsymbol{u}\|_{L^2(\mathcal{B})} + C\|\boldsymbol{\nabla}\mathcal{P}_a\boldsymbol{u}\|_{L^2(\mathcal{B})} \tag{2.33}$$

Owing to the properties (2.25) of $\mathcal{P}_a$, it is equivalent to:

$$\|\boldsymbol{v}\|_{L^2(B_a)} \leq \|\boldsymbol{u}\|_{L^2(B_a)} + Ca\|\boldsymbol{\nabla}\boldsymbol{u}\|_{L^2(B_a)}. \tag{2.34}$$

Choosing a_0 such that $B_a \Subset \Omega$ for any $a \leq a_0$, we therefore have $\|\boldsymbol{v}\|_{L^2(B_a)} \leq \max(1, a_0C)\|\boldsymbol{u}\|_{H^1(B_a)}$. Similarly, since

$$\boldsymbol{\nabla}\mathcal{P}_a\boldsymbol{v} = \left(\boldsymbol{I}^{(4)} + \boldsymbol{\nabla}\mathcal{M}\mathcal{G}^{-1}\Delta\boldsymbol{\mathcal{C}}\right)[\boldsymbol{\nabla}\mathcal{P}_a\boldsymbol{u}], \tag{2.35}$$

there exists C' such that:

$$\|\boldsymbol{\nabla}\boldsymbol{v}\|_{L^2(B_a)} \leq (1 + C')\|\boldsymbol{\nabla}\boldsymbol{u}\|_{L^2(B_a)} \leq (1 + C')\|\boldsymbol{u}\|_{H^1(B_a)} \tag{2.36}$$

Summing inequalities (2.34) and (2.36), we obtain that for $a < a_0$, there exists C_0 such that $\|\boldsymbol{\nabla}\boldsymbol{v}\|_{H^1(B_a)} \leq C_0\|\boldsymbol{\nabla}\boldsymbol{u}\|_{H^1(B_a)}$, i.e. that $\mathcal{K}_\infty{}^{-1} = \mathcal{P}_a^{-1}\mathcal{L}^{-1}\mathcal{P}_a$ is bounded uniformly in a. $\square$

Proof of Theorem 2.1. The next step is to write $\mathcal{L}_a = \mathcal{K}_\infty(\boldsymbol{I} + \mathcal{K}_\infty{}^{-1}\mathcal{K}_{\mathrm{C}})$ and to invert the second member of this product thanks to Neumann series. For that, remark that $\mathcal{K}_{\mathrm{C}}$ is an integral operator with C^∞ kernel $\boldsymbol{\nabla}\boldsymbol{G}_{\mathrm{C}}$ so its norm can be readily estimated by Cauchy-Swartz inequality to obtain:

$$\begin{aligned}\|\mathcal{K}_{\mathrm{C}}[\boldsymbol{v}]\|^2_{H^1(B_a)} &\leq \|\boldsymbol{\nabla}\boldsymbol{G}_{\mathrm{C}}\|^2_{L^2(B_a\times B_a)}\|\Delta\boldsymbol{\mathcal{C}} : \boldsymbol{\nabla}\boldsymbol{v}\|^2_{L^2(B_a)} \\ &\leq a^6{C_C}^2\|\boldsymbol{\nabla}\boldsymbol{v}\|^2_{L^2(B_a)} \leq a^6{C_C}^2\|\boldsymbol{v}\|^2_{H^1(B_a)},\end{aligned} \tag{2.37}$$

so that $\|\mathcal{K}_{\mathrm{C}}\|_{H^1(B_a)} \leq a^3C_C$. Consequently, for all $c < 1$ there exists an inclusion size a_1 such that $\|\mathcal{K}_\infty{}^{-1}\mathcal{K}_{\mathrm{C}}\|_{H^1(B_a)} \leq c < 1 \;\; \forall a \leq a_0$, namely:

$$a_1 = \min\left(a_0, \left(\frac{c}{C_0C_C}\right)^{1/3}\right)$$

As a result, $\forall a < a_1$, $\boldsymbol{I} + \mathcal{K}_\infty{}^{-1}\mathcal{K}_{\mathrm{C}}$ is invertible by Neumann series, with bounded inverse:

$$\|(\boldsymbol{I} + \mathcal{K}_\infty{}^{-1}\mathcal{K}_{\mathrm{C}})^{-1}\|_{H^1(B_a)} \leq \frac{1}{1 - \|\mathcal{K}_\infty{}^{-1}\mathcal{K}_{\mathrm{C}}\|_{H^1(B_a)}} \leq \frac{1}{1-c}$$

The inverse of $\mathcal{L}_a$ is finally given by:

$$\mathcal{L}_a^{-1} = \left(\boldsymbol{I} + \mathcal{K}_\infty{}^{-1}\mathcal{K}_{\mathrm{C}}\right)^{-1}\mathcal{K}_\infty{}^{-1} \tag{2.38}$$

and its norm is bounded uniformly on a for $a < a_1$.

$\square$

2.2 Asymptotic behavior of perturbation displacement

The asymptotic behavior of $\boldsymbol{v}_a$ is now investigated, involving the expansion for $a \to 0$ of integral equation (2.19). To compute the integral, we use the scaling (2.22) introduced above.

2.2.1 Inner expansion

First, we look for the inner expansion of $\boldsymbol{v}_a(\boldsymbol{x})$ i.e. for $\boldsymbol{x} \in B_a$. The expansion is sought in the form:

$$\boldsymbol{v}_a(\boldsymbol{x}) \approx a\boldsymbol{V}_1(\bar{\boldsymbol{x}}) + a^2\boldsymbol{V}_2(\bar{\boldsymbol{x}}) + \frac{1}{2}a^3\boldsymbol{V}_3(\bar{\boldsymbol{x}}) + \frac{1}{6}a^4\boldsymbol{V}_4(\bar{\boldsymbol{x}}) \quad (\bar{\boldsymbol{x}} \in \mathcal{B},\ \boldsymbol{x} = \boldsymbol{z} + a\bar{\boldsymbol{x}} \in B_a) \tag{2.39}$$

in term of functions $\boldsymbol{V}_j$ of the rescaled coordinates that have to be determined. More precisely, based and this ansatz, we write the inner approximation of $\boldsymbol{v}_a$ in the form:

$$\boldsymbol{v}_a(\boldsymbol{x}) = \mathcal{P}_a^{-1}[\boldsymbol{V}_a](\boldsymbol{x}) + \boldsymbol{\delta}_a(\boldsymbol{x}), \qquad \text{with} \quad \boldsymbol{V}_a := a\boldsymbol{V}_1 + a^2\boldsymbol{V}_2 + \frac{1}{2}a^3\boldsymbol{V}_3 + \frac{1}{6}a^4\boldsymbol{V}_4, \tag{2.40}$$

and the remainder $\boldsymbol{\delta}_a$ is "small" in a sense that will be made precise later. Note that the scaling properties (2.24) imply that:

$$\begin{aligned}\boldsymbol{\nabla}\boldsymbol{v}_a(\boldsymbol{x}) &= a^{-1}\mathcal{P}_a^{-1}[\boldsymbol{\nabla}\boldsymbol{V}_a](\boldsymbol{x}) + \boldsymbol{\nabla}\boldsymbol{\delta}_a(\boldsymbol{x}) \\ &= \boldsymbol{\nabla}\boldsymbol{V}_1(\bar{\boldsymbol{x}}) + a\boldsymbol{\nabla}\boldsymbol{V}_2(\bar{\boldsymbol{x}}) + \frac{a^2}{2}\boldsymbol{\nabla}\boldsymbol{V}_3(\bar{\boldsymbol{x}}) + \frac{a^3}{6}\boldsymbol{\nabla}\boldsymbol{V}_4(\bar{\boldsymbol{x}}) + \boldsymbol{\nabla}\boldsymbol{\delta}_a(\boldsymbol{x}).\end{aligned} \tag{2.41}$$

Remark 2.2. *The expansion* (2.41) *implies in particular that* $\boldsymbol{\nabla}\boldsymbol{v}_a = O(1)$ *does not vanish as* $a \to 0$*. The difficulties arising from this observation when considering cost functionals depending on strains or stress rather than displacement were recently studied in [Delgado & Bonnet, 2015].*

Taking Taylor's expansion of $\boldsymbol{\nabla}\boldsymbol{u}$ about $\boldsymbol{z}$ provides a similar expansion for $\boldsymbol{\nabla}\boldsymbol{u}$:

$$\boldsymbol{\nabla}\boldsymbol{u}(\boldsymbol{\xi}) = \boldsymbol{\nabla}\boldsymbol{u}(\boldsymbol{z}) + a\boldsymbol{\nabla}^2\boldsymbol{u}(\boldsymbol{z}) \cdot \bar{\boldsymbol{\xi}} + \frac{a^2}{2}\boldsymbol{\nabla}^3\boldsymbol{u}(\boldsymbol{z}) : \bar{\boldsymbol{\xi}}^{\otimes 2} + \frac{a^3}{6}\boldsymbol{\nabla}^4\boldsymbol{u}(\boldsymbol{z}) \bullet \bar{\boldsymbol{\xi}}^{\otimes 3} + O(a^4). \tag{2.42}$$

Invoking the decomposition (2.16) of $\boldsymbol{G}(\boldsymbol{\xi}, \boldsymbol{x})$, the homogeneity property (1.30) and differentiability of $\boldsymbol{G}_\mathrm{C}$ in B_a, one has

$$\begin{aligned}\boldsymbol{\nabla}_1\boldsymbol{G}(\boldsymbol{\xi}, \boldsymbol{x}) =& a^{-2}\boldsymbol{\nabla}\boldsymbol{G}_\infty(\bar{\boldsymbol{\xi}} - \bar{\boldsymbol{x}}) + \boldsymbol{\nabla}_1\boldsymbol{G}_\mathrm{C}(\boldsymbol{z}, \boldsymbol{z}) \\ &+ a(\boldsymbol{\nabla}_{11}\boldsymbol{G}_\mathrm{C}(\boldsymbol{z}, \boldsymbol{z}) \cdot \bar{\boldsymbol{\xi}} + \boldsymbol{\nabla}_{21}\boldsymbol{G}_\mathrm{C}(\boldsymbol{z}, \boldsymbol{z}) \cdot \bar{\boldsymbol{x}}) + o(a)\end{aligned} \tag{2.43}$$

Finally, the integral equation $\mathcal{L}_a[\boldsymbol{v}_a](\boldsymbol{x}) = -\langle \boldsymbol{u}, \boldsymbol{G}(\cdot, \boldsymbol{x})\rangle_{B_a}^{\Delta\mathcal{C}}$ (2.19) is expanded as:

$$\sum_{j=1}^{4} \frac{a^j}{(j-1)!}\left(\mathcal{L}[\boldsymbol{V}_j](\bar{\boldsymbol{x}}) - \mathcal{F}_j(\bar{\boldsymbol{x}})\right) + o(a^4) = 0, \tag{2.44}$$

where the right-hand sides $\mathcal{F}_j$ are given by:

$$
\begin{aligned}
\mathcal{F}_1(\bar{\boldsymbol{x}}) &= -\int_{\mathcal{B}} \boldsymbol{\nabla}\boldsymbol{u}(\boldsymbol{z}) : \Delta\boldsymbol{\mathcal{C}} : \boldsymbol{\nabla}\boldsymbol{G}_\infty(\bar{\boldsymbol{\xi}} - \bar{\boldsymbol{x}})\, \mathrm{d}V_{\bar{\xi}} \\
\mathcal{F}_2(\bar{\boldsymbol{x}}) &= -\int_{\mathcal{B}} \left(\boldsymbol{\nabla}^2\boldsymbol{u}(\boldsymbol{z}) \cdot \bar{\boldsymbol{\xi}}\right) : \Delta\boldsymbol{\mathcal{C}} : \boldsymbol{\nabla}\boldsymbol{G}_\infty(\bar{\boldsymbol{\xi}} - \bar{\boldsymbol{x}})\, \mathrm{d}V_{\bar{\xi}} \\
\mathcal{F}_3(\bar{\boldsymbol{x}}) &= -\int_{\mathcal{B}} \left(\boldsymbol{\nabla}^3\boldsymbol{u}(\boldsymbol{z}) : \bar{\boldsymbol{\xi}}^{\otimes 2}\right) : \Delta\boldsymbol{\mathcal{C}} : \boldsymbol{\nabla}\boldsymbol{G}_\infty(\bar{\boldsymbol{\xi}} - \bar{\boldsymbol{x}})\, \mathrm{d}V_{\bar{\xi}} \\
&\quad - 2\int_{\mathcal{B}} \left(\boldsymbol{\nabla}\boldsymbol{u}(\boldsymbol{z}) + \boldsymbol{\nabla}\boldsymbol{V}_1(\bar{\boldsymbol{\xi}})\right) : \Delta\boldsymbol{\mathcal{C}} : \boldsymbol{\nabla}_1\boldsymbol{G}_{\mathrm{C}}(\boldsymbol{z}, \boldsymbol{z})\, \mathrm{d}V_{\bar{\xi}} \\
\mathcal{F}_4(\bar{\boldsymbol{x}}) &= -\int_{\mathcal{B}} \left(\boldsymbol{\nabla}^4\boldsymbol{u}(\boldsymbol{z}) \bullet \bar{\boldsymbol{\xi}}^{\otimes 3}\right) : \Delta\boldsymbol{\mathcal{C}} : \boldsymbol{\nabla}\boldsymbol{G}_\infty(\bar{\boldsymbol{\xi}} - \bar{\boldsymbol{x}})\, \mathrm{d}V_{\bar{\xi}} \\
&\quad - 6\int_{\mathcal{B}} \left(\boldsymbol{\nabla}^2\boldsymbol{u}(\boldsymbol{z}) \cdot \bar{\boldsymbol{\xi}} + \boldsymbol{\nabla}\boldsymbol{V}_2(\bar{\boldsymbol{\xi}})\right) : \Delta\boldsymbol{\mathcal{C}} : \boldsymbol{\nabla}_1\boldsymbol{G}_{\mathrm{C}}(\boldsymbol{z}, \boldsymbol{z})\, \mathrm{d}V_{\bar{\xi}} \\
&\quad - 6\int_{\mathcal{B}} \left(\boldsymbol{\nabla}\boldsymbol{u}(\boldsymbol{z}) + \boldsymbol{\nabla}\boldsymbol{V}_1(\bar{\boldsymbol{\xi}})\right) : \Delta\boldsymbol{\mathcal{C}} : \left(\boldsymbol{\nabla}_{11}\boldsymbol{G}_{\mathrm{C}}(\boldsymbol{z}, \boldsymbol{z}) \cdot \bar{\boldsymbol{\xi}} + \boldsymbol{\nabla}_{21}\boldsymbol{G}_{\mathrm{C}}(\boldsymbol{z}, \boldsymbol{z}) \cdot \bar{\boldsymbol{x}}\right)\, \mathrm{d}V_{\bar{\xi}}
\end{aligned}
\tag{2.45}
$$

Cancelling each order contribution in (2.44), the terms of the expansion of $\boldsymbol{v}_a$ are found to be the solutions to the equations:

$$
\mathcal{L}[\boldsymbol{V}_j](\bar{\boldsymbol{x}}) - \mathcal{F}_j(\bar{\boldsymbol{x}}) = 0 \Leftrightarrow \mathcal{L}[\boldsymbol{V}_j](\bar{\boldsymbol{x}}) = \mathcal{F}_j(\bar{\boldsymbol{x}}),\ j \in \{1..4\}.
$$

Resolution The solutions of these equations are those of the FSTPs with polynomial background displacement described in Section 1.3. More precisely, rewriting the RHS (2.45) with the help of notations $\boldsymbol{\varphi}_j[\boldsymbol{\nabla}^j\boldsymbol{u}(\boldsymbol{z})]$ for homogeneous polynomial displacements driven by the gradients of $\boldsymbol{u}$, the first and second-order equations are:

$$
\begin{aligned}
\mathcal{L}[\boldsymbol{V}_1](\bar{\boldsymbol{x}}) &= -\left\langle \boldsymbol{\varphi}_1[\boldsymbol{\nabla}\boldsymbol{u}(\boldsymbol{z})], \boldsymbol{G}_\infty(\cdot - \bar{\boldsymbol{x}})\right\rangle_{\mathcal{B}}^{\Delta\mathcal{C}} \\
\mathcal{L}[\boldsymbol{V}_2](\bar{\boldsymbol{x}}) &= -\left\langle \boldsymbol{\varphi}_2[\boldsymbol{\nabla}^2\boldsymbol{u}(\boldsymbol{z})], \boldsymbol{G}_\infty(\cdot - \bar{\boldsymbol{x}})\right\rangle_{\mathcal{B}}^{\Delta\mathcal{C}}
\end{aligned}
\tag{2.46}
$$

Consequently, $\boldsymbol{V}_1$ and $\boldsymbol{V}_2$ are the corresponding FSTP solutions:

$$
\boldsymbol{V}_1 = \boldsymbol{v}_{\mathcal{B}}^{(1)}[\boldsymbol{\nabla}\boldsymbol{u}(\boldsymbol{z})], \qquad \boldsymbol{V}_2 = \boldsymbol{v}_{\mathcal{B}}^{(2)}[\boldsymbol{\nabla}^2\boldsymbol{u}(\boldsymbol{z})]. \tag{2.47}
$$

The third and fourth-order equations, involving complementary parts coming from the contribution of $\boldsymbol{G}_{\mathrm{C}}$, then are:

$$
\begin{aligned}
\mathcal{L}[\boldsymbol{V}_3](\bar{\boldsymbol{x}}) &= -\left\langle \boldsymbol{\varphi}_3[\boldsymbol{\nabla}^2\boldsymbol{u}(\boldsymbol{z})], \boldsymbol{G}_\infty(\cdot - \bar{\boldsymbol{x}})\right\rangle_{\mathcal{B}}^{\Delta\mathcal{C}} - 2\ \boldsymbol{q}_3(\boldsymbol{z}) \\
\mathcal{L}[\boldsymbol{V}_4](\bar{\boldsymbol{x}}) &= -\left\langle \boldsymbol{\varphi}_4[\boldsymbol{\nabla}^4\boldsymbol{u}(\boldsymbol{z})], \boldsymbol{G}_\infty(\cdot - \bar{\boldsymbol{x}})\right\rangle_{\mathcal{B}}^{\Delta\mathcal{C}} - 6\left(\boldsymbol{q}_4(\boldsymbol{z}) + \boldsymbol{L}(\boldsymbol{z}) \cdot \bar{\boldsymbol{x}}\right)
\end{aligned}
\tag{2.48}
$$

where the vectors $\boldsymbol{q}_3(\boldsymbol{z})$ and $\boldsymbol{q}_4(\boldsymbol{z})$ collect the constant terms w.r.t. $\bar{\boldsymbol{x}}$ in $\mathcal{F}_3$ and $\mathcal{F}_4$, and $\boldsymbol{L}(\boldsymbol{z}) \cdot \bar{\boldsymbol{x}}$ accounts for the linear term in $\mathcal{F}_4$. Introducing the solutions (2.47) into (2.45), and using the elastic moment tensors defined in Section 1.3.3, they are written:

$$
\begin{aligned}
\boldsymbol{q}_3(\boldsymbol{z}) &= \boldsymbol{\nabla}\boldsymbol{u}(\boldsymbol{z}) : \boldsymbol{\mathcal{A}} : \boldsymbol{\nabla}_1\boldsymbol{G}_{\mathrm{C}}(\boldsymbol{z}, \boldsymbol{z}) \\
\boldsymbol{q}_4(\boldsymbol{z}) &= \boldsymbol{\nabla}^2\boldsymbol{u}(\boldsymbol{z}) \bullet \boldsymbol{\mathcal{A}}_{21} : \boldsymbol{\nabla}_1\boldsymbol{G}_{\mathrm{C}}(\boldsymbol{z}, \boldsymbol{z}) + \boldsymbol{\nabla}\boldsymbol{u}(\boldsymbol{z}) : \boldsymbol{\mathcal{A}}_{12} \bullet \boldsymbol{\nabla}_{11}\boldsymbol{G}_{\mathrm{C}}(\boldsymbol{z}, \boldsymbol{z}) \\
\boldsymbol{L}(\boldsymbol{z}) &= \boldsymbol{\nabla}\boldsymbol{u}(\boldsymbol{z}) : \boldsymbol{\mathcal{A}} : \boldsymbol{\nabla}_{21}\boldsymbol{G}_{\mathrm{C}}(\boldsymbol{z}, \boldsymbol{z})
\end{aligned}
\tag{2.49}
$$

The solutions $\boldsymbol{V}_3$ and $\boldsymbol{V}_4$ are therefore given by:

$$\boldsymbol{V}_3 = \boldsymbol{v}_{\mathcal{B}}^{(3)}[\boldsymbol{\nabla}^3\boldsymbol{u}(\boldsymbol{z})] + 2\boldsymbol{v}_{3\mathrm{C}}, \qquad \boldsymbol{V}_4 = \boldsymbol{v}_{\mathcal{B}}^{(4)}[\boldsymbol{\nabla}^4\boldsymbol{u}(\boldsymbol{z})] + 6\boldsymbol{v}_{4\mathrm{C}}, \tag{2.50}$$

where the complementary parts are defined accordingly to (2.48) and using the solution for first-order FSTP by:

$$\boldsymbol{v}_{3\mathrm{C}}(\bar{\boldsymbol{x}};\boldsymbol{z}) := -\boldsymbol{q}_3(\boldsymbol{z}), \qquad \boldsymbol{v}_{4\mathrm{C}}(\bar{\boldsymbol{x}};\boldsymbol{z}) := -\boldsymbol{q}_4(\boldsymbol{z}) - \boldsymbol{u}_{\mathcal{B}}^{(1)}[\boldsymbol{L}(\boldsymbol{z})](\bar{\boldsymbol{x}}). \tag{2.51}$$

Inserting all these solutions into (2.40), the inner approximation $\mathcal{P}_a^{-1}\boldsymbol{V}_a$ of $\boldsymbol{v}_a$ is finally defined by:

$$\begin{aligned}\boldsymbol{V}_a := a\boldsymbol{v}_{\mathcal{B}}^{(1)}[\boldsymbol{\nabla}\boldsymbol{u}(\boldsymbol{z})] + a^2\boldsymbol{v}_{\mathcal{B}}^{(2)}[\boldsymbol{\nabla}^2\boldsymbol{u}(\boldsymbol{z})]\\ + a^3\left(\frac{1}{2}\boldsymbol{v}_{\mathcal{B}}^{(3)}[\boldsymbol{\nabla}^3\boldsymbol{u}(\boldsymbol{z})] + \boldsymbol{v}_{3\mathrm{C}}\right) + a^4\left(\frac{1}{6}\boldsymbol{v}_{\mathcal{B}}^{(4)}[\boldsymbol{\nabla}^4\boldsymbol{u}(\boldsymbol{z})] + \boldsymbol{v}_{4\mathrm{C}}\right)\end{aligned} \tag{2.52}$$

2.2.2 Remainder estimate

Eventually, the $O(a^4)$ inner approximation we obtained is justified by the following estimate.

Theorem 2.3. *(Error estimate on the inner approximation of displacement): Assume that the background and inhomogeneity elasticity tensors $\boldsymbol{\mathcal{C}}$ and $\boldsymbol{\mathcal{C}}^\star$ are both positive definite and bounded. Then there exists a bound $a_1 > 0$ and a constant $C > 0$ independent of the size a such that:*

$$\|\boldsymbol{\delta}_a\|_{H^1(B_a)} \leq Ca^{11/2} \quad \forall a < a_1. \tag{2.53}$$

Proof. Combining (2.19) and (2.44), the error $\boldsymbol{\delta}_a$ is found to satisfy an integral equation:

$$\mathcal{L}_a[\boldsymbol{\delta}_a](\boldsymbol{x}) = \boldsymbol{\gamma}_a(\boldsymbol{x}) \tag{2.54}$$

The proof then relies on (i) the existence and boundedness of the inverse operator $\mathcal{L}_a^{-1} : \boldsymbol{H}^1(B_a) \to \boldsymbol{H}^1(B_a)$ uniformly in a, which was proven in Theorem 2.1 for a smaller than a fixed bound a_1 and (ii) estimate of the second member $\boldsymbol{\gamma}_a$, that we provide now.

Subtracting the RHS $\mathcal{F}_j$ defined by (2.45) to the RHS $-\langle \boldsymbol{u}, \boldsymbol{G}(\cdot,\boldsymbol{x})\rangle_{B_a}^{\Delta\mathcal{C}}$ of the integral equation satisfied by the exact perturbation $\boldsymbol{v}_a$ (after adequate scaling), the RHS $\boldsymbol{\gamma}_a$ is written as the sum of convolutions:

$$\boldsymbol{\gamma}_a(\boldsymbol{x}) = -\int_{B_a} \boldsymbol{F}_0 : \Delta\boldsymbol{\mathcal{C}} : \boldsymbol{\nabla}\boldsymbol{G}_\infty(\cdot - \boldsymbol{x})\,\mathrm{d}V - \sum_{j=1}^{4}\int_{B_a} \boldsymbol{F}_j : \Delta\boldsymbol{\mathcal{C}} : \boldsymbol{H}_j(\cdot,\boldsymbol{x})\,\mathrm{d}V, \tag{2.55}$$

where the functions $\boldsymbol{F}_j$ and kernels $\boldsymbol{H}_j$ will be specified below. In particular, these kernels are bounded and smooth enough so that the gradient $\boldsymbol{\nabla}\boldsymbol{\gamma}_a$ is computed as:

$$\boldsymbol{\nabla}\boldsymbol{\gamma}_a(\boldsymbol{x}) = -\boldsymbol{\nabla}_{\boldsymbol{x}}\int_{B_a} \boldsymbol{F}_0 : \Delta\boldsymbol{\mathcal{C}} : \boldsymbol{\nabla}\boldsymbol{G}_\infty(\cdot - \boldsymbol{x})\,\mathrm{d}V - \sum_{j=1}^{4}\int_{B_a} \boldsymbol{F}_j : \Delta\boldsymbol{\mathcal{C}} : \boldsymbol{\nabla}_2\boldsymbol{H}_j(\cdot,\boldsymbol{x})\,\mathrm{d}V. \tag{2.56}$$

Definition and estimates for the functions $\boldsymbol{F}_j$: The functions $\boldsymbol{F}_0$ and $\boldsymbol{F}_1$ are remainders of Taylor's expansion of $\boldsymbol{\nabla u}$ about $\boldsymbol{z}$:

$$\begin{aligned} \boldsymbol{F}_0(\boldsymbol{\xi}) &= \boldsymbol{\nabla u}(\boldsymbol{\xi}) - \left[\boldsymbol{\nabla u}(\boldsymbol{z}) + a\boldsymbol{\nabla u}^2(\boldsymbol{z}) \cdot \bar{\boldsymbol{\xi}} + \frac{a^2}{2}\boldsymbol{\nabla}^3\boldsymbol{u}(\boldsymbol{z}) : \bar{\boldsymbol{\xi}}^{\otimes 2} + \frac{a^3}{6}\boldsymbol{\nabla}^4\boldsymbol{u}(\boldsymbol{z}) \bullet \bar{\boldsymbol{\xi}}^{\otimes 3} \right], \\ \boldsymbol{F}_1(\boldsymbol{\xi}) &= \left[\boldsymbol{\nabla u}(\boldsymbol{\xi}) - \boldsymbol{\nabla u}(\boldsymbol{z}) - a\boldsymbol{\nabla}^2\boldsymbol{u}(\boldsymbol{z}) \cdot \bar{\boldsymbol{\xi}} \right], \end{aligned} \tag{2.57}$$

where we used the scaled variable $\bar{\boldsymbol{\xi}} = (\boldsymbol{\xi} - \boldsymbol{z})/a$. Consequently, their leading-order contributions are so that:

$$\begin{aligned} \boldsymbol{F}_0(\boldsymbol{\xi}) &= \frac{a^4}{24}\boldsymbol{\nabla}^5\boldsymbol{u}(\boldsymbol{z}) \bullet \bar{\boldsymbol{\xi}}^{\otimes 4} + o(a^4) = \frac{a^4}{24}\mathcal{P}_a^{-1}\left[\boldsymbol{\nabla}\boldsymbol{\varphi}_5[\boldsymbol{\nabla}^5\boldsymbol{u}(\boldsymbol{z})] \right](\boldsymbol{\xi}) + o(a^4), \\ \boldsymbol{F}_1(\boldsymbol{\xi}) &= \frac{a^2}{2}\boldsymbol{\nabla}^3\boldsymbol{u}(\boldsymbol{z}) : \bar{\boldsymbol{\xi}}^{\otimes 2} + o(a^2) = \frac{a^2}{2}\mathcal{P}_a^{-1}\left[\boldsymbol{\nabla}\boldsymbol{\varphi}_3[\boldsymbol{\nabla}^3\boldsymbol{u}(\boldsymbol{z})] \right](\boldsymbol{\xi}) + o(a^2), \end{aligned} \tag{2.58}$$

Similarly, the other functions $\boldsymbol{F}_j$ for $j \geq 2$ are found to be:

$$\begin{aligned} \boldsymbol{F}_2(\boldsymbol{\xi}) &= \mathcal{P}_a^{-1}\left[\boldsymbol{\nabla u}_{\mathcal{B}}^{(1)}[\boldsymbol{\nabla u}(\boldsymbol{z})] \right](\boldsymbol{\xi}), \\ \boldsymbol{F}_3(\boldsymbol{\xi}) &= a\mathcal{P}_a^{-1}\left[\boldsymbol{\nabla u}_{\mathcal{B}}^{(2)}[\boldsymbol{\nabla}^2\boldsymbol{u}(\boldsymbol{z})] \right](\boldsymbol{\xi}), \\ \boldsymbol{F}_4(\boldsymbol{\xi}) &= \frac{a^2}{2}\mathcal{P}_a^{-1}\left[\boldsymbol{\nabla v}_{\mathcal{B}}^{(3)}[\boldsymbol{\nabla}^3\boldsymbol{u}(\boldsymbol{z})] + \frac{a}{3}\boldsymbol{\nabla}\left(\boldsymbol{v}_{\mathcal{B}}^{(4)}[\boldsymbol{\nabla}^4\boldsymbol{u}(\boldsymbol{z})] - 6\boldsymbol{u}_{\mathcal{B}}^{(1)}[\boldsymbol{L}(\boldsymbol{z})] \right) \right](\boldsymbol{\xi}). \end{aligned} \tag{2.59}$$

From the expressions (2.58) and (2.59) and since $\|\mathcal{P}_a^{-1}\tilde{\boldsymbol{F}}\|_{L^2(B_a)} = O(a^{3/2})$ for any function $\tilde{\boldsymbol{F}} \in \boldsymbol{H}^1(\mathcal{B})$ independent of a as specified by (2.25), we obtain the following estimates:

$$\begin{aligned} &\|\boldsymbol{F}_0\|_{L^2(B_a)} = O(a^{11/2}), \quad \|\boldsymbol{F}_1\|_{L^2(B_a)} = O(a^{7/2}), \\ &\|\boldsymbol{F}_2\|_{L^2(B_a)} = O(a^{3/2}), \quad \|\boldsymbol{F}_3\|_{L^2(B_a)} = O(a^{5/2}), \quad \|\boldsymbol{F}_4\|_{L^2(B_a)} = O(a^{7/2}). \end{aligned} \tag{2.60}$$

Definition and estimates for the kernels $\boldsymbol{H}_j$: These kernels are:

$$\begin{aligned} \boldsymbol{H}_1(\boldsymbol{\xi}, \boldsymbol{x}) &= \boldsymbol{H}_4(\boldsymbol{\xi}, \boldsymbol{x}) = \boldsymbol{\nabla G}_{\mathrm{C}}(\boldsymbol{\xi}, \boldsymbol{x}), \\ \boldsymbol{H}_2(\boldsymbol{\xi}, \boldsymbol{x}) &= \boldsymbol{\nabla G}_{\mathrm{C}}(\boldsymbol{\xi}, \boldsymbol{x}) - \boldsymbol{\nabla G}_{\mathrm{C}}(\boldsymbol{z}, \boldsymbol{z}) - a\left(\boldsymbol{\nabla}_{11}\boldsymbol{G}_{\mathrm{C}}(\boldsymbol{z}, \boldsymbol{z}) \cdot \bar{\boldsymbol{\xi}} + \boldsymbol{\nabla}_{21}\boldsymbol{G}_{\mathrm{C}}(\boldsymbol{z}, \boldsymbol{z}) \cdot \bar{\boldsymbol{x}} \right), \\ \boldsymbol{H}_3(\boldsymbol{\xi}, \boldsymbol{x}) &= \boldsymbol{\nabla G}_{\mathrm{C}}(\boldsymbol{\xi}, \boldsymbol{x}) - \boldsymbol{\nabla G}_{\mathrm{C}}(\boldsymbol{z}, \boldsymbol{z}). \end{aligned} \tag{2.61}$$

and are therefore bounded by virtue of the C^∞ regularity of $\boldsymbol{G}_{\mathrm{C}}$. Their gradients are also bounded and defined by:

$$\begin{aligned} \boldsymbol{\nabla}_2\boldsymbol{H}_j(\boldsymbol{\xi}, \boldsymbol{x}) &= \boldsymbol{\nabla}_{21}\boldsymbol{G}_{\mathrm{C}}(\boldsymbol{\xi}, \boldsymbol{x}) \quad \text{for } j \in \{1, 3, 4\}, \\ \boldsymbol{\nabla}_2\boldsymbol{H}_2(\boldsymbol{\xi}, \boldsymbol{x}) &= \boldsymbol{\nabla}_{21}\boldsymbol{G}_{\mathrm{C}}(\boldsymbol{\xi}, \boldsymbol{x}) - \boldsymbol{\nabla}_{21}\boldsymbol{G}_{\mathrm{C}}(\boldsymbol{z}, \boldsymbol{z}). \end{aligned} \tag{2.62}$$

As for $\boldsymbol{F}_0$ and $\boldsymbol{F}_1$, these kernels are remainders of Taylor expansions of $\boldsymbol{\nabla G}_{\mathrm{C}}$ about $(\boldsymbol{z}, \boldsymbol{z})$ whose leading-order contribution can be determined similarly to (2.58). Since $\|\mathcal{P}_a^{-1}\tilde{\boldsymbol{H}}\|_{L^2(B_a \times B_a)} = O(a^3)$ for any function $\tilde{\boldsymbol{H}} \in \boldsymbol{L}^2(\mathcal{B} \times \mathcal{B})$ independent of a, one easily obtains the estimates:

$$\begin{aligned} &\|\boldsymbol{H}_j\|_{L^2(B_a \times B_a)} = O(a^3) \text{ for } j \in \{1, 4\}, \quad \|\boldsymbol{H}_2\|_{L^2(B_a \times B_a)} = O(a^5) \\ \text{and} \quad &\|\boldsymbol{H}_3\|_{L^2(B_a \times B_a)} = O(a^4), \end{aligned} \tag{2.63}$$

and similarly, for the gradients,

$$\|\boldsymbol{\nabla}_2\boldsymbol{H}_j\|_{L^2(B_a \times B_a)} = O(a^3) \text{ for } j \in \{1, 3, 4\} \quad \text{and} \quad \|\boldsymbol{\nabla}_2\boldsymbol{H}_2\|_{L^2(B_a \times B_a)} = O(a^4). \tag{2.64}$$

Estimation of γ_a: Remark that the first term of (2.55) writes $-\mathcal{M}[\Delta\boldsymbol{\mathcal{C}}_a : \boldsymbol{F}_0]$, with $\Delta\boldsymbol{\mathcal{C}}_a := \chi_{B_a}\Delta\boldsymbol{\mathcal{C}}$ and $\mathcal{M} : L^2_{\text{comp}}(\mathbb{R}^3;\mathbb{R}^{3\times3}_{\text{sym}}) \to \boldsymbol{H}^1_{\text{loc}}(\mathbb{R}^3)$ is shown to be continuous by Lemma 1.4. Therefore, there exists $C > 0$ such that the following inequality holds:

$$\left\| \int_{B_a} \boldsymbol{F}_0 : \Delta\boldsymbol{\mathcal{C}} : \boldsymbol{\nabla G}_\infty(\cdot - \boldsymbol{x}) \,\mathrm{d}V \right\|_{H^1(B_a)} \leq C\|\boldsymbol{F}_0\|_{L^2(B_a)} = Ca^{11/2} + o\left(a^{11/2}\right). \tag{2.65}$$

For the remaining terms, we use Cauchy-Schwartz inequality twice to assert similarly that there exists $C > 0$ such that:

$$\left\| \int_{B_a} \boldsymbol{F} : \Delta\boldsymbol{\mathcal{C}} : \boldsymbol{H}(\cdot, \boldsymbol{x}) \,\mathrm{d}V \right\|_{L^2(B_a)} \leq C\|\boldsymbol{F}\|_{L^2(B_a)}\|\boldsymbol{H}\|_{L^2(B_a\times B_a)}$$
$$\forall(\boldsymbol{F}, \boldsymbol{H}) \in \boldsymbol{L}^2(B_a) \times \boldsymbol{L}^2(B_a \times B_a). \tag{2.66}$$

We then apply (2.66) to the products of functions $\boldsymbol{F}_j$ and kernels $\boldsymbol{H}_j$ (resp. $\boldsymbol{\nabla}_2\boldsymbol{H}_j$) and introduce the estimates (2.60) and (2.63) to evaluate the $\boldsymbol{L}^2$ norm of $\boldsymbol{\gamma}_a$ (resp. of $\boldsymbol{\nabla\gamma}_a$). Combining those norms finally yields the sought estimate:

$$\|\boldsymbol{\gamma}_a\|_{H^1(B_a)} \leq Ca^{11/2} + o\left(a^{11/2}\right). \tag{2.67}$$

□

2.2.3 Outer expansion

We now look for the outer expansion of $\boldsymbol{v}_a$, i.e. for $\boldsymbol{x} \notin \overline{B_a}$. Recall that $\boldsymbol{v}_a(\boldsymbol{x})$ is then given by the integral representation

$$\boldsymbol{v}_a(\boldsymbol{x}) = -\int_{B_a} \boldsymbol{\nabla}(\boldsymbol{u} + \boldsymbol{v}_a) : \Delta\boldsymbol{\mathcal{C}} : \boldsymbol{\nabla}_1\boldsymbol{G}(\cdot, \boldsymbol{x}) \,\mathrm{d}V, \quad \boldsymbol{x} \in \Omega \setminus \overline{B_a}. \tag{2.68}$$

In this case, the singular behavior of $\boldsymbol{G}(\boldsymbol{\xi}, \boldsymbol{x})$ is not activated, and one therefore has:

$$\boldsymbol{\nabla}_1\boldsymbol{G}(\boldsymbol{\xi}, \boldsymbol{x}) = \boldsymbol{\nabla}_1\boldsymbol{G}(\boldsymbol{z}, \boldsymbol{x}) + O(a), \qquad \boldsymbol{\xi} \in B_a, \boldsymbol{x} \notin B_a.$$

Using the first order inner expansion $\boldsymbol{v}_a = a\mathcal{P}_a^{-1}[\boldsymbol{V}_1] + o(a)$ and $\boldsymbol{V}_1 = \boldsymbol{v}_{\mathcal{B}}^{(1)}[\boldsymbol{\nabla u}(\boldsymbol{z})]$, one moreover has:

$$\boldsymbol{\nabla}(\boldsymbol{u} + \boldsymbol{v}_a)(\boldsymbol{\xi}) = \boldsymbol{\nabla u}(\boldsymbol{z}) + \mathcal{P}_a^{-1}[\boldsymbol{\nabla V}_1](\boldsymbol{\xi}) + O(a) = \mathcal{P}_a^{-1}\left[\boldsymbol{\nabla u}_{\mathcal{B}}^{(1)}[\boldsymbol{\nabla u}(\boldsymbol{z})]\right](\boldsymbol{\xi}), \quad \boldsymbol{\xi} \in B_a.$$

Scaling the representation (2.68), retaining only the leading-order terms and expressing the resulting integral thanks to the elastic moment tensor $\boldsymbol{\mathcal{A}}$, we finally obtain the well-known leading-order outer perturbation [Ammari et al., 2002]:

$$\boldsymbol{v}_a(\boldsymbol{x}) = a^3\boldsymbol{v}_{\text{out}}(\boldsymbol{x}; \boldsymbol{z}) + O(a^4), \quad \boldsymbol{x} \in \Omega \setminus \overline{B_a} \tag{2.69}$$

where:

$$\boldsymbol{v}_{\text{out}}(\boldsymbol{x}; \boldsymbol{z}) := -\boldsymbol{\nabla u}(\boldsymbol{z}) : \boldsymbol{\mathcal{A}} : \boldsymbol{\nabla}_1\boldsymbol{G}(\boldsymbol{z}, \boldsymbol{x}). \tag{2.70}$$

2.3 Misfit function expansion

Now that we know both the inner and outer expansion of the perturbation $\boldsymbol{v}_a$, we are in position to provide and justify the sixth-order expansion of the cost functional $\mathbb{J}(B_a)$. We begin by stating the Theorem 2.4, which addresses the general case and constitutes the main result of this chapter. The possible simplifications for centrally symmetric shapes are then specified, with focus on ellipsoidal and spherical shapes. We finally discuss shortly the issues raised by the practical computation of this expansion.

2.3.1 Inhomogeneity of arbitrary shape

Theorem 2.4. *The sixth-order expansion of any misfit functional fulfilling the requirements presented in Section 2.1.2 is of the form:*

$$J(\boldsymbol{u}_a) = J(\boldsymbol{u}) + a^3\mathcal{T}_3(\boldsymbol{z}) + a^4\mathcal{T}_4(\boldsymbol{z}) + a^5\mathcal{T}_5(\boldsymbol{z}) + a^6\mathcal{T}_6(\boldsymbol{z}) + o(a^6), \tag{2.71}$$

where the topological derivatives $\mathcal{T}_j$ *are given by:*

$$\begin{aligned}
\mathcal{T}_3(\boldsymbol{z}) =& -\boldsymbol{\nabla}\boldsymbol{u}(\boldsymbol{z}) : \boldsymbol{\mathcal{A}} : \boldsymbol{\nabla}\boldsymbol{p}(\boldsymbol{z}),\\
\mathcal{T}_4(\boldsymbol{z}) =& -\boldsymbol{\nabla}\boldsymbol{u}(\boldsymbol{z}) : \boldsymbol{\mathcal{A}}_{12} \bullet \boldsymbol{\nabla}^2\boldsymbol{p}(\boldsymbol{z}) - \boldsymbol{\nabla}\boldsymbol{p}(\boldsymbol{z}) : \boldsymbol{\mathcal{A}}_{12} \bullet \boldsymbol{\nabla}^2\boldsymbol{u}(\boldsymbol{z}),\\
\mathcal{T}_5(\boldsymbol{z}) =& -\frac{1}{2}\boldsymbol{\nabla}\boldsymbol{u}(\boldsymbol{z}) : \boldsymbol{\mathcal{A}}_{13} \bullet \boldsymbol{\nabla}^3\boldsymbol{p}(\boldsymbol{z}) - \boldsymbol{\nabla}^2\boldsymbol{u}(\boldsymbol{z}) \bullet \boldsymbol{\mathcal{A}}_{22} \bullet \boldsymbol{\nabla}^2\boldsymbol{p}(\boldsymbol{z}) - \frac{1}{2}\boldsymbol{\nabla}\boldsymbol{p}(\boldsymbol{z}) : \boldsymbol{\mathcal{A}}_{13} \bullet \boldsymbol{\nabla}^3\boldsymbol{u}(\boldsymbol{z}),\\
\mathcal{T}_6(\boldsymbol{z}) =& -\frac{1}{6}\boldsymbol{\nabla}\boldsymbol{u}(\boldsymbol{z}) : \boldsymbol{\mathcal{A}}_{14} \bullet \boldsymbol{\nabla}^4\boldsymbol{p}(\boldsymbol{z}) - \frac{1}{2}\boldsymbol{\nabla}^2\boldsymbol{u}(\boldsymbol{z}) \bullet \boldsymbol{\mathcal{A}}_{23} \bullet \boldsymbol{\nabla}^3\boldsymbol{p}(\boldsymbol{z})\\
&- \frac{1}{2}\boldsymbol{\nabla}^2\boldsymbol{p}(\boldsymbol{z}) \bullet \boldsymbol{\mathcal{A}}_{23} \bullet \boldsymbol{\nabla}^3\boldsymbol{u}(\boldsymbol{z}) - \frac{1}{6}\boldsymbol{\nabla}\boldsymbol{p}(\boldsymbol{z}) : \boldsymbol{\mathcal{A}}_{14} \bullet \boldsymbol{\nabla}^4\boldsymbol{u}(\boldsymbol{z})\\
&+ \boldsymbol{\nabla}\boldsymbol{u}(\boldsymbol{z}) : \boldsymbol{\mathcal{A}} : \boldsymbol{\nabla}_{21}\boldsymbol{G}_{\mathrm{C}}(\boldsymbol{z},\boldsymbol{z}) : \boldsymbol{\mathcal{A}} : \boldsymbol{\nabla}\boldsymbol{p}(\boldsymbol{z}) + \frac{1}{2}J''(\boldsymbol{u};\boldsymbol{v}_{\mathrm{out}}(\cdot;\boldsymbol{z})),
\end{aligned} \tag{2.72}$$

in terms of (i) the direct and adjoint fields $\boldsymbol{u}$ *and* $\boldsymbol{p}$ *solutions of the problems* (2.1) *and* (2.10) *posed on the homogeneous domain* $(\Omega, \boldsymbol{\mathcal{C}})$, *(ii) the elastic moment tensors* $\boldsymbol{\mathcal{A}}_{pq}$ *defined in Section 1.3.3, and (iii) the Green's tensor* $\boldsymbol{G}$ *defined by* (2.15), *which intervenes in* $\mathcal{T}_6$ *through its complementary part* $\boldsymbol{G}_{\mathrm{C}} = \boldsymbol{G} - \boldsymbol{G}_\infty$ *and in the definition* (2.70) *of* $\boldsymbol{v}_{\mathrm{out}}$.

Proof. Recall that J is expanded in Section 2.1.2 as:

$$J(\boldsymbol{u}_a) = J(\boldsymbol{u}) + J'(\boldsymbol{u};\boldsymbol{v}_a) + \frac{1}{2}J''(\boldsymbol{u};\boldsymbol{v}_a) + R(\boldsymbol{u};\boldsymbol{v}_a). \tag{2.73}$$

The expansion in powers of a is therefore obtained by evaluating successively each of these terms.

First derivative J' is computed thanks to the adjoint field $\boldsymbol{p}$ defined by (2.10) as:

$$J'(\boldsymbol{u};\boldsymbol{v}_a) = -\langle \boldsymbol{p}, \boldsymbol{u}_a\rangle^{\Delta\mathcal{C}}_{B_a} = -\left\langle \boldsymbol{p}, \boldsymbol{u} + \mathcal{P}_a^{-1}[\boldsymbol{V}_a]\right\rangle^{\Delta\mathcal{C}}_{B_a} - \langle \boldsymbol{p}, \boldsymbol{\delta}_a\rangle^{\Delta\mathcal{C}}_{B_a}, \tag{2.74}$$

where the inner expansion (2.39) was introduced for the second equality. The first term is expanded up to order $O(a^6)$ by (i) expressing the integral using the scaling $B_a \to \mathcal{B}$, (ii) introducing the definition (2.52) of $\boldsymbol{V}_a$, (iii) using Taylor expansion (2.42) of $\mathcal{P}_a[\boldsymbol{\nabla u}]$ and $\mathcal{P}_a[\boldsymbol{\nabla p}]$ and (iv) using the notation $\boldsymbol{u}_{\mathcal{B}}^{(p)}[\boldsymbol{E}_p] = \boldsymbol{\varphi}_p[\boldsymbol{E}_p] + \boldsymbol{v}_{\mathcal{B}}^{(p)}[\boldsymbol{E}_p]$ for compactness. We obtain:

$$\begin{aligned}\big\langle \boldsymbol{p}, \boldsymbol{u} + \mathcal{P}_a^{-1}[\boldsymbol{V}_a]\big\rangle_{B_a}^{\Delta\mathcal{C}} = a^3 \int_{\mathcal{B}} &\left[\sum_{q=1}^{4} \frac{a^{q-1}}{(q-1)!} \boldsymbol{\nabla}^q \boldsymbol{p}(\boldsymbol{z}) \bullet \bar{\boldsymbol{\xi}}^{\otimes q-1}\right] \\ &: \Delta\boldsymbol{\mathcal{C}} : \left[\sum_{p=1}^{4} \frac{a^{p-1}}{(p-1)!} \boldsymbol{\nabla u}_{\mathcal{B}}^{(p)}[\boldsymbol{\nabla}^p \boldsymbol{u}(\boldsymbol{z})] - a^3 \boldsymbol{\nabla u}_{\mathcal{B}}^{(1)}[\boldsymbol{L}(\boldsymbol{z})]\right] (\bar{\boldsymbol{\xi}})\, \mathrm{d}V_{\bar{\xi}} + o(a^6). \end{aligned} \tag{2.75}$$

Owing to the fact that only the gradients of $\boldsymbol{v}_{3,4\mathrm{C}}$ defined by (2.51) intervene, one can note that $\boldsymbol{\nabla u}_{\mathcal{B}}^{(1)}[\boldsymbol{L}(\boldsymbol{z})]$ is the only remaining contribution of these "complementary" terms in (2.75).

Moreover, the $o(a^6)$ behavior of the second term $\langle \boldsymbol{p}, \boldsymbol{\delta}_a\rangle_{B_a}^{\Delta\mathcal{C}}$ in (2.74) is obtained thanks to the estimate $\|\boldsymbol{\delta}_a\|_{H^1(B_a)} \le Ca^{11/2}$ given by the Theorem 2.3 so that:

$$\left|\langle \boldsymbol{p}, \boldsymbol{\delta}_a\rangle_{B_a}^{\Delta\mathcal{C}}\right| \le \|\Delta\boldsymbol{\mathcal{C}} : \boldsymbol{\nabla p}\|_{L^2(B_a)} \|\boldsymbol{\nabla\delta}_a\|_{L^2(B_a)} \le Ca^{3/2}a^{11/2} \le Ca^7. \tag{2.76}$$

Second derivative To evaluate $J''(\boldsymbol{u}; \boldsymbol{v}_a)$, under the assumptions $\Omega^{\mathrm{m}} \cap B_a = \emptyset$ and $\Gamma^{\mathrm{m}} \cap B_a = \emptyset$ made earlier, we use only the outer expansion of $\boldsymbol{v}_a$ (2.69) to obtain:

$$\begin{aligned} J''(\boldsymbol{u}; \boldsymbol{v}_a) &= a^6 J''(\boldsymbol{u}; \boldsymbol{v}_{\mathrm{out}}) + o(a^6) \\ &= a^6 \left[\int_{\Omega^{\mathrm{m}}} \boldsymbol{\nabla}_{22}\Psi_\Omega(\cdot; \boldsymbol{u}) : \boldsymbol{v}_{\mathrm{out}}^{\otimes 2}\, \mathrm{d}V + \int_{\Gamma^{\mathrm{m}}} \boldsymbol{\nabla}_{22}\Psi_\Gamma(\cdot; \boldsymbol{u}) : \boldsymbol{v}_{\mathrm{out}}^{\otimes 2}\, \mathrm{d}S\right] + o(a^6). \end{aligned} \tag{2.77}$$

Remainder $R(\boldsymbol{u}; \boldsymbol{v}_a)$ can be put in the form (considering only the surface integral on Γ^{m} for brievety)

$$R(\boldsymbol{u}; \boldsymbol{v}_a) = \int_0^1 (1-t) \int_{\Gamma^{\mathrm{m}}} [\boldsymbol{\nabla}_{22}\Psi_\Gamma(\boldsymbol{x}; \boldsymbol{u}(\boldsymbol{x}) + t\boldsymbol{v}_a(\boldsymbol{x})) - \boldsymbol{\nabla}_{22}\Psi_\Gamma(\boldsymbol{x}; \boldsymbol{u}(\boldsymbol{x}))] : (\boldsymbol{v}_a \otimes \boldsymbol{v}_a)(\boldsymbol{x})\, \mathrm{d}S_x\, \mathrm{d}t. \tag{2.78}$$

The $C^{0,\gamma}$ assumption on $\boldsymbol{\nabla}_{22}\Psi_\Gamma$ and the outer expansion (2.69) then yield the estimate:

$$\begin{aligned} \big|\, [\boldsymbol{\nabla}_{22}\Psi_\Gamma(\boldsymbol{x}; \boldsymbol{u}(\boldsymbol{x}) + t\boldsymbol{v}_a(\boldsymbol{x})) - \boldsymbol{\nabla}_{22}\Psi_\Gamma(\boldsymbol{x}; \boldsymbol{u}(\boldsymbol{x}))] : (\boldsymbol{v}_a \otimes \boldsymbol{v}_a)(\boldsymbol{x})\big| \\ \le Ca^{6+3\gamma}\big(|\boldsymbol{v}_{\mathrm{out}}(\boldsymbol{x}; \boldsymbol{z})|^{2+\gamma} t^\gamma + o(1)\big) \end{aligned} \tag{2.79}$$

for some constant C. Consequently, the following estimate holds:

$$R(\boldsymbol{u}; \boldsymbol{v}_a) \le O(a^{6+3\gamma}) = o(a^6) \tag{2.80}$$

Final computations The expansion (2.71) finally follows directly from the expansions above by (i) expanding the inner product (2.75) into a sum of inner products ordered by increasing powers of incsize, (ii) remarking that these products are of the form (1.115) used as the definition of elastic moment tensors and (iii) adding the $O(a^6)$ contribution of J'' (2.77). Owing to the $o(a^6)$ behavior of both remainder (2.76) and (2.80), one obtains the sought expansion. Remark also that we also used the definition (2.49) of $\boldsymbol{L}(\boldsymbol{z})$ in $\mathcal{T}_6$ to emphasize the dependency on the complementary Green's tensor $\boldsymbol{G}_{\mathrm{C}}$. □

2.3.2 Simplifications for particular shapes

We now adress some of the simplifications that can be obtained when considering particular shapes of inclusion.

Centrally symmetric inhomogeneities: Centrally symmetric shapes $\mathcal{B}$ cover many simple shapes such as balls, ellipsoids or cuboids. As a consequence of Lemma 1.9 asserting that $\boldsymbol{\mathcal{A}}_{pq} = \mathbf{0}$ for odd $p+q$, all of $\mathcal{T}_4$ and much of $\mathcal{T}_6$ vanish in (2.72) and the topological derivatives are given as:

$$
\begin{aligned}
&\mathcal{T}_3(\boldsymbol{z}) = -\,\boldsymbol{\nabla u}(\boldsymbol{z}) : \boldsymbol{\mathcal{A}} : \boldsymbol{\nabla p}(\boldsymbol{z}),\\
&\mathcal{T}_4(\boldsymbol{z}) = 0,\\
&\mathcal{T}_5(\boldsymbol{z}) = -\,\frac{1}{2}\boldsymbol{\nabla u}(\boldsymbol{z}) : \boldsymbol{\mathcal{A}}_{13} : \boldsymbol{\nabla}^3\boldsymbol{p}(\boldsymbol{z}) - \boldsymbol{\nabla}^2\boldsymbol{u}(\boldsymbol{z}) \bullet \boldsymbol{\mathcal{A}}_{22} \bullet \boldsymbol{\nabla}^2\boldsymbol{p}(\boldsymbol{z}) - \frac{1}{2}\boldsymbol{\nabla p}(\boldsymbol{z}) : \boldsymbol{\mathcal{A}}_{13} : \boldsymbol{\nabla}^3\boldsymbol{u}(\boldsymbol{z}),\\
&\mathcal{T}_6(\boldsymbol{z}) = \boldsymbol{\nabla u}(\boldsymbol{z}) : \boldsymbol{\mathcal{A}} : \boldsymbol{\nabla}_{21}\boldsymbol{G}_{\mathrm{C}}(\boldsymbol{z},\boldsymbol{z}) : \boldsymbol{\mathcal{A}} : \boldsymbol{\nabla p}(\boldsymbol{z}) + \frac{1}{2}J''(\boldsymbol{u}; \boldsymbol{v}_{\mathrm{out}}(\cdot;\boldsymbol{z}))
\end{aligned}
\tag{2.81}
$$

Note in particular that since $\mathcal{T}_4 = 0$, $\mathbb{J}(\emptyset) + a^3\mathcal{T}_3(\boldsymbol{z})$ is a fourth-order (and not third-order) approximation of $\mathbb{J}(B_a)$ in a in this case.

Remark 2.3. *In the expansion of $\boldsymbol{v}_a$, one can observe that the constant part $\boldsymbol{q}_4$ of $\boldsymbol{v}_{4\mathrm{C}}$ (2.51) vanishes for any centrally symmetric shape, since it involves first-order integrals of $\bar{\boldsymbol{\xi}}$ on $\mathcal{B}$.*

Ellipsoidal inhomogeneities: Ellipsoids are a particular case of centrally-symmetric shapes for which the $\boldsymbol{\nabla u}_{\mathcal{B}}^{(j)}[\boldsymbol{E}_j]$ are polynomials whose terms have degrees $j-1$, $j-3$ ...as explained in Section 1.3. The particular cases $j=1$ and $j=2$ and the way to compute the corresponding moment tensors are detailed in sections 1.3.2 and 1.3.3, in particular the following simplification holds:

$$
\boldsymbol{\mathcal{A}}_{13} = \frac{1}{|\mathcal{B}|}\boldsymbol{\mathcal{A}} \otimes \boldsymbol{M}^{(2)},
\tag{2.82}
$$

$\boldsymbol{M}^{(2)}$ being $\mathcal{B}$'s geometrical inertia tensor defined by (1.123). The topological derivatives are then expressed with the help of $\boldsymbol{\mathcal{A}}$ and $\boldsymbol{\mathcal{A}}_{22}$ only:

$$
\begin{aligned}
&\mathcal{T}_3(\boldsymbol{z}) = -\,\boldsymbol{\nabla u}(\boldsymbol{z}) : \boldsymbol{\mathcal{A}} : \boldsymbol{\nabla p}(\boldsymbol{z})\\
&\mathcal{T}_4(\boldsymbol{z}) = 0\\
&\mathcal{T}_5(\boldsymbol{z}) = -\,\frac{1}{2|\mathcal{B}|}\Big[\boldsymbol{\nabla u}(\boldsymbol{z}) : \boldsymbol{\mathcal{A}} : \Big(\boldsymbol{\nabla}^3\boldsymbol{p}(\boldsymbol{z}) : \boldsymbol{M}^{(2)}\Big) + \boldsymbol{\nabla p}(\boldsymbol{z}) : \boldsymbol{\mathcal{A}} : \Big(\boldsymbol{\nabla}^3\boldsymbol{u}(\boldsymbol{z}) : \boldsymbol{M}^{(2)}\Big)\Big]\\
&\qquad\qquad - \boldsymbol{\nabla}^2\boldsymbol{u}(\boldsymbol{z}) \bullet \boldsymbol{\mathcal{A}}_{22} \bullet \boldsymbol{\nabla}^2\boldsymbol{p}(\boldsymbol{z})\\
&\mathcal{T}_6(\boldsymbol{z}) = \boldsymbol{\nabla u}(\boldsymbol{z}) : \boldsymbol{\mathcal{A}} : \boldsymbol{\nabla}_{21}\boldsymbol{G}_{\mathrm{C}}(\boldsymbol{z},\boldsymbol{z}) : \boldsymbol{\mathcal{A}} : \boldsymbol{\nabla p}(\boldsymbol{z}) + \frac{1}{2}J''(\boldsymbol{u}; \boldsymbol{v}_{\mathrm{out}}(\cdot;\boldsymbol{z}))
\end{aligned}
\tag{2.83}
$$

Spherical inhomogeneities: If $\mathcal{B}$ is the unit sphere, then we easily compute:

$$
|\mathcal{B}| = \frac{4\pi}{3}, \qquad \boldsymbol{M}^{(2)} = \frac{4\pi}{15}\boldsymbol{I} \quad \text{and} \quad \boldsymbol{\nabla}^3\boldsymbol{u} : \boldsymbol{I} = \boldsymbol{\nabla}\boldsymbol{\Delta u},
\tag{2.84}
$$

so that $\mathcal{T}_5$ becomes:

$$
\mathcal{T}_5(\boldsymbol{z}) = -\frac{1}{10}\Big[\boldsymbol{\nabla u}(\boldsymbol{z}) : \boldsymbol{\mathcal{A}} : \boldsymbol{\nabla\Delta p}(\boldsymbol{z}) + \boldsymbol{\nabla p}(\boldsymbol{z}) : \boldsymbol{\mathcal{A}} : \boldsymbol{\nabla\Delta u}(\boldsymbol{z})\Big] - \boldsymbol{\nabla}^2\boldsymbol{u}(\boldsymbol{z}) \bullet \boldsymbol{\mathcal{A}}_{22} \bullet \boldsymbol{\nabla}^2\boldsymbol{p}(\boldsymbol{z}),
\tag{2.85}
$$

and $\boldsymbol{\mathcal{A}}$ have the closed-form expression (1.119) for isotropic materials.

2.3.3 Practical evaluation of the topological derivatives

The practical evaluation of the topological derivatives $\mathcal{T}_3$ to $\mathcal{T}_6$ rely on the following ingredients:

(a) Background and adjoint solutions: each needs to be computed just once, irrespective of the number of inhomogeneity sites $\boldsymbol{z}$ considered. As derivatives of $\boldsymbol{u}$ and $\boldsymbol{p}$ of order up to four in $\mathcal{T}_6$ (or only up to three in $\mathcal{T}_5$ for centrally symmetric shapes) are required, suitable solution or post-processing methods are needed. One possibility is to use integral representation formulas, since they can be differentiated at arbitrary order.

(b) Elastic moment tensors: each needs to be computed just once for given inhomogeneity shape and material properties. Their computation requires knowing the FSTP solutions $\boldsymbol{u}_{\mathcal{B}}^{(p)}$ for $p \in \{1,2,3,4\}$ in the general case and $p \in \{1,2\}$ in the centrally symmetric case. The latter are known explicitly for ellipsoidal inhomogeneities, except for the need to (i) evaluate Eshelby tensors given by integrals for anisotropic background properties, and (ii) solve numerically a small matrix system for computing $\boldsymbol{u}_{\mathcal{B}}^{(2)}$ via (1.104). For non-ellipsoidal inhomogeneities, one needs to solve numerically the FSTPs (1.88).

(c) Derivatives of either the Green's tensor $\boldsymbol{G}(\cdot,\boldsymbol{z})$ or its complementary part $\boldsymbol{G}_{\mathrm{C}}(\cdot,\boldsymbol{z})$ are needed for the evaluation of $\mathcal{T}_6$.

Evaluations of contributions related to the Green's tensor Item (c) above deserves elaboration. If an infinite medium is considered ($\Omega = \mathbb{R}^3$), then of course $\boldsymbol{G} = \boldsymbol{G}_\infty$ and $\boldsymbol{G}_{\mathrm{C}} = 0$. In a few other cases, in particular that of a semi-infinite elastic medium with a traction-free plane surface, the Green's tensor $\boldsymbol{G}$ is known in closed form. In most situations, however, contributions of $\boldsymbol{G}(\cdot,\boldsymbol{z})$ or $\boldsymbol{G}_{\mathrm{C}}(\cdot,\boldsymbol{z})$ to the topological derivative $\mathcal{T}_6$ will have to be computed numerically. We now briefly discuss the implications of this requirement.

First, the derivatives $\boldsymbol{\nabla}_1\boldsymbol{G}(\cdot,\boldsymbol{z})$ are involved, through the expression (2.70) of $\boldsymbol{v}_{\mathrm{out}}$, in $J''(\boldsymbol{u};\boldsymbol{v}_{\mathrm{out}})$. This looks inconvenient as all Green's tensors with source points on Γ^{m} and Ω^{m} are a priori needed. However, we note that the well-known symmetry property $\boldsymbol{G}(\boldsymbol{z},\boldsymbol{x}) = \boldsymbol{G}^{\mathrm{T}}(\boldsymbol{x},\boldsymbol{z})$ implies the property $\boldsymbol{\nabla}_1\boldsymbol{G}(\boldsymbol{z},\boldsymbol{x}) = \boldsymbol{\nabla}_2\boldsymbol{G}^{\mathrm{T}}(\boldsymbol{x},\boldsymbol{z})$. This allows to evaluate $J''(\boldsymbol{u};\boldsymbol{v}_{\mathrm{out}})$ for given $\boldsymbol{z}$ by means of the Green's tensor having $\boldsymbol{z}$ as source point.

In fact, the derivatives $\boldsymbol{H}^{(p)}(\cdot,\boldsymbol{z}) := \partial_{z_p}\boldsymbol{G}_{\mathrm{C}}(\cdot,\boldsymbol{z})$ can be found as solutions to problems obtained by differentiating the problem (2.17) satisfied by $\boldsymbol{G}_{\mathrm{C}}$ with respect to the coordinates of $\boldsymbol{z}$ (which acts therein as a parameter):

$$\left|\begin{aligned} &\operatorname{div}(\boldsymbol{\mathcal{C}} : \boldsymbol{\nabla}\boldsymbol{H}^{(p)}(\cdot,\boldsymbol{z})) = \boldsymbol{0} && \text{in } \Omega,\\ &\boldsymbol{H}^{(p)}(\cdot,\boldsymbol{z}) = \partial_p\boldsymbol{G}_\infty(\cdot-\boldsymbol{z}) && \text{on } \Gamma_{\mathrm{D}},\\ &\boldsymbol{t}[\boldsymbol{H}^{(p)}(\cdot,\boldsymbol{z})] = \boldsymbol{t}[\partial_p\boldsymbol{G}_\infty(\cdot-\boldsymbol{z})] && \text{on } \Gamma_{\mathrm{N}}.\end{aligned}\right. \tag{2.86}$$

Problems above are ordinary elastostatic problems with smooth boundary data (since $\boldsymbol{z} \in \Omega$). Then, $\mathcal{T}_6(\boldsymbol{z})$ also involves the second-order derivative $\boldsymbol{\nabla}_{12}\boldsymbol{G}_{\mathrm{C}}(\boldsymbol{z},\boldsymbol{z})$, which can be evaluated using first-order derivatives of $\boldsymbol{x} \mapsto \boldsymbol{H}^{(p)}(\boldsymbol{x},\boldsymbol{z})$ at $\boldsymbol{x} = \boldsymbol{z}$.

If the expansion of $\mathbb{J}(B_a)$ is to be evaluated for many inhomogeneity sites $\boldsymbol{z}$, the induced need to solve many problems of the form (2.86) becomes impractical. One possible remedy then consists in using a (truncated) separable representation of $\boldsymbol{G}_\infty(\boldsymbol{x}-\boldsymbol{z})$, of the form

$$\boldsymbol{G}_\infty(\boldsymbol{x}-\boldsymbol{z}) = \sum_{q=1}^{p} \boldsymbol{\alpha}_q(\boldsymbol{x}) \otimes \boldsymbol{\beta}_q(\boldsymbol{z}) + \boldsymbol{\varepsilon}_p. \tag{2.87}$$

Such representations are provided by e.g. multipole expansions [Fu et al., 1998] or the sparse cardinal sine decomposition of [Alouges & Aussal, 2015], with bounds on the truncation error ε_p. Then, the computational effort associated with solving problems of type (2.86) becomes $O(p)$ irrespective of the number of inhomogeneity sites $\boldsymbol{z}$.

2.4 Conclusions

This chapter was about the perturbations due to the presence of an inhomogeneity $(B_a, \boldsymbol{\mathcal{C}}^\star)$ in an otherwise homogeneous medium, and their asymptotic behavior as the size a of such inhomogeneity becomes smaller.

We first established the expansions of the perturbation $\boldsymbol{v}_a$ of the displacement due to external loads, up to $O(a^4)$ for the *inner* expansion (inside B_a) and to $O(a^3)$ - the leading order - for the *outer* expansion (outside $\overline{B_a}$). The practical computation of these expansions lean on the free-space transmission solutions $\boldsymbol{u}_{\mathcal{B}}^{(p)}$ addressed in Chapter 1, with analytical expressions available for ellipsoids. As an illustration, a full analytical example of the computation of the second-order inner expansion (up to $O(a^2)$) is provided in appendix 2.A.

These expansions of the perturbation displacement were then used to compute the expansion up to $O(a^6)$ of any cost functional $\mathbb{J}$ that depend implicitly on the inhomogeneity $(B_a, \boldsymbol{\mathcal{C}}^\star)$ through this perturbation $\boldsymbol{v}_a$ and that satisfies some regularity assumptions. Thanks especially to the adjoint state method that we used to expand the first functional derivative of $\mathbb{J}$, the terms $\mathcal{T}_j$, $j = 3, ..., 6$ of the expansion of $\mathbb{J}$, called the *topological derivatives* of $\mathbb{J}$, were given in closed-form by Theorem 2.4. The remainder of the expansion was rigorously proven to be of higher-order, i.e. $o(a^6)$. Finally, some of the difficulties raised by their practical computation were discussed briefly, along with some tracks to address these difficulties.

We now delay further discussion, particularly on how to use such expansion for identification, to the next chapter.

2.A Analytical example of perturbation expansion: concentric spheres

This part is meant to illustrate the expansion of the perturbation of the displacement. Consider two concentric spheres S_a and S, of radii a and b, S_a being embedded in S ($a < b$). We note $S_\mathrm{C} = S \backslash \overline{S_a}$ the complementary part of S_a. An homogeneous isotropic "background" material occupies S_C and is characterized by shear modulus and Poisson coefficient (μ, ν). Another isotropic homogeneous material occupies "the inhomogeneity" S_a and is similarly characterized by $(\mu^\star, \nu^\star)$. These notations are summarized on figure 2.1.

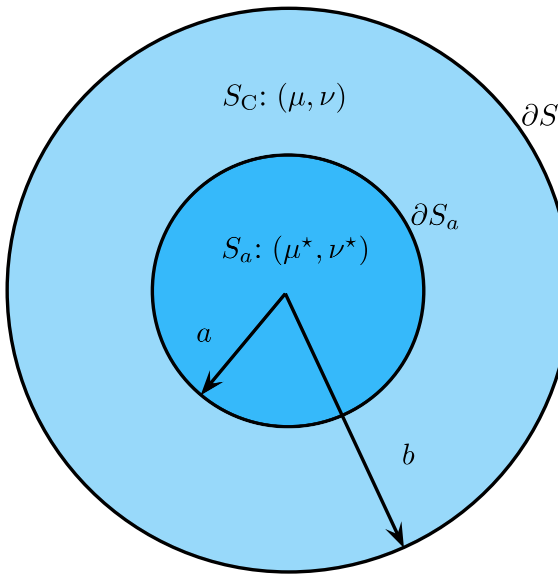

Figure 2.1: Concentric spheres: notations.

Applying some tractions (to be defined later) on the exterior boundary ∂S, we note in this section:

- $\boldsymbol{u}$ the "background" displacement, i.e. the displacement that would lie in S if it was homogeneous with properties (μ, ν).
- $\boldsymbol{u}^\mathrm{ex}$ the exact total displacement, and $\boldsymbol{v}^\mathrm{ex} = \boldsymbol{u}^\mathrm{ex} - \boldsymbol{u}$ the exact perturbation displacement due to the presence of S_a.
- $\boldsymbol{v}_a$ the second-order approximation of $\boldsymbol{v}^\mathrm{ex}$ obtained by an asymptotic expansion as $a \to 0$.

The goal of this study is to compute the first terms of $\boldsymbol{v}_a$ and compare it to $\boldsymbol{v}^\mathrm{ex}$. Some numerical illustrations are provided, performed with Matlab and the tensor toolbox [Bader et al., 2012].

2.A.1 Preliminary computations: exact and background fields

2.A.1.1 Solution of Navier equations in spherical coordinates

General solutions to the elastic equilibrium equation $\mathrm{div}(\boldsymbol{\mathcal{C}} : \boldsymbol{\nabla u}) = \boldsymbol{0}$ for isotropic materials are given in spherical coordinates (r, θ, φ) in [Parton et al., 1984]. We limit ourselves to axisymmetrical problems, for which the solutions are the harmonics $\boldsymbol{u}^{(n)}(r,\theta)$ defined for each harmonics by four constants (A,B,C,D) as:

$$
\begin{aligned}
u_r^{(n)} &= \Big[A(n+1)(n-2+4\nu)r^{n+1} + Bnr^{n-1} + Cn(n+3-4\nu)r^{-n} - D(n+1)r^{-(n+2)}\Big]\, P_n(\cos(\theta))\\
u_\theta^{(n)} &= \Big[A(n+5-4\nu)r^{n+1} + Br^{n-1} + C(-n+4-4\nu)r^{-n} + Dr^{-(n+2)}\Big]\, \partial_\theta P_n(\cos(\theta)),
\end{aligned}
\tag{2.88}
$$

where $\partial_\theta = \partial/\partial\theta$ and P_n are Legendre polynomials. The first ones and their derivatives are:

$$
\begin{aligned}
&P_0(\cos(\theta)) = 1 && \partial_\theta P_0(\cos(\theta)) = 0\\
&P_1(\cos(\theta)) = \cos(\theta) && \partial_\theta P_1(\cos(\theta)) = -\sin(\theta)\\
&P_2(\cos(\theta)) = \frac{1}{2}(3\cos^2(\theta)-1) && \partial_\theta P_2(\cos(\theta)) = -3\cos(\theta)\sin(\theta)
\end{aligned}
\tag{2.89}
$$

Such fields are physically acceptable in a bounded domain that does not contain the origin (typically S_{C}) while $C = D = 0$ is required for a solution computed in a bounded domain containing the origin (typically S or S_a). The corresponding components of the traction vector in the radial direction $\boldsymbol{t}^{(n)} = \boldsymbol{\sigma}^{(n)} \cdot \boldsymbol{e}_r$ are:

$$
\begin{aligned}
t_r^{(n)} &= 2\mu\Big[A(n+1)(n^2-n-2-2\nu)r^n + Bn(n-1)r^{n-2}\\
&\qquad - Cn(n^2+3n-2\nu)r^{-(n+1)} + D(n+1)(n+2)r^{-(n+3)}\Big]P_n(\cos(\theta))\\
t_\theta^{(n)} &= 2\mu\Big[A(n^2+2n-1+2\nu)r^n + B(n-1)r^{n-2}\\
&\qquad + C(n^2-2+2\nu)r^{-(n+1)} - D(n+2)r^{-(n+3)}\Big]\partial_\theta P_n(\cos(\theta))
\end{aligned}
\tag{2.90}
$$

2.A.1.2 Solution under surface harmonic loading

As showed by (2.88), one displacement harmonic is entirely defined by up to four coefficients (A, B, C and D) depending if the domain of study contains the origin and/or is bounded. These coefficients are to be determined for each problem by the boundary and/or interface conditions. For simplicity, we chose to consider a surface harmonic loading on the exterior surface ∂S, i.e.

$$
\boldsymbol{t}^{(n)}_{|\partial S} = t_r P_n(\cos(\theta))\boldsymbol{e}_r + t_\theta \partial_\theta P_n(\cos(\theta))\boldsymbol{e}_\theta \tag{2.91}
$$

for some $(t_r, t_\theta) \in \mathbb{R}^2$. The corresponding force per unit length on a vertical half-circle as $\theta \in [0,\pi]$ is $\boldsymbol{t}^{(n)}\sin(\theta)$ ($\sin(\theta)\mathrm{d}\varphi$ being the contribution of the surface element in the direction $\boldsymbol{e}_\varphi$) and is represented on Figure 2.2.

This loading, must be balanced (zero resultant force and moment). The only global equilibrium condition that is not trivially verified for loads of the form (2.91) is

$$
\int_{\partial S} \boldsymbol{t}\cdot\boldsymbol{e}_3 \,\mathrm{d}S = 0 \tag{2.92}
$$

i.e.

$$
2\pi \int_0^\pi \big[t_r P_n(\cos(\theta))\cos(\theta) - t_\theta \sin(\theta)\partial_\theta P_n(\cos(\theta))\big]\sin(\theta)\,\mathrm{d}\theta = 0 \tag{2.93}
$$

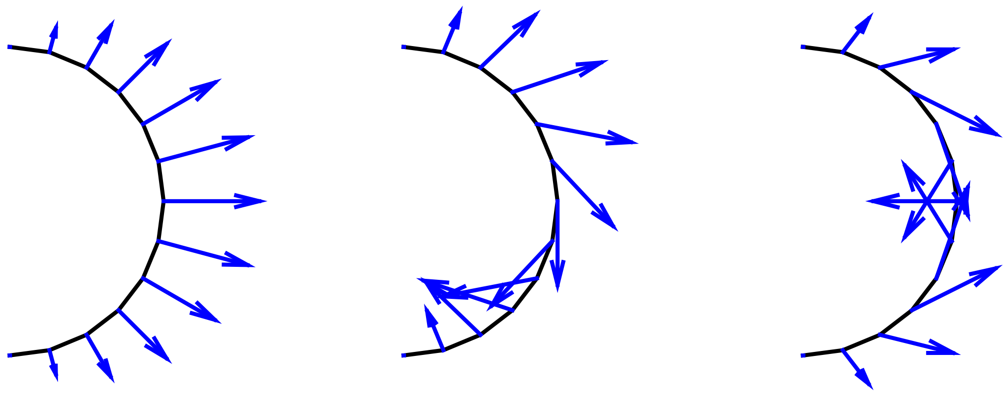

Figure 2.2: Force per unit length $\boldsymbol{t}^{(n)}\sin(\theta)$ applied on ∂S for $(t_r, t_\theta) = (1, -0.5)$ such that $t_r + 2t_\theta = 0$.

or, integrating by parts the 2nd term in the integral and using $\partial_\theta \sin^2(\theta) = 2\sin(\theta)\cos(\theta)$ and $\cos(\theta) = P_1(\cos(\theta))$:

$$2\pi \int_0^\pi \big[t_r + 2t_\theta\big] P_n(\cos(\theta)) P_1(\cos(\theta)) \sin(\theta)\, \mathrm{d}\theta = 0 \tag{2.94}$$

Orthogonality properties of the Legendre polynomials show that the above is automatically satisfied for $n \neq 1$, whereas one must assume $t_r + 2t_\theta = 0$ if $n = 1$. Figure 2.2 gives a graphical confirmation of the global equilibrium under such constraint.

Finally, this choice of surface harmonic traction loading was made such that, thanks to the orthogonality of the Legendre polynomials, only the corresponding (n^{th}) harmonic composing the traction and displacement field is excited inside S. The background and exact solutions are therefore easily computed.

Background solution: Since $\boldsymbol{u}$ is defined on S which contains the origin, only A and B are nonzero for each harmonic. These coefficients are computed from the traction boundary conditions on ∂S, i.e. for $r = b$, which result on the system:

$$\begin{aligned} A(n+1)(n^2 - n - 2 - 2\nu)b^n + Bn(n-1)b^{n-2} &= \frac{t_r}{2\mu} \\ A(n^2 + 2n - 1 + 2\nu)b^n + B(n-1)b^{n-2} &= \frac{t_\theta}{2\mu} \end{aligned} \tag{2.95}$$

Exact solution: $\boldsymbol{u}^{\mathrm{ex}}$ is defined by parts on (i) S_a containing the origin, by two coefficients A_1 and B_1 and (ii) S_{C} bounded and not containing the origin by four coefficients A_2, B_2, C_2 and D_2. The transmission conditions (continuity of the displacement and traction vector) on ∂S_a $(r = a)$

then read:

$$
\begin{aligned}
&\left[A_2(n-2+4\nu)-A_1(n-2+4\nu^\star)\right](n+1)a^{n+1}+(B_2-B_1)na^{n-1}\\
&\qquad\qquad\qquad\qquad + C_2n(n+3-4\nu)a^{-n}-D_2(n+1)a^{-(n+2)}=0\\
&\left[A_2(n+5-4\nu)-A_1(n+5-4\nu^\star)\right]a^{n+1}+(B_2-B_1)a^{n-1}\\
&\qquad\qquad\qquad\qquad + C_2(-n+4-4\nu)a^{-n}+D_2a^{-(n+2)}=0\\
&\left[A_2(n^2-n-2-2\nu)-\gamma A_1(n^2-n-2-2\nu^\star)\right](n+1)a^{n}+(B_2-\gamma B_1)n(n-1)a^{n-2}\\
&\qquad\qquad\qquad\qquad - C_2n(n^2+3n-2\nu)a^{-(n+1)}+D_2(n+1)(n+2)a^{-(n+3)}=0\\
&\left[A_2(n^2+2n-1+2\nu)-\gamma A_1(n^2+2n-1+2\nu^\star)\right]a^{n}+(B_2-\gamma B_1)(n-1)a^{n-2}\\
&\qquad\qquad\qquad\qquad + C_2(n^2-2+2\nu)a^{-(n+1)}-D_2(n+2)a^{-(n+3)}=0
\end{aligned}
\tag{2.96}
$$

where the stiffness contrast γ is:

$$
\gamma=\frac{\mu^\star}{\mu}
\tag{2.97}
$$

Similarly, the boundary conditions on ∂S $(r=b)$ are written:

$$
\begin{aligned}
&A_2(n+1)(n^2-n-2-2\nu)b^n+B_2n(n-1)b^{n-2}\\
&\qquad\qquad - C_2n(n^2+3n-2\nu)b^{-(n+1)}+D_2(n+1)(n+2)b^{-(n+3)}=\frac{t_r}{2\mu}\\
&A_2(n^2+2n-1+2\nu)b^n+B_2(n-1)b^{n-2}\\
&\qquad\qquad + C_2(n^2-2+2\nu)b^{-(n+1)}-D_2(n+2)b^{-(n+3)}=\frac{t_\theta}{2\mu}
\end{aligned}
\tag{2.98}
$$

for a total of six equations that can be written as a linear system :

$$
\begin{bmatrix}
-f_r^\star(a) & -g_r(a) & f_r(a) & g_r(a) & h_r(a) & k_r(a)\\
-f_\theta^\star(a) & -g_\theta(a) & f_\theta(a) & g_\theta(a) & h_\theta(a) & k_\theta(a)\\
-\gamma F_r^\star(a) & -\gamma G_r(a) & F_r(a) & G_r(a) & H_r(a) & K_r(a)\\
-\gamma F_\theta^\star(a) & -\gamma G_\theta(a) & F_\theta(a) & G_\theta(a) & H_\theta(a) & K_\theta(a)\\
0 & 0 & F_r(b) & G_r(b) & H_r(b) & K_r(b)\\
0 & 0 & F_\theta(b) & G_\theta(b) & H_\theta(b) & K_\theta(b)
\end{bmatrix}
\begin{Bmatrix} A_1\\ B_1\\ A_2\\ B_2\\ C_2\\ D_2 \end{Bmatrix}
=
\begin{Bmatrix} 0\\ 0\\ 0\\ 0\\ t_r/2\mu\\ t_\theta/2\mu \end{Bmatrix},
\tag{2.99}
$$

where the functions $F, G, f, g...$ are defined as the coefficients in (2.96) and (2.98). Note that $F^\star = F$ and $f^\star = f$ if $\nu^\star = \nu$. This system is solved numerically in the Matlab code.

2.A.1.3 The case n=1

When $n=1$, for the background solution, the boundary conditions (2.95) become:

$$
-4A(1+\nu)b=\frac{t_r}{2\mu}\quad\text{and}\quad 2A(1+\nu)b=\frac{t_\theta}{2\mu}.
\tag{2.100}
$$

They provide another justification to the necessary condition $t_r+2t_\theta=0$ already established in part 2.A.1.2, and gives:

$$
A=-\frac{t_r}{8\mu(1+\nu)b}=-\frac{t_r}{4Eb},
\tag{2.101}
$$

E being the Young's modulus of the background material. For the exact solution, since $G_r(r) = n(n-1)r^{n-2} = 0$ and $G_\theta(r) = (n-1)r^{n-2} = 0$, the matrix of the system (2.99) is:

$$\begin{bmatrix} -f_r(a) & -g_r(a) & f_r(a) & g_r(a) & h_r(a) & k_r(a) \\ -f_\theta(a) & -g_\theta(a) & f_\theta(a) & g_\theta(a) & h_\theta(a) & k_\theta(a) \\ -\gamma F_r^\star(a) & 0 & F_r(a) & 0 & H_r(a) & K_r(a) \\ -\gamma F_\theta^\star(a) & 0 & F_\theta(a) & 0 & H_\theta(a) & K_\theta(a) \\ 0 & 0 & F_r(b) & 0 & H_r(b) & K_r(b) \\ 0 & 0 & F_\theta(b) & 0 & H_\theta(b) & K_\theta(b) \end{bmatrix} \tag{2.102}$$

and is no more invertible since the second and fourth columns are each other opposite : the kernel of the matrix is the one-dimensional space defined by $B_1 = B_2$, and zero other coefficients. As the motion associated to the coefficient B is a rigid body translation toward the $\boldsymbol{e}_3$ direction ($\boldsymbol{u}_B = B(\cos(\theta)\boldsymbol{e}_r - \sin(\theta)\boldsymbol{e}_\theta) = B\boldsymbol{e}_3$), this kernel physically corresponds to the rigid body translation of the whole sphere S. Consequently, an additional assumption involving B_2 and/or B_1 is necessary for the system to be solved.

2.A.1.4 Gradients of the background field

The gradients $\boldsymbol{\nabla}\boldsymbol{u}(\boldsymbol{0})$ and $\boldsymbol{\nabla}^2\boldsymbol{u}(\boldsymbol{0})$ of the background field act as the source terms of the FSTPs satisfied by the terms of the expansion of $\boldsymbol{v}_a$. They are therefore computed in this part.

General case $n \geq 1$, expressed in spherical coordinates: Since $\boldsymbol{u}$ is defined on S containing the origin, it can be written as a sum of harmonics $\boldsymbol{u}^{(n)}$ with positive powers of r:

$$\begin{aligned} u_r^{(n)} &= \left[A_r^{(n)} r^{n+1} + B_r^{(n)} r^{n-1}\right] P_n \\ u_\theta^{(n)} &= \left[A_\theta^{(n)} r^{n+1} + B_\theta^{(n)} r^{n-1}\right] \partial_\theta P_n, \end{aligned} \tag{2.103}$$

where we introduced the notations:

$$\begin{aligned} A_r^{(n)} &= A(n+1)(n-2+4\nu) & \qquad B_r^{(n)} &= Bn \\ A_\theta^{(n)} &= A(n+5-4\nu) & \qquad B_\theta^{(n)} &= B \end{aligned}$$

∂_θ still stands for $\partial/\partial\theta$, and the dependency $P_n = P_n(\cos(\theta))$ is kept implicit to ease the lecture. Its first gradient, in spherical coordinates, is:

$$\boldsymbol{\mathcal{D}}^{(n)} := \boldsymbol{\nabla}\boldsymbol{u}^{(n)} = \begin{bmatrix} \mathcal{D}_{rr}^{(n)} & \mathcal{D}_{r\theta}^{(n)} & 0 \\ \mathcal{D}_{\theta r}^{(n)} & \mathcal{D}_{\theta\theta}^{(n)} & 0 \\ 0 & 0 & \mathcal{D}_{\varphi\varphi}^{(n)} \end{bmatrix}, \tag{2.104}$$

with:

$$\begin{aligned}
\mathcal{D}_{rr}^{(n)} &= \left[(n+1)A_r^{(n)}r^n + (n-1)B_r^{(n)}r^{n-2}\right] P_n \\
\mathcal{D}_{r\theta}^{(n)} &= \left[(A_r^{(n)} - A_\theta^{(n)})r^n + (B_r^{(n)} - B_\theta^{(n)})r^{n-2}\right] \partial_\theta P_n \\
\mathcal{D}_{\theta r}^{(n)} &= \left[(n+1)A_\theta^{(n)}r^n + (n-1)B_\theta^{(n)}r^{n-2}\right] \partial_\theta P_n \\
\mathcal{D}_{\theta\theta}^{(n)} &= \left[A_\theta^{(n)}r^n + B_\theta^{(n)}r^{n-2}\right] \partial_\theta^2 P_n + \left[A_r^{(n)}r^n + B_r^{(n)}r^{n-2}\right] P_n \\
\mathcal{D}_{\varphi\varphi}^{(n)} &= \left[A_\theta^{(n)}r^n + B_\theta^{(n)}r^{n-2}\right] \frac{\partial_\theta P_n}{\tan\theta} + \left[A_r^{(n)}r^n + B_r^{(n)}r^{n-2}\right] P_n
\end{aligned} \tag{2.105}$$

The above expression is also valid for $n = 1$, since $P_1(\cos(\theta)) = \cos(\theta)$ and some alebra show that all the coefficients in front of the $r^{n-2} = r^{-1}$ vanish. In particular, we have:

$$\boldsymbol{\nabla u}^{(1)}(\mathbf{0}) = \mathbf{0}, \quad \boldsymbol{\nabla u}^{(2)}(\mathbf{0}) = B \begin{bmatrix} 3\cos^2(\theta) - 1 & -3\cos(\theta)\sin(\theta) & 0 \\ -3\cos(\theta)\sin(\theta) & -3\cos^2(\theta) + 2 & 0 \\ 0 & 0 & -1 \end{bmatrix} \tag{2.106}$$

The couple (θ, φ) in the later expression defines the basis $(\boldsymbol{e}_r, \boldsymbol{e}_\theta, \boldsymbol{e}_\varphi)$ in which this gradient is expressed. For example, taking $\theta = \varphi = 0$, the spherical basis is a direct permutation of the Cartesian basis: $(\boldsymbol{e}_r, \boldsymbol{e}_\theta, \boldsymbol{e}_\varphi) = (\boldsymbol{e}_3, \boldsymbol{e}_1, \boldsymbol{e}_2)$ so that:

$$\boldsymbol{\nabla u}^{(2)}(\mathbf{0}) = \begin{bmatrix} -B & 0 & 0 \\ 0 & -B & 0 \\ 0 & 0 & 2B \end{bmatrix}_{(\boldsymbol{e}_1, \boldsymbol{e}_2, \boldsymbol{e}_3)} \tag{2.107}$$

Noting $\boldsymbol{\mathcal{E}}^{(n)} = \boldsymbol{\nabla}^2 \boldsymbol{u}^{(n)}$, the relation $\mathrm{d}\boldsymbol{\mathcal{D}}^{(n)} = \boldsymbol{\mathcal{E}}^{(n)} \cdot \mathrm{d}\boldsymbol{r}$ holds, where the differential of $\boldsymbol{\mathcal{D}}^{(n)}$ is computed as:

$$\mathrm{d}\left(\mathcal{D}_{\alpha\beta}^{(n)} \boldsymbol{e}_\alpha \otimes \boldsymbol{e}_\beta\right) = \mathrm{d}\mathcal{D}_{\alpha\beta}^{(n)} \boldsymbol{e}_\alpha \otimes \boldsymbol{e}_\beta + \mathcal{D}_{\alpha\beta}^{(n)} \mathrm{d}\boldsymbol{e}_\alpha \otimes \boldsymbol{e}_\beta + \mathcal{D}_{\alpha\beta}^{(n)} \boldsymbol{e}_\alpha \otimes \mathrm{d}\boldsymbol{e}_\beta \tag{2.108}$$

for $(\alpha, \beta) \in (r, \theta, \varphi)^2$, those of the basis vectors are:

$$\begin{aligned}
\mathrm{d}\boldsymbol{e}_r &= \mathrm{d}\theta \boldsymbol{e}_\theta + \sin(\theta)\mathrm{d}\varphi \boldsymbol{e}_\theta \\
\mathrm{d}\boldsymbol{e}_\theta &= -\mathrm{d}\theta \boldsymbol{e}_r + \cos(\theta)\mathrm{d}\varphi \boldsymbol{e}_\theta \\
\mathrm{d}\boldsymbol{e}_\varphi &= -\mathrm{d}\varphi\left(\sin(\theta)\boldsymbol{e}_r + \cos(\theta)\boldsymbol{e}_\theta\right),
\end{aligned} \tag{2.109}$$

and this of the position vector $\boldsymbol{r} = r\boldsymbol{e}_r$ is:

$$\mathrm{d}\boldsymbol{r} = \mathrm{d}r \boldsymbol{e}_r + r\mathrm{d}\theta \boldsymbol{e}_\theta + r\sin(\theta)\mathrm{d}\varphi \boldsymbol{e}_\varphi \tag{2.110}$$

Then, identifying the terms containing $\mathrm{d}r$, $\mathrm{d}\theta$ and $\mathrm{d}\varphi$ in (2.108), we obtain the nonzero components of the second gradient $\boldsymbol{\mathcal{E}}^{(n)}$:

$$
\begin{aligned}
\mathcal{E}^{(n)}_{rrr} &= \left[(n+1)nA^{(n)}_r r^{n-1} + (n-1)(n-2)B^{(n)}_r r^{n-3}\right] P_n \\
\mathcal{E}^{(n)}_{rr\theta} = \mathcal{E}^{(n)}_{r\theta r} &= \left[n(A^{(n)}_r - A^{(n)}_\theta) r^{n-1} + (n-2)(B^{(n)}_r - B^{(n)}_\theta) r^{n-3}\right] \partial_\theta P_n \\
\mathcal{E}^{(n)}_{r\theta\theta} &= \left[(A^{(n)}_r - 2A^{(n)}_\theta) r^{n-1} + (B^{(n)}_r - 2B^{(n)}_\theta) r^{n-3}\right] \partial^2_\theta P_n \\
&+ \left[nA^{(n)}_r r^{n-1} + (n-2)B^{(n)}_r r^{n-3}\right] P_n \\
\mathcal{E}^{(n)}_{r\varphi\varphi} &= \left[nA^{(n)}_r r^{n-1} + (n-2)B^{(n)}_r r^{n-3}\right] P_n \\
&+ \left[(A^{(n)}_r - 2A^{(n)}_\theta) r^{n-1} + (B^{(n)}_r - 2B^{(n)}_\theta) r^{n-3}\right] \frac{\partial_\theta P_n}{\tan\theta} \\
\mathcal{E}^{(n)}_{\theta rr} &= \left[(n+1)nA^{(n)}_\theta r^{n-1} + (n-1)(n-2)B^{(n)}_\theta r^{n-3}\right] \partial_\theta P_n \\
\mathcal{E}^{(n)}_{\theta r\theta} = \mathcal{E}^{(n)}_{\theta\theta r} &= \left[nA^{(n)}_\theta r^{n-1} + (n-2)B^{(n)}_\theta r^{n-3}\right] \partial^2_\theta P_n \\
&+ \left[nA^{(n)}_r r^{n-1} + (n-2)B^{(n)}_r r^{n-3}\right] P_n \\
\mathcal{E}^{(n)}_{\theta\theta\theta} &= \left[A^{(n)}_\theta r^{n-1} + B^{(n)}_\theta r^{n-3}\right] \partial^3_\theta P_n \\
&+ \left[(2A^{(n)}_r + nA^{(n)}_\theta) r^{n-1} + (2B^{(n)}_r + (n-2)B^{(n)}_\theta) r^{n-3}\right] \partial_\theta P_n \\
\mathcal{E}^{(n)}_{\theta\varphi\varphi} &= \left[(n+1)A^{(n)}_\theta r^{n-1} + (n-1)B^{(n)}_\theta r^{n-3}\right] \partial_\theta P_n \\
&+ \left[A^{(n)}_\theta r^{n-1} + B^{(n)}_\theta r^{n-3}\right] \left(\frac{\partial^2_\theta P_n}{\tan\theta} - \frac{\partial_\theta P_n}{\tan^2\theta}\right) \\
\mathcal{E}^{(n)}_{\varphi r\varphi} = \mathcal{E}^{(n)}_{\varphi\varphi r} &= \left[nA^{(n)}_\theta r^{n-1} + (n-2)B^{(n)}_\theta r^{n-3}\right] \frac{\partial_\theta P_n}{\tan\theta} \\
&+ \left[nA^{(n)}_r r^{n-1} + (n-2)B^{(n)}_r r^{n-3}\right] P_n \\
\mathcal{E}^{(n)}_{\varphi\theta\varphi} = \mathcal{E}^{(n)}_{\varphi\varphi\theta} &= \left[A^{(n)}_\theta r^{n-1} + B^{(n)}_\theta r^{n-3}\right] \left(\frac{\partial^2_\theta P_n}{\tan\theta} - \frac{\partial_\theta P_n}{\sin^2\theta}\right) \\
&+ \left[A^{(n)}_r r^{n-1} + B^{(n)}_r r^{n-3}\right] \partial_\theta P_n
\end{aligned}
\tag{2.111}
$$

Similarly than for the first gradient, these expressions are also valid for $n = 1$ and $n = 2$, since in these case the coefficients in front of the negative powers of r vanish. In particular, $\boldsymbol{\nabla}^2\boldsymbol{u}^{(2)}$ is found to be linear in r, so that $\boldsymbol{\nabla}^2\boldsymbol{u}^{(2)}(\mathbf{0}) = \mathbf{0}$.

Gradients for $n = 1$ in Cartesian coordinates Taking $n = 1$ in (2.103), we obtain for $\boldsymbol{u}^{(1)}$ defined on S:

$$
\begin{aligned}
u^{(1)}_r &= \left[2A(4\nu - 1)r^2 + B\right] \cos(\theta) \\
u^{(1)}_\theta &= \left[2A(3 - 2\nu)r^2 + B\right] (-\sin(\theta)).
\end{aligned}
\tag{2.112}
$$

In the Cartesian basis $(\boldsymbol{e}_1, \boldsymbol{e}_2, \boldsymbol{e}_3)$,

$$
\cos(\theta)\boldsymbol{e}_r = \frac{1}{r^2}\begin{bmatrix} x_1x_3 \\ x_2x_3 \\ x_3^2 \end{bmatrix} \quad \text{and} \quad -\sin(\theta)\boldsymbol{e}_\theta = \frac{1}{r^2}\begin{bmatrix} -x_1x_3 \\ -x_2x_3 \\ \rho^2 \end{bmatrix}, \quad \text{with } \rho^2 = x_1^2 + x_2^2, \tag{2.113}
$$

and $\boldsymbol{u}^{(1)}$ is therefore given by:

$$\boldsymbol{u}^{(1)}(\boldsymbol{x}) = \begin{bmatrix} 4A(3\nu-2)x_1x_3 \\ 4A(3\nu-2)x_2x_3 \\ 2A\left[(4\nu-1)x_3^2 + (3-2\nu)\rho^2\right] + B \end{bmatrix}. \tag{2.114}$$

Is gradient is then found to be:

$$\boldsymbol{\nabla u}^{(1)}(\boldsymbol{x}) = 4A \begin{bmatrix} (3\nu-2)x_3 & 0 & (3\nu-2)x_1 \\ 0 & (3\nu-2)x_3 & (3\nu-2)x_2 \\ (3-2\nu)x_1 & (3-2\nu)x_2 & (4\nu-1)x_3 \end{bmatrix} \tag{2.115}$$

and in particular vanishes at the origin $\boldsymbol{x} = \boldsymbol{0}$ as already seen in (2.106). Noting the second gradient $\boldsymbol{\mathcal{E}}^{(1)} := \boldsymbol{\nabla}^2\boldsymbol{u}^{(1)}$, most of its components are zero except seven that are constants:

$$\begin{array}{lll} \mathcal{E}^{(1)}_{113} = 4A(3\nu-2) & & \mathcal{E}^{(1)}_{131} = 4A(3\nu-2) \\ & \mathcal{E}^{(1)}_{223} = 4A(3\nu-2) & \mathcal{E}^{(1)}_{232} = 4A(3\nu-2) \\ \mathcal{E}^{(1)}_{311} = 4A(3-2\nu) & \mathcal{E}^{(1)}_{322} = 4A(3-2\nu) & \mathcal{E}^{(1)}_{333} = 4A(4\nu-1) \end{array} \tag{2.116}$$

One can check that these expressions correspond to the general formulae (2.105) and (2.111) for $n = 1$, $\theta = \varphi = 0$ and after proper index permutation.

2.A.2 Second-order approximation of displacement

The inner approximation is given up to the second-order term as:

$$\boldsymbol{v}_a(\boldsymbol{x}) = a\boldsymbol{v}^{(1)}_{\mathcal{B}}\left[\boldsymbol{\nabla u}(\boldsymbol{0})\right](\bar{\boldsymbol{x}}) + a^2\boldsymbol{v}^{(2)}_{\mathcal{B}}\left[\boldsymbol{\nabla}^2\boldsymbol{u}(\boldsymbol{0})\right](\bar{\boldsymbol{x}}) + o(a^2) \tag{2.117}$$

where $\boldsymbol{x} \in S_a$ and $\bar{\boldsymbol{x}} = \boldsymbol{x}/a$ belongs to the unit sphere. We recall for convenience the solutions of the first and second Eshelby problems for ellipsoids, studied in section 1.3.2.1 and 1.3.2.2:

$$\boldsymbol{v}^{(1)}_{\mathcal{B}}[\boldsymbol{E}_1](\bar{\boldsymbol{x}}) = (\boldsymbol{A}_1 : \boldsymbol{E}_1)\cdot\bar{\boldsymbol{x}}, \qquad \boldsymbol{v}^{(2)}_{\mathcal{B}}[\boldsymbol{E}_2](\bar{\boldsymbol{x}}) = \frac{1}{2}\left((\boldsymbol{\mathcal{F}}\bullet\boldsymbol{A}_2)\bullet\boldsymbol{E}_2\right) : (\bar{\boldsymbol{x}}\otimes\bar{\boldsymbol{x}}), \tag{2.118}$$

where $\boldsymbol{A}_1$ and $\boldsymbol{A}_2$ are computed from the resolution of Eshelby's equivalent stress equation, and $\boldsymbol{\mathcal{F}}$ accounts for the integration of a linear strain.

2.A.2.1 The case n = 1

The various (exact, background, Eshelby) solutions for $n=1$ are now considered in some detail.

The two-sphere transmission problem. The axisymmetric solution $\boldsymbol{u}^{\text{ex}}$ for $n=1$ of the two-sphere transmission problem is given, from (2.88), by

$$\begin{aligned} u^{(1)}_r &= [2(4\nu^\star-1)A^{\text{ex}}_1 r^2 + B^{\text{ex}}_1]\cos(\theta) \\ u^{(1)}_\theta &= -[(6-4\nu^\star)A^{\text{ex}}_1 r^2 + B^{\text{ex}}_1]\sin(\theta) \end{aligned}$$

in S_a, and by

$$\begin{aligned} u^{(1)}_r &= \left[2(4\nu-1)A^{\text{ex}}_2 r^2 + B^{\text{ex}}_2 + 4(1-\nu)C^{\text{ex}}_2 r^{-1} - 2D^{\text{ex}}_2 r^{-3}\right]\cos(\theta) \\ u^{(1)}_\theta &= -\left[(6-4\nu)A^{\text{ex}}_2 r^2 + B^{\text{ex}}_2 + (3-4\nu)C^{\text{ex}}_2 r^{-1} + D^{\text{ex}}_2 r^{-3)}\right]\sin(\theta) \end{aligned}$$

in S_{C}. The transmission conditions (2.98) become

$$\begin{bmatrix} (2-8\nu^{\star})a^2 & -1 & (8\nu-2)a^2 & 1 & 4(1-\nu)a^{-1} & -2a^{-3} \\ (4\nu^{\star}-6)a^2 & -1 & (6-4\nu)a^2 & 1 & (3-4\nu)a^{-1} & a^{-3} \\ 4\gamma(1+\nu^{\star})a^2 & 0 & -4(1+\nu)a^2 & 0 & (4-2\nu)a^{-1} & 6a^{-3} \\ -2\gamma(1+\nu^{\star})a^2 & 0 & 2(1+\nu)a^2 & 0 & (2\nu-1)a^{-1} & -3a^{-3} \\ 0 & 0 & -4(1+\nu)b & 0 & (2\nu-4)b^{-2} & 6b^{-4} \\ 0 & 0 & 2(1+\nu)b & 0 & (2\nu-1)b^{-2} & -3b^{-4} \end{bmatrix} \begin{Bmatrix} A_1 \\ B_1 \\ A_2 \\ B_2 \\ C_2 \\ D_2 \end{Bmatrix}^{\mathrm{ex}} = \frac{t_r}{4\mu} \begin{Bmatrix} 0 \\ 0 \\ 0 \\ 0 \\ 2 \\ -1 \end{Bmatrix} \tag{2.119}$$

i.e.

$$\left[A_2^{\mathrm{ex}}(4\nu-1) - A_1^{\mathrm{ex}}(4\nu^{\star}-1)\right] 2a^2 + B_2^{\mathrm{ex}} - B_1^{\mathrm{ex}} + 4C_2^{\mathrm{ex}}(1-\nu)a^{-1} - 2D_2^{\mathrm{ex}}a^{-3} = 0 \tag{2.120a}$$

$$\left[A_2^{\mathrm{ex}}(6-4\nu) - A_1^{\mathrm{ex}}(6-4\nu^{\star})\right] a^2 + B_2^{\mathrm{ex}} - B_1^{\mathrm{ex}} + C_2^{\mathrm{ex}}(3-4\nu)a^{-1} + D_2^{\mathrm{ex}}a^{-3} = 0 \tag{2.120b}$$

$$\left[-A_2^{\mathrm{ex}}(2+2\nu) + \gamma A_1^{\mathrm{ex}}(2+2\nu^{\star})\right] 2a - C_2^{\mathrm{ex}}(4-2\nu)a^{-2} + 6D_2^{\mathrm{ex}}a^{-4} = 0 \tag{2.120c}$$

$$\left[A_2^{\mathrm{ex}}(2+2\nu) - \gamma A_1^{\mathrm{ex}}(2+2\nu^{\star})\right] a + C_2^{\mathrm{ex}}(2\nu-1)a^{-2} - 3D_2^{\mathrm{ex}}a^{-4} = 0 \tag{2.120d}$$

$$-2A_2^{\mathrm{ex}}(2+2\nu)b - C_2^{\mathrm{ex}}(4-2\nu)b^{-2} + 6D_2^{\mathrm{ex}}b^{-4} = t_r/2\mu \tag{2.120e}$$

$$A_2^{\mathrm{ex}}(2+2\nu)b + C_2^{\mathrm{ex}}(2\nu-1)b^{-2} - 3D_2^{\mathrm{ex}}b^{-4} = -t_r/4\mu \tag{2.120f}$$

where the equilibrium condition $t_r + 2t_\theta = 0$ has been taken into account.

Writing (2.120e) + 2(2.120f) gives $6C_2^{\mathrm{ex}}(\nu-1)b^{-2} = 0$ so $C_2^{\mathrm{ex}} = 0$. Then the equations (c-d) and (e-f) are identical, and finally solving the four left independent equations (e.g. eqs (a-b-c-e)) for the four independent constants $A_1^{\mathrm{ex}}, A_2^{\mathrm{ex}}, B_2^{\mathrm{ex}} - B_1^{\mathrm{ex}}, D_2^{\mathrm{ex}}$ yields

$$A_1^{\mathrm{ex}} = \frac{5(1-\nu)}{q_1\alpha^5 - (1+\nu)q_2}\,\frac{t_r}{8\mu b} \tag{2.121a}$$

$$A_2^{\mathrm{ex}} = \frac{q_2}{q_1\alpha^5 - (1+\nu)q_2}\,\frac{t_r}{8\mu b} \tag{2.121b}$$

$$B_2^{\mathrm{ex}} - B_1^{\mathrm{ex}} = \frac{5(1-\nu) - q_2}{q_1\alpha^5 - (1+\nu)q_2}\,\frac{5b\alpha^2 t_r}{12\mu} \tag{2.121c}$$

$$C_2^{\mathrm{ex}} = 0 \tag{2.121d}$$

$$D_2^{\mathrm{ex}} = \frac{q_1}{q_1\alpha^5 - (1+\nu)q_2}\,\frac{b^4\alpha^5 t_r}{12\mu}, \tag{2.121e}$$

with $\alpha := a/b$ and the constants q_1, q_2 defined by

$$q_1 = 10(\nu-\nu^{\star}) + (1+\nu^{\star})(6\nu-4)(\gamma-1), \qquad q_2 = 5(1-\nu^{\star}) + (1+\nu^{\star})(\gamma-1) \tag{2.122}$$

Finally, a separate determination of B_1^{ex} and B_2^{ex} is achieved by imposing a kinematic constraint, namely that the mean displacement vanish on S_{C}. This translates into

$$4(1+\nu)b^2 A_2^{\mathrm{ex}} + 2B_2^{\mathrm{ex}} - b^{-3}D_2^{\mathrm{ex}} = 0 \tag{2.123}$$

i.e.

$$\begin{aligned} B_2^{\mathrm{ex}} &= \Big(\frac{q_1\alpha^5}{q_1\alpha^5 - (1+\nu)q_2} - \frac{6q_2(1+\nu)}{q_1\alpha^5 - (1+\nu)q_2}\Big)\frac{t_r b}{24\mu} \\ &= \Big(6 - \frac{5q_1\alpha^5}{q_1\alpha^5 - (1+\nu)q_2}\Big)\frac{t_r b}{24\mu} \end{aligned}$$

Background solution. This solution $\boldsymbol{u}$ corresponds to the previous solution (2.121a–e) when the two materials are identical ($\nu^\star = \nu$ and $\gamma = \mu^\star/\mu = 1$). In that case, $q_1 = 0$ and $q_2 = 5(1-\nu)$, and the relevant coefficients are given (still with the zero-mean constraint on S_C) by

$$A_1 = A_2 = A = -\frac{t_r}{8\mu b(1+\nu)} = -\frac{t_r}{4bE}, \qquad B_2 = \frac{t_r b}{4\mu}, \qquad C_2 = D_2 = 0, \tag{2.124}$$

which, as expected, is identical to (2.95). Moreover:

$$\begin{aligned}
A_2^{\text{ex}} - A_2 &= \frac{q_1\alpha^5}{(q_1\alpha^5 - (1+\nu)q_2)(1+\nu)} \frac{t_r}{8\mu b} \\
B_2^{\text{ex}} - B_2 &= -\frac{5q_1\alpha^5}{q_1\alpha^5 - (1+\nu)q_2} \frac{t_r b}{24\mu} \\
C_2^{\text{ex}} - C_2 &= 0 \\
D_2^{\text{ex}} - D_2 &= \frac{q_1}{q_1\alpha^5 - (1+\nu)q_2} \frac{b^4\alpha^5 t_r}{12\mu}
\end{aligned}$$

Second Eshelby solution. For $n = 1$, the background solution $\boldsymbol{u}$ defined by (2.112) and (2.124) is a quadratic polynomial displacement. The second Eshelby solution is therefore the solution $\boldsymbol{u}_\mathcal{B}^{(2)}$ to the transmission problem for S_a taken as the unit sphere and S as the free-space (i.e. $a=1$ and $b=+\infty$). The Eshelby solution is of the form (2.88), with its coefficients satisfying the transmission conditions (2.120a–d) with $a=1$ together with the condition

$$A_2^{(2)} = A = -\frac{t_r}{8\mu b(1+\nu)} \tag{2.125}$$

ensuring that $\boldsymbol{u}_\mathcal{B}^{(2)} - \boldsymbol{u} = o(1)$ at infinity. Solving (2.120a–d) for the remaining constants $A_1^{(2)}$, $B_2^{(2)}$, $C_2^{(2)}$ and $D_2^{(2)}$ yields

$$A_1^{(2)} = -\frac{5(1-\nu)t_r}{8\mu b(1+\nu)q_2} \tag{2.126}$$

$$B_2^{(2)} = -\frac{5[5(1-\nu) - q_2]t_r}{24\mu b(1+\nu)q_2} \tag{2.127}$$

$$C_2^{(2)} = 0 \tag{2.128}$$

$$D_2^{(2)} = -\frac{q_1 t_r}{12\mu b(1+\nu)q_2} \tag{2.129}$$

In particular, one has $A_1^{(2)} = [5(1-\nu)/q_2]A$, so that the (constant) second gradients of the Eshelby perturbation $\boldsymbol{v}_\mathcal{B}^{(2)}$ and background solutions $\boldsymbol{u}$ (noted respectively $\boldsymbol{E}_2^{(2)}$ and $\boldsymbol{E}_2$) are such that

$$\boldsymbol{E}_2^{(2)} = \left(\frac{5(1-\nu)}{q_2} - 1\right)\boldsymbol{E}_2 \tag{2.130}$$

This gives (among other things) a possible test for checking the numerical procedure solving the second Eshelby problem.

Interior expansion of transmission solution. The interior expansion of $\boldsymbol{u}^{\mathrm{ex}}$ at $\boldsymbol{z}=\boldsymbol{0}$ is given (since $\boldsymbol{\nabla}\boldsymbol{u}(\boldsymbol{0})=\boldsymbol{0}$) by

$$\begin{aligned}\boldsymbol{u}_a(\boldsymbol{x}) &:= \boldsymbol{u}(\boldsymbol{x}) + a^2\boldsymbol{v}^{(2)}_{\mathcal{B}}\big[\boldsymbol{\nabla}^2\boldsymbol{u}(\boldsymbol{0})\big](\bar{\boldsymbol{x}})\\ &= -\frac{t_r}{8\mu b(1+\nu)}\frac{5(1-\nu)}{q_2}\big[(8\nu-2)\cos(\theta)\boldsymbol{e}_r + (4\nu-6)\sin(\theta)\boldsymbol{e}_\theta\big]r^2\end{aligned}$$

The truncation error is thus

$$\begin{aligned}\boldsymbol{u}^{\mathrm{ex}} - \boldsymbol{u}_a &= \frac{t_r}{8\mu b(1+\nu)}\Big(\frac{5(1-\nu^2)}{q_1\alpha^5-(1+\nu)q_2} + \frac{5(1-\nu)}{q_2}\Big)\big[(8\nu-2)\cos(\theta)\boldsymbol{e}_r + (4\nu-6)\sin(\theta)\boldsymbol{e}_\theta\big]r^2\\ &= \frac{5(1-\nu)t_r}{8\mu b(1+\nu)}\,\frac{q_1\alpha^5}{q_2[q_1\alpha^5-(1+\nu)q_2]}r^2 = O(a^5) = o(a^2)\end{aligned} \tag{2.131}$$

2.A.3 Numerical illustrations

We now provide some examples of exact and approximated fields computed with the methods described above. In the upcoming results, the characteristics of S_{C} are : radius $b=1$, shear modulus $\mu=1$ and Poisson ratio $\nu=0.3$. The displacement fields $\boldsymbol{u}^{\mathrm{ex}}$, $\boldsymbol{u}$, $\boldsymbol{v}^{\mathrm{ex}}$ and $\boldsymbol{v}_a$ are plotted in S_a for $a=0.2$ and Poisson ratio $\nu^\star=\nu=0.3$.

We computed a numerical error on the radial component as:

$$E_r = \frac{|v^{\mathrm{ex}}_r - v_{ar}|}{|v_{ar}|} \text{ with: } |v| = \sum_{p=1}^{N_p}|v_p|, \tag{2.132}$$

N_p being the number of points where these fields are computed. We similarly compute E_θ. This error is computed for several inner radii so that we can check that it follows the predicted order of convergence.

A soft inclusion is considered: the shear modulus is lower in S_a: $\mu^\star=0.1\mu$ while $\mu=1$. For the computed loadings ($n=0,1$), the second-order approximation $\boldsymbol{v}_a$ is found to approximate the exact perturbation $\boldsymbol{v}^{\mathrm{ex}}$ with at least the sought order $O(a^3)$.

For $n=1$, the only case where the second-order term is actually computed since $\boldsymbol{v}^{(2)}_{\mathcal{B}}=\boldsymbol{0}$ in the other cases, the error is found to be in $O(a^5)$ as observed on Figure 2.6 as it was predicted by (2.131).

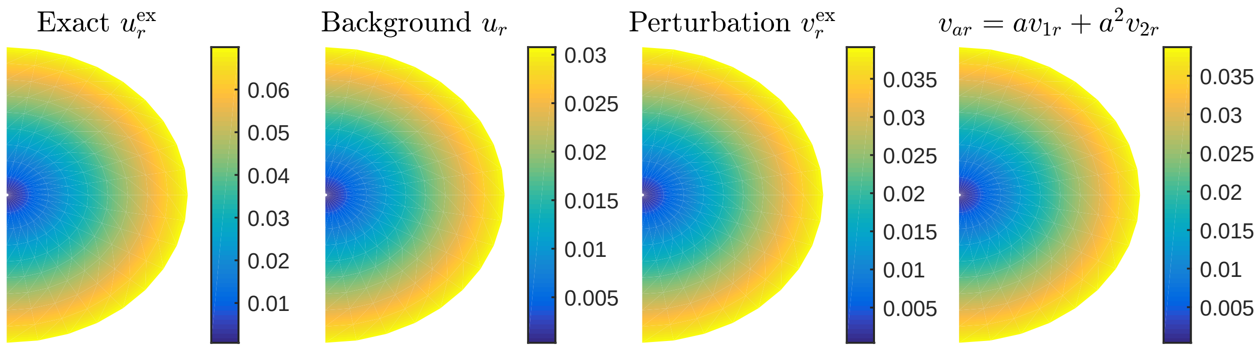

Figure 2.3: Exact, background and approximated displacement inside S_a, for $\mu^\star = 0.1\mu$, $a = 0.2$ and $n = 0$ ($u_\theta = 0$ in this case, as well as the θ-components of the other fields)

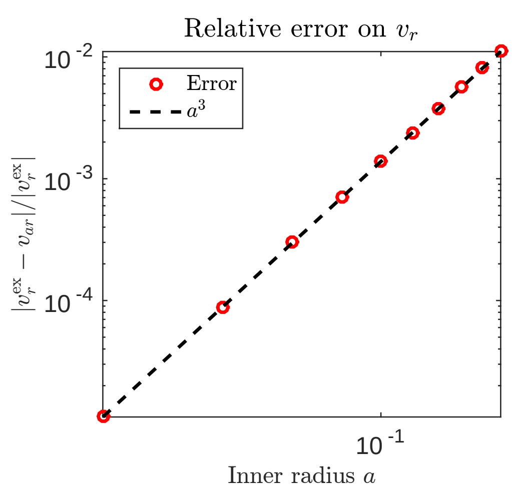

Figure 2.4: Relative error on the displacement in S_a for $n = 0$ and $a \in [0.02, 0.2]$.

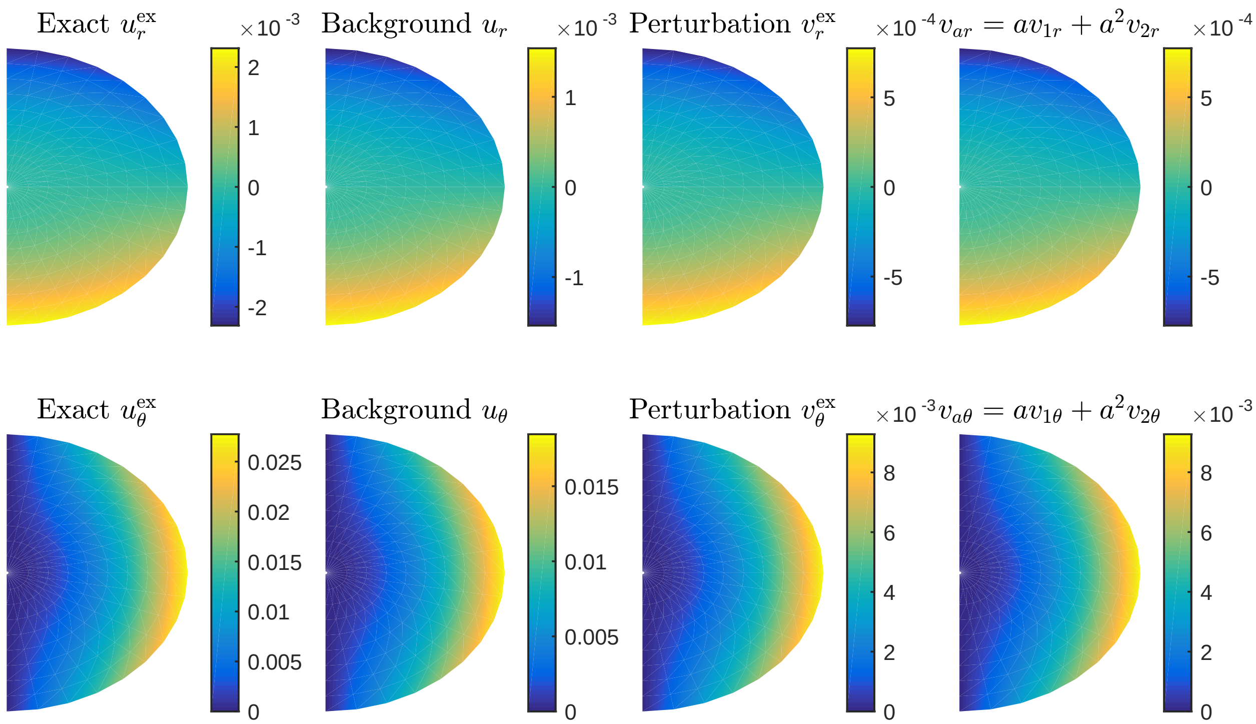

Figure 2.5: Exact, backgound and approximated displacement inside S_a, for $\mu^\star = 0.1\mu$, $a = 0.2$ and $n = 1$.

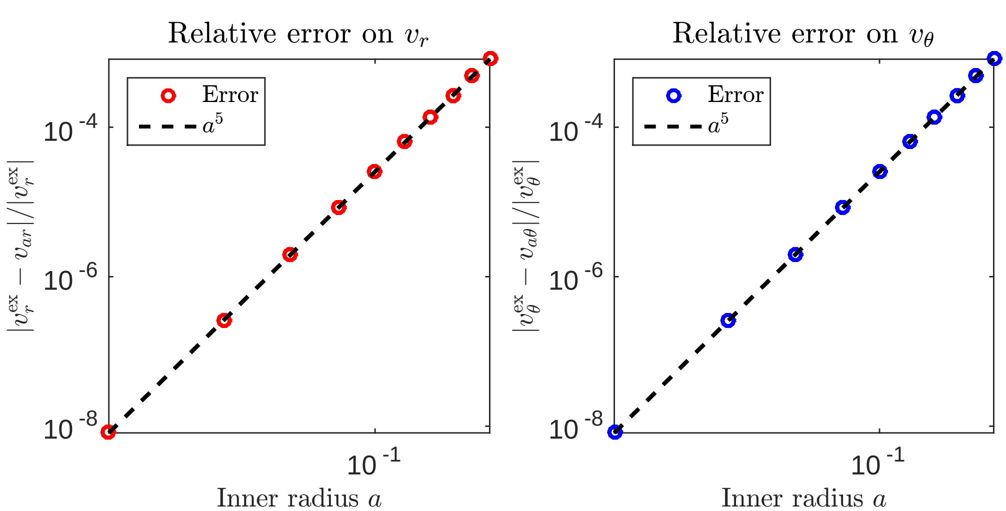

Figure 2.6: Relative error on the displacement in S_a for $n = 1$ and $a \in [0.02, 0.2]$.

Chapter 3

Misfit function expansion for time-harmonic elastodynamics and identification of a penetrable obstacle

Contents

This chapter is dedicated to the time-harmonic follow-up of the previous chapter. The elastic solid occupying the domain Ω is now supposed to be submitted to time-harmonic dynamic excitations, so that the implicit time dependence of all considered fields is $e^{\mathrm{i}\omega t}$. This dependence will be omitted in the sequel: we consider only the space-dependent part of these fields (which are now complex-valued). We furthermore suppose that none of the boundary-value problems into consideration admits the circular frequency ω as an eigenvalue.

We follow the exact same steps than in the previous chapter: Section 3.1 presents the scattering problem associated to a trial inhomogeneity B_a, the equivalent integral formulation and the invertibility of the resulting integral operator. Sections 3.2 and 3.3 then address the expansions of the scattered displacement and of the misfit function, with emphasis on the new terms that appear in the dynamical case. Finally, Section 3.4 shows some identification results obtained thanks to this expansion. Some tedious computations were delayed to the appendices to ease the lecture.

3.1 Scattering problem and integral formulation

3.1.1 Incident, total and scattered displacements

Consider an elastic solid occupying the domain Ω and characterized by both Hooke's tensor $\boldsymbol{\mathcal{C}}$ and density ρ. For prescribed time-harmonic displacements $\boldsymbol{u}_{\mathrm{D}}$ on Γ_{D}, tractions $\boldsymbol{t}_{\mathrm{N}}$ on Γ_{N} and volume forces $\boldsymbol{f}$, the background (or incident) displacement $\boldsymbol{u}$ satisfies:

$$\left| \begin{array}{ll} \mathrm{div}(\boldsymbol{\mathcal{C}} : \boldsymbol{\nabla u}) + \rho\omega^2 \boldsymbol{u} + \boldsymbol{f} = \boldsymbol{0} & \text{in } \Omega, \\ \boldsymbol{u} = \boldsymbol{u}_D & \text{on } \Gamma_{\mathrm{D}}, \\ \boldsymbol{t}[\boldsymbol{u}] = \boldsymbol{t}_N & \text{on } \Gamma_{\mathrm{N}}. \end{array} \right. \tag{3.1}$$

The associated variational formulation is:

$$\text{Find } \boldsymbol{u} \in \boldsymbol{W}(\boldsymbol{u}_{\mathrm{D}}),\ \ \langle \boldsymbol{u}, \boldsymbol{w} \rangle_\Omega^{\mathcal{C}} - \omega^2 (\boldsymbol{u}, \boldsymbol{w})_\Omega^\rho = F(\boldsymbol{w}), \quad \forall \boldsymbol{w} \in \boldsymbol{W}_0, \tag{3.2}$$

where $\langle \cdot, \cdot \rangle_D^{\mathcal{C}}$ denotes the bilinear elastic energy form as previously, and $(\cdot, \cdot)_D^\rho$ denotes the kinetic energy bilinear form associated with domain D and density ρ, i.e.:

$$\langle \boldsymbol{u}, \boldsymbol{w} \rangle_D^{\mathcal{C}} = \int_D \boldsymbol{\nabla u} : \boldsymbol{\mathcal{C}} : \boldsymbol{\nabla w} \,\mathrm{d}V \quad \text{and} \quad (\boldsymbol{u}, \boldsymbol{w})_D^\rho := \int_D \rho \ \boldsymbol{u} \cdot \boldsymbol{w} \,\mathrm{d}V, \tag{3.3}$$

the linear form F is defined as:

$$F(\boldsymbol{w}) = \int_\Omega \boldsymbol{f} \cdot \boldsymbol{w} \,\mathrm{d}V + \int_{\Gamma_{\mathrm{N}}} \boldsymbol{t}_{\mathrm{N}} \cdot \boldsymbol{w} \,\mathrm{d}S, \tag{3.4}$$

and the same notations were kept for the functional spaces, although the fields are now complex-valued:

$$\boldsymbol{W}(\boldsymbol{u}_{\mathrm{D}}) = \left\{ \ \boldsymbol{w} \in H^1(\Omega);\ \boldsymbol{w} = \boldsymbol{u}_{\mathrm{D}} \text{ on } \Gamma_{\mathrm{D}} \right\}, \qquad \boldsymbol{W}_0 = \boldsymbol{W}(\boldsymbol{0}). \tag{3.5}$$

The inhomogeneity $B_a = \boldsymbol{z} + a\mathcal{B}$, which now supports a constant density contrast $\Delta\rho$ along with the previously studied elastic coefficients contrast $\Delta\boldsymbol{\mathcal{C}}$, is then taken into account. In the perturbed domain, the total displacement $\boldsymbol{u}_a^\omega$ is the solution of the variational problem:

$$\text{Find } \boldsymbol{u}_a^\omega \in \boldsymbol{W}(\boldsymbol{u}_{\mathrm{D}}),\ \ \langle \boldsymbol{u}_a^\omega, \boldsymbol{w} \rangle_\Omega^{\mathcal{C}} + \langle \boldsymbol{u}_a^\omega, \boldsymbol{w} \rangle_{B_a}^{\Delta\mathcal{C}} - \omega^2 \left[(\boldsymbol{u}_a^\omega, \boldsymbol{w})_\Omega^\rho + (\boldsymbol{u}_a^\omega, \boldsymbol{w})_{B_a}^{\Delta\rho} \right] = F(\boldsymbol{w}), \quad \forall \boldsymbol{w} \in \boldsymbol{W}_0. \tag{3.6}$$

Finally, subtracting (3.2) from (3.6), the *scattered displacement* $\boldsymbol{v}_a^\omega := \boldsymbol{u}_a^\omega - \boldsymbol{u}$ is found to satisfy the weak formulation:

$$\text{Find } \boldsymbol{v}_a^\omega \in \boldsymbol{W}_0, \quad \langle \boldsymbol{v}_a^\omega, \boldsymbol{w} \rangle_\Omega^{\mathcal{C}} + \langle \boldsymbol{v}_a^\omega, \boldsymbol{w} \rangle_{B_a}^{\Delta\mathcal{C}} - \omega^2 \left[(\boldsymbol{v}_a^\omega, \boldsymbol{w})_\Omega^\rho + (\boldsymbol{v}_a^\omega, \boldsymbol{w})_{B_a}^{\Delta\rho} \right] \\ = - \langle \boldsymbol{u}, \boldsymbol{w} \rangle_{B_a}^{\Delta\mathcal{C}} + \omega^2 (\boldsymbol{u}, \boldsymbol{w})_{B_a}^{\Delta\rho} \qquad \forall \boldsymbol{w} \in \boldsymbol{W}_0, \quad (3.7)$$

whose source terms are expressed only as a function of the incident field. To derive the integral equation corresponding to this scattering problem, we now need a proper Green's tensor.

3.1.2 Time harmonic Green's tensor

Green's tensor $\boldsymbol{G}^\omega(\cdot, \boldsymbol{x})$ associated to problem (3.1) is defined similarly to the static case as the tensor whose components represent the displacements resulting from time-harmonic point-like forces applied at $\boldsymbol{x}$, and that satisfies homogeneous boundary conditions on Γ_D and Γ_N:

$$\left| \begin{array}{ll} \operatorname{div}(\boldsymbol{\mathcal{C}} : \boldsymbol{\nabla} \boldsymbol{G}^\omega(\cdot, \boldsymbol{x})) + \rho\omega^2 \boldsymbol{G}^\omega(\cdot, \boldsymbol{x}) + \delta(\cdot - \boldsymbol{x}) \boldsymbol{I} = \boldsymbol{0} & \text{in } \Omega, \\ \boldsymbol{G}^\omega(\cdot, \boldsymbol{x}) = \boldsymbol{0} & \text{on } \Gamma_\mathrm{D}, \\ \boldsymbol{t}[\boldsymbol{G}^\omega(\cdot, \boldsymbol{x})] = \boldsymbol{0} & \text{on } \Gamma_\mathrm{N}. \end{array} \right. \tag{3.8}$$

It satisfies the integral equality:

$$\langle \boldsymbol{G}^\omega(\cdot, \boldsymbol{x}), \boldsymbol{w} \rangle_\Omega^{\mathcal{C}} - (\boldsymbol{G}^\omega(\cdot, \boldsymbol{x}), \boldsymbol{w})_\Omega^\rho = \boldsymbol{w}(\boldsymbol{x}) \quad \forall \boldsymbol{w} \in \boldsymbol{W}_0 \cap C^1(\omega_{\boldsymbol{x}}), \tag{3.9}$$

where $\omega_{\boldsymbol{x}}$ is a neighborhood of $\boldsymbol{x}$.

3.1.2.1 First decomposition: fundamental solution and complementary part

As for the static case, we split $\boldsymbol{G}^\omega$ into the time-harmonic fundamental solution $\boldsymbol{G}_\infty^\omega$ and a complementary part $\boldsymbol{G}_\mathrm{C}^\omega$ as:

$$\boldsymbol{G}^\omega(\boldsymbol{\xi}, \boldsymbol{x}) = \boldsymbol{G}_\infty^\omega(\boldsymbol{\xi} - \boldsymbol{x}) + \boldsymbol{G}_\mathrm{C}^\omega(\boldsymbol{\xi}, \boldsymbol{x}), \tag{3.10}$$

where $\boldsymbol{G}_\infty^\omega$ satisfies:

$$\operatorname{div}(\boldsymbol{\mathcal{C}} : \boldsymbol{\nabla} \boldsymbol{G}_\infty^\omega(\boldsymbol{r})) + \rho\omega^2 \boldsymbol{G}_\infty^\omega(\boldsymbol{r}) + \delta(\boldsymbol{r}) \boldsymbol{I} = \boldsymbol{0}, \qquad \boldsymbol{r} \in \mathbb{R}^3, \tag{3.11}$$

along with radiation conditions that ensure that $\boldsymbol{G}_\infty^\omega$ corresponds to outgoing waves. A convenient expression is computed in [Wang & Achenbach, 1995] for general anisotropic materials, by means of Radon transform on equation (3.11) and inverse transform of the result. For isotropic materials, it is called the Helmholtz solution, and given by [Achenbach et al., 1982] as:

$$\boldsymbol{G}_\infty^\omega(\boldsymbol{r}) = \frac{1}{\mu} \left\{ \frac{1}{k_\mathrm{S}^2} \boldsymbol{\nabla}^2 \Big[-G(r; k_\mathrm{P}) + G(r; k_\mathrm{S}) \Big] + G(r; k_\mathrm{S}) \boldsymbol{I} \right\}, \quad r = |\boldsymbol{r}|, \tag{3.12}$$

where k_P and k_S are the wave numbers associated with pressure and shear waves (or "primary" and "secondary" waves) defined by:

$$k_\mathrm{P}^2 = \frac{\rho\omega^2}{\lambda + 2\mu} \qquad \text{and} \qquad k_\mathrm{S}^2 = \frac{\rho\omega^2}{\mu}, \tag{3.13}$$

and $G(r; k)$ is the fundamental solution for the scalar Helmholtz operator $(\Delta + k^2)$ given as:

$$G(r; k) = \frac{e^{ikr}}{4\pi r}. \tag{3.14}$$

Remark 3.1. *Alternative expressions of $\boldsymbol{G}^{\omega}_{\infty}$ exist for isotropic materials, see Appendix 3.B. The choice of a particular expression depends on the most convenient way to compute this tensor and its derivatives for a particular situation.*

The complementary part $\boldsymbol{G}^{\omega}_{\mathrm{C}}$ in the decomposition (3.10) accounts for the homogeneous boundary conditions on $\partial\Omega$ and thus is defined for each source point $\boldsymbol{x}$ as the solution of the following boundary-value problem:

$$\left|\begin{array}{ll} \operatorname{div}(\boldsymbol{\mathcal{C}} : \boldsymbol{\nabla}\boldsymbol{G}^{\omega}_{\mathrm{C}}(\cdot,\boldsymbol{x})) + \rho\omega^2\boldsymbol{G}^{\omega}_{\mathrm{C}}(\cdot,\boldsymbol{x}) = \boldsymbol{0} & \text{in } \Omega, \\ \boldsymbol{G}^{\omega}_{\mathrm{C}}(\cdot,\boldsymbol{x}) = -\boldsymbol{G}^{\omega}_{\infty}(\cdot-\boldsymbol{x}) & \text{on } \Gamma_{\mathrm{D}}, \\ \boldsymbol{t}[\boldsymbol{G}^{\omega}_{\mathrm{C}}(\cdot,\boldsymbol{x})] = -\boldsymbol{t}[\boldsymbol{G}^{\omega}_{\infty}(\cdot-\boldsymbol{x})] & \text{on } \Gamma_{\mathrm{N}}. \end{array}\right. \tag{3.15}$$

In particular, $\boldsymbol{G}^{\omega}_{\mathrm{C}}(\cdot,\boldsymbol{x}) \in C^{\infty}(\Omega)\ \forall\boldsymbol{x}\in\Omega$.

3.1.2.2 Second decomposition involving the static fundamental solution

Further decomposition is available featuring the *static* fundamental solution $\boldsymbol{G}_{\infty}$, which shares the same singular behavior with $\boldsymbol{G}^{\omega}_{\infty}$. We define $\boldsymbol{G}^{\omega}_{\mathrm{C}\infty}(\boldsymbol{r}) := \boldsymbol{G}^{\omega}_{\infty}(\boldsymbol{r}) - \boldsymbol{G}_{\infty}(\boldsymbol{r})$, so that a second decomposition for $\boldsymbol{G}^{\omega}$ holds:

$$\boldsymbol{G}^{\omega}(\boldsymbol{\xi},\boldsymbol{x}) = \boldsymbol{G}_{\infty}(\boldsymbol{\xi}-\boldsymbol{x}) + \boldsymbol{G}^{\omega}_{\mathrm{C}\infty}(\boldsymbol{\xi}-\boldsymbol{x}) + \boldsymbol{G}^{\omega}_{\mathrm{C}}(\boldsymbol{\xi},\boldsymbol{x}). \tag{3.16}$$

This difference $\boldsymbol{G}^{\omega}_{\mathrm{C}\infty}$ between time-harmonic and static fundamental solutions is now studied in further details. Again, we refer to [Wang & Achenbach, 1995][1] for anisotropic materials. For isotropic materials, we use the decomposition from [Bonnet, 1999, Part 8.5] to establish the expression:

$$\boldsymbol{G}^{\omega}_{\mathrm{C}\infty}(\boldsymbol{r}) = \frac{1}{4\pi\mu r}(A(r)\boldsymbol{I} + B(r)\hat{\boldsymbol{r}}\otimes\hat{\boldsymbol{r}}), \tag{3.17}$$

where A and B are given as:

$$A(r) = \sum_{p\geq 1}\frac{1+p+\beta^{p+2}}{p!(p+2)}(\mathrm{i}k_{\mathrm{S}}r)^p, \quad B(r) = \sum_{p\geq 1}\frac{(1-\beta^{p+2})(1-p)}{p!(p+2)}(\mathrm{i}k_{\mathrm{S}}r)^p, \tag{3.18}$$

and β is defined by:

$$\beta = \frac{k_{\mathrm{P}}}{k_{\mathrm{S}}} = \frac{c_{\mathrm{S}}}{c_{\mathrm{P}}} = \sqrt{\frac{\mu}{\lambda+2\mu}}. \tag{3.19}$$

As seen in the static case, the asymptotic behavior of $\boldsymbol{G}^{\omega}_{\mathrm{C}\infty}(\boldsymbol{r})$ and of its gradient when applying the scaling $\boldsymbol{r} = a\bar{\boldsymbol{r}}$ and letting $a\to 0$ will be required. We therefore define their first-order expansions as:

$$\begin{aligned} \boldsymbol{G}^{\omega}_{\mathrm{C}\infty}(a\bar{\boldsymbol{r}}) &= \mathrm{i}\boldsymbol{G}^{\omega(0)} + a\boldsymbol{G}^{\omega(1)}(\bar{\boldsymbol{r}}) + o(a) \\ \boldsymbol{\nabla}\boldsymbol{G}^{\omega}_{\mathrm{C}\infty}(a\bar{\boldsymbol{r}}) &= \boldsymbol{H}^{\omega(0)}(\bar{\boldsymbol{r}}) + a\mathrm{i}\boldsymbol{H}^{\omega(1)}(\bar{\boldsymbol{r}}) + o(a). \end{aligned} \tag{3.20}$$

[1] where the notation $\boldsymbol{g}^R(\boldsymbol{r},\omega)$ is adopted for this complementary part

This form was chosen so that the terms $\boldsymbol{G}^{\omega(j)}$ and $\boldsymbol{H}^{\omega(j)}$ are real-valued tensors for an isotropic material. Indeed, from (3.17) and (3.18), they are given in this case by:

$$\begin{aligned}
\boldsymbol{G}^{\omega(0)} &= \frac{k_{\mathrm{S}}}{12\pi\mu}(2+\beta^3)\boldsymbol{I}, \\
\boldsymbol{G}^{\omega(1)}(\bar{\boldsymbol{r}}) &= \frac{k_{\mathrm{S}}^2\bar{r}}{32\pi\mu}\left(-(3+\beta^4)\boldsymbol{I} + (1-\beta^4)\hat{\boldsymbol{r}}\otimes\hat{\boldsymbol{r}}\right), \\
\boldsymbol{H}^{\omega(0)}(\bar{\boldsymbol{r}}) &= \frac{k_{\mathrm{S}}^2}{32\pi\mu}\left(-4\boldsymbol{I}\otimes\hat{\boldsymbol{r}} + (1-\beta^4)\boldsymbol{k}^{2,1}(\hat{\boldsymbol{r}}) + (1-\beta^4)\hat{\boldsymbol{r}}^{\otimes 3}\right), \\
\boldsymbol{H}^{\omega(1)}(\bar{\boldsymbol{r}}) &= \frac{k_{\mathrm{S}}^3\bar{r}}{60\pi\mu}\left(-5\boldsymbol{I}\otimes\hat{\boldsymbol{r}} + (1-\beta^5)\boldsymbol{k}^{2,1}(\hat{\boldsymbol{r}})\right),
\end{aligned} \tag{3.21}$$

where $\hat{\boldsymbol{r}} = \boldsymbol{r}/r$ and $k^{2,1}_{mnp}(\boldsymbol{r}) = \delta_{mn}r_p + \delta_{mp}r_n + r_m\delta_{np}$.

3.1.3 Volume integral equation formulation

Introducing Green's tensor $\boldsymbol{G}^{\omega}(\cdot,\boldsymbol{x})$ as test function in (3.7), and using identity (3.9) with $\boldsymbol{w} = \boldsymbol{v}_a^{\omega}$, we obtain the integral equation:

$$\mathcal{L}_a^{\omega}[\boldsymbol{v}_a^{\omega}](\boldsymbol{x}) = -\langle \boldsymbol{u}, \boldsymbol{G}^{\omega}(\cdot,\boldsymbol{x})\rangle_{B_a}^{\Delta\mathcal{C}} + \omega^2(\boldsymbol{u}, \boldsymbol{G}^{\omega}(\cdot,\boldsymbol{x}))_{B_a}^{\Delta\rho}, \tag{3.22}$$

where the linear integral operator $\mathcal{L}_a^{\omega}$ is defined by

$$\mathcal{L}_a^{\omega}[\boldsymbol{v}](\boldsymbol{x}) = \boldsymbol{v}(\boldsymbol{x}) + \langle \boldsymbol{v}, \boldsymbol{G}^{\omega}(\cdot,\boldsymbol{x})\rangle_{B_a}^{\Delta\mathcal{C}} - \omega^2(\boldsymbol{v}, \boldsymbol{G}^{\omega}(\cdot,\boldsymbol{x}))_{B_a}^{\Delta\rho}. \tag{3.23}$$

Owing to (i) the decomposition (3.16) of Green's tensor $\boldsymbol{G}^{\omega}$ and (ii) the homogeneity properties of the static fundamental solution $\boldsymbol{G}_{\infty}$ given by (1.30) while applying the scaling $B_a \to \mathcal{B}$, $\mathcal{L}_a^{\omega}$ can be decomposed as:

$$\mathcal{L}_a^{\omega}[\boldsymbol{v}] = \mathcal{K}_{\infty}[\boldsymbol{v}] - a^2\omega^2\mathcal{P}_a^{-1}\mathcal{V}\mathcal{P}_a[\Delta\rho\,\boldsymbol{v}] + \mathcal{K}_{\mathrm{C}\infty}^{\omega}[\boldsymbol{v}] + \mathcal{K}_{\mathrm{C}}^{\omega}[\boldsymbol{v}]. \tag{3.24}$$

where $\mathcal{P}_a : \boldsymbol{H}^1(B_a) \to \boldsymbol{H}^1(\mathcal{B})$ is the "scaling operator" defined in Section 2.1.3.3, $\mathcal{K}_{\infty} = \mathcal{P}_a^{-1}\mathcal{L}\mathcal{P}_a$, and $\mathcal{L}$ (the integral operator associated to the free-space transmission problem by $\mathcal{B}$) and $\mathcal{V}$ (the Newtonian potential associated to $\mathcal{B}$) are given by:

$$\mathcal{L}[\boldsymbol{v}](\boldsymbol{x}) = \boldsymbol{v}(\boldsymbol{x}) + \int_{\mathcal{B}} \boldsymbol{\nabla}\boldsymbol{v} : \Delta\boldsymbol{\mathcal{C}} : \boldsymbol{\nabla}\boldsymbol{G}_{\infty}(\cdot - \boldsymbol{x})\,\mathrm{d}V \quad \text{and} \quad \mathcal{V}[\boldsymbol{\varphi}](\boldsymbol{x}) = \int_{\mathcal{B}} \boldsymbol{\varphi}\cdot\boldsymbol{G}_{\infty}(\cdot - \boldsymbol{x})\,\mathrm{d}V. \tag{3.25}$$

The complementary operators $\mathcal{K}_{\mathrm{C}\infty}^{\omega}$ and $\mathcal{K}_{\mathrm{C}}^{\omega}$ are classical integral operators with bounded kernels $\boldsymbol{G}_{\mathrm{C}\infty}^{\omega}$ and $\boldsymbol{G}_{\mathrm{C}}^{\omega}$:

$$\begin{aligned}
\mathcal{K}_{\mathrm{C}\infty}^{\omega}[\boldsymbol{v}](\boldsymbol{x}) &:= \int_{B_a} \boldsymbol{\nabla}\boldsymbol{v} : \Delta\boldsymbol{\mathcal{C}} : \boldsymbol{\nabla}\boldsymbol{G}_{\mathrm{C}\infty}^{\omega}(\cdot - \boldsymbol{x})\,\mathrm{d}V - \omega^2\int_{B_a} \Delta\rho\,\boldsymbol{v}\cdot\boldsymbol{G}_{\mathrm{C}\infty}^{\omega}(\cdot - \boldsymbol{x})\,\mathrm{d}V, \\
\mathcal{K}_{\mathrm{C}}^{\omega}[\boldsymbol{v}](\boldsymbol{x}) &:= \int_{B_a} \boldsymbol{\nabla}\boldsymbol{v} : \Delta\boldsymbol{\mathcal{C}} : \boldsymbol{\nabla}\boldsymbol{G}_{\mathrm{C}}^{\omega}(\cdot,\boldsymbol{x})\,\mathrm{d}V - \omega^2\int_{B_a} \Delta\rho\,\boldsymbol{v}\cdot\boldsymbol{G}_{\mathrm{C}}^{\omega}(\cdot,\boldsymbol{x})\,\mathrm{d}V.
\end{aligned} \tag{3.26}$$

We are now in position to assert the following invertibility theorem:

Theorem 3.1. *Suppose that both elasticity tensors $\boldsymbol{\mathcal{C}}$ and $\boldsymbol{\mathcal{C}}^{\star} = \boldsymbol{\mathcal{C}} + \Delta\boldsymbol{\mathcal{C}}$ are positive and bounded. Then there exists $a_0^{\omega} > 0$ such that the integro-differential operator $\mathcal{L}_a^{\omega} : \boldsymbol{H}^1(B_a) \to \boldsymbol{H}^1(B_a)$ corresponding to the scattering problem by an inhomogeneity $(B_a, \boldsymbol{\mathcal{C}}^{\star})$ embedded in the finite domain Ω, defined by* (3.23) *and decomposition* (3.24)*, is invertible and its inverse is bounded independently of the size a of B_a for all $a < a_0^{\omega}$.*

Proof. Using the decomposition (3.24) and the fact that $\mathcal{K}_\infty := \mathcal{P}_a^{-1}\mathcal{L}\mathcal{P}_a$ is invertible with bounded inverse independently of a as shown by Lemma 2.2, we have:

$$\mathcal{L}_a^\omega = \mathcal{K}_\infty \left(\boldsymbol{I} + \mathcal{K}_\infty{}^{-1}\mathcal{K}_{\mathrm{Ctot}}^\omega\right) \tag{3.27}$$

where we noted for convenience:

$$\mathcal{K}_{\mathrm{Ctot}}^\omega := -a^2\omega^2\mathcal{P}_a^{-1}\mathcal{V}\mathcal{P}_a[\Delta\rho\ \cdot] + \mathcal{K}_{\mathrm{C}\infty}^\omega + \mathcal{K}_{\mathrm{C}}^\omega. \tag{3.28}$$

We then rely on the following estimate for the norm of $\mathcal{K}_{\mathrm{Ctot}}^\omega$:

Lemma 3.2. *The integro-differential operator $\mathcal{K}_{\mathrm{Ctot}}^\omega : H^1(B_a) \to \boldsymbol{H}^1(B_a)$ defined by (3.28) is continuous, and there exists $C_{\mathcal{V}}^\omega > 0$ such that its norm satisfies $\|\mathcal{K}_{\mathrm{Ctot}}^\omega\|_{H^1(B_a)} \leq aC_{\mathcal{V}}^\omega + o(a)$ as $a \to 0$.*

Proof. The proof is given by estimating the three operators involved in $\mathcal{K}_{\mathrm{Ctot}}^\omega$. It is found that the $O(a)$ contribution of the norm comes from the first one (hence the chosen notation for $C_{\mathcal{V}}^\omega$), while the contributions of $\mathcal{K}_{\mathrm{C}}^\omega$ and $\mathcal{K}_{\mathrm{C}\infty}^\omega$ are of higher order ($O(a^3)$).

Indeed, the Newtonian potential $\mathcal{V} : \boldsymbol{H}^1(\mathcal{B}) \to \boldsymbol{H}^1(\mathcal{B})$ is bounded due to the fact that both $\mathcal{V}$ and $\boldsymbol{\nabla}\mathcal{V}$ are integral operators with weakly singular kernels [Kress, 1989, Problem 4.5]. Owing to the properties of the scaling operators $\mathcal{P}_a$ and $\mathcal{P}_a^{-1}$ (2.25), there exists a constant $C_{\mathcal{V}}^\omega$ independent of a such that:

$$\|a^2\omega^2\mathcal{P}_a^{-1}\mathcal{V}\mathcal{P}_a[\Delta\rho\ \cdot]\|_{H^1(B_a)} \leq a^2\omega^2 \left(a^{1/2}\|\mathcal{V}\|_{H^1(\mathcal{B})}a^{-3/2}|\Delta\rho|\right) \leq C_{\mathcal{V}}^\omega a \tag{3.29}$$

with:

$$C_{\mathcal{V}}^\omega = \omega^2|\Delta\rho|\|\mathcal{V}\|_{H^1(\mathcal{B})}. \tag{3.30}$$

On the other hand, $\mathcal{K}_{\mathrm{C}}^\omega$ is a sum of integral operator with bounded kernels. Moreover, the derivatives of these kernels are also bounded (owing to the C^∞ regularity of $\boldsymbol{G}_{\mathrm{C}}^\omega$). The norm of $\mathcal{K}_{\mathrm{C}}^\omega$ can therefore be readily estimated by Cauchy-Schwarz inequalities:

$$\begin{aligned}\|\mathcal{K}_{\mathrm{C}}^\omega[\boldsymbol{v}]\|_{H^1(B_a)}^2 \leq &\left(\|\boldsymbol{\nabla}_1\boldsymbol{G}_{\mathrm{C}}^\omega\|_{L^2(B_a)\times L^2(B_a)}^2 + \|\boldsymbol{\nabla}_{12}\boldsymbol{G}_{\mathrm{C}}^\omega\|_{L^2(B_a)\times L^2(B_a)}^2\right)\|\Delta\boldsymbol{\mathcal{C}} : \boldsymbol{\nabla}\boldsymbol{v}\|_{L^2(B_a)}^2 \\ &+ \omega^2\left(\|\boldsymbol{G}_{\mathrm{C}}^\omega\|_{L^2(B_a)\times L^2(B_a)}^2 + \|\boldsymbol{\nabla}_2\boldsymbol{G}_{\mathrm{C}}^\omega\|_{L^2(B_a)\times L^2(B_a)}^2\right)\|\Delta\rho\ \boldsymbol{v}\|_{L^2(B_a)}^2 \\ \leq &\ (C_C^\omega)^2\ a^6\ \|\boldsymbol{v}\|_{H^1(B_a)}^2\end{aligned} \tag{3.31}$$

so that $\|\mathcal{K}_{\mathrm{C}}^\omega\|_{H^1(B_a)} \leq C_C^\omega a^3$. Similarly, the kernels of the integral operators involved in $\mathcal{K}_{\mathrm{C}\infty}^\omega$ and $\boldsymbol{\nabla}\mathcal{K}_{\mathrm{C}\infty}^\omega$ are bounded, except for $\boldsymbol{\nabla}_{12}\boldsymbol{G}_{\mathrm{C}\infty}^\omega$ that is square-integrable. A similar Cauchy-Schwarz inequality holds and shows that there exists $C_{C\infty}^\omega > 0$ independent of a so that $\|\mathcal{K}_{\mathrm{C}\infty}^\omega\|_{H^1(B_a)} \leq C_{C\infty}^\omega a^3$.

The norm of $\mathcal{K}_{\mathrm{Ctot}}^\omega$ is therefore dominated by the one of the first term as $a \to 0$ and we obtain:

$$\|\mathcal{K}_{\mathrm{Ctot}}^\omega\|_{H^1(B_a)} \leq C_{\mathcal{V}}^\omega a + o(a), \tag{3.32}$$

where $C_{\mathcal{V}}^\omega$ is defined by (3.30).

□

We are now able to conclude the proof of Theorem 3.1. Recall that $\mathcal{L}_a^\omega$ is written as:

$$\mathcal{L}_a^\omega = \mathcal{K}_\infty(\boldsymbol{I} + \mathcal{K}_\infty{}^{-1}\mathcal{K}_{\mathrm{Ctot}}^\omega).$$

For all $c < 1$ there exists an inclusion size a_0^ω such that $\|\mathcal{K}_\infty{}^{-1}\mathcal{K}_{\mathrm{Ctot}}^\omega\|_{H^1(B_a)} \leq c < 1\ \forall a \leq a_0^\omega$, namely, from Lemma 3.2:

$$a_0^\omega = \frac{c}{C_{\mathcal{V}}^\omega \|\mathcal{K}_\infty{}^{-1}\|_{H^1(B_a)}}. \tag{3.33}$$

Then, $\forall a < a_0^\omega$, $\boldsymbol{I} + \mathcal{K}_\infty{}^{-1}\mathcal{K}_{\mathrm{Ctot}}^\omega$ is invertible by Neumann series, with bounded inverse:

$$\|(\boldsymbol{I} + \mathcal{K}_\infty{}^{-1}\mathcal{K}_{\mathrm{Ctot}}^\omega)^{-1}\|_{H^1(B_a)} \leq \frac{1}{1 - \|\mathcal{L}^{-1}\mathcal{K}_{\mathrm{Ctot}}^\omega\|_{H^1(B_a)}} \leq \frac{1}{1-c}.$$

And finally, $\forall a < a_0^\omega$, the inverse of $\mathcal{L}_a^\omega$ exists and is given by:

$$\mathcal{L}_a^{\omega-1} = (\boldsymbol{I} + \mathcal{K}_\infty{}^{-1}\mathcal{K}_{\mathrm{Ctot}}^\omega)^{-1}\mathcal{K}_\infty{}^{-1}, \tag{3.34}$$

and its norm is bounded as showed by:

$$\|\mathcal{L}_a^{\omega-1}\|_{H^1(B_a)} \leq \|(\boldsymbol{I} + \mathcal{K}_\infty{}^{-1}\mathcal{K}_{\mathrm{Ctot}}^\omega)^{-1}\|_{H^1(B_a)}\|\mathcal{K}_\infty{}^{-1}\|_{H^1(B_a)} \leq \frac{1}{1-c}\|\mathcal{K}_\infty{}^{-1}\|_{H^1(B_a)}. \tag{3.35}$$

□

3.2 Scattered displacement expansion

Relying on the integral equation framework that we set above, we now look at the asymptotic behavior of the scattered displacement $\boldsymbol{v}_a^\omega$ as $a \to 0$. Since computing $\boldsymbol{v}_a^\omega$ requires (i) to solve the integral equation (3.22) for $\boldsymbol{x} \in B_a$ and (ii) to use this equation as an integral representation for $\boldsymbol{x} \notin \overline{B_a}$, we address successively the *inner* and *outer* expansions of $\boldsymbol{v}_a^\omega$.

3.2.1 Inner expansion

First, we look for the inner expansion of $\boldsymbol{v}_a^\omega(\boldsymbol{x})$ i.e. $\boldsymbol{x} \in B_a$. In this goal, we apply the scaling $B_a \to \mathcal{B}$ described in Section 2.1.3.3 (and therefore the variable change $(\boldsymbol{x}, \boldsymbol{\xi}) \to (\bar{\boldsymbol{x}}, \bar{\boldsymbol{\xi}})$) to the integral equation (3.22) and use the following expansions:

- The sought decomposition for $\boldsymbol{v}_a^\omega$ is given in terms of functions $\boldsymbol{V}_j^\omega$ of the scaled variable $\bar{\boldsymbol{x}}$ as:

$$\begin{gathered}\boldsymbol{v}_a^\omega(\boldsymbol{x}) = \boldsymbol{V}_a^\omega\left(\frac{\boldsymbol{x}-\boldsymbol{z}}{a}\right) + \boldsymbol{\delta}_a^\omega(\boldsymbol{x}) = \mathcal{P}_a[\boldsymbol{V}_a^\omega](\boldsymbol{x}) + \boldsymbol{\delta}_a^\omega(\boldsymbol{x}),\\ \text{with: } \boldsymbol{V}_a^\omega(\bar{\boldsymbol{x}}) := a\boldsymbol{V}_1^\omega(\bar{\boldsymbol{x}}) + a^2\boldsymbol{V}_2^\omega(\bar{\boldsymbol{x}}) + \frac{1}{2}a^3\boldsymbol{V}_3^\omega(\bar{\boldsymbol{x}}) + \frac{1}{6}a^4\boldsymbol{V}_4^\omega(\bar{\boldsymbol{x}}),\end{gathered} \tag{3.36}$$

  and the remainder $\boldsymbol{\delta}_a^\omega$ will later be proven to be "small" in some sense.

- The expansions of $\boldsymbol{u}$, $\boldsymbol{\nabla u}$, $\boldsymbol{G}_{\mathrm{C}}^\omega$ and $\boldsymbol{\nabla G}_{\mathrm{C}}^\omega$ are given by their Taylor expansions about $\boldsymbol{z}$.

- The expansion of $\boldsymbol{G}_{\mathrm{C}\infty}^\omega(\boldsymbol{\xi} - \boldsymbol{x}) = \boldsymbol{G}_{\mathrm{C}\infty}^\omega(a(\bar{\boldsymbol{\xi}} - \bar{\boldsymbol{x}}))$ is given by (3.20).

Regrouping all the powers of a, and owing to the $O(1)$ behavior of $\mathcal{P}_a^{-1}\mathcal{L}\mathcal{P}_a$ in the decomposition of $\mathcal{L}_a^\omega$ (3.24) as $a \to 0$, the integral equation (3.22) is expanded as:

$$\sum_{j=1}^{4} \frac{a^j}{(j-1)!}(\mathcal{L}[\boldsymbol{V}_j^\omega](\bar{\boldsymbol{x}}) - \mathcal{F}_j^\omega(\bar{\boldsymbol{x}})) + o(a^4) = 0. \tag{3.37}$$

The definition of $\mathcal{L}$ is given in (3.25) and those of the terms $\mathcal{F}_j$ are:

$$\begin{aligned}
\mathcal{F}_1^\omega(\bar{\boldsymbol{x}}) =& -\int_{\mathcal{B}} \boldsymbol{\nabla}\boldsymbol{u}(\boldsymbol{z}) : \Delta\boldsymbol{\mathcal{C}} : \boldsymbol{\nabla}\boldsymbol{G}_\infty(\bar{\boldsymbol{\xi}} - \bar{\boldsymbol{x}})\,\mathrm{d}V_{\bar{\xi}}, \\
\mathcal{F}_2^\omega(\bar{\boldsymbol{x}}) =& -\int_{\mathcal{B}} \left(\boldsymbol{\nabla}^2\boldsymbol{u}(\boldsymbol{z})\cdot\bar{\boldsymbol{\xi}}\right) : \Delta\boldsymbol{\mathcal{C}} : \boldsymbol{\nabla}\boldsymbol{G}_\infty(\bar{\boldsymbol{\xi}} - \bar{\boldsymbol{x}})\,\mathrm{d}V_{\bar{\xi}} \\
&+ \omega^2 \int_{\mathcal{B}} \Delta\rho\ \boldsymbol{u}(\boldsymbol{z})\cdot\boldsymbol{G}_\infty(\bar{\boldsymbol{\xi}} - \bar{\boldsymbol{x}})\,\mathrm{d}V_{\bar{\xi}}, \\
\mathcal{F}_3^\omega(\bar{\boldsymbol{x}}) =& -\int_{\mathcal{B}} \left(\boldsymbol{\nabla}^3\boldsymbol{u}(\boldsymbol{z}) : \bar{\boldsymbol{\xi}}^{\otimes 2}\right) : \Delta\boldsymbol{\mathcal{C}} : \boldsymbol{\nabla}\boldsymbol{G}_\infty(\bar{\boldsymbol{\xi}} - \bar{\boldsymbol{x}})\,\mathrm{d}V_{\bar{\xi}} \\
&+ 2\,\omega^2 \int_{\mathcal{B}} \Delta\rho\ \left(\boldsymbol{\nabla}\boldsymbol{u}(\boldsymbol{z})\cdot\bar{\boldsymbol{\xi}} + \boldsymbol{V}_1^\omega(\bar{\boldsymbol{\xi}})\right)\cdot\boldsymbol{G}_\infty(\bar{\boldsymbol{\xi}} - \bar{\boldsymbol{x}})\,\mathrm{d}V_{\bar{\xi}} \\
&- 2\int_{\mathcal{B}} (\boldsymbol{\nabla}\boldsymbol{u}(\boldsymbol{z}) + \boldsymbol{\nabla}\boldsymbol{V}_1^\omega) : \Delta\boldsymbol{\mathcal{C}} : \left(\boldsymbol{\nabla}_1\boldsymbol{G}_{\mathrm{C}}(\boldsymbol{z},\boldsymbol{z}) + \boldsymbol{H}^{\omega(0)}(\bar{\boldsymbol{\xi}} - \bar{\boldsymbol{x}})\right)\,\mathrm{d}V_{\bar{\xi}} \\
&+ 2\,\omega^2 \int_{\mathcal{B}} \Delta\rho\ \boldsymbol{u}(\boldsymbol{z})\cdot\left(\boldsymbol{G}_{\mathrm{C}}^\omega(\boldsymbol{z},\boldsymbol{z}) + \mathrm{i}\boldsymbol{G}^{\omega(0)}\right)\,\mathrm{d}V_{\bar{\xi}},
\end{aligned} \tag{3.38}$$

and:

$$\begin{aligned}
\mathcal{F}_4^\omega(\bar{\boldsymbol{x}}) =& -\int_{\mathcal{B}} \left(\boldsymbol{\nabla}^4\boldsymbol{u}(\boldsymbol{z}) \bullet \bar{\boldsymbol{\xi}}^{\otimes 3}\right) : \Delta\boldsymbol{\mathcal{C}} : \boldsymbol{\nabla}\boldsymbol{G}_\infty(\bar{\boldsymbol{\xi}} - \bar{\boldsymbol{x}})\,\mathrm{d}V_{\bar{\xi}} \\
&+ 6\,\omega^2 \int_{\mathcal{B}} \Delta\rho\ \left(\frac{\boldsymbol{\nabla}^2\boldsymbol{u}(\boldsymbol{z}) : \bar{\boldsymbol{\xi}}^{\otimes 2}}{2} + \boldsymbol{V}_2^\omega(\bar{\boldsymbol{\xi}})\right)\cdot\boldsymbol{G}_\infty(\bar{\boldsymbol{\xi}} - \bar{\boldsymbol{x}})\,\mathrm{d}V_{\bar{\xi}} \\
&- 6\int_{\mathcal{B}} \left(\boldsymbol{\nabla}^2\boldsymbol{u}(\boldsymbol{z})\cdot\bar{\boldsymbol{\xi}} + \boldsymbol{\nabla}\boldsymbol{V}_2^\omega(\bar{\boldsymbol{\xi}})\right) : \Delta\boldsymbol{\mathcal{C}} : \left(\boldsymbol{\nabla}_1\boldsymbol{G}_{\mathrm{C}}(\boldsymbol{z},\boldsymbol{z}) + \boldsymbol{H}^{\omega(0)}(\bar{\boldsymbol{\xi}} - \bar{\boldsymbol{x}})\right)\,\mathrm{d}V_{\bar{\xi}} \\
&- 6\int_{\mathcal{B}} \left(\boldsymbol{\nabla}\boldsymbol{u}(\boldsymbol{z}) + \boldsymbol{\nabla}\boldsymbol{V}_1^\omega(\bar{\boldsymbol{\xi}})\right) : \Delta\boldsymbol{\mathcal{C}} : \left(\boldsymbol{\nabla}_{11}\boldsymbol{G}_{\mathrm{C}}(\boldsymbol{z},\boldsymbol{z})\cdot\bar{\boldsymbol{\xi}} + \boldsymbol{\nabla}_{21}\boldsymbol{G}_{\mathrm{C}}(\boldsymbol{z},\boldsymbol{z})\cdot\bar{\boldsymbol{x}}\right)\,\mathrm{d}V_{\bar{\xi}} \\
&- 6\int_{\mathcal{B}} \left(\boldsymbol{\nabla}\boldsymbol{u}(\boldsymbol{z}) + \boldsymbol{\nabla}\boldsymbol{V}_1^\omega(\bar{\boldsymbol{\xi}})\right) : \Delta\boldsymbol{\mathcal{C}} : \mathrm{i}\boldsymbol{H}^{\omega(1)}(\bar{\boldsymbol{\xi}} - \bar{\boldsymbol{x}})\,\mathrm{d}V_{\bar{\xi}} \\
&+ 6\,\omega^2 \int_{\mathcal{B}} \Delta\rho\ \left(\boldsymbol{\nabla}\boldsymbol{u}(\boldsymbol{z})\cdot\bar{\boldsymbol{\xi}} + \boldsymbol{V}_1^\omega(\bar{\boldsymbol{\xi}})\right)\cdot\left(\boldsymbol{G}_{\mathrm{C}}^\omega(\boldsymbol{z},\boldsymbol{z}) + \mathrm{i}\boldsymbol{G}^{\omega(0)}\right)\,\mathrm{d}V_{\bar{\xi}} \\
&+ 6\,\omega^2 \int_{\mathcal{B}} \Delta\rho\ \boldsymbol{u}(\boldsymbol{z})\cdot\left(\boldsymbol{\nabla}_1\boldsymbol{G}_{\mathrm{C}}^\omega(\boldsymbol{z},\boldsymbol{z})\cdot\bar{\boldsymbol{\xi}} + \boldsymbol{\nabla}_2\boldsymbol{G}_{\mathrm{C}}^\omega(\boldsymbol{z},\boldsymbol{z})\cdot\bar{\boldsymbol{x}} + \boldsymbol{G}^{\omega(1)}(\bar{\boldsymbol{\xi}} - \bar{\boldsymbol{x}})\right)\,\mathrm{d}V_{\bar{\xi}}.
\end{aligned} \tag{3.39}$$

Canceling each order of the expansion (3.37), the terms $\boldsymbol{V}_j^\omega$ of the expansion (3.36) are found to be the solutions of the following equations corresponding to *static* free-space transmission problems:

$$\mathcal{L}[\boldsymbol{V}_j^\omega](\bar{\boldsymbol{x}}) = \mathcal{F}_j^\omega(\bar{\boldsymbol{x}}),\ \ j \in \{1,2,3,4\} \tag{3.40}$$

Owing to the linearity of equations (3.40), and the different terms involved in the right-hand-sides $\mathcal{F}_j^\omega$ as explained below, the following decomposition holds:

$$\begin{aligned}
\boldsymbol{V}_1^\omega &= \boldsymbol{v}_\mathcal{B}^{(1)}[\boldsymbol{\nabla}\boldsymbol{u}(\boldsymbol{z})] \\
\boldsymbol{V}_2^\omega &= \boldsymbol{v}_\mathcal{B}^{(2)}[\boldsymbol{\nabla}^2\boldsymbol{u}(\boldsymbol{z})] + \boldsymbol{U}^{(0)}[\boldsymbol{u}(\boldsymbol{z})] \\
\boldsymbol{V}_3^\omega &= \boldsymbol{v}_\mathcal{B}^{(3)}[\boldsymbol{\nabla}^3\boldsymbol{u}(\boldsymbol{z})] + 2\ \boldsymbol{U}^{(1)}\left[\boldsymbol{u}_\mathcal{B}^{(1)}[\boldsymbol{\nabla}\boldsymbol{u}(\boldsymbol{z})]\right] + 2\ \boldsymbol{v}_{3\mathrm{C}}^\omega \\
\boldsymbol{V}_4^\omega &= \boldsymbol{v}_\mathcal{B}^{(4)}[\boldsymbol{\nabla}^4\boldsymbol{u}(\boldsymbol{z})] + 6\ \boldsymbol{U}^{(2)}\left[\boldsymbol{u}_\mathcal{B}^{(2)}[\boldsymbol{\nabla}^2\boldsymbol{u}(\boldsymbol{z})] + \boldsymbol{U}^{(0)}[\boldsymbol{u}(\boldsymbol{z})]\right] + 6\ \boldsymbol{v}_{4\mathrm{C}}^\omega,
\end{aligned} \tag{3.41}$$

where:

- The $\boldsymbol{v}_\mathcal{B}^{(p)}$ are the perturbation displacement solutions of FSTPs featuring background polynomial displacements:

  $$\mathcal{L}\left[\boldsymbol{v}_\mathcal{B}^{(p)}[\boldsymbol{\nabla}^p\boldsymbol{u}(\boldsymbol{z})]\right] = -\left\langle \boldsymbol{\varphi}_p[\boldsymbol{\nabla}^p\boldsymbol{u}(\boldsymbol{z})], \boldsymbol{G}_\infty(\cdot - \bar{\boldsymbol{x}})\right\rangle_\mathcal{B}^{\Delta\mathcal{C}} \tag{3.42}$$

  These problems and their solutions (that we called the Eshelby solutions) were extensively addressed in Section 1.3.

- The $\boldsymbol{U}^{(p)}$ are solutions of FSTPs for which the background displacement is defined as a Newtonian potential involving a "source" displacement $\boldsymbol{u}^{(p)}$:

  $$\mathcal{L}\left[\boldsymbol{U}^{(p)}[\boldsymbol{u}^{(p)}]\right](\boldsymbol{x}) = \omega^2\left(\boldsymbol{u}^{(p)}, \boldsymbol{G}_\infty(\cdot - \boldsymbol{x})\right)_\mathcal{B}^{\Delta\rho} = \omega^2\mathcal{V}[\Delta\rho\boldsymbol{u}^{(p)}](\bar{\boldsymbol{x}}). \tag{3.43}$$

  These problems are examined in details below, in Section 3.2.1.1.

- Finally, the "complementary terms" $\boldsymbol{v}_{3\mathrm{C}}^\omega$ and $\boldsymbol{v}_{4\mathrm{C}}^\omega$ account for the contribution of Green's tensor complementary part $\boldsymbol{G}_{\mathrm{C}\infty}^\omega + \boldsymbol{G}_\mathrm{C}^\omega$. The corresponding FSTPs and their solutions, are also addressed below in Section 3.2.1.2.

3.2.1.1 Additional inertial terms

From any "source" displacement noted $\boldsymbol{u}_\mathrm{s}$ in this section, let us define the displacement $\boldsymbol{P}[\boldsymbol{u}_\mathrm{s}]$ as:

$$\boldsymbol{P}[\boldsymbol{u}_\mathrm{s}](\bar{\boldsymbol{x}}) = \omega^2\left(\boldsymbol{u}, \boldsymbol{G}_\infty(\cdot - \bar{\boldsymbol{x}})\right)_\mathcal{B}^{\Delta\rho} = \omega^2\mathcal{V}[\Delta\rho\boldsymbol{u}_\mathrm{s}](\bar{\boldsymbol{x}}). \tag{3.44}$$

Then the displacement $\boldsymbol{U}[\boldsymbol{u}_\mathrm{s}] := \boldsymbol{u}_\mathcal{B}[\boldsymbol{P}[\boldsymbol{u}_\mathrm{s}]]$, i.e. the solution of the transmission problem involving $\mathcal{B}$ with background displacement $\boldsymbol{P}[\boldsymbol{u}_\mathrm{s}]$ is such that:

$$\mathcal{L}[\boldsymbol{U}[\boldsymbol{u}_\mathrm{s}]](\bar{\boldsymbol{x}}) = \boldsymbol{P}[\boldsymbol{u}_\mathrm{s}](\bar{\boldsymbol{x}}). \tag{3.45}$$

Physically, $\boldsymbol{P}[\boldsymbol{u}_\mathrm{s}]$ may be seen as the displacement due to a repartition of volume forces $\boldsymbol{f} = \omega^2\Delta\rho\ \boldsymbol{u}_\mathrm{s}$ on the domain $\mathcal{B}$ in the background medium. Remark that $\boldsymbol{P} \in \boldsymbol{W}_\infty$. $\boldsymbol{U}[\boldsymbol{u}_\mathrm{s}]$ is the displacement due to the same repartition of forces, $\mathcal{B}$ furthermore supporting the elasticity contrast $\Delta\boldsymbol{\mathcal{C}}$. They satisfy the identities:

$$\begin{aligned}
\int_{\mathbb{R}^3} \boldsymbol{\nabla}\boldsymbol{P}[\boldsymbol{u}_\mathrm{s}] : \boldsymbol{\mathcal{C}} : \boldsymbol{\nabla}\boldsymbol{w}\ \mathrm{d}V &= \omega^2\int_\mathcal{B} \Delta\rho\ \boldsymbol{u}_\mathrm{s}\cdot\boldsymbol{w}\ \mathrm{d}V \quad \forall\boldsymbol{w}\in W_\infty, \\
\int_{\mathbb{R}^3} \boldsymbol{\nabla}\boldsymbol{U}[\boldsymbol{u}_\mathrm{s}] : \boldsymbol{\mathcal{C}}_\mathcal{B} : \boldsymbol{\nabla}\boldsymbol{w}\ \mathrm{d}V &= \omega^2\int_\mathcal{B} \Delta\rho\ \boldsymbol{u}_\mathrm{s}\cdot\boldsymbol{w}\ \mathrm{d}V \quad \forall\boldsymbol{w}\in W_\infty.
\end{aligned} \tag{3.46}$$

The reciprocity identity stated by Lemma 1.2 applied to two of these solutions with two source fields $\boldsymbol{u}_{\rm s}$ and $\boldsymbol{u}'_{\rm s}$ therefore reads:

$$\int_{\mathcal{B}} \Delta\rho \; \boldsymbol{u}_{\rm s} \cdot \boldsymbol{U}[\boldsymbol{u}'_{\rm s}] \;{\rm d}V = \int_{\mathcal{B}} \Delta\rho \; \boldsymbol{U}[\boldsymbol{u}_{\rm s}] \cdot \boldsymbol{u}'_{\rm s} \;{\rm d}V. \tag{3.47}$$

Moreover, for any tensor $\boldsymbol{E}_p$ and "source" displacement $\boldsymbol{u}_{\rm s}$, the same reciprocity relation applied to an Eshelby solution $\boldsymbol{u}^{(p)}_{\mathcal{B}}[\boldsymbol{E}_p]$ and $\boldsymbol{U}[\boldsymbol{u}_{\rm s}] = \boldsymbol{u}_{\mathcal{B}}[\boldsymbol{P}[\boldsymbol{u}_{\rm s}]]$ reads:

$$\begin{aligned}\int_{\mathcal{B}} \boldsymbol{\nabla}\boldsymbol{U}[\boldsymbol{u}_{\rm s}] : \Delta\boldsymbol{\mathcal{C}} : \boldsymbol{\nabla}\boldsymbol{\varphi}_p[\boldsymbol{E}_p] \;{\rm d}V &= \int_{\mathcal{B}} \boldsymbol{\nabla}\boldsymbol{P}[\boldsymbol{u}_{\rm s}] : \Delta\boldsymbol{\mathcal{C}} : \boldsymbol{\nabla}\boldsymbol{u}^{(p)}_{\mathcal{B}}[\boldsymbol{E}_p] \;{\rm d}V \\ &= -\omega^2 \int_{\mathcal{B}} \Delta\rho \; \boldsymbol{u}_{\rm s} \cdot \boldsymbol{v}^{(p)}_{\mathcal{B}}[\boldsymbol{E}_p] \;{\rm d}V.\end{aligned} \tag{3.48}$$

For ellipsoidal inclusions, the source displacements $\boldsymbol{u}_{\rm s}$ that we have to consider in the scattered displacement expansion (3.41) are polynomial displacements of order p in $\bar{\boldsymbol{\xi}}$, not necessarily homogeneous, that we note $\boldsymbol{u}^{(p)}$. We therefore note $\boldsymbol{P}^{(p)}[\boldsymbol{u}^{(p)}]$ and $\boldsymbol{U}^{(p)}[\boldsymbol{u}^{(p)}]$ for the fields $\boldsymbol{P}$ and $\boldsymbol{U}$ associated to such displacements.

The computation of $\boldsymbol{P}^{(p)}[\boldsymbol{u}^{(p)}]$ for an ellipsoidal inhomogeneity and isotropic materials uses the decomposition of Kelvin solution on harmonic and biharmonic potentials presented in [Mura, 1982] and is addressed in Appendix 3.A.1. The important property arising from this computation is: since $\boldsymbol{u}^{(p)}$ is a polynomial of degree p, $\boldsymbol{P}^{(p)}[\boldsymbol{u}^{(p)}]$ inside the inclusion will also be a polynomial with terms of degree $p+2$, p, $p-2$ ... So will be the Eshelby solution $\boldsymbol{U}^{(p)}$.

Note that the reciprocity relations (3.47) and (3.48) will permit to limit the required expressions in the misfit function expansion to these of $\boldsymbol{P}^{(0)}$ and $\boldsymbol{U}^{(0)}$. These expressions are given by (3.123) and (3.129). We also provided the expression of $\boldsymbol{P}^{(1)}$ and the general method to obtain these expressions.

3.2.1.2 Complementary terms

The complementary terms $\boldsymbol{v}^{\omega}_{3{\rm C}}$ and $\boldsymbol{v}^{\omega}_{4{\rm C}}$ which embed the contribution of the complementary part of $\boldsymbol{G}^{\omega}$ are now addressed.

Third order complementary term Introducing the solution for the first order term $\boldsymbol{V}^{\omega}_1 = \boldsymbol{v}^{(1)}_{\mathcal{B}}[\boldsymbol{\nabla}\boldsymbol{u}(\boldsymbol{z})]$ into $\mathcal{F}^{\omega}_3$ (3.38), and consequently expressing the resulting integral thanks to the elastic moment tensor $\boldsymbol{\mathcal{A}}$, $\boldsymbol{v}^{\omega}_{3{\rm C}}$ is defined as the solution of:

$$\begin{aligned}\mathcal{L}[\boldsymbol{v}^{\omega}_{3{\rm C}}](\bar{\boldsymbol{x}}) = &- \boldsymbol{\nabla}\boldsymbol{u}(\boldsymbol{z}) : \boldsymbol{\mathcal{A}} : \boldsymbol{\nabla}_1 \boldsymbol{G}^{\omega}_{\rm C}(\boldsymbol{z},\boldsymbol{z}) + \omega^2 |\mathcal{B}| \Delta\rho \; \boldsymbol{u}(\boldsymbol{z}) \cdot \Big({\rm i}\boldsymbol{G}^{\omega(0)} + \boldsymbol{G}^{\omega}_{\rm C}(\boldsymbol{z},\boldsymbol{z}) \Big) \\ &- \int_{\mathcal{B}} \boldsymbol{\nabla}\boldsymbol{u}^{(1)}_{\mathcal{B}}[\boldsymbol{\nabla}\boldsymbol{u}(\boldsymbol{z})] : \Delta\boldsymbol{\mathcal{C}} : \boldsymbol{H}^{\omega(0)}(\cdot - \bar{\boldsymbol{x}}) \;{\rm d}V.\end{aligned} \tag{3.49}$$

We reordered the right-hand-side of (3.49) so that the first line is seen to be independent of $\bar{\boldsymbol{x}}$, the difficulty lying therefore in the computation of the integral involving $\boldsymbol{H}^{\omega(0)}$.

The general case is not addressed, but for ellipsoids and isotropic materials, the computation of this integral is explained in Appendix 3.A.2, and the resulting contribution is found to be polynomial in $\bar{\boldsymbol{x}}$:

$$\int_{\mathcal{B}} \boldsymbol{\nabla}\boldsymbol{u}^{(1)}_{\mathcal{B}}[\boldsymbol{\nabla}\boldsymbol{u}(\boldsymbol{z})] : \Delta\boldsymbol{\mathcal{C}} : \boldsymbol{H}^{\omega(0)}(\cdot - \bar{\boldsymbol{x}}) \;{\rm d}V = \boldsymbol{J}^{H0}_1(\boldsymbol{z}) \cdot \bar{\boldsymbol{x}} + \boldsymbol{J}^{H0}_3(\boldsymbol{z}) \bullet \bar{\boldsymbol{x}}^{\otimes 3}, \tag{3.50}$$

where the tensors $\boldsymbol{J}_p^{H0}$ are expressed as:

$$\boldsymbol{J}_p^{H0}(\boldsymbol{z}) = \boldsymbol{\nabla}\boldsymbol{u}(\boldsymbol{z}) : \boldsymbol{\mathcal{A}} : \boldsymbol{I}_p^{H0} \qquad p = \{1, 3\}, \tag{3.51}$$

in terms of constant tensors $\boldsymbol{I}_p^{H0}$, whose computation is explained in Appendix 3.A.2. For a sphere, these computations provide the closed-form expressions:

$$\begin{aligned}
\boldsymbol{J}_1^{H0}(\boldsymbol{z}) &= \frac{k_{\mathrm{S}}^2}{80\pi\mu}\boldsymbol{\nabla}\boldsymbol{u}(\boldsymbol{z}) : \boldsymbol{\mathcal{A}} : \left[15(1+\beta^4)\boldsymbol{\mathcal{J}} - 6(1-\beta^4)\boldsymbol{\mathcal{K}}\right], \\
\boldsymbol{J}_3^{H0}(\boldsymbol{z}) &= -\frac{k_{\mathrm{S}}^2}{560\pi\mu}\boldsymbol{\nabla}\boldsymbol{u}(\boldsymbol{z}) : \boldsymbol{\mathcal{A}} : \left[\left[(17+25\beta^4)\boldsymbol{\mathcal{J}} - 10(1-\beta^4)\boldsymbol{\mathcal{K}}\right] \otimes \boldsymbol{I} + 4\,\boldsymbol{I}^{(6)}\right].
\end{aligned} \tag{3.52}$$

Eventually, in these cases, equation (3.49) also corresponds to the integral formulation of a FSTP with non-homogeneous polynomial background displacement, and its solution is expressed thanks to the corresponding Eshelby solutions $\boldsymbol{u}_{\mathcal{B}}^{(p)}$ as:

$$\begin{aligned}
\boldsymbol{v}_{3\mathrm{C}}^{\omega} = &- \boldsymbol{\nabla}\boldsymbol{u}(\boldsymbol{z}) : \boldsymbol{\mathcal{A}} : \boldsymbol{\nabla}_1\boldsymbol{G}_{\mathrm{C}}^{\omega}(\boldsymbol{z},\boldsymbol{z}) + \omega^2|\mathcal{B}|\Delta\rho\ \boldsymbol{u}(\boldsymbol{z}) \cdot \left(\mathrm{i}\boldsymbol{G}^{\omega(0)} + \boldsymbol{G}_{\mathrm{C}}^{\omega}(\boldsymbol{z},\boldsymbol{z})\right) \\
&- \boldsymbol{u}_{\mathcal{B}}^{(1)}\left[\boldsymbol{J}_1^{H0}(\boldsymbol{z})\right] - \boldsymbol{u}_{\mathcal{B}}^{(3)}\left[\boldsymbol{J}_3^{H0}(\boldsymbol{z})\right].
\end{aligned} \tag{3.53}$$

Fourth order complementary term Introducing the expressions (3.41) of $\boldsymbol{V}_1^{\omega}$ and $\boldsymbol{V}_2^{\omega}$ into the remaining terms in $\mathcal{F}_4$ (3.39), using reciprocity relation (3.48), and expressing the arising "stiffness" and "mass" products thanks to the elastic moment tensors and inertial polarization tensors whenever possible, $\boldsymbol{v}_{4\mathrm{C}}^{\omega}$ is found to be the solution of:

$$\begin{aligned}
\mathcal{L}[\boldsymbol{v}_{4\mathrm{C}}^{\omega}](\bar{\boldsymbol{x}}) = &- \boldsymbol{\nabla}\boldsymbol{u}(\boldsymbol{z}) : \boldsymbol{\mathcal{A}}_{12} \bullet \boldsymbol{\nabla}_{11}\boldsymbol{G}_{\mathrm{C}}^{\omega}(\boldsymbol{z},\boldsymbol{z}) - \boldsymbol{\nabla}^2\boldsymbol{u}(\boldsymbol{z}) \bullet \boldsymbol{\mathcal{A}}_{21} : \boldsymbol{\nabla}_1\boldsymbol{G}_{\mathrm{C}}^{\omega}(\boldsymbol{z},\boldsymbol{z}) \\
&+ \omega^2\Delta\rho\ \left[\boldsymbol{u}(\boldsymbol{z}) \cdot \boldsymbol{\mathcal{Q}}_{01} : \boldsymbol{\nabla}_1\boldsymbol{G}_{\mathrm{C}}^{\omega}(\boldsymbol{z},\boldsymbol{z}) + \boldsymbol{\nabla}\boldsymbol{u}(\boldsymbol{z}) : \boldsymbol{\mathcal{Q}}_{10} \cdot \left(\mathrm{i}\boldsymbol{G}^{\omega(0)} + \boldsymbol{G}_{\mathrm{C}}^{\omega}(\boldsymbol{z},\boldsymbol{z})\right)\right] \\
&- \left[\boldsymbol{\nabla}\boldsymbol{u}(\boldsymbol{z}) : \boldsymbol{\mathcal{A}} : \boldsymbol{\nabla}_{21}\boldsymbol{G}_{\mathrm{C}}^{\omega}(\boldsymbol{z},\boldsymbol{z}) - \omega^2|\mathcal{B}|\Delta\rho\ \boldsymbol{u}(\boldsymbol{z}) \cdot \boldsymbol{\nabla}_2\boldsymbol{G}_{\mathrm{C}}^{\omega}(\boldsymbol{z},\boldsymbol{z})\right] \cdot \bar{\boldsymbol{x}} \\
&- \int_{\mathcal{B}} \boldsymbol{\nabla}\boldsymbol{u}_{\mathcal{B}}^{(1)}[\boldsymbol{\nabla}\boldsymbol{u}(\boldsymbol{z})] : \Delta\boldsymbol{\mathcal{C}} : \mathrm{i}\boldsymbol{H}^{\omega(1)}(\cdot - \bar{\boldsymbol{x}})\ \mathrm{d}V \\
&- \int_{\mathcal{B}} \boldsymbol{\nabla}\left(\boldsymbol{u}_{\mathcal{B}}^{(2)}[\boldsymbol{\nabla}^2\boldsymbol{u}(\boldsymbol{z})] + \boldsymbol{U}^{(0)}[\boldsymbol{u}(\boldsymbol{z})]\right) : \Delta\boldsymbol{\mathcal{C}} : \boldsymbol{H}^{\omega(0)}(\cdot - \bar{\boldsymbol{x}})\ \mathrm{d}V \\
&+ \omega^2\Delta\rho\ \boldsymbol{u}(\boldsymbol{z}) \cdot \int_{\mathcal{B}} \boldsymbol{G}^{\omega(1)}(\cdot - \bar{\boldsymbol{x}})\ \mathrm{d}V
\end{aligned} \tag{3.54}$$

As above for $\boldsymbol{v}_{3\mathrm{C}}^{\omega}$, we reordered some terms to make clear that the right-hand-side of (3.54) includes three kind of contributions: (i) constant terms w.r.t $\bar{\boldsymbol{x}}$ (first and second lines), (ii) linear terms w.r.t. $\bar{\boldsymbol{x}}$ (third line) and (iii) contributions of the expansion of $\boldsymbol{G}_{\mathrm{C}\infty}^{\omega}$.

Again, we focus on the case of ellipsoids and isotropic materials, for which closed-form expressions are available. First remark that all the constant terms vanish owing to the cancellation of $\boldsymbol{\mathcal{A}}_{pq}$ and $\boldsymbol{\mathcal{Q}}_{pq}$ whenever $p+q$ is odd for centrally symmetric shapes $\mathcal{B}$ (Lemmas 1.9 and 1.10). Then, we recall that $\boldsymbol{\nabla}\boldsymbol{u}_{\mathcal{B}}^{(1)}[\boldsymbol{\nabla}\boldsymbol{u}(\boldsymbol{z})]$ is constant for ellipsoids, and that the expressions (1.108) for $\boldsymbol{u}_{\mathcal{B}}^{(2)}$ and (3.130) for $\boldsymbol{U}^{(0)}$ imply:

$$\boldsymbol{\varepsilon}\left[\boldsymbol{u}_{\mathcal{B}}^{(2)}[\boldsymbol{\nabla}^2\boldsymbol{u}(\boldsymbol{z})] + \boldsymbol{U}^{(0)}[\boldsymbol{u}(\boldsymbol{z})]\right](\bar{\boldsymbol{\xi}}) = \left[\left(\boldsymbol{\mathcal{I}}^{(6)} + \boldsymbol{A}_2\right) \bullet \left(\boldsymbol{\nabla}^2\boldsymbol{u}(\boldsymbol{z}) + \omega^2\Delta\rho\ \boldsymbol{\mathcal{E}}_3^{(0)} \cdot \boldsymbol{u}(\boldsymbol{z})\right)\right] \cdot \bar{\boldsymbol{\xi}}, \tag{3.55}$$

so that completing the evaluation of the right-hand side of (3.54) requires the computation of the integrals:

$$\int_{\mathcal{B}} \boldsymbol{H}^{\omega(1)}(\cdot - \bar{\boldsymbol{x}}) \, \mathrm{d}V, \quad \int_{\mathcal{B}} \bar{\boldsymbol{\xi}} \otimes \boldsymbol{H}^{\omega(0)}(\bar{\boldsymbol{\xi}} - \bar{\boldsymbol{x}}) \, \mathrm{d}V_{\bar{\xi}} \quad \text{and} \quad \int_{\mathcal{B}} \boldsymbol{G}^{\omega(1)}(\cdot - \bar{\boldsymbol{x}}) \, \mathrm{d}V. \tag{3.56}$$

After some algebra, delayed to Appendix 3.A.2, these integrals are found to be polynomials in $\bar{\boldsymbol{x}}$. Finally, the equation (3.54) is again seen to be the formulation of a FSTP with polynomial source terms, and its solution is therefore written in terms of the corresponding Eshelby solutions $\boldsymbol{u}_{\mathcal{B}}^{(p)}$ as:

$$\begin{aligned} \boldsymbol{v}_{4\mathrm{C}}^{\omega} = & - \boldsymbol{u}_{\mathcal{B}}^{(1)} \left[\left(\boldsymbol{L}^{\Delta\mathcal{C}} - \omega^2 \boldsymbol{L}^{\Delta\rho} + \mathrm{i} \boldsymbol{J}_1^{H1} \right) (\boldsymbol{z}) \right] \\ & - \left(\boldsymbol{J}_0^{\xi H0}(\boldsymbol{z}) + \boldsymbol{u}_{\mathcal{B}}^{(2)} \left[\boldsymbol{J}_2^{\xi H0}(\boldsymbol{z}) \right] + \boldsymbol{u}_{\mathcal{B}}^{(4)} \left[\boldsymbol{J}_4^{\xi H0}(\boldsymbol{z}) \right] \right) \\ & + \omega^2 \left(\boldsymbol{J}_0^{G1}(\boldsymbol{z}) + \boldsymbol{u}_{\mathcal{B}}^{(2)} \left[\boldsymbol{J}_2^{G1}(\boldsymbol{z}) \right] + \boldsymbol{u}_{\mathcal{B}}^{(4)} \left[\boldsymbol{J}_4^{G1}(\boldsymbol{z}) \right] \right), \end{aligned} \tag{3.57}$$

where:

- the tensor-valued functions $\boldsymbol{L}^{\Delta\mathcal{C}}$ and $\boldsymbol{L}^{\Delta\rho}$ are given by:

$$\boldsymbol{L}^{\Delta\mathcal{C}}(\boldsymbol{z}) = \boldsymbol{\nabla}\boldsymbol{u}(\boldsymbol{z}) : \boldsymbol{\mathcal{A}} : \boldsymbol{\nabla}_{21}\boldsymbol{G}_{\mathrm{C}}^{\omega}(\boldsymbol{z}, \boldsymbol{z}) \quad \text{and} \quad \boldsymbol{L}^{\Delta\rho}(\boldsymbol{z}) = |\mathcal{B}|\Delta\rho \, \boldsymbol{u}(\boldsymbol{z}) \cdot \boldsymbol{\nabla}_2\boldsymbol{G}_{\mathrm{C}}^{\omega}(\boldsymbol{z}, \boldsymbol{z}), \tag{3.58}$$

- the tensor $\boldsymbol{J}_1^{H1}$ is given by

$$\boldsymbol{J}_1^{H1}(\boldsymbol{z}) = \boldsymbol{\nabla}\boldsymbol{u}(\boldsymbol{z}) : \boldsymbol{\mathcal{A}} : \boldsymbol{I}_1^{H1}, \tag{3.59}$$

  where the computation of the constant tensor $\boldsymbol{I}_1^{H1}$ for any ellipsoid is explained in Appendix 3.A.2. When $\mathcal{B}$ is a sphere, it results in:

$$\boldsymbol{J}_1^{H1}(\boldsymbol{z}) = \frac{k_{\mathrm{S}}^3}{60\pi\mu} \boldsymbol{\nabla}\boldsymbol{u}(\boldsymbol{z}) : \boldsymbol{\mathcal{A}} : \left[5(2+\beta^5)\boldsymbol{\mathcal{J}} - 2(1-\beta^5)\boldsymbol{\mathcal{K}} \right], \tag{3.60}$$

- the contributions of the tensors $\boldsymbol{J}_p^{G1}$ and $\boldsymbol{J}_p^{\xi H0}$ will be found to vanish in the upcoming misfit function expansion. Consequently, we provide only partially explicit expression for these tensors. The tensors $\boldsymbol{J}_p^{G1}$ are given as function of constant tensors $\boldsymbol{I}_p^{G1}$ as:

$$\boldsymbol{J}_p^{G1} = |\mathcal{B}|\Delta\rho \, \boldsymbol{u}(\boldsymbol{z}) \cdot \boldsymbol{I}_p^{G1}, \tag{3.61}$$

  and the tensors $\boldsymbol{J}_p^{\xi H0}$ are the polynomial coefficients of the integral below:

$$\begin{aligned} & \int_{\mathcal{B}} \boldsymbol{\nabla} \left(\boldsymbol{u}_{\mathcal{B}}^{(2)}[\boldsymbol{\nabla}^2\boldsymbol{u}(\boldsymbol{z})] + \boldsymbol{U}^{(0)}[\boldsymbol{u}(\boldsymbol{z})] \right) : \Delta\boldsymbol{\mathcal{C}} : \boldsymbol{H}^{\omega(0)}(\cdot - \bar{\boldsymbol{x}}) \, \mathrm{d}V \\ & \qquad = \boldsymbol{J}_0^{\xi H0}(\boldsymbol{z}) + \boldsymbol{J}_2^{\xi H0}(\boldsymbol{z}) : \bar{\boldsymbol{x}}^{\otimes 2} + \boldsymbol{J}_4^{\xi H0}(\boldsymbol{z}) \bullet \bar{\boldsymbol{x}}^{\otimes 4}. \end{aligned} \tag{3.62}$$

  The setting for complete computations, along with preliminary expressions, are provided in Appendix 3.A.2.

3.2.2 Remainder estimate for the inner expansion

The inner approximation $\boldsymbol{V}_a^\omega$ of $\boldsymbol{v}_a^\omega$ being given by (3.41), we now provide an estimate of the remainder $\boldsymbol{\delta}_a^\omega = \boldsymbol{v}_a^\omega - \mathcal{P}_a^{-1}\boldsymbol{V}_a^\omega$.

Proposition 3.1. *(Error estimation on the inner expansion of the displacement) Consider the inner expansion $\boldsymbol{v}_a^\omega = \mathcal{P}_a^{-1}\boldsymbol{V}_a^\omega + \boldsymbol{\delta}_a^\omega$ of the scattered field by an inhomogeneity $(B_a, \boldsymbol{\mathcal{C}}^\star)$, with $\boldsymbol{V}_a^\omega$ defined by expressions* (3.41)*. If both $\boldsymbol{\mathcal{C}}$ and $\boldsymbol{\mathcal{C}}^\star$ are bounded and positive, there exists a constant $C_\delta^\omega > 0$ independent of the size a such that*

$$\|\boldsymbol{\delta}_a^\omega\|_{H^1(B_a)} \leq C_\delta^\omega a^{11/2} \qquad \textit{as } a \to 0. \tag{3.63}$$

Proof. Subtracting the integral equations satisfied by the terms $\boldsymbol{V}_j^\omega$ of the inner expansion (3.37) to the one satisfied by $\boldsymbol{v}_a^\omega$ (3.22), $\boldsymbol{\delta}_a^\omega$ is found to satisfy the integral equation $\mathcal{L}_a^\omega[\boldsymbol{\delta}_a^\omega](\boldsymbol{x}) = \boldsymbol{\gamma}_a^\omega(\boldsymbol{x})$ where $\boldsymbol{\gamma}_a^\omega$ is written as the sum:

$$\begin{aligned}\boldsymbol{\gamma}_a^\omega(\boldsymbol{x}) = &-\int_{B_a} \boldsymbol{F}_0(\boldsymbol{\xi}) : \Delta\boldsymbol{\mathcal{C}} : \boldsymbol{\nabla}\boldsymbol{G}_\infty(\boldsymbol{\xi}-\boldsymbol{x})\,\mathrm{d}V_\xi + \omega^2\int_{B_a}\Delta\rho\;\boldsymbol{f}_0(\boldsymbol{\xi})\cdot\boldsymbol{G}_\infty(\boldsymbol{\xi}-\boldsymbol{x})\,\mathrm{d}V_\xi\\ &+\sum_{i=1}^{3}\left[-\int_{B_a}\boldsymbol{F}_p(\boldsymbol{\xi}) : \Delta\boldsymbol{\mathcal{C}} : \boldsymbol{H}_p(\boldsymbol{\xi},\boldsymbol{x})\,\mathrm{d}V_\xi + \omega^2\int_{B_a}\Delta\rho\;\boldsymbol{f}_p(\boldsymbol{\xi})\cdot\boldsymbol{h}_p(\boldsymbol{\xi},\boldsymbol{x})\,\mathrm{d}V_\xi\right],\end{aligned} \tag{3.64}$$

where the functions $\boldsymbol{F}_p$ and $\boldsymbol{f}_p$ come from the expansion of $\boldsymbol{u}_a^\omega$:

$$\begin{aligned}
\boldsymbol{F}_0(\boldsymbol{\xi}) &= \boldsymbol{\nabla}\boldsymbol{u}(\boldsymbol{\xi}) - \left[\boldsymbol{\nabla}\boldsymbol{u}(\boldsymbol{z}) + a\boldsymbol{\nabla}\boldsymbol{u}^2(\boldsymbol{z})\cdot\bar{\boldsymbol{\xi}} + \frac{a^2}{2}\boldsymbol{\nabla}^3\boldsymbol{u}(\boldsymbol{z}) : \bar{\boldsymbol{\xi}}^{\otimes 2} + \frac{a^3}{6}\boldsymbol{\nabla}^4\boldsymbol{u}(\boldsymbol{z})\bullet\bar{\boldsymbol{\xi}}^{\otimes 3}\right],\\
\boldsymbol{F}_1(\boldsymbol{\xi}) &= \boldsymbol{\nabla}\boldsymbol{u}(\boldsymbol{\xi}) - \left[\boldsymbol{\nabla}\boldsymbol{u}(\boldsymbol{z}) + a\boldsymbol{\nabla}^2\boldsymbol{u}(\boldsymbol{z})\cdot\bar{\boldsymbol{\xi}}\right] + \frac{a^2}{2}\bar{\boldsymbol{\nabla}}\boldsymbol{V}_3^\omega(\bar{\boldsymbol{\xi}}) + \frac{a^3}{6}\bar{\boldsymbol{\nabla}}\boldsymbol{V}_4^\omega(\bar{\boldsymbol{\xi}}),\\
\boldsymbol{F}_2(\boldsymbol{\xi}) &= a\bar{\boldsymbol{\nabla}}\boldsymbol{V}_2^\omega(\bar{\boldsymbol{\xi}}),\\
\boldsymbol{F}_3(\boldsymbol{\xi}) &= \bar{\boldsymbol{\nabla}}\boldsymbol{V}_1^\omega(\bar{\boldsymbol{\xi}}),\\
\boldsymbol{f}_0(\boldsymbol{\xi}) &= \boldsymbol{u}(\boldsymbol{\xi}) - \left[\boldsymbol{u}(\boldsymbol{z}) + a\boldsymbol{\nabla}\boldsymbol{u}(\boldsymbol{z})\cdot\bar{\boldsymbol{\xi}} + \frac{a^2}{2}\boldsymbol{\nabla}^2\boldsymbol{u}(\boldsymbol{z}) : \bar{\boldsymbol{\xi}}^{\otimes 2}\right] + \frac{a^3}{2}\boldsymbol{V}_3^\omega(\bar{\boldsymbol{\xi}}) + \frac{a^4}{6}\boldsymbol{V}_4^\omega(\bar{\boldsymbol{\xi}}),\\
\boldsymbol{f}_1(\boldsymbol{\xi}) &= \boldsymbol{u}(\boldsymbol{\xi}) - \left[\boldsymbol{u}(\boldsymbol{z}) + a\boldsymbol{\nabla}\boldsymbol{u}(\boldsymbol{z})\cdot\bar{\boldsymbol{\xi}}\right] + a^2\boldsymbol{V}_2^\omega(\bar{\boldsymbol{\xi}}),\\
\boldsymbol{f}_2(\boldsymbol{\xi}) &= a\left[\boldsymbol{\nabla}\boldsymbol{u}(\boldsymbol{z})\cdot\bar{\boldsymbol{\xi}} + \boldsymbol{V}_1^\omega(\bar{\boldsymbol{\xi}})\right],\\
\boldsymbol{f}_3(\boldsymbol{\xi}) &= \boldsymbol{u}(\boldsymbol{z}),
\end{aligned} \tag{3.65}$$

and the bounded kernels $\boldsymbol{H}_p(\boldsymbol{\xi},\boldsymbol{x})$ and $\boldsymbol{h}_p(\boldsymbol{\xi},\boldsymbol{x})$ come form the expansion of $\boldsymbol{G}_{\mathrm{C}\infty}^\omega + \boldsymbol{G}_{\mathrm{C}}^\omega$:

$$\begin{aligned}
\boldsymbol{H}_1(\boldsymbol{\xi},\boldsymbol{x}) &= \boldsymbol{\nabla}\boldsymbol{G}_{\mathrm{C}\infty}^\omega(\boldsymbol{\xi}-\boldsymbol{x}) + \boldsymbol{\nabla}_1\boldsymbol{G}_{\mathrm{C}}^\omega(\boldsymbol{\xi},\boldsymbol{x}),\\
\boldsymbol{H}_2(\boldsymbol{\xi},\boldsymbol{x}) &= \boldsymbol{H}_1(\boldsymbol{\xi},\boldsymbol{x}) - \left[\boldsymbol{H}^{\omega(0)}(\bar{\boldsymbol{\xi}}-\bar{\boldsymbol{x}}) + \boldsymbol{\nabla}\boldsymbol{G}_{\mathrm{C}}^\omega(\boldsymbol{z},\boldsymbol{z})\right],\\
\boldsymbol{H}_3(\boldsymbol{\xi},\boldsymbol{x}) &= \boldsymbol{H}_2(\boldsymbol{\xi},\boldsymbol{x}) - a\left[\mathrm{i}\boldsymbol{H}^{\omega(1)}(\bar{\boldsymbol{\xi}}-\bar{\boldsymbol{x}}) + \boldsymbol{\nabla}_{11}\boldsymbol{G}_{\mathrm{C}}^\omega(\boldsymbol{z},\boldsymbol{z})\cdot\bar{\boldsymbol{\xi}} + \boldsymbol{\nabla}_{21}\boldsymbol{G}_{\mathrm{C}}^\omega(\boldsymbol{z},\boldsymbol{z})\cdot\bar{\boldsymbol{x}}\right],\\
\boldsymbol{h}_1(\boldsymbol{\xi},\boldsymbol{x}) &= \boldsymbol{G}_{\mathrm{C}\infty}^\omega(\boldsymbol{\xi}-\boldsymbol{x}) + \boldsymbol{G}_{\mathrm{C}}^\omega(\boldsymbol{\xi},\boldsymbol{x}),\\
\boldsymbol{h}_2(\boldsymbol{\xi},\boldsymbol{x}) &= \boldsymbol{h}_1(\boldsymbol{\xi},\boldsymbol{x}) - \left[\mathrm{i}\boldsymbol{G}^{\omega(0)} + \boldsymbol{G}_{\mathrm{C}}^\omega(\boldsymbol{z},\boldsymbol{z})\right],\\
\boldsymbol{h}_3(\boldsymbol{\xi},\boldsymbol{x}) &= \boldsymbol{h}_2(\boldsymbol{\xi},\boldsymbol{x}) - a\left[\boldsymbol{G}^{\omega(1)}(\bar{\boldsymbol{\xi}}-\bar{\boldsymbol{x}}) + \boldsymbol{\nabla}_1\boldsymbol{G}_{\mathrm{C}}^\omega(\boldsymbol{z},\boldsymbol{z})\cdot\bar{\boldsymbol{\xi}} + \boldsymbol{\nabla}_2\boldsymbol{G}_{\mathrm{C}}^\omega(\boldsymbol{z},\boldsymbol{z})\cdot\bar{\boldsymbol{x}}\right].
\end{aligned} \tag{3.66}$$

The gradient of this right-hand-side is then:

$$\nabla\gamma_a^\omega(\boldsymbol{x}) = -\nabla_{\boldsymbol{x}}\int_{B_a}\boldsymbol{F}_0(\boldsymbol{\xi}):\Delta\boldsymbol{\mathcal{C}}:\nabla\boldsymbol{G}_\infty(\boldsymbol{\xi}-\boldsymbol{x})\,\mathrm{d}V_\xi - \omega^2\int_{B_a}\Delta\rho\boldsymbol{f}_0\cdot\nabla\boldsymbol{G}_\infty(\boldsymbol{\xi}-\boldsymbol{x})\,\mathrm{d}V_\xi$$
$$+\sum_{i=1}^{3}\left[-\int_{B_a}\boldsymbol{F}_p(\boldsymbol{\xi}):\Delta\boldsymbol{\mathcal{C}}:\nabla_2\boldsymbol{H}_p(\boldsymbol{\xi},\boldsymbol{x})\,\mathrm{d}V_\xi + \omega^2\int_{B_a}\Delta\rho\;\boldsymbol{f}_p(\boldsymbol{\xi})\cdot\nabla_2\boldsymbol{h}_p(\boldsymbol{\xi},\boldsymbol{x})\,\mathrm{d}V_\xi\right]. \tag{3.67}$$

We know from Theorem 3.1 that $\mathcal{L}_a^\omega$ is invertible with bounded inverse independently of a for $a < a_0^\omega$, so that:

$$\exists C > 0,\ \|\boldsymbol{\delta}_a^\omega\|_{H^1(B_a)} \leq C\|\boldsymbol{\gamma}_a^\omega\|_{H^1(B_a)} \quad \forall a < a_0^\omega. \tag{3.68}$$

Our goal is therefore to show that $\|\boldsymbol{\gamma}_a^\omega\|_{H^1(B_a)} = O(a^{11/2})$. We successively deal with the three terms in (3.64):

(i) Remark that the first term of (2.55) writes $-\mathcal{M}[\Delta\boldsymbol{\mathcal{C}}_a : \boldsymbol{F}_0]$, with $\Delta\boldsymbol{\mathcal{C}}_a := \chi_{B_a}\Delta\boldsymbol{\mathcal{C}}$ and $\mathcal{M} : L^2_{\text{comp}}(\mathbb{R}^3;\mathbb{R}^{3\times3}_{\text{sym}}) \to \boldsymbol{H}^1_{\text{loc}}(\mathbb{R}^3)$ is shown to be continuous by Lemma 1.4. The following inequality therefore holds:

$$\exists C > 0,\ \left\|\int_{B_a}\boldsymbol{F}_0:\Delta\boldsymbol{\mathcal{C}}:\nabla\boldsymbol{G}_\infty(\cdot-\boldsymbol{x})\,\mathrm{d}V\right\|_{H^1(B_a)} \leq C\|\boldsymbol{F}_0\|_{L^2(B_a)} = Ca^{11/2} + o\left(a^{11/2}\right). \tag{3.69}$$

(ii) Similarly than in the proof of Lemma 3.2 (see eq. (3.29)), we have:

$$\begin{aligned}\|\omega^2\left(\boldsymbol{f}_0, \boldsymbol{G}_\infty(\cdot-\boldsymbol{x})\right)^{\Delta\rho}_{B_a}\|_{H^1(B_a)} &\leq a^{5/2}C^\omega_{\mathcal{V}}\|\mathcal{P}_a\boldsymbol{f}_0\|_{H^1(\mathcal{B})}\\ &\leq a^{5/2}C^\omega_{\mathcal{V}}\left(\frac{a^3}{2}\left\|\boldsymbol{\varphi}_3\left[\nabla^3\boldsymbol{u}(\boldsymbol{z})\right]+\boldsymbol{V}_3^\omega\right\|_{H^1(\mathcal{B})}+o(a^3)\right)\\ &\leq Ca^{11/2}+o\left(a^{11/2}\right)\end{aligned} \tag{3.70}$$

(iii) For all the other terms, we have to bound the $\boldsymbol{H}^1$-norm of functions defined by the convolutions $(\boldsymbol{F}_p, \Delta\boldsymbol{\mathcal{C}} : \boldsymbol{H}_p(\cdot,\boldsymbol{x}))_{L^2(B_a)}$ and $\omega^2(\boldsymbol{f}_p, \boldsymbol{h}_p(\cdot,\boldsymbol{x}))^{\Delta\rho}_{B_a}$. Since $\boldsymbol{H}_p$ and $\boldsymbol{h}_p$ are bounded kernels, and their gradients $\nabla_2\boldsymbol{H}_p$ and $\nabla_2\boldsymbol{h}_p$ that intervene in (3.67) are respectively square-integrable and bounded kernels, we can apply Cauchy-Schwarz inequality twice. From the definitions (3.65) and (3.66), it is straightforward that:

$$\begin{aligned}&\|\boldsymbol{F}_p\|_{L^2(B_a)} \sim \|\boldsymbol{f}_p\|_{L^2(B_a)} = O\left(a^{3/2+(3-p)}\right) \quad \forall p\in\{1,2,3\}\\ \text{and}\quad &\|\boldsymbol{H}_p\|_{H^1(B_a)\times H^1(B_a)} \sim \|\boldsymbol{h}_p\|_{H^1(B_a)\times H^1(B_a)} = O\left(a^{3+(p-1)}\right) \quad \forall p\in\{1,2,3\}\end{aligned} \tag{3.71}$$

Multiplying these orders of magnitude, one obtains:

$$\begin{aligned}&\|(\boldsymbol{F}_p, \Delta\boldsymbol{\mathcal{C}} : \boldsymbol{H}_p(\cdot,\boldsymbol{x}))_{L^2(B_a)}\|_{H^1(B_a)} = O\left(a^{13/2}\right) \quad \forall p\in\{1,2,3\}\\ \text{and}\quad &\|(\boldsymbol{f}_p, \boldsymbol{h}_p(\cdot,\boldsymbol{x}))^{\Delta\rho}_{B_a}\|_{H^1(B_a)} = O\left(a^{13/2}\right) \quad \forall p\in\{1,2,3\}\end{aligned} \tag{3.72}$$

And we can conclude the estimation of $\boldsymbol{\gamma}_a^\omega$ and the proof of Proposition 3.1 by:

$$\exists C_\delta^\omega,\quad \|\boldsymbol{\gamma}_a^\omega\|_{H^1(B_a)} \leq C_\delta^\omega a^{11/2} + o(a^{11/2}) \tag{3.73}$$

□

Remark 3.2. *Evaluating successively the $\boldsymbol{L}^2$-norms of the fields considered in step (i) and (ii) above and those of their gradients (instead of evaluating directly their $\boldsymbol{H}^1$-norms), one could additionally show that:*

$$\exists C, \quad \|\gamma_a^\omega\|_{L^2(B_a)} \leq C a^{13/2} + o(a^{13/2}), \tag{3.74}$$

so that the $O(a^{11/2})$ estimate (3.73) *comes from $\|\boldsymbol{\nabla}\gamma_a^\omega\|_{L^2(B_a)}$. Similar observation then holds for $\|\boldsymbol{\delta}_a^\omega\|_{L^2(B_a)}$ and $\|\boldsymbol{\nabla}\boldsymbol{\delta}_a^\omega\|_{L^2(B_a)}$.*

3.2.3 Outer expansion

We now look for the outer expansion of $\boldsymbol{v}_a^\omega$. Let's recall that for $\boldsymbol{x} \notin \overline{B_a}$, $\boldsymbol{v}_a^\omega(\boldsymbol{x})$ is given by the integral representation:

$$\boldsymbol{v}_a^\omega(\boldsymbol{x}) = -\int_{B_a} \boldsymbol{\nabla}\left(\boldsymbol{u} + \boldsymbol{v}_a^\omega\right) : \Delta\boldsymbol{\mathcal{C}} : \boldsymbol{\nabla}_1 \boldsymbol{G}^\omega(\cdot, \boldsymbol{x})\, \mathrm{d}V + \omega^2 \int_{B_a} \Delta\rho\, \left(\boldsymbol{u} + \boldsymbol{v}_a^\omega\right) \cdot \boldsymbol{G}^\omega(\cdot, \boldsymbol{x})\, \mathrm{d}V. \tag{3.75}$$

In this case, the singular behavior of $\boldsymbol{G}^\omega(\boldsymbol{\xi}, \boldsymbol{x})$ is not activated, and one therefore has:

$$\begin{aligned} \boldsymbol{G}^\omega(\boldsymbol{\xi}, \boldsymbol{x}) &= \boldsymbol{G}^\omega(\boldsymbol{z}, \boldsymbol{x}) + O(a), \qquad && \boldsymbol{\xi} \in B_a, \boldsymbol{x} \notin \overline{B_a}. \\ \boldsymbol{\nabla}_1\boldsymbol{G}^\omega(\boldsymbol{\xi}, \boldsymbol{x}) &= \boldsymbol{\nabla}_1\boldsymbol{G}^\omega(\boldsymbol{z}, \boldsymbol{x}) + O(a), \qquad && \boldsymbol{\xi} \in B_a, \boldsymbol{x} \notin \overline{B_a}. \end{aligned} \tag{3.76}$$

Using the leading-order inner expansion of $\boldsymbol{v}_a^\omega$, one moreover has :

$$\begin{aligned} \boldsymbol{u}(\boldsymbol{\xi}) + \boldsymbol{v}_a^\omega(\boldsymbol{\xi}) &= \boldsymbol{u}(\boldsymbol{z}) + O(a), && \boldsymbol{\xi} \in B_a \\ \boldsymbol{\nabla}(\boldsymbol{u}(\boldsymbol{\xi}) + \boldsymbol{v}_a^\omega(\boldsymbol{\xi})) &= \boldsymbol{\nabla}\boldsymbol{u}(\boldsymbol{z}) + \mathcal{P}_a^{-1}\left[\boldsymbol{\nabla}\boldsymbol{V}_1^\omega\right](\boldsymbol{\xi}) + O(a), && \boldsymbol{\xi} \in B_a \\ &= \boldsymbol{\nabla}\boldsymbol{u}_{\mathcal{B}}^{(1)}[\boldsymbol{\nabla}\boldsymbol{u}(\boldsymbol{z})]\left(\frac{\boldsymbol{\xi} - \boldsymbol{z}}{a}\right) + O(a), && \boldsymbol{\xi} \in B_a. \end{aligned} \tag{3.77}$$

Inserting (3.76) and (3.77) into (3.75), and scaling the integrals over B_a as usual, we finally obtain the well-known leading-order outer expansion given in [Guzina & Chikichev, 2007]:

$$\boldsymbol{v}_a^\omega(\boldsymbol{x}) = a^3 \boldsymbol{v}_{\text{out}}^\omega(\boldsymbol{x}) + O(a^4) \qquad \boldsymbol{x} \notin \overline{B_a}, \tag{3.78}$$

with:

$$\begin{aligned} \boldsymbol{v}_{\text{out}}^\omega(\boldsymbol{x}) &= -\int_{\mathcal{B}} \boldsymbol{\nabla}\boldsymbol{u}_{\mathcal{B}}^{(1)}[\boldsymbol{\nabla}\boldsymbol{u}(\boldsymbol{z})] : \Delta\boldsymbol{\mathcal{C}} : \boldsymbol{\nabla}_1\boldsymbol{G}^\omega(\boldsymbol{z}, \boldsymbol{x})\, \mathrm{d}V + \omega^2 \int_{\mathcal{B}} \Delta\rho\, \boldsymbol{u}(\boldsymbol{z}) \cdot \boldsymbol{G}^\omega(\boldsymbol{z}, \boldsymbol{x})\, \mathrm{d}V \\ &= -\boldsymbol{\nabla}\boldsymbol{u}(\boldsymbol{z}) : \boldsymbol{\mathcal{A}} : \boldsymbol{\nabla}_1\boldsymbol{G}^\omega(\boldsymbol{z}, \boldsymbol{x}) + \omega^2 |\mathcal{B}| \Delta\rho\, \boldsymbol{u}(\boldsymbol{z}) \cdot \boldsymbol{G}^\omega(\boldsymbol{z}, \boldsymbol{x}). \end{aligned} \tag{3.79}$$

As it was observed in the previous chapter for the static case, and as we will show in the next section, only this leading-order approximation is required to reach the sought sixth order for the expansion of a misfit functional.

3.3 Misfit function: definition and expansion

After we established the inner and outer expansion of the scattered displacement $\boldsymbol{v}_a^\omega$ by an inhomogeneity $(B_a, \Delta\boldsymbol{\mathcal{C}}, \Delta\rho)$, we are in position to compute such expansion for a misfit functional depending implicitly on B_a through $\boldsymbol{v}_a^\omega$.

3.3.1 Notations and adjoint displacement

We consider misfit functions $\mathbb{J}(B_a)$ taking the exact same form than in the static case, as described in Section 2.1.2. In particular, $\mathbb{J}(B_a) = J(\boldsymbol{u}_a^\omega)$ with J defined in terms of volume and surface densities Ψ_Ω and Ψ_Γ as:

$$J(\boldsymbol{w}) := \int_{\Omega^\mathrm{m}} \Psi_\Omega(\boldsymbol{x}; \boldsymbol{w}(\boldsymbol{x}))\, \mathrm{d}V_x + \int_{\Gamma^\mathrm{m}} \Psi_\Gamma(\boldsymbol{x}; \boldsymbol{w}(\boldsymbol{x}))\, \mathrm{d}S_x, \tag{3.80}$$

and these densities are twice differentiable so that the following expansion about $\boldsymbol{u}$ holds:

$$J(\boldsymbol{u}_a^\omega) = J(\boldsymbol{u}) + J'(\boldsymbol{u}; \boldsymbol{v}_a^\omega) + J''(\boldsymbol{u}; \boldsymbol{v}_a^\omega) + R(\boldsymbol{u}; \boldsymbol{v}_a^\omega). \tag{3.81}$$

A difference with the static case appears now in the definition of J', J'' and R to account for the fact that all the fields are (possibly) complex-valued. Following e.g. [Guzina & Chikichev, 2007; Bonnet, 2008], J' is written as:

$$J'(\boldsymbol{u}; \boldsymbol{w}) := \Re\left\{ \int_{\Omega^\mathrm{m}} \widetilde{\boldsymbol{\nabla}}_2 \Psi_\Omega(\cdot; \boldsymbol{u}) \cdot \boldsymbol{w}\, \mathrm{d}V + \int_{\Gamma^\mathrm{m}} \widetilde{\boldsymbol{\nabla}}_2 \Psi_\Gamma(\cdot; \boldsymbol{u}) \cdot \boldsymbol{w}\, \mathrm{d}S \right\}, \tag{3.82}$$

where, for a complex-valued field $\boldsymbol{u}$, noting $\boldsymbol{u}_\mathrm{R} = \Re\boldsymbol{u}$ and $\boldsymbol{u}_\mathrm{I} = \Im\boldsymbol{u}$, $\widetilde{\boldsymbol{\nabla}}$ is defined by:

$$\widetilde{\boldsymbol{\nabla}}\psi(\boldsymbol{u}) = \widetilde{\boldsymbol{\nabla}}\psi(\boldsymbol{u}_\mathrm{R} + \mathrm{i}\boldsymbol{u}_\mathrm{I}) := \boldsymbol{\nabla}_{\boldsymbol{u}_\mathrm{R}}\psi - \mathrm{i}\boldsymbol{\nabla}_{\boldsymbol{u}_\mathrm{I}}\psi. \tag{3.83}$$

Consequently, we define the adjoint solution $\boldsymbol{p}$ as the solution of the weak formulation

$$\begin{aligned}\text{Find } \boldsymbol{p} \in \boldsymbol{W}_0, \qquad & \langle \boldsymbol{p}, \boldsymbol{w} \rangle_\Omega^\mathcal{C} - \omega^2 (\boldsymbol{p}, \boldsymbol{w})_\Omega^\rho \\ & = \int_{\Omega^\mathrm{m}} \widetilde{\boldsymbol{\nabla}}_2 \Psi_\Omega(\cdot; \boldsymbol{u}) \cdot \boldsymbol{w}\, \mathrm{d}V + \int_{\Gamma^\mathrm{m}} \widetilde{\boldsymbol{\nabla}}_2 \Psi_\Gamma(\cdot; \boldsymbol{u}) \cdot \boldsymbol{w}\, \mathrm{d}S, \quad \forall \boldsymbol{w} \in \boldsymbol{W}_0.\end{aligned} \tag{3.84}$$

Then, on setting $\boldsymbol{w} = \boldsymbol{p}$ in (3.7) and $\boldsymbol{w} = \boldsymbol{v}_a^\omega$ in (3.84), combining the resulting identities, exploiting the symmetry of the energy bilinear forms, and finally retaining only the real part of the result to retrieve the first derivative (3.82), one obtains

$$J'(\boldsymbol{u}; \boldsymbol{v}_a^\omega) = \Re\left\{ -\langle \boldsymbol{p}, \boldsymbol{u}_a^\omega \rangle_{B_a}^{\Delta\mathcal{C}} + \omega^2 (\boldsymbol{p}, \boldsymbol{u}_a^\omega)_{B_a}^{\Delta\rho} \right\}. \tag{3.85}$$

The second directional derivative J'' is similarly given as in [Bonnet, 2008] by:

$$\begin{aligned} J''(\boldsymbol{u}; \boldsymbol{w}) := \frac{1}{2} \sum_{\alpha,\beta=\mathrm{R},\mathrm{I}} \Bigg[& \int_{\Omega^\mathrm{m}} \boldsymbol{\nabla}_{\boldsymbol{u}_\alpha \boldsymbol{u}_\beta} \Psi_\Omega(\cdot; \boldsymbol{u}) : (\boldsymbol{w}_\alpha \otimes \boldsymbol{w}_\beta)\, \mathrm{d}V \\ & + \int_{\Gamma^\mathrm{m}} \boldsymbol{\nabla}_{\boldsymbol{u}_\alpha \boldsymbol{u}_\beta} \Psi_\Gamma(\cdot; \boldsymbol{u}) : (\boldsymbol{w}_\alpha \otimes \boldsymbol{w}_\beta)\, \mathrm{d}S \Bigg], \end{aligned} \tag{3.86}$$

and the remainder R is defined exactly as in the static case by:

$$R(\boldsymbol{u}; \boldsymbol{w}) := \int_0^1 (1-t) J''(\boldsymbol{u} + t\boldsymbol{w}; \boldsymbol{w})\, \mathrm{d}t - \frac{1}{2} J''(\boldsymbol{u}; \boldsymbol{w}). \tag{3.87}$$

Example of the least-square cost functional To illustrate the definitions above, let's again consider the least-square cost functional defined for some measurements $\boldsymbol{u}^{\mathrm{m}}$ as:

$$J(\boldsymbol{w}) = \frac{1}{2}\int_{\Gamma^{\mathrm{m}}} |\boldsymbol{w} - \boldsymbol{u}^{\mathrm{m}}|^2 \,\mathrm{d}S, \tag{3.88}$$

for which the expansion (3.81) is exact, i.e. $R(\boldsymbol{u};\boldsymbol{v}_a^{\omega}) = 0$. Its first derivative is:

$$J'(\boldsymbol{u};\boldsymbol{v}_a) = \frac{1}{2}\int_{\Gamma^{\mathrm{m}}} \left[\overline{(\boldsymbol{u}-\boldsymbol{u}^{\mathrm{m}})}\cdot\boldsymbol{v}_a + (\boldsymbol{u}-\boldsymbol{u}^{\mathrm{m}})\cdot\overline{\boldsymbol{v}_a}\right] \mathrm{d}S = \Re\left\{\int_{\Gamma^{\mathrm{m}}} \overline{(\boldsymbol{u}-\boldsymbol{u}^{\mathrm{m}})}\cdot\boldsymbol{v}_a \,\mathrm{d}S\right\}. \tag{3.89}$$

The adjoint solution $\boldsymbol{p}$ is therefore the solution of:

$$\text{Find } \boldsymbol{p}\in\boldsymbol{W}_0, \qquad \langle \boldsymbol{p},\boldsymbol{w}\rangle_{\Omega}^{\mathcal{C}} - \omega^2(\boldsymbol{p},\boldsymbol{w})_{\Omega}^{\rho} = \int_{\Gamma^{\mathrm{m}}} \overline{(\boldsymbol{u}-\boldsymbol{u}^{\mathrm{m}})}\cdot\boldsymbol{w}\,\mathrm{d}S, \quad \forall \boldsymbol{w}\in\boldsymbol{W}_0. \tag{3.90}$$

The second derivative of J is:

$$J''(\boldsymbol{u};\boldsymbol{v}_a^{\omega}) = \frac{1}{2}\int_{\Gamma^{\mathrm{m}}} |\boldsymbol{v}_a^{\omega}|^2 \,\mathrm{d}S \tag{3.91}$$

3.3.2 Expansion in the general case

We are now in position to state the main result of this chapter:

Theorem 3.3. *Misfit functionals of the form* (3.81)*, with the regularity hypothesis on* Ψ_Ω *and* Ψ_Γ *stated in Section 2.1.2, admit the* $O(a^6)$ *expansion:*

$$J(\boldsymbol{u}_a^{\omega}) = J(\boldsymbol{u}) + a^3\mathcal{T}_3^{\omega}(\boldsymbol{z}) + a^4\mathcal{T}_4^{\omega}(\boldsymbol{z}) + a^5\mathcal{T}_5^{\omega}(\boldsymbol{z}) + a^6\mathcal{T}_6^{\omega}(\boldsymbol{z}) + o(a^6), \tag{3.92}$$

and the topological derivatives $\mathcal{T}_j^{\omega}$ *are computed as bilinear forms of the incident displacement* $\boldsymbol{u}$ *and the adjoint displacement* $\boldsymbol{p}$ *defined by* (3.84) *as explained below.* $\mathcal{T}_6^{\omega}$ *moreover embeds the leading-order contribution of the second-order derivative* J'' *of* J*. More precisely, the well-known leading-order topological derivative* $\mathcal{T}_3^{\omega}$ *is recalled by* (3.96)*, and* $\mathcal{T}_4^{\omega}$*,* $\mathcal{T}_5^{\omega}$ *and* $\mathcal{T}_6^{\omega}$ *are given resp. by* (3.98)*,* (3.101) *and* (3.105)*. Closed-form expressions in the special case of ellipsoidal shapes and isotropic materials are also provided in Section 3.3.3.*

Proof. We begin the proof by isolating the higher-order terms (in $o(a^6)$). First, inserting the inner expansion (3.36) in the expression (3.85) of J' gives:

$$J'(\boldsymbol{u};\boldsymbol{v}_a^{\omega}) \;=\; \Re\Big\{ -\langle \boldsymbol{p},\boldsymbol{u}+\mathcal{P}_a^{-1}\boldsymbol{V}_a^{\omega}\rangle_{B_a}^{\Delta\mathcal{C}} + \omega^2\left(\boldsymbol{p},\boldsymbol{u}+\mathcal{P}_a^{-1}\boldsymbol{V}_a^{\omega}\right)_{B_a}^{\Delta\rho} - \langle \boldsymbol{p},\boldsymbol{\delta}_a^{\omega}\rangle_{B_a}^{\Delta\mathcal{C}} + \omega^2\left(\boldsymbol{p},\boldsymbol{\delta}_a^{\omega}\right)_{B_a}^{\Delta\rho}\Big\}. \tag{3.93}$$

The $o(a^6)$ behavior of the terms involving $\boldsymbol{\delta}_a^{\omega}$ is then justified by Proposition 3.1: there exists $C>0$ so that:

$$\begin{aligned}\left|-\langle \boldsymbol{p},\boldsymbol{\delta}_a^{\omega}\rangle_{B_a}^{\Delta\mathcal{C}} + \omega^2(\boldsymbol{p},\boldsymbol{\delta}_a^{\omega})_{B_a}^{\Delta\rho}\right| &\le C\|\boldsymbol{p}\|_{H^1(B_a)}\|\boldsymbol{\delta}_a^{\omega}\|_{H^1(B_a)} \\ &\le Ca^{3/2}\left(C_\delta^{\omega}a^{11/2} + o(a^{11/2})\right) \\ &\le CC_\delta^{\omega}a^7 + o(a^7).\end{aligned} \tag{3.94}$$

To evaluate the second derivative $J''(\boldsymbol{u};\boldsymbol{v}_a^\omega,\boldsymbol{v}_a^\omega)$, still supposing that J'' does not use the evaluation of $\boldsymbol{v}_a^\omega$ inside B_a, we use the outer expansion of $\boldsymbol{v}_a^\omega$ (3.78) and obtain:

$$J''(\boldsymbol{u};\boldsymbol{v}_a^\omega) = a^6 J''(\boldsymbol{u};\boldsymbol{v}_{\text{out}}^\omega) + o(a^6). \tag{3.95}$$

Finally, the remainder $R(\boldsymbol{u};\boldsymbol{v}_a^\omega)$ in (3.81) is shown to be of order $o(a^6)$ the same way than for the static case (see Section 2.3).

The rest of the proof consists in introducing (i) the decomposition (3.41) of $\boldsymbol{V}_a^\omega$ and (ii) the Taylor expansions about $\boldsymbol{z}$ of $\boldsymbol{u}$, $\boldsymbol{\nabla u}$, $\boldsymbol{p}$ and $\boldsymbol{\nabla p}$ into the expression (3.93). Adding $a^6 J''(\boldsymbol{u};\boldsymbol{v}_{\text{out}}^\omega)$ from (3.95) to the obtained sum and collecting the contributions of the different powers of a then provides the expressions of the topological derivatives, as given below.

In the computation of these topological derivatives, we use the reciprocity relations (3.48) wherever possible to obtain expressions featuring the lowest-order Eshelby problems. Each specific use of these relations will be specified for clarity. □

Leading-order topological derivative The third-order topological derivative $\mathcal{T}_3^\omega$ is found to have the well-known expression already given by [Guzina & Chikichev, 2007]:

$$\mathcal{T}_3^\omega(\boldsymbol{z}) = \Re\left\{-\boldsymbol{\nabla u}(\boldsymbol{z}) : \boldsymbol{\mathcal{A}} : \boldsymbol{\nabla p}(\boldsymbol{z}) + \omega^2|\mathcal{B}|\Delta\rho\, \boldsymbol{u}(\boldsymbol{z})\cdot\boldsymbol{p}(\boldsymbol{z})\right\}. \tag{3.96}$$

Fourth order topological derivative For the fourth topological derivative $\mathcal{T}_4^\omega$, to avoid later computation of $\boldsymbol{U}^{(0)}$, we use the reciprocity relation:

$$\left\langle \boldsymbol{U}^{(0)}[\boldsymbol{u}(\boldsymbol{z})], \boldsymbol{\varphi}_1[\boldsymbol{\nabla p}(\boldsymbol{z})]\right\rangle_{\mathcal{B}}^{\Delta\mathcal{C}} = -\omega^2\left(\boldsymbol{u}(\boldsymbol{z}), \boldsymbol{v}_{\mathcal{B}}^{(1)}[\boldsymbol{\nabla p}(\boldsymbol{z})]\right)_{\mathcal{B}}^{\Delta\rho}, \tag{3.97}$$

and obtain:

$$\begin{aligned}\mathcal{T}_4^\omega(\boldsymbol{z}) =\Re\Big\{ &-\left\langle \boldsymbol{\varphi}_2\left[\boldsymbol{\nabla}^2\boldsymbol{u}(\boldsymbol{z})\right], \boldsymbol{u}_{\mathcal{B}}^{(1)}[\boldsymbol{p}(\boldsymbol{z})]\right\rangle_{\mathcal{B}}^{\Delta\mathcal{C}} - \left\langle \boldsymbol{u}_{\mathcal{B}}^{(1)}[\boldsymbol{u}(\boldsymbol{z})], \boldsymbol{\varphi}_2\left[\boldsymbol{\nabla}^2\boldsymbol{p}(\boldsymbol{z})\right]\right\rangle_{\mathcal{B}}^{\Delta\mathcal{C}} \\ &+\omega^2\left(\boldsymbol{u}(\boldsymbol{z}), \boldsymbol{u}_{\mathcal{B}}^{(1)}[\boldsymbol{\nabla p}(\boldsymbol{z})]\right)_{\mathcal{B}}^{\Delta\rho} + \omega^2\left(\boldsymbol{u}_{\mathcal{B}}^{(1)}[\boldsymbol{\nabla u}(\boldsymbol{z})], \boldsymbol{p}(\boldsymbol{z})\right)_{\mathcal{B}}^{\Delta\rho}\Big\}.\end{aligned} \tag{3.98}$$

Introducing the elastic moment tensors $\boldsymbol{\mathcal{A}}_{21}$ and $\boldsymbol{\mathcal{A}}_{12}$ and the inertial polarization tensor $\boldsymbol{\mathcal{Q}}_{01}$, this expression becomes:

$$\begin{aligned}\mathcal{T}_4^\omega(\boldsymbol{z}) =\Re\Big\{ &-\boldsymbol{\nabla}^2\boldsymbol{u}(\boldsymbol{z}) \bullet \boldsymbol{\mathcal{A}}_{21} : \boldsymbol{\nabla p}(\boldsymbol{z}) - \boldsymbol{\nabla u}(\boldsymbol{z}) : \boldsymbol{\mathcal{A}}_{12} \bullet \boldsymbol{\nabla}^2\boldsymbol{p}(\boldsymbol{z}) \\ &+\omega^2\Delta\rho\big[\boldsymbol{u}(\boldsymbol{z})\cdot\boldsymbol{\mathcal{Q}}_{01} : \boldsymbol{\nabla p}(\boldsymbol{z}) + \boldsymbol{\nabla u}(\boldsymbol{z}) : \boldsymbol{\mathcal{Q}}_{10}\cdot\boldsymbol{p}(\boldsymbol{z})\big]\Big\}.\end{aligned} \tag{3.99}$$

Fifth order topological derivative For $\mathcal{T}_5^\omega$, to avoid the computation of $\boldsymbol{U}^{(1)}$, we similarly use the relation:

$$\left\langle \boldsymbol{U}^{(1)}\left[\boldsymbol{u}_{\mathcal{B}}^{(1)}[\boldsymbol{\nabla u}(\boldsymbol{z})]\right], \boldsymbol{\varphi}_1[\boldsymbol{\nabla p}(\boldsymbol{z})]\right\rangle_{\mathcal{B}}^{\Delta\mathcal{C}} = -\omega^2\left(\boldsymbol{u}_{\mathcal{B}}^{(1)}[\boldsymbol{\nabla u}(\boldsymbol{z})], \boldsymbol{v}_{\mathcal{B}}^{(1)}[\boldsymbol{\nabla p}(\boldsymbol{z})]\right)_{\mathcal{B}}^{\Delta\rho}, \tag{3.100}$$

and find:

$$\begin{aligned}\mathcal{T}_5^\omega(\boldsymbol{z}) =\Re\Bigg\{ &- \frac{1}{2}\left\langle \boldsymbol{\varphi}_3\left[\boldsymbol{\nabla}^3\boldsymbol{u}(\boldsymbol{z})\right], \boldsymbol{u}_{\mathcal{B}}^{(1)}[\boldsymbol{\nabla}\boldsymbol{p}(\boldsymbol{z})]\right\rangle_{\mathcal{B}}^{\Delta\mathcal{C}} - \frac{1}{2}\left\langle \boldsymbol{u}_{\mathcal{B}}^{(1)}[\boldsymbol{\nabla}\boldsymbol{u}(\boldsymbol{z})], \boldsymbol{\varphi}_3\left[\boldsymbol{\nabla}^3\boldsymbol{p}(\boldsymbol{z})\right]\right\rangle_{\mathcal{B}}^{\Delta\mathcal{C}} \\ &- \left\langle \boldsymbol{u}_{\mathcal{B}}^{(2)}[\boldsymbol{\nabla}^2\boldsymbol{u}(\boldsymbol{z})], \boldsymbol{\varphi}_2\left[\boldsymbol{\nabla}^2\boldsymbol{p}(\boldsymbol{z})\right]\right\rangle_{\mathcal{B}}^{\Delta\mathcal{C}} \\ &- \left\langle \boldsymbol{v}_{3\mathrm{C}}^{\omega}, \boldsymbol{\varphi}_1[\boldsymbol{\nabla}\boldsymbol{p}(\boldsymbol{z})]\right\rangle_{\mathcal{B}}^{\Delta\mathcal{C}} \\ &+ \omega^2\left(\boldsymbol{u}_{\mathcal{B}}^{(2)}[\boldsymbol{\nabla}^2\boldsymbol{u}(\boldsymbol{z})], \boldsymbol{p}(\boldsymbol{z})\right)_{\mathcal{B}}^{\Delta\rho} + \omega^2\left(\boldsymbol{u}(\boldsymbol{z}), \boldsymbol{u}_{\mathcal{B}}^{(2)}[\boldsymbol{\nabla}^2\boldsymbol{p}(\boldsymbol{z})]\right)_{\mathcal{B}}^{\Delta\rho} \\ &+ \omega^2\left(\boldsymbol{u}_{\mathcal{B}}^{(1)}[\boldsymbol{\nabla}\boldsymbol{u}(\boldsymbol{z})], \boldsymbol{u}_{\mathcal{B}}^{(1)}[\boldsymbol{\nabla}\boldsymbol{p}(\boldsymbol{z})]\right)_{\mathcal{B}}^{\Delta\rho} \\ &+ \omega^2\left(\boldsymbol{U}^{(0)}[\boldsymbol{u}(\boldsymbol{z})], \boldsymbol{p}(\boldsymbol{z})\right)_{\mathcal{B}}^{\Delta\rho}\Bigg\}.\end{aligned} \tag{3.101}$$

Since we did not compute a closed-form expression for the term $\boldsymbol{v}_{3\mathrm{C}}^{\omega}$ in the general case, further simplification is provided in the next section.

Sixth order topological derivative Finally, for $\mathcal{T}_6^\omega$, to avoid the computation of $\boldsymbol{U}^{(2)}$ and $\boldsymbol{U}^{(1)}$, we use both relations:

$$\begin{aligned}&\left\langle \boldsymbol{U}^{(2)}\left[\boldsymbol{u}_{\mathcal{B}}^{(2)}[\boldsymbol{\nabla}^2\boldsymbol{u}(\boldsymbol{z})] + \boldsymbol{U}^{(0)}[\boldsymbol{u}(\boldsymbol{z})]\right], \boldsymbol{\varphi}_1\left[\boldsymbol{\nabla}\boldsymbol{p}(\boldsymbol{z})\right]\right\rangle_{\mathcal{B}}^{\Delta\mathcal{C}} \\ &\qquad = -\omega^2\left(\boldsymbol{u}_{\mathcal{B}}^{(2)}[\boldsymbol{\nabla}^2\boldsymbol{u}(\boldsymbol{z})] + \boldsymbol{U}^{(0)}[\boldsymbol{u}(\boldsymbol{z})], \boldsymbol{v}_{\mathcal{B}}^{(1)}[\boldsymbol{\nabla}\boldsymbol{p}(\boldsymbol{z})]\right)_{\mathcal{B}}^{\Delta\rho},\end{aligned} \tag{3.102}$$

and:

$$\left\langle \boldsymbol{U}^{(1)}\left[\boldsymbol{u}_{\mathcal{B}}^{(1)}[\boldsymbol{\nabla}\boldsymbol{u}(\boldsymbol{z})]\right], \boldsymbol{\varphi}_2\left[\boldsymbol{\nabla}^2\boldsymbol{p}(\boldsymbol{z})\right]\right\rangle_{\mathcal{B}}^{\Delta\mathcal{C}} = -\omega^2\left(\boldsymbol{u}_{\mathcal{B}}^{(1)}[\boldsymbol{\nabla}\boldsymbol{u}(\boldsymbol{z})], \boldsymbol{v}_{\mathcal{B}}^{(2)}[\boldsymbol{\nabla}^2\boldsymbol{p}(\boldsymbol{z})]\right)_{\mathcal{B}}^{\Delta\rho}. \tag{3.103}$$

To compute the inertial product involving $\boldsymbol{v}_{\mathcal{B}}^{(3)}$ without solving the third Eshelby problem, we also use the reciprocal identity:

$$\omega^2\left(\boldsymbol{v}_{\mathcal{B}}^{(3)}[\boldsymbol{\nabla}\boldsymbol{u}^3(\boldsymbol{z})], \boldsymbol{p}(\boldsymbol{z})\right)_{\mathcal{B}}^{\Delta\rho} = -\left\langle \boldsymbol{\varphi}_3\left[\boldsymbol{\nabla}^3\boldsymbol{u}(\boldsymbol{z})\right], \boldsymbol{U}^{(0)}[\boldsymbol{p}(\boldsymbol{z})]\right\rangle_{\mathcal{B}}^{\Delta\mathcal{C}}. \tag{3.104}$$

Finally, the sixth-order Topological derivative is given by:

$$
\begin{aligned}
\mathcal{T}_6^\omega(\boldsymbol{z}) =\Re\Big\{ &-\frac{1}{6}\Big\langle \boldsymbol{\varphi}_4\left[\boldsymbol{\nabla}^4\boldsymbol{u}(\boldsymbol{z})\right], \boldsymbol{u}_{\mathcal{B}}^{(1)}[\boldsymbol{\nabla}\boldsymbol{p}(\boldsymbol{z})]\Big\rangle_{\mathcal{B}}^{\Delta\mathcal{C}} - \frac{1}{6}\Big\langle \boldsymbol{u}_{\mathcal{B}}^{(1)}[\boldsymbol{\nabla}\boldsymbol{u}(\boldsymbol{z})], \boldsymbol{\varphi}_4\left[\boldsymbol{\nabla}^4\boldsymbol{p}(\boldsymbol{z})\right]\Big\rangle_{\mathcal{B}}^{\Delta\mathcal{C}} \\
&- \frac{1}{2}\Big\langle \boldsymbol{\varphi}_3\left[\boldsymbol{\nabla}^3\boldsymbol{u}(\boldsymbol{z})\right], \boldsymbol{u}_{\mathcal{B}}^{(2)}[\boldsymbol{\nabla}^2\boldsymbol{p}(\boldsymbol{z})] + \boldsymbol{U}^{(0)}[\boldsymbol{p}(\boldsymbol{z})]\Big\rangle_{\mathcal{B}}^{\Delta\mathcal{C}} \\
&- \frac{1}{2}\Big\langle \boldsymbol{u}_{\mathcal{B}}^{(2)}[\boldsymbol{\nabla}^2\boldsymbol{u}(\boldsymbol{z})] + \boldsymbol{U}^{(0)}[\boldsymbol{u}(\boldsymbol{z})], \boldsymbol{\varphi}_3\left[\boldsymbol{\nabla}^3\boldsymbol{p}(\boldsymbol{z})\right]\Big\rangle_{\mathcal{B}}^{\Delta\mathcal{C}} \\
&- \Big\langle \boldsymbol{v}_{3\mathrm{C}}^\omega, \boldsymbol{\varphi}_2[\boldsymbol{\nabla}^2\boldsymbol{p}(\boldsymbol{z})]\Big\rangle_{\mathcal{B}}^{\Delta\mathcal{C}} - \Big\langle \boldsymbol{v}_{4\mathrm{C}}^\omega, \boldsymbol{\varphi}_1[\boldsymbol{\nabla}\boldsymbol{p}(\boldsymbol{z})]\Big\rangle_{\mathcal{B}}^{\Delta\mathcal{C}} \\
&+ \frac{1}{2}\omega^2\left[\Big(\boldsymbol{\varphi}_3\left[\boldsymbol{\nabla}^3\boldsymbol{u}(\boldsymbol{z})\right], \boldsymbol{p}(\boldsymbol{z})\Big)_{\mathcal{B}}^{\Delta\rho} + \Big(\boldsymbol{u}(\boldsymbol{z}), \boldsymbol{\varphi}_3\left[\boldsymbol{\nabla}^3\boldsymbol{p}(\boldsymbol{z})\right]\Big)_{\mathcal{B}}^{\Delta\rho}\right] \\
&+ \omega^2\Big(\boldsymbol{u}_{\mathcal{B}}^{(1)}[\boldsymbol{\nabla}\boldsymbol{u}(\boldsymbol{z})], \boldsymbol{u}_{\mathcal{B}}^{(2)}[\boldsymbol{\nabla}^2\boldsymbol{p}(\boldsymbol{z})] + \boldsymbol{U}^{(0)}[\boldsymbol{p}(\boldsymbol{z})]\Big)_{\mathcal{B}}^{\Delta\rho} \\
&+ \omega^2\Big(\boldsymbol{u}_{\mathcal{B}}^{(2)}[\boldsymbol{\nabla}^2\boldsymbol{u}(\boldsymbol{z})] + \boldsymbol{U}^{(0)}[\boldsymbol{u}(\boldsymbol{z})], \boldsymbol{u}_{\mathcal{B}}^{(1)}[\boldsymbol{\nabla}\boldsymbol{p}(\boldsymbol{z})]\Big)_{\mathcal{B}}^{\Delta\rho} \\
&+ \omega^2\Big(\boldsymbol{v}_{3\mathrm{C}}^\omega, \boldsymbol{p}(\boldsymbol{z})\Big)_{\mathcal{B}}^{\Delta\rho}\Big\} \\
&+ J''(\boldsymbol{u}; \boldsymbol{v}_{\mathrm{out}}^\omega).
\end{aligned}
\tag{3.105}
$$

Since neither the solution $\boldsymbol{U}^{(0)}$ nor the "complementary" terms $\boldsymbol{v}_{3\mathrm{C}}^\omega$ and $\boldsymbol{v}_{4\mathrm{C}}^\omega$ have closed-form expressions in the general case, we delay further simplifications of this expression to the next section.

General simplifications Provided some additional assumption on $\mathcal{B}$, some simplifications may hold. Choosing $\boldsymbol{z}$ as the gravity center of B_a (i.e. $\mathbf{0}$ as the gravity center of $\mathcal{B}$), which is done without any loss of generality, all "1st order" integrals on $\bar{\boldsymbol{\xi}}$ are canceled. Moreover, for any centrally symmetric inclusion, invoking Lemmas 1.9 and 1.10, all odd-order tensors $\boldsymbol{\mathcal{A}}_{pq}$ and $\boldsymbol{\mathcal{Q}}_{pq}$ vanish, so does $\mathcal{T}_4^\omega$ and most of the terms in $\mathcal{T}_6^\omega$.

3.3.3 Ellipsoidal shapes and isotropic materials

We now consider the specific case case for which all materials are isotropic and $\mathcal{B}$ is an ellipsoid. The expression of the required polarization tensors are then computed explicitly in Sections 1.3.3 and 1.3.4, and some terms in the expansion of the scattered displacement $\boldsymbol{v}_a^\omega$ are available in closed-form. In this case,

(i) $\mathcal{T}_3^\omega$ is still given by (3.96), with $\boldsymbol{\mathcal{A}}$ given by (1.117).
(ii) $\mathcal{T}_4^\omega$ entirely vanishes.
(iii) For $\mathcal{T}_5^\omega$, most of the terms in (3.101) are available in closed form:

- The elastic moment tensors $\boldsymbol{\mathcal{A}}$ and $\boldsymbol{\mathcal{A}}_{22}$ are given by (1.118) and (1.127), and $\boldsymbol{\mathcal{A}}_{13} = \boldsymbol{\mathcal{A}} \otimes \boldsymbol{M}^{(2)}/|\mathcal{B}|$ from (1.122).
- The inertial polarization tensors $\boldsymbol{\mathcal{Q}}_{02}$ and $\boldsymbol{\mathcal{Q}}_{11}$ are given by (1.133) and (1.135).
- The solution $\boldsymbol{U}^{(0)}$ is expressed as:

$$
\boldsymbol{U}^{(0)}[\boldsymbol{u}(\boldsymbol{z})](\boldsymbol{x}) = \omega^2\Delta\rho\left[\mathcal{E}^{(0)}\ \boldsymbol{u}(\boldsymbol{z}) + \boldsymbol{u}_{\mathcal{B}}^{(2)}[\boldsymbol{\mathcal{E}}_3^{(0)} \cdot \boldsymbol{u}(\boldsymbol{z})](\boldsymbol{x})\right],
\tag{3.106}
$$

and the way to compute the constant $\mathcal{E}^{(0)}$ and the tensor $\boldsymbol{\mathcal{E}}_3^{(0)}$ is explained in Appendix 3.A.1.

- From (3.53), the only contribution of the "complementary" terms is:

$$\boldsymbol{\nabla}\boldsymbol{v}_{3\mathrm{C}}^{\omega} = -\boldsymbol{\nabla}\boldsymbol{u}_{\mathcal{B}}^{(1)}\left[\boldsymbol{J}_1^{H0}(\boldsymbol{z})\right] - \boldsymbol{\nabla}\boldsymbol{u}_{\mathcal{B}}^{(3)}\left[\boldsymbol{J}_3^{H0}(\boldsymbol{z})\right], \tag{3.107}$$

  where $\boldsymbol{J}_p^{H0}(\boldsymbol{z}) = \boldsymbol{\nabla}\boldsymbol{u}(\boldsymbol{z}) : \boldsymbol{\mathcal{A}} : \boldsymbol{I}_p^{H0}$ for $p = \{1,3\}$, and the way to compute the expressions of the tensors $\boldsymbol{I}_{1,3}^{H0}$ is explained in Appendix 3.A.2.

Inserting all these expressions into the general expression (3.101) for $\mathcal{T}_5^{\omega}$ leads to:

$$\begin{aligned}
\mathcal{T}_5^{\omega}(\boldsymbol{z}) =\Re\Big\{ & -\frac{1}{2|\mathcal{B}|}\left[\left(\boldsymbol{\nabla}^3\boldsymbol{u}(\boldsymbol{z}) : \boldsymbol{M}^{(2)}\right) : \boldsymbol{\mathcal{A}} : \boldsymbol{\nabla}\boldsymbol{p}(\boldsymbol{z}) + \boldsymbol{\nabla}\boldsymbol{u}(\boldsymbol{z}) : \boldsymbol{\mathcal{A}} : \left(\boldsymbol{\nabla}^3\boldsymbol{p}(\boldsymbol{z}) : \boldsymbol{M}^{(2)}\right)\right] \\
& - \boldsymbol{\nabla}^2\boldsymbol{u}(\boldsymbol{z}) \bullet \boldsymbol{\mathcal{A}}_{22} \bullet \boldsymbol{\nabla}^2\boldsymbol{p}(\boldsymbol{z}) \\
& + \boldsymbol{\nabla}\boldsymbol{p}(\boldsymbol{z}) : \boldsymbol{\mathcal{A}} : \left[\boldsymbol{I}_1^{H0} + \frac{1}{|\mathcal{B}|}\boldsymbol{I}_3^{H0} : \boldsymbol{M}^{(2)}\right] : \boldsymbol{\mathcal{A}} : \boldsymbol{\nabla}\boldsymbol{u}(\boldsymbol{z}) \\
& + \omega^2\Delta\rho\ \left[\boldsymbol{\nabla}^2\boldsymbol{u}(\boldsymbol{z}) \bullet \boldsymbol{\mathcal{Q}}_{20} \cdot \boldsymbol{p}(\boldsymbol{z}) + \boldsymbol{u}(\boldsymbol{z}) \cdot \boldsymbol{\mathcal{Q}}_{02} \bullet \boldsymbol{\nabla}^2\boldsymbol{p}(\boldsymbol{z})\right] \\
& + \omega^2\Delta\rho\ \boldsymbol{\nabla}\boldsymbol{u}(\boldsymbol{z}) : \boldsymbol{\mathcal{Q}}_{11} : \boldsymbol{\nabla}\boldsymbol{p}(\boldsymbol{z}) \\
& + \left(\omega^2\Delta\rho\right)^2\ \boldsymbol{p}(\boldsymbol{z}) \cdot \left[\mathcal{E}^{(0)}\boldsymbol{I} + \boldsymbol{\mathcal{Q}}_{02} \bullet \boldsymbol{\mathcal{E}}_3^{(0)}\right] \cdot \boldsymbol{u}(\boldsymbol{z})\Big\}.
\end{aligned} \tag{3.108}$$

(iv) Finally, for $\mathcal{T}_6^{\omega}$, nearly all terms in the expression (3.105) that come from the expansion of $J'(\boldsymbol{v}_a^{\omega})$ vanish, except the contribution of $\boldsymbol{v}_{4\mathrm{C}}^{\omega}$ in $\langle \boldsymbol{v}_{4\mathrm{C}}^{\omega}, \boldsymbol{\varphi}_1[\boldsymbol{\nabla}\boldsymbol{p}(\boldsymbol{z})]\rangle_{\mathcal{B}}^{\Delta\mathcal{C}}$ and that of $\boldsymbol{v}_{3\mathrm{C}}^{\omega}$ in $(\boldsymbol{v}_{3\mathrm{C}}^{\omega}, \boldsymbol{p}(\boldsymbol{z}))_{\mathcal{B}}^{\Delta\rho}$. Inserting the expressions (3.53) for $\boldsymbol{v}_{3\mathrm{C}}^{\omega}$ and (3.57) for $\boldsymbol{v}_{4\mathrm{C}}^{\omega}$ into these products leads to:

$$\begin{aligned}
\mathcal{T}_6^{\omega}(\boldsymbol{z}) =\Re\Big\{ & \boldsymbol{\nabla}\boldsymbol{u}(\boldsymbol{z}) : \boldsymbol{\mathcal{A}} : \left(\mathrm{i}\boldsymbol{I}_1^{H1} + \boldsymbol{\nabla}_{21}\boldsymbol{G}_{\mathrm{C}}^{\omega}(\boldsymbol{z},\boldsymbol{z})\right) : \boldsymbol{\mathcal{A}} : \boldsymbol{\nabla}\boldsymbol{p}(\boldsymbol{z}) \\
& - \omega^2|\mathcal{B}|\Delta\rho\ \left[\boldsymbol{u}(\boldsymbol{z}) \cdot \boldsymbol{\nabla}_2\boldsymbol{G}_{\mathrm{C}}^{\omega}(\boldsymbol{z},\boldsymbol{z}) : \boldsymbol{\mathcal{A}} : \boldsymbol{\nabla}\boldsymbol{p}(\boldsymbol{z}) + \boldsymbol{\nabla}\boldsymbol{u}(\boldsymbol{z}) : \boldsymbol{\mathcal{A}} : \boldsymbol{\nabla}_1\boldsymbol{G}_{\mathrm{C}}^{\omega}(\boldsymbol{z},\boldsymbol{z}) \cdot \boldsymbol{p}(\boldsymbol{z})\right] \\
& + \left(\omega^2|\mathcal{B}|\Delta\rho\right)^2 \boldsymbol{u}(\boldsymbol{z}) \cdot \left(\mathrm{i}\boldsymbol{G}^{\omega(0)} + \boldsymbol{G}_{\mathrm{C}}^{\omega}(\boldsymbol{z},\boldsymbol{z})\right) \cdot \boldsymbol{p}(\boldsymbol{z})\Big\} \\
& + J''(\boldsymbol{u}; \boldsymbol{v}_{\mathrm{out}}^{\omega}).
\end{aligned} \tag{3.109}$$

Spherical inhomogeneity If $\mathcal{B}$ is the unit sphere,

$$|\mathcal{B}| = \frac{4\pi}{3}, \quad \boldsymbol{M}^{(2)} = \frac{4\pi}{15}\boldsymbol{I} = \frac{|\mathcal{B}|}{5}\boldsymbol{I}, \quad \boldsymbol{\nabla}^3\boldsymbol{u} : \boldsymbol{M}^{(2)} = \frac{|\mathcal{B}|}{5}\boldsymbol{\nabla}(\boldsymbol{\Delta}\boldsymbol{u}), \tag{3.110}$$

and $\boldsymbol{\mathcal{A}}$ is given by (1.119). $\mathcal{T}_5^\omega$ therefore becomes:

$$
\begin{aligned}
\mathcal{T}_5^\omega(\boldsymbol{z}) =\Re\Big\{ & -\frac{1}{10}\Big[\boldsymbol{\nabla}(\boldsymbol{\Delta u})(\boldsymbol{z}) : \boldsymbol{\mathcal{A}} : \boldsymbol{\nabla p}(\boldsymbol{z}) + \boldsymbol{\nabla u}(\boldsymbol{z}) : \boldsymbol{\mathcal{A}} : \boldsymbol{\nabla}(\boldsymbol{\Delta p})(\boldsymbol{z}) + \Big] \\
& - \boldsymbol{\nabla}^2\boldsymbol{u}(\boldsymbol{z}) \bullet \boldsymbol{\mathcal{A}}_{22} \bullet \boldsymbol{\nabla}^2\boldsymbol{p}(\boldsymbol{z}) \\
& + \boldsymbol{\nabla p}(\boldsymbol{z}) : \boldsymbol{\mathcal{A}} : \Big[\boldsymbol{I}_1^{H0} + \frac{1}{5}\boldsymbol{I}_3^{H0} : \boldsymbol{I}\Big] : \boldsymbol{\mathcal{A}} : \boldsymbol{\nabla u}(\boldsymbol{z}) \\
& + \omega^2\Delta\rho\,\Big[\boldsymbol{\nabla}^2\boldsymbol{u}(\boldsymbol{z}) \bullet \boldsymbol{\mathcal{Q}}_{20} \cdot \boldsymbol{p}(\boldsymbol{z}) + \boldsymbol{u}(\boldsymbol{z}) \cdot \boldsymbol{\mathcal{Q}}_{02} \bullet \boldsymbol{\nabla}^2\boldsymbol{p}(\boldsymbol{z})\Big] \\
& + \omega^2\Delta\rho\ \boldsymbol{\nabla u}(\boldsymbol{z}) : \boldsymbol{\mathcal{Q}}_{11} : \boldsymbol{\nabla p}(\boldsymbol{z}) \\
& + \left(\omega^2\Delta\rho\right)^2\ \boldsymbol{p}(\boldsymbol{z}) \cdot \Big[\mathcal{E}^{(0)}\boldsymbol{I} + \boldsymbol{\mathcal{Q}}_{02} \bullet \boldsymbol{\mathcal{E}}_3^{(0)}\Big] \cdot \boldsymbol{u}(\boldsymbol{z})\Big\},
\end{aligned}
\tag{3.111}
$$

where $\boldsymbol{I}_1^{H0}$ and $\boldsymbol{I}_3^{H0}$ are given by (3.151) and $\mathcal{E}^{(0)}$ and $\boldsymbol{\mathcal{E}}_3^{(0)}$ are given by (3.126). $\mathcal{T}_6^\omega$ becomes:

$$
\begin{aligned}
\mathcal{T}_6^\omega(\boldsymbol{z}) =\Re\Big\{ & \boldsymbol{\nabla u}(\boldsymbol{z}) : \boldsymbol{\mathcal{A}} : \big(\mathrm{i}\boldsymbol{I}_1^{H1} + \boldsymbol{\nabla}_{21}\boldsymbol{G}_{\mathrm{C}}^\omega(\boldsymbol{z},\boldsymbol{z})\big) : \boldsymbol{\mathcal{A}} : \boldsymbol{\nabla p}(\boldsymbol{z}) \\
& - \frac{4\pi}{3}\omega^2\Delta\rho\Big[\boldsymbol{u}(\boldsymbol{z}) \cdot \boldsymbol{\nabla}_2\boldsymbol{G}_{\mathrm{C}}^\omega(\boldsymbol{z},\boldsymbol{z}) : \boldsymbol{\mathcal{A}} : \boldsymbol{\nabla p}(\boldsymbol{z}) + \boldsymbol{\nabla u}(\boldsymbol{z}) : \boldsymbol{\mathcal{A}} : \boldsymbol{\nabla}_1\boldsymbol{G}_{\mathrm{C}}^\omega(\boldsymbol{z},\boldsymbol{z}) \cdot \boldsymbol{p}(\boldsymbol{z})\Big] \\
& + \left(\frac{4\pi}{3}\omega^2\Delta\rho\right)^2 \boldsymbol{u}(\boldsymbol{z}) \cdot \Big(\mathrm{i}\boldsymbol{G}^{\omega(0)} + \boldsymbol{G}_{\mathrm{C}}^\omega(\boldsymbol{z},\boldsymbol{z})\Big) \cdot \boldsymbol{p}(\boldsymbol{z})\Big\} \\
& + J''(\boldsymbol{u};\boldsymbol{v}_{\mathrm{out}}^\omega)
\end{aligned}
\tag{3.112}
$$

and $\boldsymbol{I}_1^{H1}$ is given by (3.143).

3.4 Identification of a penetrable scatter

In this section, we eventually address the use of the misfit function expansion we derive for identification of a penetrable scatterer. We therefore seek estimations $(\boldsymbol{z}^{\mathrm{est}}, a^{\mathrm{est}})$ of the location $\boldsymbol{z}^{\mathrm{true}}$ and size a^{true} of an homogeneity B^{true}, in a test domain Ω^{test} (chosen in practice as a discrete research grid) and for all a. We first describe a procedure to obtain these estimates, then apply this procedure to a simple setting.

3.4.1 General identification procedure

For any cost functional $\mathbb{J}(B_a) = J(\boldsymbol{u}_a)$, we define:

$$
J_6(a,\boldsymbol{z}) := a^3\mathcal{T}_3(\boldsymbol{z}) + a^4\mathcal{T}_4(\boldsymbol{z}) + a^5\mathcal{T}_5(\boldsymbol{z}) + a^6\mathcal{T}_6(\boldsymbol{z}) \tag{3.113}
$$

so that the sixth-order approximation $\mathbb{J}(B_a) = \mathbb{J}(\emptyset) + J_6(a,\boldsymbol{z}) + o(a^6)$ holds. The identification procedure then reads:

1. "Probe" the solid occupying Ω with an incident wave $\boldsymbol{u}$, and compute its values for all $\boldsymbol{z} \in \Omega^{\mathrm{test}}$.

2. From this incident field, compute the directional derivative $J'(\boldsymbol{u};\boldsymbol{w})$ of $\mathbb{J}$, then compute the adjoint displacement $\boldsymbol{p}$ defined by the weak formulation (3.84) for all $\boldsymbol{z} \in \Omega^{\mathrm{test}}$.

3. From $\boldsymbol{u}$, $\boldsymbol{p}$ and the second directional derivative $J''(\boldsymbol{u}; \boldsymbol{v}^{\omega}_{\text{out}})$ of $\mathbb{J}$, compute the topological derivatives $\mathcal{T}_j(\boldsymbol{z})$ for all $\boldsymbol{z} \in \Omega^{\text{test}}$.

4. Define $a^{\min}(\boldsymbol{z}) := \arg\min_{a} J_6(a, \boldsymbol{z})$, $\boldsymbol{z} \in \Omega^{\text{test}}$.

5. Estimate the location as: $\boldsymbol{z}^{\text{est}} := \arg\min_{\boldsymbol{z}\in\Omega^{\text{test}}} J_6(a^{\min}(\boldsymbol{z}), \boldsymbol{z})$.

6. Estimate the size as: $a^{\text{est}} := a^{\min}(\boldsymbol{z}^{\text{est}})$.

The most costly of these operations are steps (1) and (2) for most cases, i.e. when we don't have access to analytical expressions for $\boldsymbol{u}$ and $\boldsymbol{p}$ and have to rely on a numerical method (finite elements, boundary elements ...) to solve the direct and adjoint problems. An additional constraint is that such method must accurately compute high-order derivatives of both these fields, at least into Ω^{test}, as discussed in Section 2.3.3.

Step (3) consists on computing all the bilinear forms implied in the topological derivatives, plus the quadratic term $J''(\boldsymbol{u}; \boldsymbol{v}^{\omega}_{\text{out}})$, which may deserve special attention since it involves Green's tensor $\boldsymbol{G}^{\omega}$ for Ω, including complementary part $\boldsymbol{G}^{\omega}_{\text{C}}$. The arising difficulties were addressed in Section 2.3.3. These computations were implemented in a Matlab code, limited for now to $\Omega = \mathbb{R}^3$, i.e. $\boldsymbol{G}^{\omega}_{\text{C}} = \boldsymbol{0}$, to spherical shapes and to isotropic materials. The tensor formalism was maintained in this code thanks to the Matlab tensor toolbox [Bader et al., 2012].[2]

Step (4) is straightforward since it is just a minimization of a polynomial in a for each $\boldsymbol{z}$. It could be achieved analytically, but in the following we rely on numerical tools provided by Matlab. Note also that $J_6(a^{\min}(\boldsymbol{z}), \boldsymbol{z})$ minimizes $J_6(a, \boldsymbol{z})$ on a for each $\boldsymbol{z}$, and thus can be used similarly to $\mathcal{T}_3$ as an indicator function.

Finally, step (5) is just a search of a minimum over the research grid Ω^{test}, and again we rely on Matlab to do so.

Remark 3.3. *In this section, unless specified, the contrasts $(\Delta\boldsymbol{\mathcal{C}}, \Delta\rho)$ that characterize the real inclusion B^{true} are assumed to be known and they are used in the computation of the topological derivatives $\mathcal{T}_j$ (i.e. the trial inhomogeneity B_a is characterized by the same contrasts).*

3.4.2 Identification of a spherical scatterer in full-space and for isotropic materials

We suppose that measurements data $\boldsymbol{u}^{\text{m}}$ of the scattered field by a spherical obstacle B^{true} for some incident plane P-wave $\boldsymbol{u}$ are available on a discrete array of "captors" : $\Gamma^{\text{m}} = \cup_{n=1}^{N} \boldsymbol{x}_n$ such that $\Gamma^{\text{m}} \cap \Omega^{\text{test}} = \emptyset$. For convenience, we consider the least-square misfit function:

$$\mathbb{J}(B_a) = J(\boldsymbol{u}^{\omega}_a) = \sum_{n=1}^{N} |\boldsymbol{u}^{\omega}_a(\boldsymbol{x}_n) - \boldsymbol{u}^{\text{m}}(\boldsymbol{x}_n)|^2 \tag{3.114}$$

In full-space, when both materials are isotropic, all the required fields can be computed analytically:

- The incident field is a single plane P-wave in the direction $\boldsymbol{d}$ defined by the angle θ as shown on figure 3.1:

$$\boldsymbol{u}(\boldsymbol{x}) = u_0\, e^{ik_{\text{P}}(\boldsymbol{d}\cdot\boldsymbol{x})}\boldsymbol{d} \quad \text{with : } \boldsymbol{d} = \cos(\theta)\boldsymbol{e}_1 + \sin(\theta)\boldsymbol{e}_3 \tag{3.115}$$

[2]available at http://www.sandia.gov/ tgkolda/TensorToolbox/index-2.6.html

- Since the solution of the scattering problem for a incident plane P-wave and a penetrable sphere is known ([Eringen & Suhubi, 1975, Sect. 9.12]), measurements $\boldsymbol{u}^{\mathrm{m}}$ can be simulated analytically.

- The adjoint field, in the case of the least-square cost functional (3.114), is then computed using the full-space Green's tensor $\boldsymbol{G}^{\omega}_{\infty}$, i.e. the Helmholtz solution given by (3.12), as:

$$\boldsymbol{p}(\boldsymbol{x}) = \sum_{n=1}^{N} \overline{(\boldsymbol{u} - \boldsymbol{u}^{\mathrm{m}})}(\boldsymbol{x}_n) \cdot \boldsymbol{G}^{\omega}_{\infty}(\boldsymbol{x}_n, \boldsymbol{x}). \tag{3.116}$$

  Note that since high-order derivatives of $\boldsymbol{p}$ are required, high-order derivatives of $\boldsymbol{G}^{\omega}_{\infty}$ must be computed. These straightforward but tedious computations are addressed in Appendix 3.B.

Material and geometrical parameters: The examples below are intended to provide a first illustration of the identification method given above and not to mimic any physically realistic situation. Consequently, all the parameters we use are fixed to meaningless "mathematical" values. In particular, we do not precise any unit.

The considered circular frequency is $\omega = 1$ and the materials are fixed as follow:

- The background coefficients are $(\mu, \nu, \rho) = (1, 0.3, 10)$ and, so that the pressure and shear wavelengths are $\lambda_{\mathrm{P}} \approx 3.7$ and $\lambda_{\mathrm{S}} \approx 2.0$. A "small" size is thus supposed to be $a \ll \lambda_{\mathrm{S}} \approx 2.0$.

- The material in the scatterer is characterized by: $(\mu^\star, \nu^\star, \rho^\star) = (1.2, 0.3, 12)$ i.e $\Delta\boldsymbol{\mathcal{C}} = 0.2\boldsymbol{\mathcal{C}}$ and $\Delta\rho = 0.2\rho$.

The "screen" Γ^{m} of 5×5 captors spaced by $2 = \lambda_{\mathrm{S}}$ is kept fixed on the plane $x_1 = 10$. The angle θ which defines the incident direction $\boldsymbol{d}$ varies to study the influence of the "illumination" direction, as represented on Figure 3.1. The results are compared to those obtained on a "full aperture" configuration, for which Γ^{m} is a spherical array of 50 "captors", of radius $R = 5$ and centered on the origin.

The sample domain Ω^{test} we used for localization attempts is a cubic grid with $11 \times 11 \times 11$ sampling points spaced by $0.1 \approx \lambda_{\mathrm{S}}/20$, so that its side length is $1 \approx \lambda_{\mathrm{S}}/2$, centered on $\boldsymbol{z}^{\mathrm{true}}$ as shown on Figure 3.1.

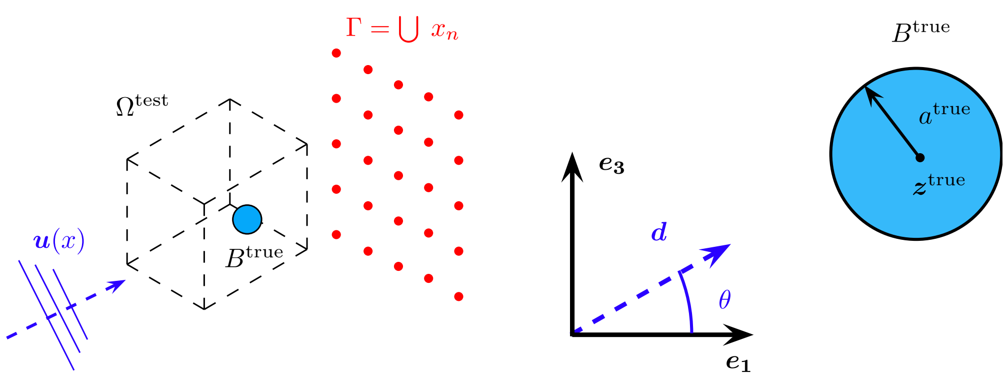

Figure 3.1: 3D representation and notations for the scattering by a spherical obstacle B^{true}

Reflexion configuration: We begin by looking at a "reflexion" configuration that we define by setting $\theta = \pi$ so that the incident direction is $\boldsymbol{d} = -\boldsymbol{e}_1$: the displacement measured on Γ^{m} therefore corresponds to the wave "reflected" by the obstacle. This might correspond to situations in which only one face of the domain Ω is reachable, so both captors and the device that produces the incident wave (e.g. transducers) have to be placed on it.

In this configuration, as seen on Figure 3.2, the minimum values of the topological derivative $\mathcal{T}_3(\boldsymbol{z})$ already provides a very good localization of the obstacle, only the peak of $J_6(a^{\min}(\boldsymbol{z}), \boldsymbol{z})$ is sharper. Figure 3.3 presents the errors in localization and size estimation. Over the tested range of sizes $a \in [0.025\lambda_{\mathrm{S}}, 0.25\lambda_{\mathrm{S}}]$, it is seen that perfect localization is provided by all indicator functions, even $\mathcal{T}_3$ for partial aperture measurements. The improvement brought by J_6 therefore lies only on the size estimate, which is performed with reasonable mistake.

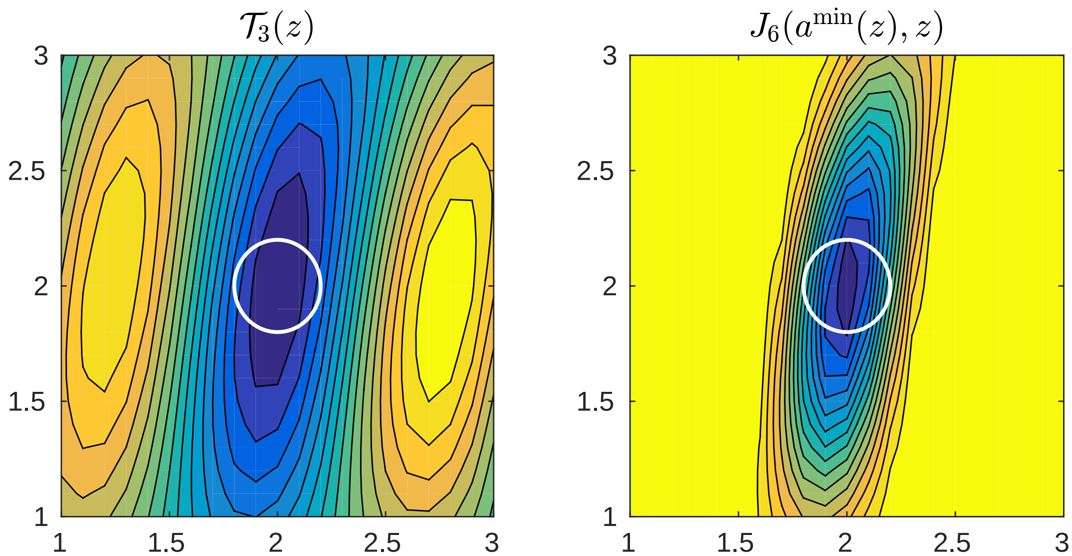

Figure 3.2: Isovalues of $\mathcal{T}_3(\boldsymbol{z})$ and $J_6(a^{\min}(\boldsymbol{z}), \boldsymbol{z})$ in the x_1x_3-plane passing by $\boldsymbol{z}^{\mathrm{true}} = (2, 2, 2)$, and with $a^{\mathrm{true}} = 0.2 = \lambda_{\mathrm{S}}/10$, for the reflexion configuration ($\theta = \pi$)

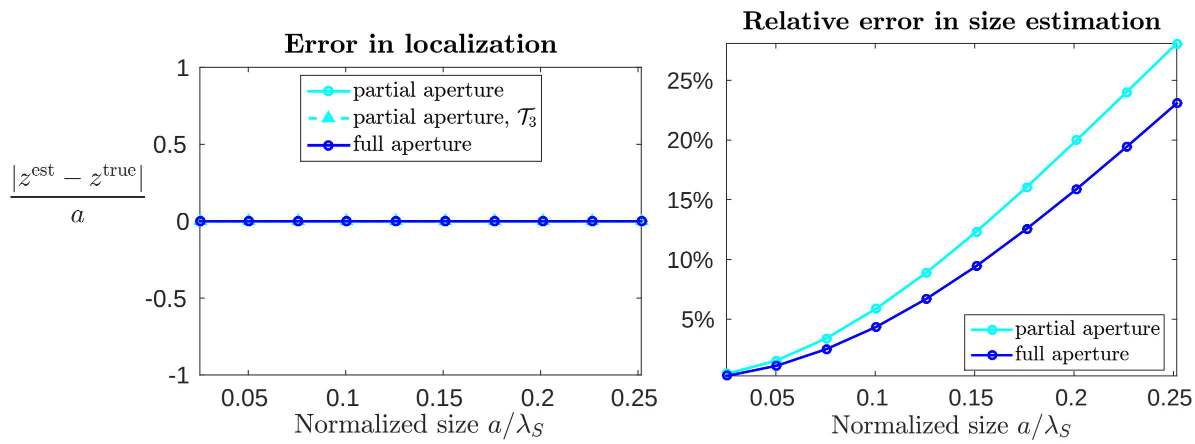

Figure 3.3: Errors in localization and size estimation of a penetrable sphere in full-space, for weak contrast, $\boldsymbol{z}^{\mathrm{true}} = (2, 2, 2)$ and reflexion configuration ($\theta = \pi$).

Transmission configuration We define the transmission configuration by $\theta = 0$ (so that the incident direction is $\boldsymbol{d} = \boldsymbol{e}_1$): the displacement is measured *behind* the obstacle.

Figure 3.4 presents the indicator functions $\mathcal{T}_3(\boldsymbol{z})$ and $J_6(a^{\min}(\boldsymbol{z}), \boldsymbol{z})$ for a scatterer placed at $\boldsymbol{z}^{\mathrm{true}} = (2, 2, 2)$ and with radius $a^{\mathrm{true}} = 0.2 = \lambda_{\mathrm{S}}/10$. This configuration was chosen as an example because the minimum of the sole topological derivative $\mathcal{T}_3$ is seen to be outside B^{true}. At the contrary the indicator function $J_6(a^{\min}(\boldsymbol{z}), \boldsymbol{z})$ computed from the above procedure presents a sharp peak closer to the position of B^{true}. For this configuration, we find $\boldsymbol{z}^{\mathrm{est}} = (1.8, 2, 2)$ and $a^{\mathrm{est}} = 0.207$.

Figure 3.5 presents for the same case the contributions of each term $a^j \mathcal{T}_j$ of the approximation to $J_6(a, \boldsymbol{z})$, for $\boldsymbol{z} = \boldsymbol{z}^{\mathrm{est}}$. It emphasizes the importance of the highest-order term $a^6 \mathcal{T}_6$: at least in this case, both $\mathcal{T}_3$ and $\mathcal{T}_5$ are negative, so stopping the expansion of $\mathbb{J}$ to order 5 would have provided no minimum to estimate a.

Figure 3.6 investigates the asymptotic accuracy of the identification method as $a^{\mathrm{true}} \to 0$. The distance to the exact location $\boldsymbol{z}^{\mathrm{true}}$ does not exceed $2a^{\mathrm{true}}$, up to $a^{\mathrm{true}} = \lambda_{\mathrm{S}}/4$. The full aperture measurements enable to reach exactly $\boldsymbol{z}^{\mathrm{true}}$, but in this case, $\mathcal{T}_3$ already gave such information. The estimate of a from the partial aperture measurements is quite precise (less than 20% error) up to $a^{\mathrm{true}} = 0.2\lambda_{\mathrm{S}}$, where a “jump” that we don't explain yet occurs.

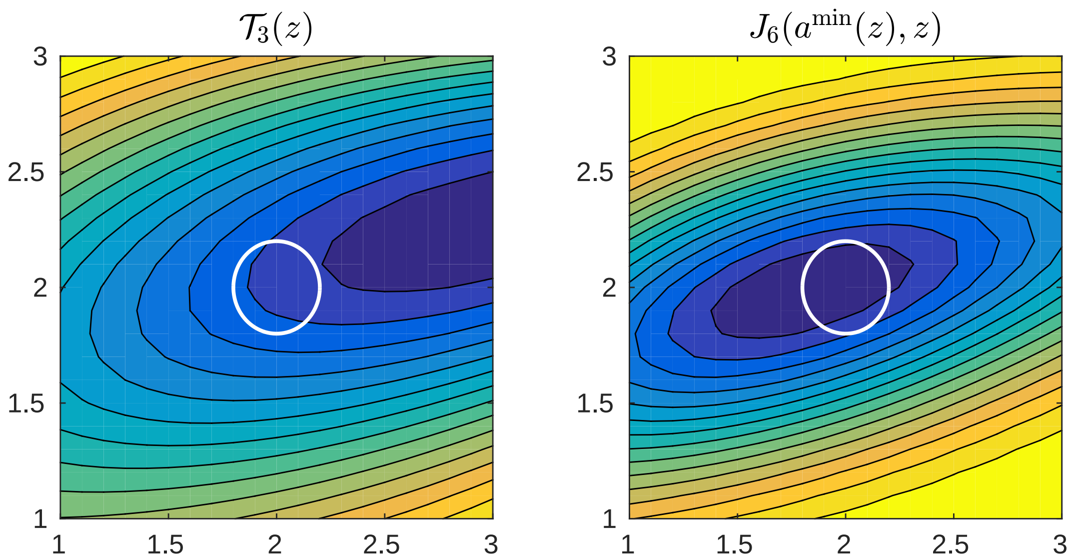

Figure 3.4: Isovalues of $\mathcal{T}_3(\boldsymbol{z})$ and $J_6(a^{\min}(\boldsymbol{z}), \boldsymbol{z})$ in the x_1x_3-plane passing by $\boldsymbol{z}^{\text{true}} = (2, 2, 2)$, and with $a^{\text{true}} = 0.2 \approx \lambda_{\text{S}}/10$.

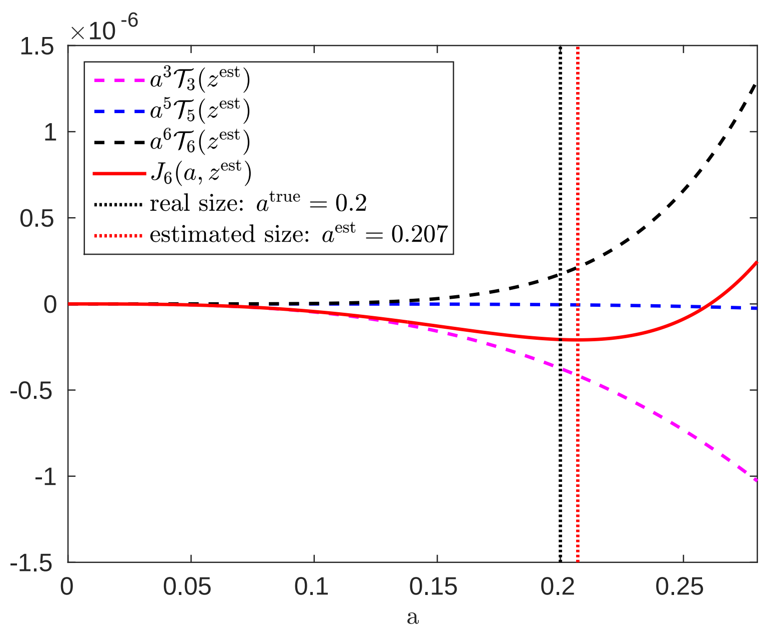

Figure 3.5: Contributions to $J_6(a, \boldsymbol{z}^{\text{est}})$ for the weak-contrast transmission configuration.

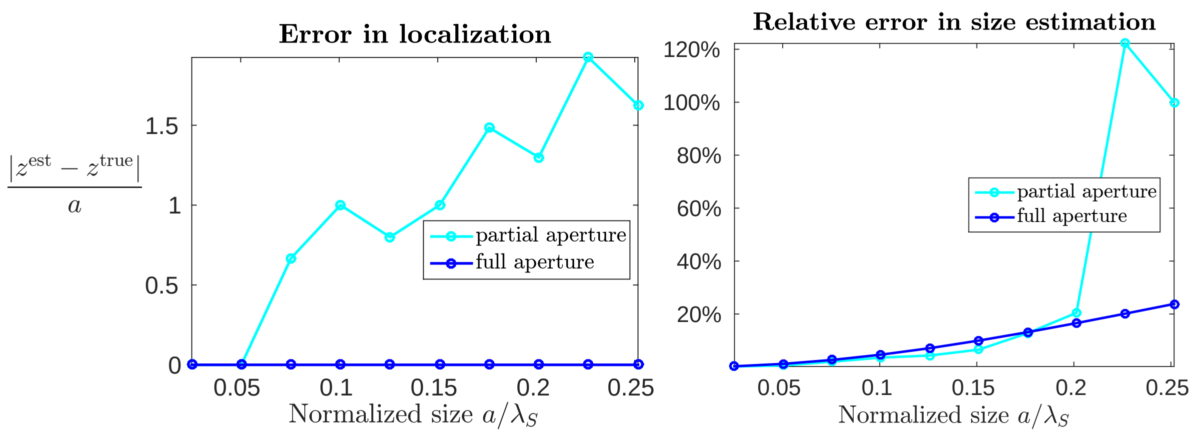

Figure 3.6: Errors in localization and size estimation of a penetrable sphere in full-space, for weak contrast and $\boldsymbol{z}^{\mathrm{true}} = (2, 2, 2)$.

Unknown material coefficients: An interesting case is the one for which we do not know the exact material coefficient of the obstacle, but rather its "kind" (i.e. stiffer / softer or more or less dense than the background medium). We investigate the case where the obstacle is still the "weak contrast" obstacle B^{true} described above, that is $(\mu^\star, \nu^\star, \rho^\star) = (1.2, 0.3, 12)$, but the coefficient associated to B_a and therefore used in the computation of the topological derivatives are those for a "generic" stiffer and denser obstacle: $(\mu^{\text{test}}, \nu^{\text{test}}, \rho^{\text{test}}) = (2, 0.3, 20)$, i.e. $\boldsymbol{\mathcal{C}}^{\text{test}} = 2\boldsymbol{\mathcal{C}}$ and $\rho^{\text{test}} = 2\rho$. For the transmission configuration defined above ($\boldsymbol{d} = \boldsymbol{e}_1$), Figure 3.7 shows that the localization is still quite precise, and certainly more than using $\mathcal{T}_3$ alone.

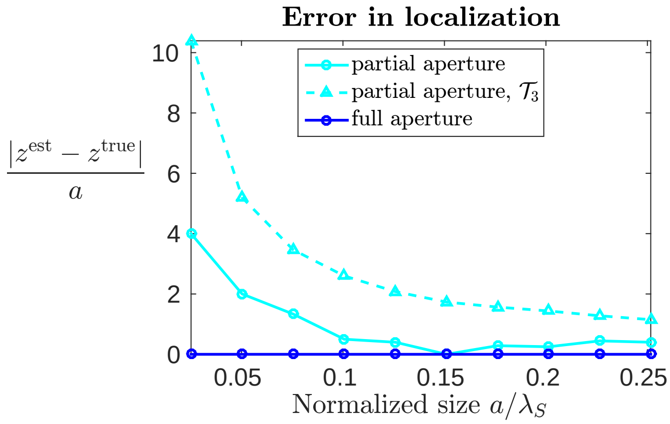

Figure 3.7: Errors in localization of a penetrable sphere in full-space, for unknown material coefficients: $(\mu^\star, \nu^\star, \rho^\star) = (1.2, 0.3, 12)$ in the true obstacle whereas $(\mu^{\text{test}}, \nu^{\text{test}}, \rho^{\text{test}}) = (2, 0.3, 20)$ were used in the computation. The estimate given by the minimum of the first topological derivative $\mathcal{T}_3$ is also plotted.

Other possible experiments Many other numerical experiments could be conduced over this simple framework. In particular, one could investigate the influence of the distance between the scatterer and the "screen", that of the number of "captors", the limit cases of a cavity (i.e. $\mu^\star \to 0$) or a rigid scatterer $\mu^\star \to +\infty$) and many more. However, our goal in this part was to show some preliminary illustrations of chosen configuration for which the usefulness of using the high-order expansion of $\mathbb{J}$ clearly appears. Further attempts and a more systematic experimental study are to be considered afterwards.

3.5 Conclusions and future work

In this chapter, we first established the fourth-order expansion of displacement field inside a small penetrable scatterer. It is to be noted that the leading-order contribution of the considered time-harmonic integral operator is still the operator addressed in detail in Chapter 1 corresponding to *static* free-space transmission problem. As a consequence, all terms in the expansion are computed as the solutions of such static problems and the frequency ω acts only as a parameter in the source terms of these problems.

Under the same assumptions for the studied cost functionals than in the previous chapter, we then computed the sixth-order expansion of such a cost functional. The higher-order topological derivatives are expressed similarly than in the static case as bilinear forms of incident and adjoint displacements, plus and additional term in $\mathcal{T}_6$ involving the full Green's tensor of the domain Ω.

Eventually, we presented a method relying on this sixth-order polynomial approximation to estimate the position and size of an unknown scatterer. Some examples were provided in the simple case of a spherical scatterer illuminated by an incident plane wave, and for isotropic materials. In particular, in specific configurations, our high-order method improves the quality of the localization compared to the one obtained when using only the first topological derivative $\mathcal{T}_3$.

Many works could follow from these results. First of all, we stated all the general results for anisotropic materials and any obstacle shape, but we addressed only isotropic materials and spherical shapes to provide explicit expressions. A natural follow-up to this work would therefore be to provide explicit expressions for more general cases. Beginning with ellipsoidal shapes, for which the necessary tools are provided all along this dissertation, would permit for instance to address thin obstacles that cannot be approached by spheres.

Another issue is the practical computation of these topological derivative. The two main issues one will have to deal with are (i) the computation of high-order derivatives of the incident and adjoint displacements, which requires accurate enough numerical methods, and (ii) the computation of $\mathcal{T}_6$ in bounded domains, for which the complementary part $\boldsymbol{G}_{\mathrm{C}}^{\omega}$ of Green's tensor must be known. These issues were already discussed in Section 2.3.3 of Chapter 2, to which we refer since the conceptual difficulties do not depend on whether we consider static or time-harmonic fields.

Eventually, many other identification process could be imagined from the knowledge of the sixth-order approximation J_6 of the cost functional. An example which comes naturally to mind is attempting to perform *material* identification rather than only geometrical identification. Indeed, a preliminary example in Section 3.4 showed that quite precise localization can be obtained without precise knowledge of the material of the scatterer. One could therefore imagine to fix the sampling point $\boldsymbol{z}$ to this first estimate and to minimize $J_6(\boldsymbol{z})$ w.r.t. other parameters. More generally, conducing a minimization of J_6 w.r.t. parameters other than the position $\boldsymbol{z}$, which intervenes very implicitly through the direct and adjoint fields, could benefit from the closed-form formula we derived.

3.A Time-harmonic terms in scattered displacement expansion

This section presents the computation of the additionnal terms which appear in the scattered displacement expansion:

- Some come from the inertial term in the bilinear form, so that the new terms are the solutions of equations $\mathcal{L}[\boldsymbol{v}](\boldsymbol{x}) = (\boldsymbol{u}_\mathrm{s}, \boldsymbol{G}_\infty(\cdot - \boldsymbol{x}))_\mathcal{B}^{\Delta\rho}$, $\boldsymbol{u}_\mathrm{s}$ being some "source" displacement as explained in section 3.2.1.1

- Some come from the expansion of elastodynamic Green's complementary part $\boldsymbol{G}^\omega_{\mathrm{C}\infty}$ (3.20) and the resulting contributions are parts of the "complementary" displacement $\boldsymbol{v}^\omega_{3C}$ and $\boldsymbol{v}^\omega_{4C}$ as explained in section 3.2.1.2.

We address successively these two cases, the main tool being the harmonic and biharmonic potentials detailed in section 1.A.

Remark 3.4. *Since this appendix addresses only problems posed on the reference shape $\mathcal{B}$ with no reference to the initial inhomogeneity B_a, variables $\boldsymbol{x}$ and $\boldsymbol{\xi}$ will be used rather than $\bar{\boldsymbol{x}}$ and $\bar{\boldsymbol{\xi}}$ to simplify notations.*

3.A.1 Contribution of inertial additionnal terms for ellipsoids

For ellipsoids, the source displacement $\boldsymbol{u}_\mathrm{s}$ into consideration is a polynomial:

$$[\boldsymbol{u}_\mathrm{s}]_p(\boldsymbol{\xi}) = E_p + E_{pa}\xi_a + E_{pab}\xi_a\xi_b + ... \tag{3.117}$$

and recall that the right-hand sides $\boldsymbol{P}[\boldsymbol{u}_\mathrm{s}]$ of the FSTPs to be solved are:

$$\boldsymbol{P}[\boldsymbol{u}_\mathrm{s}](\boldsymbol{x}) = \omega^2(\boldsymbol{u}, \boldsymbol{G}_\infty(\cdot - \boldsymbol{x}))_\mathcal{B}^{\Delta\rho} = \omega^2 \int_\mathcal{B} \Delta\rho\ \boldsymbol{u}_\mathrm{s}(\boldsymbol{\xi}) \cdot \boldsymbol{G}_\infty(\boldsymbol{\xi} - \boldsymbol{x})\ \mathrm{d}V_\xi, \tag{3.118}$$

In this part, we adress only the cases where $\Delta\rho$ is constant in $\mathcal{B}$. Since the fundamental static solution may be written:

$$\boldsymbol{G}_\infty(\boldsymbol{\xi} - \boldsymbol{x}) = \frac{1}{4\pi\mu|\boldsymbol{\xi} - \boldsymbol{x}|}\boldsymbol{I} + \frac{1}{16\pi\mu(1-\nu)}\boldsymbol{\nabla}^2_{\boldsymbol{x}}|\boldsymbol{\xi} - \boldsymbol{x}| \tag{3.119}$$

then $\boldsymbol{P}$ can be expressed thanks to the harmonic and biharmonic potentials $\phi_{ab...m}$ and $\psi_{ab...m}$ (1.137) as:

$$\begin{aligned} P_j[\boldsymbol{u}_\mathrm{s}](\boldsymbol{x}) =& \frac{\omega^2\Delta\rho}{4\pi\mu}\left(E_p\phi(\boldsymbol{x}) + E_{pa}\phi_a(\boldsymbol{x}) + E_{pab}\phi_{ab}(\boldsymbol{x}) + ...\right)\delta_{pj} \\ &- \frac{\omega^2\Delta\rho}{16\pi\mu(1-\nu)}\left(E_p\psi_{,pj}(\boldsymbol{x}) + E_{pa}\psi_{a,pj}(\boldsymbol{x}) + E_{pab}\psi_{ab,pj}(\boldsymbol{x}) + ...\right) \end{aligned} \tag{3.120}$$

3.A.1.1 Constant source displacement

This part adresses the simplest case for which $\boldsymbol{u}_{\rm s} = \boldsymbol{e}$ is a constant vector.

Displacement $\boldsymbol{P}^{(0)}[\boldsymbol{e}](\boldsymbol{x})$:

$$\boldsymbol{P}^{(0)}[\boldsymbol{e}](\boldsymbol{x}) = \omega^2 \int_{\mathcal{B}} \Delta\rho \; \boldsymbol{e} \cdot \boldsymbol{G}_\infty(\boldsymbol{\xi} - \boldsymbol{x}) \; {\rm d}V_\xi = \omega^2 \Delta\rho \; \boldsymbol{e} \cdot \int_{\mathcal{B}} \boldsymbol{G}_\infty(\boldsymbol{\xi} - \boldsymbol{x}) \; {\rm d}V_\xi, \tag{3.121}$$

and from (3.120) and $\mathcal{B}$ an ellipsoid,

$$\begin{aligned}\left[\int_{\mathcal{B}} \boldsymbol{G}_\infty(\boldsymbol{\xi} - \boldsymbol{x}) \; {\rm d}V_\xi\right]_{jp} &= \frac{1}{4\pi\mu}\phi(\boldsymbol{x})\delta_{jp} + \frac{1}{16\pi\mu(1-\nu)}\psi_{,jp}(\boldsymbol{x}) \\ &= \frac{1}{8\pi\mu}(I - x_r x_r I_R)\delta_{jp} \\ &\quad + \frac{1}{32\pi\mu(1-\nu)}\left(I - x_r x_r I_R - a_P^2(I_P - x_r x_r I_{RP}))\delta_{jp} - (I_J - a_P^2 I_{JP})x_j x_p\right)\end{aligned} \tag{3.122}$$

Remark 3.5. *Recall that terms written $\delta_{jp} a_P^2 I_P$ do not represent tensors proportionnal to $\boldsymbol{I}$ but diagonal tensors with $a_P^2 I_P$ as p-th diagonal values.*

Introducing (3.122) into (3.121), $\boldsymbol{P}^{(0)}[\boldsymbol{e}]$ is found to be a second-order polynomial displacement, and we define the constant $\mathcal{E}^{(0)}$ and the fourth-order tensor $\boldsymbol{\mathcal{E}}_3^{(0)}$ such that:

$$\boldsymbol{P}^{(0)}[\boldsymbol{e}](\boldsymbol{x}) = \omega^2 \Delta\rho \left[\mathcal{E}^{(0)}\boldsymbol{e} + \frac{1}{2}\left(\boldsymbol{\mathcal{E}}_3^{(0)} \cdot \boldsymbol{e}\right) : (\boldsymbol{x} \otimes \boldsymbol{x})\right] \tag{3.123}$$

For the unit sphere, thanks to the expression (1.140) of elliptic integrals, (3.122) becomes:

$$\int_{\mathcal{B}} \boldsymbol{G}_\infty(\boldsymbol{\xi} - \boldsymbol{x}) \; {\rm d}V_\xi = \frac{1}{6\mu(1-\nu)}\left[\frac{1}{2}(7 - 6\nu - (3 - 2\nu)|\boldsymbol{x}|^2)\boldsymbol{I} - \frac{1}{5}\boldsymbol{x} \otimes \boldsymbol{x}\right] \tag{3.124}$$

so that $\boldsymbol{P}^{(0)}[\boldsymbol{e}]$ is given by

$$\boldsymbol{P}^{(0)}[\boldsymbol{e}](\boldsymbol{x}) = \frac{\omega^2 \Delta\rho}{6\mu(1-\nu)}\left[\frac{1}{2}(7 - 6\nu - (3 - 2\nu)|\boldsymbol{x}|^2)\boldsymbol{e} - \frac{1}{5}\boldsymbol{e} \cdot (\boldsymbol{x} \otimes \boldsymbol{x})\right] \tag{3.125}$$

and, with reference to (3.123), $\mathcal{E}^{(0)}$ and $\boldsymbol{\mathcal{E}}_3^{(0)}$ are found to be:

$$\begin{aligned}\mathcal{E}^{(0)} &= \frac{(7-6\nu)}{12\mu(1-\nu)} \\ \left[\boldsymbol{\mathcal{E}}_3^{(0)}\right]_{ijkl} &= -\frac{1}{30\mu(1-\nu)}\left[(15 - 10\nu)\delta_{il}\delta_{jk} + 2\delta_{ik}\delta_{jl}\right]\end{aligned} \tag{3.126}$$

Strain $\boldsymbol{\varepsilon}[\boldsymbol{P}^{(0)}[\boldsymbol{e}]](\boldsymbol{x})$: The associated strain is obtained by symmetrizing $\boldsymbol{\mathcal{E}}_3^{(0)}$ over its two first indexes: we obtain

$$\boldsymbol{\varepsilon}[\boldsymbol{P}^{(0)}[\boldsymbol{e}]](\boldsymbol{x}) = \omega^2 \Delta\rho \; \left(\boldsymbol{\mathcal{E}}_3^{(0){\rm s}} \cdot \boldsymbol{e}\right) \cdot \boldsymbol{x} \tag{3.127}$$

with:

$$\begin{aligned}\left[\boldsymbol{\mathcal{E}}_3^{(0){\rm s}}\right]_{ijkl} &= -\frac{1}{30\mu(1-\nu)}\left[(8 - 5\nu)(\delta_{il}\delta_{jk} + \delta_{ik}\delta_{jl}) + \delta_{ij}\delta_{kl}\right] \\ \text{i.e.} \quad \boldsymbol{\mathcal{E}}_3^{(0){\rm s}} &= -\frac{1}{30\mu(1-\nu)}\left[(19 - 10\nu)\boldsymbol{\mathcal{J}} + (16 - 10\nu)\boldsymbol{\mathcal{K}}\right]\end{aligned} \tag{3.128}$$

Solution $\boldsymbol{U}^{(0)}[\boldsymbol{e}]$ of corresponding Eshelby problem: $\boldsymbol{U}^{(0)}[\boldsymbol{e}]$ satisfies $\mathcal{L}[\boldsymbol{U}^{(0)}[\boldsymbol{e}]] = \boldsymbol{P}^{(0)}[\boldsymbol{e}]$ and is therefore given for an ellipsoid by:

$$\boldsymbol{U}^{(0)}[\boldsymbol{e}] = \omega^2 \Delta\rho \left[\mathcal{E}^{(0)}\ \boldsymbol{e} + \boldsymbol{u}^{(2)}_{\mathcal{B}} \left[\boldsymbol{\mathcal{E}}^{(0)}_3 \cdot \boldsymbol{e}\right]\right] \tag{3.129}$$

i.e., using the expression of the second Eshelby solution (1.114),

$$\boldsymbol{U}^{(0)}[\boldsymbol{e}](\boldsymbol{x}) = \omega^2 \Delta\rho \left[\mathcal{E}^{(0)}\ \boldsymbol{e} + \frac{1}{2}\left(\left(\boldsymbol{I}^{(6)} + \boldsymbol{\mathcal{F}} \bullet \boldsymbol{A}_2\right) \bullet \left(\boldsymbol{\mathcal{E}}^{(0)}_3 \cdot \boldsymbol{e}\right)\right) : (\boldsymbol{x} \otimes \boldsymbol{x})\right] \tag{3.130}$$

3.A.1.2 Linear source displacement

The case of a linear source displacement $\boldsymbol{u}_{\mathrm{s}}(\boldsymbol{x}) = \boldsymbol{E} \cdot \boldsymbol{x}$, while not necessary to compute the topological derivatives, is of interest for the expansion of the scattered displacement.

Displacement $\boldsymbol{P}^{(1)}[\boldsymbol{E}](\boldsymbol{x})$:

$$\begin{aligned} \boldsymbol{P}^{(1)}[\boldsymbol{E}](\boldsymbol{x}) &= \omega^2 \int_{\mathcal{B}} \Delta\rho\ (\boldsymbol{E} \cdot \boldsymbol{\xi}) \cdot \boldsymbol{G}_\infty(\boldsymbol{\xi} - \boldsymbol{x})\ \mathrm{d}V_\xi \\ \text{i.e.}\quad P^{(1)}_j[\boldsymbol{E}](\boldsymbol{x}) &= \omega^2 \Delta\rho\ E_{pa} \int_{\mathcal{B}} \xi_a G_{pj}(\boldsymbol{\xi} - \boldsymbol{x})\ \mathrm{d}V_\xi, \end{aligned} \tag{3.131}$$

where we noted G_{pj} for $[\boldsymbol{G}_\infty]_{pj}$. From (3.120) and $\mathcal{B}$ an ellipsoid,

$$\begin{aligned} \int_{\mathcal{B}} \xi_a G_{pj}(\boldsymbol{\xi} - \boldsymbol{x})\ \mathrm{d}V_\xi &= \frac{1}{4\pi\mu}\phi_a(\boldsymbol{x})\delta_{jp} + \frac{1}{16\pi\mu(1-\nu)}\psi_{a,jp}(\boldsymbol{x}) \\ &= \frac{1}{8\pi\mu} x_a a_A^2 (I_A - x_r x_r I_{RA})\delta_{jp} \\ &\quad + \frac{1}{32\pi\mu(1-\nu)} a_A^2 \Big[(x_a\delta_{jp} + \delta_{aj}x_p)(I_P - x_r x_r I_{RP} - a_A^2(I_{AP} - x_r x_r I_{RAP})) \\ &\qquad + \delta_{ap} x_j (I_J - x_r x_r I_{RJ} - a_P^2(I_{PJ} - x_r x_r I_{RPJ})) \\ &\qquad - 2(I_{PJ} - a_A^2 I_{APJ}) x_a x_j x_p\Big] \end{aligned} \tag{3.132}$$

So $\boldsymbol{P}^{(1)}$ is written:

$$\boldsymbol{P}^{(1)}[\boldsymbol{E}](\boldsymbol{x}) = \omega^2 \Delta\rho \left[\left(\boldsymbol{\mathcal{E}}^{(1)}_3 : \boldsymbol{E}\right) \cdot \boldsymbol{x} + \frac{1}{3}\left(\boldsymbol{\mathcal{E}}^{(1)}_5 : \boldsymbol{E}\right) \bullet \boldsymbol{x}^{\otimes 3}\right] \tag{3.133}$$

For the unit sphere, (3.132) becomes:

$$\begin{aligned} \int_{\mathcal{B}} \xi_a G_{pj}(\boldsymbol{\xi} - \boldsymbol{x})\ \mathrm{d}V_\xi &= \frac{1}{2\mu} x_a \left(\frac{1}{3} - \frac{1}{5}|\boldsymbol{x}|^2\right)\delta_{pj} \\ &\quad - \frac{1}{4\mu(1-\nu)}\left[\left(\frac{1}{15} - \frac{1}{35}|\boldsymbol{x}|^2\right)(x_a\delta_{jp} + \delta_{aj}x_p + \delta_{ap}x_j) - \frac{2}{35}x_a x_j x_p\right] \end{aligned} \tag{3.134}$$

and the fourth and sixth-order tensors $\boldsymbol{\mathcal{E}}^{(1)}_3$ and $\boldsymbol{\mathcal{E}}^{(1)}_5$ are given by:

$$\begin{aligned} \mathcal{E}^{(1)}_{3,jbpa} &= \frac{1}{60\mu(1-\nu)}[(9-10\nu)\delta_{jp}\delta_{ab} - \delta_{ja}\delta_{pb} - \delta_{jb}\delta_{pa}] \\ \mathcal{E}^{(1)}_{5,jbcdpa} &= -\frac{3}{140\mu(1-\nu)}\Big[[(13-14\nu)\delta_{jp}\delta_{ab} - \delta_{ja}\delta_{pb} - \delta_{jb}\delta_{pa}]\,\delta_{cd} + 2\delta_{jb}\delta_{pc}\delta_{ad}\Big] \end{aligned} \tag{3.135}$$

Strain $\boldsymbol{\varepsilon}[\boldsymbol{P}^{(1)}[\boldsymbol{E}]](\boldsymbol{x})$:

$$\boldsymbol{\varepsilon}[\boldsymbol{P}^{(1)}[\boldsymbol{E}]](\boldsymbol{x}) = \omega^2 \Delta\rho \left[\boldsymbol{\mathcal{E}}_3^{(1)\mathrm{s}} : \boldsymbol{E} + \left(\boldsymbol{\mathcal{E}}_5^{(1)\mathrm{s}} : \boldsymbol{E}\right) : \boldsymbol{x}^{\otimes 2}\right] \tag{3.136}$$

with:

$$\begin{aligned} \mathcal{E}^{(1)\mathrm{s}}_{3,jkpa} &= \frac{1}{60\mu(1-\nu)} \quad \left[(4-5\nu)(\delta_{jp}\delta_{ak} + \delta_{ja}\delta_{pk}) - \delta_{jk}\delta_{pa}\right] \\ \text{i.e. } \boldsymbol{\mathcal{E}}_3^{(1)\mathrm{s}} &= \frac{1}{60\mu(1-\nu)} \quad \left[5(1-2\nu)\boldsymbol{\mathcal{J}} + 2(4-5\nu)\boldsymbol{\mathcal{K}}\right] \end{aligned} \tag{3.137}$$

and $\boldsymbol{\mathcal{E}}_5^{(1)\mathrm{s}}$ is given by:

$$\begin{aligned} \mathcal{E}^{(1)\mathrm{s}}_{5,jkmnpa} = -\frac{3}{140\mu(1-\nu)} \Big[& \left[(6-7\nu)(\delta_{jp}\delta_{ak} + \delta_{ja}\delta_{pk}) - \delta_{jk}\delta_{pa}\right]\delta_{mn} \\ & + (12-14\nu)\left(\delta_{jp}\delta_{kn} + \delta_{jn}\delta_{kp}\right)\delta_{ma} \\ & - 2\left[\delta_{jm}\delta_{kn}\delta_{pa} + \delta_{ja}\delta_{kn}\delta_{mp} + \delta_{jm}\delta_{ka}\delta_{np} + \delta_{jk}\delta_{mp}\delta_{na}\right]\Big] \end{aligned} \tag{3.138}$$

Solution $\boldsymbol{U}^{(1)}[\boldsymbol{E}]$ of corresponding Eshelby problem $\mathcal{L}[\boldsymbol{U}^{(1)}[\boldsymbol{E}]] = \boldsymbol{P}^{(1)}[\boldsymbol{E}]$. $\boldsymbol{U}^{(1)}[\boldsymbol{E}]$ is therefore given for an ellipsoid by:

$$\boldsymbol{U}^{(1)}[\boldsymbol{u}] = \omega^2\Delta\rho \left[\boldsymbol{u}_{\mathcal{B}}^{(1)}\left[\boldsymbol{\mathcal{E}}_3^{(1)} : \boldsymbol{E}\right] + \boldsymbol{u}_{\mathcal{B}}^{(3)}\left[\boldsymbol{\mathcal{E}}_5^{(1)} : \boldsymbol{E}\right]\right]. \tag{3.139}$$

The first Eshelby solution $\boldsymbol{u}_{\mathcal{B}}^{(1)}$ is given by (1.98), but we didn't compute the third Eshelby solution $\boldsymbol{u}_{\mathcal{B}}^{(3)}$.

3.A.2 Contribution of Green's tensor complementary part for isotropic materials

As explained in Section 3.2.1.2, to compute the "complementary" terms $\boldsymbol{v}^{\omega}_{3,4C}$ we need to compute the following integrals which intervene in the right-hand sides of the integral equations (3.49) and (3.54), featuring the coefficients of the expansions of $\boldsymbol{G}^{\omega}_{\mathrm{C}\infty}$ and its gradient:

$$
\begin{aligned}
\boldsymbol{I}^{G0}(\boldsymbol{x}) &= \int_{\mathcal{B}} \boldsymbol{G}^{\omega(0)} \,\mathrm{d}V_\xi & \boldsymbol{I}^{H0}(\boldsymbol{x}) &= \int_{\mathcal{B}} \boldsymbol{H}^{\omega(0)}(\boldsymbol{\xi}-\boldsymbol{x}) \,\mathrm{d}V_\xi \\
\boldsymbol{I}^{\xi G0}(\boldsymbol{x}) &= \int_{\mathcal{B}} \boldsymbol{\xi}\otimes\boldsymbol{G}^{\omega(0)}(\boldsymbol{\xi}-\boldsymbol{x}) \,\mathrm{d}V_\xi & \boldsymbol{I}^{G1}(\boldsymbol{x}) &= \int_{\mathcal{B}} \boldsymbol{G}^{\omega(1)}(\boldsymbol{\xi}-\boldsymbol{x}) \,\mathrm{d}V_\xi \\
\boldsymbol{I}^{\xi H0}(\boldsymbol{x}) &= \int_{\mathcal{B}} \boldsymbol{\xi}\otimes\boldsymbol{H}^{\omega(0)}(\boldsymbol{\xi}-\boldsymbol{x}) \,\mathrm{d}V_\xi & \boldsymbol{I}^{H1}(\boldsymbol{x}) &= \int_{\mathcal{B}} \boldsymbol{H}^{\omega(1)}(\boldsymbol{\xi}-\boldsymbol{x}) \,\mathrm{d}V_\xi
\end{aligned}
\tag{3.140}
$$

From (3.20) the integrands:

$$
\begin{aligned}
\boldsymbol{G}^{\omega(0)} &= \frac{k_{\mathrm{S}}}{12\pi\mu}(2+\beta^3)\boldsymbol{I} \\
\boldsymbol{G}^{\omega(1)}(\boldsymbol{\xi}-\boldsymbol{x}) &= -\frac{k_{\mathrm{S}}^2}{32\pi\mu}\left[(3+\beta^4)|\boldsymbol{\xi}-\boldsymbol{x}|\boldsymbol{I} + (\beta^4-1)\frac{(\boldsymbol{\xi}-\boldsymbol{x})\otimes(\boldsymbol{\xi}-\boldsymbol{x})}{|\boldsymbol{\xi}-\boldsymbol{x}|}\right] \\
\boldsymbol{H}^{\omega(0)}(\boldsymbol{\xi}-\boldsymbol{x}) &= \frac{k_{\mathrm{S}}^2}{32\pi\mu}\left[-4\boldsymbol{I}\otimes\frac{\boldsymbol{\xi}-\boldsymbol{x}}{|\boldsymbol{\xi}-\boldsymbol{x}|} + (1-\beta^4)\left(\boldsymbol{k}^{2,1}\left(\frac{\boldsymbol{\xi}-\boldsymbol{x}}{|\boldsymbol{\xi}-\boldsymbol{x}|}\right) + \left(\frac{\boldsymbol{\xi}-\boldsymbol{x}}{|\boldsymbol{\xi}-\boldsymbol{x}|}\right)^{\otimes 3}\right)\right] \\
\boldsymbol{H}^{\omega(1)}(\boldsymbol{\xi}-\boldsymbol{x}) &= \frac{k_{\mathrm{S}}^3}{60\pi\mu}\left[-5\boldsymbol{I}\otimes(\boldsymbol{\xi}-\boldsymbol{x}) + (1-\beta^5)\boldsymbol{k}^{2,1}(\boldsymbol{\xi}-\boldsymbol{x})\right],
\end{aligned}
\tag{3.141}
$$

where $\beta = k_{\mathrm{P}}/k_{\mathrm{S}}$, and recall that $\boldsymbol{k}^{21}(\boldsymbol{r}) = (5\boldsymbol{\mathcal{J}} + 2\boldsymbol{\mathcal{K}})\cdot\boldsymbol{r}$.

General shapes Since the leading-order terme $\boldsymbol{G}^{\omega(0)}$ is constant, we have:

$$
\boldsymbol{I}^{G0}(\boldsymbol{x}) = |\mathcal{B}|\; \boldsymbol{G}^{\omega(0)} \tag{3.142}
$$

Moreover, setting $\mathbf{0}$ as the gravity center of $\mathcal{B}$ (which is done without loss of generality), so that $\int_{\mathcal{B}} \boldsymbol{\xi}\,\mathrm{d}V_\xi = \mathbf{0}$, we immediately obtain from the definitions (3.140) and (3.141):

$$
\begin{aligned}
&\boldsymbol{I}^{\xi G0}(\boldsymbol{x}) = \mathbf{0} \\
&\boldsymbol{I}^{H1}(\boldsymbol{x}) = |\mathcal{B}|\boldsymbol{I}^{H1}_1\cdot\boldsymbol{x}, \quad \text{with } \boldsymbol{I}^{H1}_1 := \frac{k_{\mathrm{S}}^3}{60\pi\mu}\left[5(2+\beta^5)\boldsymbol{\mathcal{J}} - 2(1-\beta^5)\boldsymbol{\mathcal{K}}\right]
\end{aligned}
\tag{3.143}
$$

Ellipsoidal shapes For the three other integrals, closed-form expressions are available for ellipsoids. Indeed, we use the harmonic and biharmonic potentials introduced in Appendix 1.A to evaluate the sought tensor-valued integrals:

$$
\begin{aligned}
\left[\int_{\mathcal{B}} \frac{\boldsymbol{\xi}-\boldsymbol{x}}{|\boldsymbol{\xi}-\boldsymbol{x}|}\,\mathrm{d}V_\xi\right]_a &= \phi_a(\boldsymbol{x}) - x_a\phi(\boldsymbol{x}) \\
\left[\int_{\mathcal{B}} \frac{(\boldsymbol{\xi}-\boldsymbol{x})^{\otimes 2}}{|\boldsymbol{\xi}-\boldsymbol{x}|}\,\mathrm{d}V_\xi\right]_{ab} &= \phi_{ab}(\boldsymbol{x}) - x_a\phi_b(\boldsymbol{x}) - x_b\phi_a(\boldsymbol{x}) + x_a x_b\phi(\boldsymbol{x}) \\
\left[\int_{\mathcal{B}} \left(\frac{\boldsymbol{\xi}-\boldsymbol{x}}{|\boldsymbol{\xi}-\boldsymbol{x}|}\right)^{\otimes 3}\mathrm{d}V_\xi\right]_{abc} &= (\phi_a(\boldsymbol{x}) - x_a\phi(\boldsymbol{x}))\delta_{bc} - (\psi_{a,bc}(\boldsymbol{x}) - x_a\psi_{,bc}(\boldsymbol{x}))
\end{aligned}
\tag{3.144}
$$

In particular, to obtain the third expression of (3.144), we used:

$$\left(\frac{\boldsymbol{\xi}-\boldsymbol{x}}{|\boldsymbol{\xi}-\boldsymbol{x}|}\right)^{\otimes 3} = \boldsymbol{k}^{2,1}\left(\frac{\boldsymbol{\xi}-\boldsymbol{x}}{|\boldsymbol{\xi}-\boldsymbol{x}|}\right) - \boldsymbol{\nabla}_x^2\left((\boldsymbol{\xi}-\boldsymbol{x})|\boldsymbol{\xi}-\boldsymbol{x}|\right), \tag{3.145}$$

And, recalling that $\psi_{,b} = x_b\phi - \phi_b = -(\phi_b - x_b\phi)$ (and here and therafter dropping the $\boldsymbol{x}$-dependency for simplicity):

$$\begin{aligned}
\left[\int_{\mathcal{B}}\left(\frac{\boldsymbol{\xi}-\boldsymbol{x}}{|\boldsymbol{\xi}-\boldsymbol{x}|}\right)^{\otimes 3}\,\mathrm{d}V_\xi\right]_{abc} &= (\phi_a - x_a\phi)\delta_{bc} + \delta_{ab}(\phi_c - x_c\phi) + \delta_{ac}(\phi_b - x_b\phi) \\
&\qquad - (\psi_a - x_a\psi)_{,bc} \\
&= (\phi_a - x_a\phi)\delta_{bc} + \delta_{ac}(\phi_b - x_b\phi) + \delta_{ab}(\phi_c - x_c\phi) \\
&\qquad - (\psi_{a,bc} - x_a\psi_{,bc}) + \delta_{ab}\psi_{,c} + \delta_{ac}\psi_{,b} \\
&= (\phi_a - x_a\phi)\delta_{bc} - (\psi_{a,bc} - x_a\psi_{,bc})
\end{aligned} \tag{3.146}$$

For ellipsoids, the three integrals (3.144) can thus be computed thanks to the following combinations of potentials:

$$\begin{aligned}
\phi_a - x_a\phi =& -\frac{x_a}{2}(I - a_A^2 I_A - x_r x_r(I_R - a_A^2 I_{RA})) \\
\phi_{ab} - x_a\phi_b =& \frac{a_A^2}{2}\Big\{x_a x_b\left[a_B^2(I_{AB} - x_r x_r I_{RAB}) - (I_A - x_r x_r I_{RA})\right] \\
&+ \frac{1}{4}\delta_{ab}(I - a_A^2 I_A - x_r x_r(I_R - a_A^2 I_{RA}) + x_r x_r x_s x_s(I_{RS} - a_A^2 I_{RSA}))\Big\} \\
\psi_{a,bc} - x_a\psi_{,bc} =& \frac{a_A^2}{2}\Big\{\delta_{ab}x_c(I_C - a_A^2 I_{AC} - x_r x_r(I_{RC} - a_A^2 I_{RAC})) \\
&+ \delta_{ac}x_b(I_B - a_A^2 I_{AB} - x_r x_r(I_{RB} - a_A^2 I_{RAB}))\Big\} \\
&- \frac{x_a\delta_{bc}}{2}\left(I - (a_B^2 + a_A^2)I_B + a_A^4 I_{AB} - x_r x_r(I_R - (a_B^2 + a_A^2)I_{RB} + a_A^4 I_{RAB})\right) \\
&+ x_a x_b x_c(I_C - (a_A^2 + a_B^2)I_{BC} + a_A^4 I_{ABC}),
\end{aligned} \tag{3.147}$$

whose expressions when $\mathcal{B}$ is the unit sphere are (using (1.140)):

$$\begin{aligned}
\phi_a - x_a\phi =& -4\pi x_a\left(\frac{1}{3} - \frac{1}{15}x_r x_r\right) \\
\phi_{ab} - x_a\phi_b =& -4\pi\Big\{x_a x_b\left(\frac{1}{15} - \frac{1}{35}x_r x_r\right) - \frac{1}{4}\delta_{ab}\left(\frac{1}{3} - \frac{1}{15}x_r x_r + \frac{1}{35}x_r x_r x_s x_s\right)\Big\} \\
\psi_{a,bc} - x_a\psi_{,bc} =& 4\pi\Big\{(\delta_{ab}x_c + \delta_{ac}x_b)\left(\frac{1}{15} - \frac{1}{35}x_r x_r\right) \\
&- 4x_a\delta_{bc}\left(\frac{1}{15} - \frac{1}{105}x_r x_r\right) + \frac{8}{105}x_a x_b x_c\Big\}.
\end{aligned} \tag{3.148}$$

We finally find that all the integrals are polynomials of $\boldsymbol{x}$. Adding the previously found expressions (3.143) for completeness, all the integrals defined by (3.140) are:

$$
\begin{aligned}
\boldsymbol{I}^{G0}(\boldsymbol{x}) =&|\mathcal{B}|\ \boldsymbol{G}^{\omega(0)},\\
\boldsymbol{I}^{H0}(\boldsymbol{x}) =&|\mathcal{B}|\left(\boldsymbol{I}_1^{H0}\cdot\boldsymbol{x}+\boldsymbol{I}_3^{H0}\bullet\boldsymbol{x}^{\otimes 3}\right),\\
\boldsymbol{I}^{\xi G0}(\boldsymbol{x}) =&\ \boldsymbol{0},\\
\boldsymbol{I}^{\xi H0}(\boldsymbol{x}) =&|\mathcal{B}|\left(\boldsymbol{I}_0^{\xi H0}+\boldsymbol{I}_2^{\xi H0}:\boldsymbol{x}^{\otimes 2}+\boldsymbol{I}_4^{\xi H0}\bullet\boldsymbol{x}^{\otimes 4}\right),\\
\boldsymbol{I}^{G1}(\boldsymbol{x}) =&|\mathcal{B}|\left(\boldsymbol{I}_0^{G1}+\boldsymbol{I}_2^{G1}:\boldsymbol{x}^{\otimes 2}+\boldsymbol{I}_4^{G1}\bullet\boldsymbol{x}^{\otimes 4}\right),\\
\boldsymbol{I}^{H1}(\boldsymbol{x}) =&|\mathcal{B}|\ \boldsymbol{I}_1^{H1}\cdot\boldsymbol{x},
\end{aligned}
\tag{3.149}
$$

and all the tensors-valued coefficients involved in these expressions can be computed from the formula given above. For the unit sphere, using (3.144) and (3.148), and since $|\mathcal{B}| = 4\pi/3$, we compute $\boldsymbol{I}^{H0}$ as:

$$
\begin{aligned}
I_{abc}^{H0}(\boldsymbol{x}) =& \frac{k_{\mathrm{S}}^2}{4\mu}\Big[\delta_{ab}x_c\left(\frac{7+3\beta^4}{15}-\frac{9+5\beta^4}{105}x_rx_r\right)\\
&\quad -(1-\beta^4)(x_a\delta_{bc}+\delta_{ac}x_b)\left(\frac{1}{5}-\frac{1}{21}x_rx_r\right)-\frac{4}{105}x_ax_bx_c\Big]\\
=& \frac{k_{\mathrm{S}}^2}{60\mu}\left[(7+3\beta^4)\delta_{ab}\delta_{ci}-3(1-\beta^4)(\delta_{ai}\delta_{bc}+\delta_{ac}\delta_{bi})\right]x_i\\
&-\frac{k_{\mathrm{S}}^2}{420\mu}\left[(9+5\beta^4)\delta_{ab}\delta_{ci}\delta_{jk}-5(1-\beta^4)(\delta_{ai}\delta_{bc}+\delta_{ac}\delta_{bi})\delta_{jk}+4\delta_{ai}\delta_{bj}\delta_{ck}\right]x_ix_jx_k\\
=& \frac{4\pi}{3}\left(\left[\boldsymbol{I}_1^{H0}\right]_{abci}x_i+\left[\boldsymbol{I}_3^{H0}\right]_{abcijk}x_ix_jx_k\right),
\end{aligned}
\tag{3.150}
$$

so that $\boldsymbol{I}_1^{H0}$ and $\boldsymbol{I}_3^{H0}$ are given by:

$$
\begin{aligned}
\boldsymbol{I}_1^{H0} &= \frac{k_{\mathrm{S}}^2}{80\pi\mu}\left[15(1+\beta^4)\boldsymbol{\mathcal{J}}-6(1-\beta^4)\boldsymbol{\mathcal{K}}\right],\\
\boldsymbol{I}_3^{H0} &= -\frac{k_{\mathrm{S}}^2}{560\pi\mu}\Big[\left[(17+25\beta^4)\boldsymbol{\mathcal{J}}-10(1-\beta^4)\boldsymbol{\mathcal{K}}\right]\otimes\boldsymbol{I}+4\boldsymbol{I}^{(6)}\Big].
\end{aligned}
\tag{3.151}
$$

3.B Higher-order derivatives of Green's tensors

This section gives a systematic method to compute higher derivatives of static and time-harmonic Green's tensors in full space and for isotropic material.

Green's tensors expressed as gradients of scalar functions. Kelvin's fundamental solution may be written as functions of r's derivatives as [Mura, 1982, Chap. I, Part. 5]:

$$\boldsymbol{G}_\infty(\boldsymbol{r}) = \frac{1}{16\pi\mu(1-\nu)}\left(\frac{4(1-\nu)}{r}\boldsymbol{I} - \boldsymbol{\nabla}^2 r\right). \tag{3.152}$$

Similarly, from [Chaillat et al., 2008], [Yoshida, 2001], Helmholtz' fundamental solution can also be written:

$$\begin{aligned} [\boldsymbol{G}^\omega_\infty(\boldsymbol{\xi}-\boldsymbol{x})]_{ij} &= \frac{1}{k_\mathrm{S}^2\mu}\left((\delta_{ab}\delta_{ij}-\delta_{aj}\delta_{ib})\frac{\partial}{\partial x_a}\frac{\partial}{\partial \xi_b}G(|\boldsymbol{\xi}-\boldsymbol{x}|;k_\mathrm{S}) + \frac{\partial}{\partial x_i}\frac{\partial}{\partial \xi_j}G(|\boldsymbol{\xi}-\boldsymbol{x}|;k_\mathrm{P})\right) \\ \text{i.e.}\quad [\boldsymbol{G}^\omega_\infty(\boldsymbol{r})]_{ij} &= -\frac{1}{k_\mathrm{S}^2\mu}\left((\delta_{ab}\delta_{ij}-\delta_{aj}\delta_{ib})G_{,ab}(r;k_\mathrm{S}) + G_{,ij}(r;k_\mathrm{P})\right), \end{aligned} \tag{3.153}$$

where $G(r;k) = e^{\mathrm{i}kr}/4\pi r$ and $G_{,a}$ denotes the differentiation with respect to r_a, having used $\boldsymbol{r} = \boldsymbol{\xi} - \boldsymbol{x}$ so $\boldsymbol{\nabla}_{\boldsymbol{r}} = \boldsymbol{\nabla}_{\boldsymbol{\xi}} = -\boldsymbol{\nabla}_{\boldsymbol{x}}$. We can therefore express the gradients of $\boldsymbol{G}_\infty(\boldsymbol{\xi}-\boldsymbol{x})$ and $\boldsymbol{G}^\omega_\infty(\boldsymbol{\xi}-\boldsymbol{x})$ with respect to $\boldsymbol{x}$ as:

$$\begin{aligned} \boldsymbol{\nabla}^n_{\boldsymbol{x}}\boldsymbol{G}_\infty(\boldsymbol{\xi}-\boldsymbol{x}) &= \frac{(-1)^n}{16\pi\mu(1-\nu)}\left(4(1-\nu)\boldsymbol{I}\otimes\boldsymbol{\nabla}^n_{\boldsymbol{r}}\frac{1}{r} - \boldsymbol{\nabla}^{n+2}_{\boldsymbol{r}} r\right) \\ \boldsymbol{\nabla}^n_{\boldsymbol{x}}\boldsymbol{G}^\omega_\infty(\boldsymbol{\xi}-\boldsymbol{x}) &= \frac{(-1)^{n+1}}{k_\mathrm{S}^2\mu}\left((3\boldsymbol{\mathcal{J}}-\boldsymbol{\mathcal{I}}) : \boldsymbol{\nabla}^{n+2}_{\boldsymbol{r}}G(r;k_\mathrm{S}) + \boldsymbol{\nabla}^{n+2}_{\boldsymbol{r}}G(r;k_\mathrm{P})\right) \end{aligned} \tag{3.154}$$

Remark 3.6. *In [Yoshida et al., 2001], Kelvin's fundamental solution is given only as a function of the derivatives of the distance* $r = |\boldsymbol{\xi}-\boldsymbol{x}|$*:*

$$\boldsymbol{G}_\infty(\boldsymbol{r}) = \frac{1}{8\pi\mu}\left(3\boldsymbol{\mathcal{J}} - \frac{1}{2(1-\nu)}\boldsymbol{\mathcal{I}}\right) : \boldsymbol{\nabla}^2_{\boldsymbol{r}} r, \tag{3.155}$$

which is a form closer to (3.153). *However, using* (3.152) *avoids additional inner products in numerical comptations.*

Expressions of gradients of a general scalar function. Recall that the tensors $\boldsymbol{k}^{p,q}(\boldsymbol{r})$ introduced in Section 1.1.1, with p even, are tensors of order $p+q$, invariant by any permutation of their indices, such that p indices are acounted into Kronecker's deltas, and the remaining q as $\boldsymbol{r}$'s components. The first ones of these tensors are:

$$\begin{aligned}
p+q=1: \quad & k^{0,1}_{k}(\boldsymbol{r}) = r_k \\
p+q=2: \quad & k^{2,0}_{kl}(\boldsymbol{r}) = \delta_{kl}, \\
& k^{0,2}_{kl}(\boldsymbol{r}) = r_k r_l \\
p+q=3: \quad & k^{2,1}_{klm}(\boldsymbol{r}) = \delta_{kl} r_m + \delta_{km} r_l + \delta_{lm} r_k \\
& k^{0,3}_{klm}(\boldsymbol{r}) = r_k r_l r_m \\
p+q=4: \quad & k^{4,0}_{klmn}(\boldsymbol{r}) = \delta_{kl}\delta_{mn} + \delta_{km}\delta_{ln} + \delta_{kn}\delta_{lm} \\
& k^{2,2}_{klmn}(\boldsymbol{r}) = \delta_{kl} r_m r_n + \delta_{km} r_l r_n + \delta_{kn} r_l r_m + \delta_{lm} r_k r_n + \delta_{ln} r_k r_m + \delta_{mn} r_k r_l \\
& k^{0,4}_{klmn}(\boldsymbol{r}) = r_k r_l r_m r_n
\end{aligned} \tag{3.156}$$

As mentioned earlier, these notations are not necessary for small orders since we have e.g. $\boldsymbol{k}^{0,q}(\boldsymbol{r}) = \boldsymbol{r}^{\otimes q}$ for any q, $\boldsymbol{k}^{2,0}(\boldsymbol{r}) = \boldsymbol{I}$ and $\boldsymbol{k}^{4,0}(\boldsymbol{r}) = 3\boldsymbol{\mathcal{J}} + 2\boldsymbol{\mathcal{I}} = 5\boldsymbol{\mathcal{J}} + 2\boldsymbol{\mathcal{K}}$, but emphasis the systematic differentiation properties $\boldsymbol{\nabla}\boldsymbol{k}^{p,1}(\boldsymbol{r}) = \boldsymbol{k}^{p+2,0}(\boldsymbol{r})$ and, for $q \geq 2$:

$$\boldsymbol{\nabla}\boldsymbol{k}^{p,q}(\boldsymbol{r}) = \boldsymbol{k}^{p+2,q-1}(\boldsymbol{r}) - \boldsymbol{k}^{p+2,q-2}(\boldsymbol{r}) \otimes \boldsymbol{r}, \tag{3.157}$$

and, differentiating $\boldsymbol{k}^{p,q}(\hat{\boldsymbol{r}})$ w.r.t. $\boldsymbol{r}$ (where $\hat{\boldsymbol{r}} = \boldsymbol{r}/r$), for $q \geq 2$,

$$\begin{aligned}
\boldsymbol{\nabla}_{\boldsymbol{r}}\boldsymbol{k}^{p,q}(\hat{\boldsymbol{r}}) &= \boldsymbol{\nabla}\boldsymbol{k}^{p,q}(\hat{\boldsymbol{r}}) \cdot \boldsymbol{\nabla}_{\boldsymbol{r}}\hat{\boldsymbol{r}} \\
&= \left(\boldsymbol{k}^{p+2,q-1}(\hat{\boldsymbol{r}}) - \boldsymbol{k}^{p+2,q-2}(\hat{\boldsymbol{r}}) \otimes \hat{\boldsymbol{r}}\right) \cdot \frac{1}{r}\left(\boldsymbol{I} - \hat{\boldsymbol{r}} \otimes \hat{\boldsymbol{r}}\right) \\
&= \frac{1}{r}\left(\boldsymbol{k}^{p+2,q-1}(\hat{\boldsymbol{r}}) - \boldsymbol{k}^{p+2,q-1}(\hat{\boldsymbol{r}}) \cdot (\hat{\boldsymbol{r}} \otimes \hat{\boldsymbol{r}})\right)
\end{aligned} \tag{3.158}$$

We can then express the gradients of any scalar function $f(r = |\boldsymbol{r}|)$ as functions of $\boldsymbol{k}^{p,q}(\hat{\boldsymbol{r}})$, as showed below.

$$
\begin{aligned}
\boldsymbol{\nabla}_{\boldsymbol{r}} f(r) &= f'(r)\hat{\boldsymbol{r}} \\
\boldsymbol{\nabla}_{\boldsymbol{r}}^2 f(r) &= \frac{f'(r)}{r}\boldsymbol{I} + \left(f''(r) - \frac{f'(r)}{r}\right)\hat{\boldsymbol{r}}^{\otimes 2} \\
\boldsymbol{\nabla}_{\boldsymbol{r}}^3 f(r) &= \left(\frac{f''(r)}{r} - \frac{f'(r)}{r^2}\right)\boldsymbol{k}^{2,1}(\hat{\boldsymbol{r}}) + \left(f^{(3)}(r) - 3\frac{f''(r)}{r} + 3\frac{f'(r)}{r^2}\right)\hat{\boldsymbol{r}}^{\otimes 3} \\
\boldsymbol{\nabla}_{\boldsymbol{r}}^4 f(r) &= \left(\frac{f''(r)}{r^2} - \frac{f'(r)}{r^3}\right)(5\boldsymbol{\mathcal{J}} + 2\boldsymbol{\mathcal{K}}) + \left(\frac{f^{(3)}(r)}{r} - 3\frac{f''(r)}{r^2} + 3\frac{f'(r)}{r^3}\right)\boldsymbol{k}^{2,2}(\hat{\boldsymbol{r}}) \\
&\quad + \left(f^{(4)}(r) - 6\frac{f^{(3)}(r)}{r} + 15\frac{f''(r)}{r^2} - 15\frac{f'(r)}{r^3}\right)\hat{\boldsymbol{r}}^{\otimes 4} \\
\boldsymbol{\nabla}_{\boldsymbol{r}}^5 f(r) &= \left(\frac{f^{(3)}(r)}{r^2} - 3\frac{f''(r)}{r^3} + 3\frac{f'(r)}{r^4}\right)\boldsymbol{k}^{4,1}(\hat{\boldsymbol{r}}) \\
&\quad + \left(\frac{f^{(4)}(r)}{r} - 6\frac{f^{(3)}(r)}{r^2} + 15\frac{f''(r)}{r^3} - 15\frac{f'(r)}{r^4}\right)\boldsymbol{k}^{2,3}(\hat{\boldsymbol{r}}) \\
&\quad + \left(f^{(5)}(r) - 10\frac{f^{(4)}(r)}{r} + 45\frac{f^{(3)}(r)}{r^2} - 105\frac{f''(r)}{r^3} + 105\frac{f'(r)}{r^4}\right)\hat{\boldsymbol{r}}^{\otimes 5} \\
\boldsymbol{\nabla}_{\boldsymbol{r}}^6 f(r) &= \left(\frac{f^{(3)}(r)}{r^3} - 3\frac{f''(r)}{r^4} + 3\frac{f'(r)}{r^5}\right)\boldsymbol{k}^{6,0}(\hat{\boldsymbol{r}}) \\
&\quad + \left(\frac{f^{(4)}(r)}{r^2} - 6\frac{f^{(3)}(r)}{r^3} + 15\frac{f''(r)}{r^4} - 15\frac{f'(r)}{r^5}\right)\boldsymbol{k}^{4,2}(\hat{\boldsymbol{r}}) \\
&\quad + \left(\frac{f^{(5)}(r)}{r} - 10\frac{f^{(4)}(r)}{r^2} + 45\frac{f^{(3)}(r)}{r^3} - 105\frac{f''(r)}{r^4} + 105\frac{f'(r)}{r^5}\right)\boldsymbol{k}^{2,4}(\hat{\boldsymbol{r}}) \\
&\quad + \left(f^{(6)}(r) - 15\frac{f^{(5)}(r)}{r} + 105\frac{f^{(4)}(r)}{r^2} - 420\frac{f^{(3)}(r)}{r^3} + 945\frac{f''(r)}{r^4} - 945\frac{f'(r)}{r^5}\right)\hat{\boldsymbol{r}}^{\otimes 6}
\end{aligned}
\tag{3.159}
$$

Expressions of the gradients of the required fundamental solutions. The gradients of the biharmonic fundamental solution $G(\boldsymbol{r}) = r$ are therefore:

$$
\begin{aligned}
\boldsymbol{\nabla}_{\boldsymbol{r}} r &= \hat{\boldsymbol{r}}, \\
\boldsymbol{\nabla}_{\boldsymbol{r}}^2 r &= \frac{1}{r}\left(\boldsymbol{I} - \hat{\boldsymbol{r}}^{\otimes 2}\right), \\
\boldsymbol{\nabla}_{\boldsymbol{r}}^3 r &= \frac{1}{r^2}\left(-\boldsymbol{k}^{2,1}(\hat{\boldsymbol{r}}) + 3\hat{\boldsymbol{r}}^{\otimes 3}\right), \\
\boldsymbol{\nabla}_{\boldsymbol{r}}^4 r &= \frac{1}{r^3}\left(-(5\boldsymbol{\mathcal{J}} + 2\boldsymbol{\mathcal{K}}) + 3\boldsymbol{k}^{2,2}(\hat{\boldsymbol{r}}) - 15\hat{\boldsymbol{r}}^{\otimes 4}\right), \\
\boldsymbol{\nabla}_{\boldsymbol{r}}^5 r &= \frac{1}{r^4}\left(3\boldsymbol{k}^{4,1}(\hat{\boldsymbol{r}}) - 15\boldsymbol{k}^{2,3}(\hat{\boldsymbol{r}}) + 105\hat{\boldsymbol{r}}^{\otimes 5}\right), \\
\boldsymbol{\nabla}_{\boldsymbol{r}}^6 r &= \frac{1}{r^5}\left(3\boldsymbol{k}^{6,0}(\hat{\boldsymbol{r}}) - 15\boldsymbol{k}^{4,2}(\hat{\boldsymbol{r}}) + 105\boldsymbol{k}^{2,4}(\hat{\boldsymbol{r}}) - 945\hat{\boldsymbol{r}}^{\otimes 6}\right).
\end{aligned}
\tag{3.160}
$$

The gradients of the harmonic fundamental solution $G(\boldsymbol{r}) = 1/r$ are:

$$
\begin{aligned}
\boldsymbol{\nabla}_{\boldsymbol{r}} \frac{1}{r} &= \frac{1}{r^2}(-\hat{\boldsymbol{r}}), \\
\boldsymbol{\nabla}^2_{\boldsymbol{r}} \frac{1}{r} &= \frac{1}{r^3}\left(-\boldsymbol{I} + 3\hat{\boldsymbol{r}}^{\otimes 2}\right), \\
\boldsymbol{\nabla}^3_{\boldsymbol{r}} \frac{1}{r} &= \frac{1}{r^4}\left(3\boldsymbol{k}^{2,1}(\hat{\boldsymbol{r}}) - 15\hat{\boldsymbol{r}}^{\otimes 3}\right), \\
\boldsymbol{\nabla}^4_{\boldsymbol{r}} \frac{1}{r} &= \frac{1}{r^5}\left(3(5\boldsymbol{\mathcal{J}} + 2\boldsymbol{\mathcal{K}}) - 15\boldsymbol{k}^{2,2}(\hat{\boldsymbol{r}}) + 105\hat{\boldsymbol{r}}^{\otimes 4}\right), \\
\boldsymbol{\nabla}^5_{\boldsymbol{r}} \frac{1}{r} &= \frac{1}{r^6}\left(-15\boldsymbol{k}^{4,1}(\hat{\boldsymbol{r}}) + 105\boldsymbol{k}^{2,3}(\hat{\boldsymbol{r}}) - 945\hat{\boldsymbol{r}}^{\otimes 5}\right), \\
\boldsymbol{\nabla}^6_{\boldsymbol{r}} \frac{1}{r} &= \frac{1}{r^7}\left(-15\boldsymbol{k}^{6,0}(\hat{\boldsymbol{r}}) + 105\boldsymbol{k}^{4,2}(\hat{\boldsymbol{r}}) - 945\boldsymbol{k}^{2,4}(\hat{\boldsymbol{r}}) + 10935\hat{\boldsymbol{r}}^{\otimes 6}\right).
\end{aligned}
\tag{3.161}
$$

The gradients of the fundamental solution of Helmholtz equation $G(\boldsymbol{r};k) = e^{ikr}/4\pi r$ are, noting $x := kr$:

$$
\begin{aligned}
\boldsymbol{\nabla}_{\boldsymbol{r}} G(r;k) &= \frac{e^{\mathrm{i}x}}{4\pi r^2}(\mathrm{i}x - 1)\hat{\boldsymbol{r}}, \\
\boldsymbol{\nabla}^2_{\boldsymbol{r}} G(r;k) &= \frac{e^{\mathrm{i}x}}{4\pi r^3}\Big[(\mathrm{i}x-1)\boldsymbol{I} - \left(3(\mathrm{i}x-1) + x^2\right)\hat{\boldsymbol{r}}^{\otimes 2}\Big], \\
\boldsymbol{\nabla}^3_{\boldsymbol{r}} G(r;k) &= \frac{e^{\mathrm{i}x}}{4\pi r^4}\Big[- \left(3(\mathrm{i}x-1) + x^2\right)\boldsymbol{k}^{2,1}(\hat{\boldsymbol{r}}) + \left(15(\mathrm{i}x-1) + 6x^2 - \mathrm{i}x^3\right)\hat{\boldsymbol{r}}^{\otimes 3}\Big], \\
\boldsymbol{\nabla}^4_{\boldsymbol{r}} G(r;k) &= \frac{e^{\mathrm{i}x}}{4\pi r^5}\Big[- \left(3(\mathrm{i}x-1) + x^2\right)(5\boldsymbol{\mathcal{J}} + 2\boldsymbol{\mathcal{K}}) + \left(15(\mathrm{i}x-1) + 6x^2 - \mathrm{i}x^3\right)\boldsymbol{k}^{2,2}(\hat{\boldsymbol{r}}) \\
&\qquad - \left(105(\mathrm{i}x-1) + 45x^2 - 10\mathrm{i}x^3 - x^4\right)\hat{\boldsymbol{r}}^{\otimes 4}\Big], \\
\boldsymbol{\nabla}^5_{\boldsymbol{r}} G(r;k) &= \frac{e^{\mathrm{i}x}}{4\pi r^6}\Big[- \left(15(\mathrm{i}x-1) + 6x^2 - \mathrm{i}x^3\right)\boldsymbol{k}^{4,1}(\hat{\boldsymbol{r}}) \\
&\qquad - \left(105(\mathrm{i}x-1) + 45x^2 - 10\mathrm{i}x^3 - x^4\right)\boldsymbol{k}^{2,3}(\hat{\boldsymbol{r}}) \\
&\qquad + \left(945(\mathrm{i}x-1) + 420x^2 - 105\mathrm{i}x^3 - 15x^4 + \mathrm{i}x^5\right)\hat{\boldsymbol{r}}^{\otimes 5}\Big], \\
\boldsymbol{\nabla}^6_{\boldsymbol{r}} G(r;k) &= \frac{e^{\mathrm{i}x}}{4\pi r^7}\Big[- \left(15(\mathrm{i}x-1) + 6x^2 - \mathrm{i}x^3\right)\boldsymbol{k}^{6,0}(\hat{\boldsymbol{r}}) \\
&\qquad - \left(105(\mathrm{i}x-1) + 45x^2 - 10\mathrm{i}x^3 - x^4\right)\boldsymbol{k}^{4,2}(\hat{\boldsymbol{r}}) \\
&\qquad + \left(945(\mathrm{i}x-1) + 420x^2 - 105\mathrm{i}x^3 - 15x^4 + \mathrm{i}x^5\right)\boldsymbol{k}^{2,4}(\hat{\boldsymbol{r}}) \\
&\qquad - \left(10395(\mathrm{i}x-1) + 4725x^2 - 1260\mathrm{i}x^3 - 210x^4 + 21\mathrm{i}x^5 + x^6\right)\hat{\boldsymbol{r}}^{\otimes 6}\Big].
\end{aligned}
\tag{3.162}
$$

Part II

Homogenization of a one-dimensional interior transmission problem to identify a microstructured inclusion

Chapter 4

Second-order homogenization of 1D boundary-value problems

Contents

The purpose of this chapter is to set the framework for the homogenized models used in Chapter 5. We begin by recalling in Section 4.1 recent results on higher-order two-scale homogenization for unbounded 1D periodic structures [Fish et al., 2002; Andrianov et al., 2008; Wautier & Guzina, 2015]. We then exploit the specificity of this one-dimensional case to propose local boundary conditions, expanding these results to bounded domains. Finally, the full procedure is illustrated for a layered two-phase periodic medium, for which this homogenization process, and in particular the computation of the featured cell functions, are performed analytically.

4.1 Higher-order two-scale homogenization

Here, we provide the necessary background on higher-order two-scale homogenization. We focus on the 1D time-harmonic problem, the interested reader being invited to refer to the books [Bensoussan et al., 1978; Cioranescu & Donato, 1999] for general two-scale homogenization and to [Wautier & Guzina, 2015] and the references therein for the transient time-domain case.

Consider an elastic medium characterized by the periodic Young's modulus $E_{\rm p}$ and density $\rho_{\rm p}$ varying in the x-direction with period ℓ. These coefficients satisfy physical boundedness properties:

$$0 < E_{\min} \leq E_{\rm p}(x) \leq E_{\max} < \infty \quad \text{and} \quad 0 < \rho_{\min} \leq \rho_{\rm p}(x) \leq \rho_{\max} < \infty \tag{4.1}$$

In the time-harmonic regime with circular frequency ω, the longitudinal displacement $u^{\rm p}$ in a rod with constant section and composed of such a material satisfies:

$$\left(E_{\rm p} u^{\rm p}{}_{,x}\right)_{,x} + \rho_{\rm p}\omega^2 u^{\rm p} = 0, \tag{4.2}$$

where $f_{,x} = \partial f/\partial x$ and the excitation (to be specified later on) is provided by prescribed time-harmonic boundary displacements and/or tractions.

Throughout this chapter and the following one, we also use some "reference" properties (E, ρ), together with the reference wave speed c, wavelength λ and wavenumber k that are defined by:

$$c = \sqrt{\frac{E}{\rho}}, \quad \lambda = \frac{c}{2\pi\omega} \quad \text{and} \quad k = \frac{\omega}{c}. \tag{4.3}$$

We then assume that the period ℓ is much smaller than λ, and therefore we define a small parameter ε as:

$$\varepsilon = \frac{\ell}{\lambda} = \frac{k\ell}{2\pi} \ll 1. \tag{4.4}$$

Remark 4.1. *The "reference" properties may be chosen to be e.g. (i) $(E, \rho) = (E_{\min}, \rho_{\max})$ so that λ is an upper bound to all wavlengths $\lambda_{\rm p}(x)$ encoutered in the material:*

$$\lambda_{\rm p}(x) = \frac{c_{\rm j}(x)}{2\pi\omega} = \frac{1}{2\pi\omega}\sqrt{\frac{E_{\rm p}(x)}{\rho_{\rm p}(x)}} \geq \frac{1}{2\pi\omega}\sqrt{\frac{E_{\min}}{\rho_{\max}}} = \lambda \quad \textit{and} \quad \frac{\ell}{\lambda_{\rm p}(x)} \leq \varepsilon \ll 1 \quad \forall x \tag{4.5}$$

or (ii) the properties of a "reference" homogeneous medium, typically these of a background medium when dealing with a transmission problem that involves a microstructured obstacle.

4.1.1 Two-scale expansion

The key idea of the two-scale homogenization is to introduce a *fast space variable* y and accordingly a scaled cell size $\hat{\ell}$ as:

$$y = \frac{x}{\varepsilon} \qquad \text{and} \qquad \hat{\ell} = \frac{\ell}{\varepsilon}. \tag{4.6}$$

We then write the periodic coefficients in terms of $\hat{\ell}$-periodic functions $(\hat{E}, \hat{\rho})$ as $E_{\rm p}(x) = \hat{E}(x/\varepsilon)$ and $\rho_{\rm p}(x) = \hat{\rho}(x/\varepsilon)$, while the displacement is sought as a function of both variables x and y, i.e. $u^{\rm p}(x) = \hat{u}(x, x/\varepsilon)$, so that $\hat{u}$ is $\hat{\ell}$-periodic in its second argument y. We introduce the differential and averaging operators:

$$\frac{d}{dx} = \frac{\partial}{\partial x} + \varepsilon^{-1}\frac{\partial}{\partial y} \quad \text{and} \quad \langle f \rangle = \frac{1}{\hat{\ell}}\int_0^{\hat{\ell}} f(y)\,\mathrm{d}y. \tag{4.7}$$

Inserting all these ingredients into the time-harmonic wave equation (4.2) and ordering the contributions along increasing powers of ε entails:

$$\varepsilon^{-2}\left(\hat{E}\hat{u}_{,y}\right)_{,y} + \varepsilon^{-1}\left[\left(\hat{E}\hat{u}_{,x}\right)_{,y} + \left(\hat{E}\hat{u}_{,y}\right)_{,x}\right] + \hat{E}\hat{u}_{,xx} + \hat{\rho}\omega^2\hat{u} = 0. \tag{4.8}$$

The displacement $\hat{u}$ is then sought as an expansion in powers of ε, and we note $u^{(p)}$ the restriction of this sum to the $p+1$ first terms:

$$\hat{u}(x,y) = \sum_{j\geq 0} \varepsilon^j u_j(x,y) \quad \text{and} \quad u^{(p)}(x) = \sum_{j=0}^{p} \varepsilon^j u_j\left(x, \frac{x}{\varepsilon}\right). \tag{4.9}$$

Inserting (4.9) into (4.8) leads to a cascade of partial differential equations for the u_j's. Solving these equations (which is not addressed here) yields separated-variable solutions:

$$\begin{aligned}
u_0(x,y) &= U_0(x) \\
u_1(x,y) &= U_1(x) + U_{0,x}(x)P_1(y) \\
u_2(x,y) &= U_2(x) + U_{1,x}(x)P_1(y) + U_{0,xx}(x)P_2(y) \\
u_3(x,y) &= U_3(x) + U_{2,x}(x)P_1(y) + U_{1,xx}(x)P_2(y) + U_{0,xxx}(x)P_3(y).
\end{aligned} \tag{4.10}$$

in terms of (i) *mean fields* terms U_j defined by

$$U_j(x) := \langle u_j(x,\cdot)\rangle \tag{4.11}$$

and (ii) the so-called *cell functions* P_j which are addressed in detail below.

Remark 4.2. *The cell functions are noted P, Q, R ... in [Wautier & Guzina, 2015] and often χ^i, χ^{ij} ... in other references [Bensoussan et al., 1978] for higher-dimensional problems. Indeed, in the latter case the j-th cell function is a j-th order tensor-valued function.*

Cell functions and homogenized coefficients: The first three cell functions P_1, P_2 and P_3 are solutions of the *cell problems* consisting of the differential equations:

$$\begin{aligned}
\left[\hat{E}(1+P_{1,y})\right]_{,y} &= 0 \\
\left[\hat{E}(P_1+P_{2,y})\right]_{,y} &= -\hat{E}(1+P_{1,y}) + \hat{\rho}\frac{\mathcal{E}_0}{\varrho_0} \\
\left[\hat{E}(P_2+P_{3,y})\right]_{,y} &= -\hat{E}(P_1+P_{2,y}) + \hat{\rho}P_1\frac{\mathcal{E}_0}{\varrho_0}
\end{aligned} \tag{4.12}$$

for $y \in]0,\hat{\ell}[$ together with the requirements

$$\langle P_j\rangle = 0, \quad P_j \text{ is } \hat{\ell}\text{-periodic} \quad (j=1,2,3). \tag{4.13}$$

where we set $P_0 = 1$. The homogenized coefficients $\mathcal{E}_0$ and ϱ_0 that appear in (4.12), and their higher-order counterparts $\mathcal{E}_j$ and ϱ_j are given by:

$$\mathcal{E}_j = \left\langle \hat{E}\left(P_j + P_{j+1,y}\right)\right\rangle \quad \text{and} \quad \varrho_j = \langle\hat{\rho}P_j\rangle. \tag{4.14}$$

Recall the classical result for $\mathcal{E}_0$ in 1D: $\mathcal{E}_0$ can be shown to be in fact the harmonic mean of $\hat{E}$, i.e.

$$\mathcal{E}_0 = \left\langle \hat{E}^{-1}\right\rangle^{-1}. \tag{4.15}$$

We also assert a very useful property, that is not frequently encountered but which is also valid without any additional assumption on $\hat{E}$ and $\hat{\rho}$:

Lemma 4.1. *The leading-order and first-order homogenized coefficients* $(\mathcal{E}_0, \varrho_0)$ *and* $(\mathcal{E}_1, \varrho_1)$ *satisfy:*

$$\mathcal{E}_1 = \frac{\mathcal{E}_0}{\varrho_0} \varrho_1. \tag{4.16}$$

Proof. Consider the weak form of the first two cell problems (4.12):

$$\text{Find } P_j \in \mathcal{V}, \quad \int_0^{\hat{\ell}} \hat{E} P_{j,y} w_{,y} = F_j(w) \quad \forall w \in \mathcal{V}, \tag{4.17}$$

with $\mathcal{V} = \{w \in H^1(]0, \hat{\ell}[),\ \langle w \rangle = 0, w \text{ is } \hat{\ell}\text{-periodic}\}$, and where:

$$F_1(w) = -\int_0^{\hat{\ell}} \hat{E} w_{,y}, \quad F_2(w) = -\int_0^{\hat{\ell}} \hat{E} P_1 w_{,y} + \int_0^{\hat{\ell}} \hat{E}\left(1 + P_{1,y}\right) w - \frac{\mathcal{E}_0}{\varrho_0} \int_0^{\hat{\ell}} \hat{\rho} w. \tag{4.18}$$

Setting $w = P_2$ in (4.17) for $j = 1$, and $w = P_1$ for $j = 2$, then owing to the symmetry of the left-hand side of (4.17), we obtain $F_1(P_2) = F_2(P_1)$, which leads after some simplifications to:

$$\int_0^{\hat{\ell}} \hat{E}\left(P_1 + P_{2,y}\right) - \frac{\mathcal{E}_0}{\varrho_0} \int_0^{\hat{\ell}} \hat{\rho} P_1 = 0. \tag{4.19}$$

Recalling the definition (4.14) of $(\mathcal{E}_1, \varrho_1)$ then (4.19) is exactly the desired relation (4.16). □

Remark 4.3. *Lemma 4.1 asserts in fact the simplest particular case of a more general family of relations relating the homogenized coefficients at different orders. These relations can be obtained similarly by exploiting reciprocity relations that arise from the weak formulations of the cell problems. Such relations are known from [Moskow & Vogelius, 1997] and also occur in higher dimensions [Bonnet, 2016a].*

Cell stresses and stress expansion. For convenience, we also define the *cell stresses* Σ_j as:

$$\Sigma_j := \hat{E}\left(P_{j_1} + P_{j,y}\right). \tag{4.20}$$

The cell stress are also $\hat{\ell}$-periodic functions and by definition of the homogenized Young's moduli (4.14) one has:

$$\langle \Sigma_j \rangle = \mathcal{E}_{j-1}. \tag{4.21}$$

The notation (4.20) is introduced so that computing the total derivative of the expansion (4.10) of $\hat{u}$ leads to a similar expansion for the stress:

$$\hat{E}(y)\frac{d}{dx}\hat{u}(x,y) = U_{,x}^{(2)}(x)\Sigma_1(y) + \varepsilon U_{,xx}^{(1)}(x)\Sigma_2(y) + \varepsilon^2 U_{0,xxx}(x)\Sigma_3(y) + O(\varepsilon^3). \tag{4.22}$$

Mean fields and homogenized equations. Once the cell functions defined above are known, determining u_j for $j = 0...2$ requires to determine the mean fields U_j. Once again introducing the expansion (4.9) into the wave equation (4.8), and averaging the equations of order $O(\varepsilon^j)$ for

$j = 0...2$ w.r.t. the fast variable y, leads to a cascade of "macroscopic" or "mean" equations that are written by analogy as:

$$\begin{aligned} O(1): &\quad \mathcal{E}_0 U_{0,xx} + \varrho_0 \omega^2 U_0 = 0, \\ O(\varepsilon): &\quad \mathcal{E}_0 U_{1,xx} + \varrho_0 \omega^2 U_1 + \mathcal{E}_1 U_{0,xxx} + \varrho_1 \omega^2 U_{0,x} = 0, \\ O(\varepsilon^2): &\quad \mathcal{E}_0 U_{2,xx} + \varrho_0 \omega^2 U_2 + \mathcal{E}_1 U_{1,xxx} + \varrho_1 \omega^2 U_{1,x} + \mathcal{E}_2 U_{0,xxxx} + \varrho_2 \omega^2 U_{0,xx} = 0. \end{aligned} \tag{4.23}$$

However, Lemma 4.1 permits to recursively cancel the terms involving $(\mathcal{E}_1, \varrho_1)$ in these equations. Indeed, in the $O(\varepsilon)$ equation, one has

$$\mathcal{E}_1 U_{0,xxx} + \varrho_1 \omega^2 U_{0,x} = \frac{\varrho_1}{\varrho_0} \left(\mathcal{E}_0 U_{0,xx} + \varrho_0 \omega^2 U_0 \right)_{,x} = 0. \tag{4.24}$$

and the same simplification occurs for U_1 in the $O(\varepsilon^2)$ equation. Eventually, by introducing the notations:

$$c_0 = \sqrt{\frac{\mathcal{E}_0}{\varrho_0}}, \qquad k_0 = \frac{\omega}{c_0} = \omega \sqrt{\frac{\varrho_0}{\mathcal{E}_0}} \qquad \text{and} \qquad n = \frac{k_0^2}{k^2} = \frac{E \varrho_0}{\rho \mathcal{E}_0}, \tag{4.25}$$

and dividing the equations (4.23) by $\mathcal{E}_0$, we obtain:

$$\begin{aligned} O(1): &\quad U_{0,xx} + nk^2 U_0 = 0, \\ O(\varepsilon): &\quad U_{1,xx} + nk^2 U_1 = 0, \\ O(\varepsilon^2): &\quad U_{2,xx} + nk^2 U_2 + \frac{\mathcal{E}_2}{\mathcal{E}_0} U_{0,xxxx} + \frac{\varrho_2}{\varrho_0} nk^2 U_{0,xx} = 0. \end{aligned} \tag{4.26}$$

Similarly to (4.9), we define the pth-order mean field $U^{(p)}$ as the finite sum of the $\varepsilon^j U_j$'s. In particular the first and second-order mean fields are:

$$\begin{aligned} U^{(1)}(x) &:= (U_0 + \varepsilon U_1)(x) = U_0(x) + \varepsilon \langle u_1(x, \cdot) \rangle, \\ U^{(2)}(x) &:= \sum_{j=0}^{2} \varepsilon^j U_j(x) = \left\langle \sum_{j=0}^{2} \varepsilon^j u_j(x, \cdot) \right\rangle. \end{aligned} \tag{4.27}$$

We then derive the field equations that are satisfied by these fields. The equation for U_0 is given by (4.23). For $U^{(1)}$, adding the first two equations of (4.26) yields in fact the same equation, i.e.:

$$U^{(1)}_{,xx} + nk^2 U^{(1)} = 0. \tag{4.28}$$

Similarly, for $U^{(2)}$, we add the equations (4.26) so that the averaged original equation is approximated with an $O(\varepsilon^3)$ error by:

$$U^{(2)}_{,xx} + nk^2 U^{(2)} + \varepsilon^2 \left[\frac{\mathcal{E}_2}{\mathcal{E}_0} U_{0,xxxx} + \frac{\varrho_2}{\varrho_0} nk^2 U_{0,xx} \right] = 0. \tag{4.29}$$

Furthermore, (i) the $O(1)$ equation $U_{0,xx} = -nk^2 U_0$ permits to permute the fourth, second and zero-th order derivatives of U_0 in the $O(\varepsilon^2)$ term, and (ii) noting that $U_0 = U^{(2)} + O(\varepsilon)$ allows to replace U_0 by $U^{(2)}$ in (4.29) while keeping an $O(\varepsilon^3)$ residual. Eventually, we obtain a *family* of mean second-order equations:

$$U^{(2)}_{,xx} + nk^2 U^{(2)} + \ell^2 \left(\beta_x U^{(2)}_{,xxxx} + \beta_m nk^2 U^{(2)}_{,xx} - \beta_t n^2 k^4 U^{(2)} \right) = 0, \tag{4.30}$$

where β_x, β_m and β_t are some user-chosen parameters satisfying:

$$\beta_x - \beta_m - \beta_t = \beta := \frac{\varepsilon^2}{\ell^2}\left[\frac{\mathcal{E}_2}{\mathcal{E}_0} - \frac{\varrho_2}{\varrho_0}\right]. \tag{4.31}$$

This family of equations can be reordered along decreasing orders of spatial derivatives:

$$\beta_x \ell^2 U^{(2)}_{,xxxx} + \left(1 + \beta_m n k^2 \ell^2\right) U^{(2)}_{,xx} + nk^2 \left(1 - \beta_t n k^2 \ell^2\right) U^{(2)} = 0, \tag{4.32}$$

The choice of the signs and indexes for β_x, β_m and β_t in (4.30) and (4.31) comes from the time-domain counterpart of (4.2) studied in [Wautier & Guzina, 2015], whose homogenization procedure results in fourth-order "space", "mixed" and "time" derivatives.

Note also that β is defined so that the dependency on ε in (4.32) is implicit, while the role of three new *length scales* $\sqrt{\beta_\alpha}\ell$ for $\alpha \in \{x, m, t\}$ is emphasized. In fact, it shows that the homogenization process permits to obtain such models involving higher-order derivatives and associated additional length scales and known since long as *gradient elasticity models* introduced by [Mindlin & Eshel, 1968]. We refer to the review [Askes & Aifantis, 2011] for further details on these models and their histories.

The simplest members of the family (4.32) are obtained by canceling two of the three parameters $(\beta_x, \beta_m, \beta_t)$. They will be referred to as the "space", "mixed" and "time" models and denoted respectively by (x), (m) and (t):

$$\begin{aligned}
&(x) \quad \ell^2 \beta U^{(2)}_{,xxxx} + U^{(2)}_{,xx} + nk^2 U^{(2)} = 0, \\
&(m) \quad U^{(2)}_{,xx} + n_m(k) k^2 U^{(2)} = 0 \quad \text{with } n_m(k) := \frac{n}{1 - nk^2\ell^2\beta}, \\
&(t) \quad U^{(2)}_{,xx} + n_t(k) k^2 U^{(2)} = 0 \quad \text{with } n_t(k) := n\left(1 + nk^2\ell^2\beta\right).
\end{aligned} \tag{4.33}$$

Similarly, the models retaining two of these parameters (i.e. canceling only one of them) will be denoted as (mt), (xt) and (xm), for instance:

$$(mt) \qquad U^{(2)}_{,xx} + n_{mt}(k) k^2 U^{(2)} = 0 \quad \text{with } n_{mt}(k) := \frac{n\left(1 - nk^2\ell^2\beta_t\right)}{1 + nk^2\ell^2\beta_m} \text{ and } \beta_m + \beta_t = \beta \tag{4.34}$$

while (xmt) designates the family of models retaining all of the three parameters. Some of these models and their relevance in terms of the approximation of the dispersive behavior of the structure will be addressed in Section 4.2 for a specific periodic medium.

4.1.2 Boundary value problem and boundary conditions

To introduce appropriate boundary conditions completing the mean field equations (4.28) and (4.32), we now investigate the solutions of a boundary value problem (BVP) modeling a rod that is clamped at $x = 0$ and submitted to (i) time-harmonic axial volumic forces with amplitude f on $[0, L]$ and (ii) time-harmonic axial traction with amplitude $t_L = Eku_L$ at $x = L$ (so that u_L has the dimension of a displacement). The problem reads:

$$\left|\begin{array}{ll}
\left(E_\mathrm{p} u^\mathrm{p}{}_{,x}\right)_{,x} + \rho_\mathrm{p}\omega^2 u^\mathrm{p} + f = 0 & x \in [0, L] \\
u^\mathrm{p} = 0 & x = 0 \\
E_\mathrm{p} u^\mathrm{p}{}_{,x} = Eku_L & x = L
\end{array}\right. \tag{4.35}$$

where $E_{\mathrm{p}}(x) = \hat{E}(x/\varepsilon)$ and $\rho_{\mathrm{p}}(x) = \hat{\rho}(x/\varepsilon)$. Then u^{p} satisfies the variational equation:

$$a_{\mathrm{p}}(u^{\mathrm{p}}, v) = F(v) \quad \forall v \in V \tag{4.36}$$

with

$$V = \{v \in H^1(]0, L[);\ v(0) = 0\} \tag{4.37}$$

and

$$a_{\mathrm{p}}(u, v) = \int_0^L E_{\mathrm{p}} u_{,x} v_{,x} - \omega^2 \int_0^L \rho_{\mathrm{p}} uv \quad \text{and} \quad F(v) = Eku_L v(L) + \int_0^L fv. \tag{4.38}$$

It is known (see e.g. [McLean, 2000, Thm. 4.2] or adapt [Brezis, 2011, Thm. 8.22] to the present setting) that the homogeneous counterpart of (4.35) (i.e. with $u_L = 0$) has an infinite set of positive real eigenvalues $\lambda_j = \omega_j^2 > 0$ such that $\lambda_j \to +\infty$ as $j \to +\infty$. Assuming that $\omega \neq \omega_j$, therefore (4.35) admits at most one solution. Moreover, owing to the bounds (4.1) on $(E_{\mathrm{p}}, \rho_{\mathrm{p}})$, a_{p} satisfies the Gårding inequality:

$$\left|a_{\mathrm{p}}(u, u) + 2\omega^2 \rho_{\max} \|u\|_0\right| \geq \min(E_{\min}, \omega^2 \rho_{\max}) \|u\|_1 \tag{4.39}$$

where here and thereafter $\|\cdot\|_p = \|\cdot\|_{H^p(]0,L[)}$, in particular $\|\cdot\|_0 = \|\cdot\|_{L^2(]0,L[)}$.

From (4.39), the classical Fredholm theory ensures that (4.36) is uniquely solvable, i.e. the inverse operator noted $A_{\mathrm{p}}^{-1} : (u_L, f) \mapsto u$ exists. Moreover, a_{p} being bounded, by the bounded inverse theorem, this inverse operator is bounded, so that the following stability result holds:

$$\exists C > 0, \qquad \|u^{\mathrm{p}}\|_1 \leq C \left(Ek|u_L| + \|f\|_0\right), \tag{4.40}$$

where the constant C depends on the bounds of E_{p} and ρ_{p} and on the frequency ω but not on the period ℓ (and therefore not on ε for a given ω).

Remark 4.4. *The problem* (4.35) *is written with both internal forces and boundary tractions for generality and for latter use of the stability result* (4.40)*, but we will consider $f = 0$ from now on for simplicity.*

Discussion on boundary conditions. In a general multi-dimensional setting, deriving appropriate boundary conditions for higher-order homogenized models in a domain $\Omega \subset \mathbb{R}^d$, $d \geq 2$ is a complex problem that is still an active research topic, see e.g. the nice introduction of the recent paper [Gérard-Varet & Masmoudi, 2012].

Indeed, while taking in account higher-order terms (typically $u_1(x, x/\varepsilon)$) in the two-scale expansion, one has to deal with the oscillating behavior of the trace of these terms on $\partial\Omega$. Rigorous convergence analysis is therefore possible by introducing additional functions in the expansion: the *boundary correctors* θ_j^ε, which were introduced in [Santosa & Vogelius, 1993; Moskow & Vogelius, 1997] and studied subsequently by e.g. [Allaire & Amar, 1999] and more recently [Gérard-Varet & Masmoudi, 2012; Onofrei & Vernescu, 2012; Prange, 2013] among many others.

However, these correctors are solutions of problems posed on the *periodic* (and not the homogenized) medium, and a separate asymptotic procedure is required to provide effective boundary conditions for the problems involving the mean fields. In particular, since [Santosa & Vogelius, 1993] it is shown that for polygonal domains with rational slopes, *including one-dimensional problems as a particular case*, the limit θ_j^* of θ_j^ε may not be unique and depends on the sequence of ε_k's chosen to establish such a limit.

In the case of one-dimensional problems, however, some of these difficulties can be avoided. First, boundary data at $x = 0$ and $x = L$ are real numbers. Additionally, we make the assumption that *there is an integer number N of cells in the rod*. This hypothesis implies that ℓ and ε can only take the specific values:

$$\ell = \frac{L}{N} \text{ so that } \varepsilon = \frac{L}{N\lambda}, \quad N \in \mathbb{N}. \tag{4.41}$$

In particular, the numerical convergence results presented thereafter respect this constraint, i.e. $\varepsilon \to 0$ stands for $N \to +\infty$, with λ being fixed. Consequently, the boundary values of the two-scale expansions (4.9) and (4.22) are obtained by evaluating the cell functions P_j and the cell stresses Σ_j at $y = 0$. These values thus act as fixed coefficients that define boundary conditions for the mean fields.

Remark 4.5. *The assumption* (4.41) *above is quite strong from a mathematical point of view, but realistic for many engineering applications. The extremities of a periodic structure are often chosen at a specific point of the cell, e.g. the point where the section is the largest. Note that choosing different points for the two extremities could be handled with few modifications. For instance, if the constraint is to begin the rod at the beginning of the first cell ($y = 0$ at $x = 0$) and to end at the middle of the last cell ($y = \hat{\ell}/2$ at $x = L$), we have to replace the $P_j(0)$ and $\Sigma_j(0)$ by $P_j(\hat{\ell}/2)$ and $\Sigma_j(\hat{\ell}/2)$ in the boundary conditions for the right endpoint.*

Moreover, for $\beta_x \neq 0$, the family of equations (4.32) features a fourth-order derivative $U^{(2)}_{,xxxx}$, so that the use of these field equations necessitates *additional boundary conditions* compared to the original problem (4.35). There are many ways to obtain such boundary conditions. In [Askes et al., 2008], they are derived from the variational formulation for $U^{(2)}$ so that the boundary contributions cancel in the bilinear form associated with (4.32). The coefficients in the boundary conditions are therefore completely determined by the choice of the field equation. From another point of view, [Kaplunov & Pichugin, 2009] focuses on the presence of *extraneous* (non-physical) solutions to (4.32) and the necessity to take them into account while determining relevant boundary conditions (typically, by building BCs which cancel these extraneous waves). However, no error analysis is provided with these boundary conditions, and it is not clear at this point how to make a rigorous link between them and the convergence results underlying the homogenization theory.

As a consequence, for second-order approximation, *we focus on* (mt) *models*, i.e. $\beta_x = 0$, and therefore cancel the fourth-order space derivative term. This convenient choice corresponds to retaining only higher order time derivatives for the transient counterpart of our time-harmonic models. This possibility is another specificity of one-dimensional problems as underlined by [Kaplunov & Pichugin, 2009] and showed explicitly in [Wautier & Guzina, 2015, Part 5.5] where the homogenization of a 2D chessboard-like material leads to a family of equations similar to (4.32) but which features an additional fourth-order anisotropic term that cannot be replaced by any time derivatives.

Eventually, under these assumptions and restrictions, we are able to show convergence results similar to those of [Moskow & Vogelius, 1997] for appropriately chosen first and second-order approximations of u^{p} as demonstrated below.

First-order homogenization. We define the first-order approximation $(\tilde{u}^{(1)}, \tilde{\sigma}^{(1)})$ of the displacement and stress $(u^{\mathrm{p}}, E_{\mathrm{p}} u^{\mathrm{p}}{}_{,x})$ as:

$$
\begin{aligned}
\tilde{u}^{(1)}(x) &= U^{(1)}(x) + \varepsilon P_1\left(\frac{x}{\varepsilon}\right) U^{(1)}_{,x}(x), \\
\tilde{\sigma}^{(1)}(x) &= \Sigma_1\left(\frac{x}{\varepsilon}\right) U^{(1)}_{,x}(x) + \varepsilon \Sigma_2\left(\frac{x}{\varepsilon}\right) U^{(1)}_{,xx}(x).
\end{aligned}
\tag{4.42}
$$

The first-order mean field $U^{(1)}$ is the solution of the BVP obtained by (i) using the field equation (4.28) and (ii) enforcing $\tilde{u}^{(1)}$ and $\tilde{\sigma}^{(1)}$ to satisfy exact displacement and stress boundary conditions:

$$
\left|
\begin{array}{ll}
U^{(1)}_{,xx} + nk^2 U^{(1)} = 0 & x \in [0, L] \\
U^{(1)} + \varepsilon P_1(0) U^{(1)}_{,x} = 0 & x = 0 \\
\Sigma_1(0) U^{(1)}_{,x} - \varepsilon \Sigma_2(0) nk^2 U^{(1)} = Eku_L & x = L
\end{array}
\right.
\tag{4.43}
$$

Note that we used the field equation to replace $U^{(1)}_{,xx}$ by $-nk^2 U^{(1)}$ in the stress boundary condition, obtaining Robin-like boundary conditions that are more convenient, e.g. for numerical treatment. As for the exact BVP (4.35), we suppose that k is not an eigenvalue of (4.43) so that $U^{(1)}$ is uniquely defined and depends continuously on u_L. Eventually, we note that choosing $f = 0$ as discussed in Remark 4.4 ensures that $U^{(1)} \in C^\infty([0, L])$, so that $\tilde{u}^{(1)}$, $\tilde{\sigma}^{(1)}$ and their derivatives are well-defined.

Following [Moskow & Vogelius, 1997], we then look at the errors $(z^\varepsilon, s^\varepsilon)$ defined as:

$$
\begin{aligned}
z^\varepsilon &= u^{\mathrm{p}} - \tilde{u}^{(1)} = u^{\mathrm{p}} - U^{(1)} - \varepsilon P_1 U^{(1)}_{,x}, \\
s^\varepsilon &= E_{\mathrm{p}} u^{\mathrm{p}}{}_{,x} - \tilde{\sigma}^{(1)} = E_{\mathrm{p}} u^{\mathrm{p}}{}_{,x} - \Sigma_1 U^{(1)}_{,x} - \varepsilon \Sigma_2 U^{(1)}_{,xx}.
\end{aligned}
\tag{4.44}
$$

and remark that the boundary conditions on $U^{(1)}$ in (4.43) were chosen precisely so that

$$
z^\varepsilon(0) = 0 \qquad \text{and} \qquad s^\varepsilon(L) = 0.
\tag{4.45}
$$

Moreover, differentiating these fields yields the relations:

$$
\begin{aligned}
\hat{E} z^\varepsilon_{,x} &= s^\varepsilon - \varepsilon s^{(1)} && \text{with } s^{(1)} = \hat{E} P_{2,y} U^{(1)}_{,xx} = -\hat{E} \frac{\varrho_0}{\mathcal{E}_0} \omega^2 P_{2,y} U^{(1)} \\
s^\varepsilon_{,x} &= -\omega^2 \left(\hat{\rho} z^\varepsilon - \varepsilon z^{(1)}\right) && \text{with } z^{(1)} = \left(\frac{\varrho_0}{\mathcal{E}_0} \Sigma_2 - \hat{\rho} P_1\right) U^{(1)}_{,x} = -\frac{\varrho_0}{\mathcal{E}_0} \Sigma_{3,y} U^{(1)}_{,x}
\end{aligned}
\tag{4.46}
$$

In other words, (4.45) and (4.46) mean that the error terms $(z^\varepsilon, s^\varepsilon)$ satisfy the homogeneous BVP[1] with exact boundary conditions and $O(\varepsilon)$ error in the field equation. More precisely, the justification of our choice of approximation is given by:

Lemma 4.2. *The first-order approximation $\tilde{u}^{(1)} := U^{(1)} + \varepsilon P_1 U^{(1)}_{,x}$ defined in terms of the first-order mean field $U^{(1)}$ satisfying (4.43) is such that:*

$$
\exists C > 0 \qquad \|z^\varepsilon\|_1 = \|u^{\mathrm{p}} - \tilde{u}^{(1)}\|_1 \leq C\varepsilon \|U^{(1)}\|_1.
\tag{4.47}
$$

[1] or rather the equivalent first-order system, see [Moskow & Vogelius, 1997]

Proof. We follow the duality argument of [Moskow & Vogelius, 1997] and aim at evaluating the duality product (identified to the L^2 inner product) $(z^\varepsilon, \phi)_{L^2}$ for $\phi \in H^{-1}(]0, L[)$. To this end, we define the function w^ε as the solution of a periodic BVP featuring ϕ as source term:

$$\left|\begin{array}{ll} \left(E_\mathrm{p} w^\mathrm{p}_{,x}\right)_{,x} + \rho_\mathrm{p}\omega^2 w^\mathrm{p} = \phi & x \in [0, L] \\ w^\mathrm{p} = 0 & x = 0 \\ E_\mathrm{p} w^\mathrm{p}_{,x} = 0 & x = L \end{array}\right. \tag{4.48}$$

and compute:

$$\begin{aligned} (z^\varepsilon, \phi)_{L^2} &= \int_0^L z^\varepsilon \left[\left(E_\mathrm{p} w^\mathrm{p}_{,x}\right)_{,x} + \rho_\mathrm{p}\omega^2 w^\mathrm{p}\right] \mathrm{d}x \\ &= \left[E_\mathrm{p} w^\mathrm{p}_{,x} z^\varepsilon\right]_0^L - \int_0^L (s^\varepsilon - \varepsilon s^{(1)}) w^\mathrm{p}_{,x} - \rho_\mathrm{p}\omega^2 z^\varepsilon w^\mathrm{p} \, \mathrm{d}x \\ &= \left[E_\mathrm{p} w^\mathrm{p}_{,x} z^\varepsilon\right]_0^L - \left[s^\varepsilon w^\mathrm{p}\right]_0^L + \varepsilon \int_0^L s^{(1)} w^\mathrm{p}_{,x} - \omega^2 z^{(1)} w^\mathrm{p} \, \mathrm{d}x \end{aligned} \tag{4.49}$$

where we used (4.46) when integrating by parts. Because of the boundary conditions (4.45) and (4.48), the boundary terms cancel out and expanding $s^{(1)}$ and $z^{(1)}$ we are left with:

$$(z^\varepsilon, \phi)_{L^2} = -\varepsilon \frac{\varrho_0}{\mathcal{E}_0}\omega^2 \int_0^L \hat{E} P_{2,y} U^{(1)} w^\mathrm{p}_{,x} - \left[\hat{E}\left(P_2 + P_{3,y}\right)\right]_{,y} U^{(1)}_{,x} w^\mathrm{p} \, \mathrm{d}x, \tag{4.50}$$

where $\hat{E}$ and the cell functions P_j have to be understood as functions of (x/ε). We deduce that:

$$\exists C_1,\ C_2 > 0, \qquad |(z^\varepsilon, \phi)_{L^2}| \leq C_1 \varepsilon \|U^{(1)}\|_1 \|w^\mathrm{p}\|_1 \leq C_2 \varepsilon \|U^{(1)}\|_1 \|\phi\|_{-1}, \tag{4.51}$$

the second inequality coming from the well-posedness of the problem (4.48) which is another particular case of the periodic BVP (4.35). Then, taking the supremum over all $\phi \in H^{-1}(]0, L[)$ and invoking [Brezis, 2011, Corollary 1.4] concludes the proof. $\square$

Remark 4.6. *The result* (4.47) *is classical for 1D homogenization problems, and in fact it does not require boundary corrections to hold. Indeed, without them, the contribution on boundary terms in* (4.49) *would not cancel but be in $O(\varepsilon)$. On the contrary, in higher dimension, the oscillating behavior of such boundary term would result in an $O(\varepsilon^{1/2})$ error estimate in $H^1(\Omega)$-norm without boundary corrections, see [Cioranescu & Donato, 1999, Thm. 6.3].*

However, the main contribution of these corrections will become clear when looking at the L^2-norm of $u^\mathrm{p} - \tilde{u}^{(1)}$, which analysis requires to pursue the homogenization process.

Second order homogenization. We move now to the second-order homogenization, following the exact sames steps as above. The second-order approximation $(\tilde{u}^{(2)}, \tilde{\sigma}^{(2)})$ is sought as:

$$\begin{aligned} \tilde{u}^{(2)}(x) &= U^{(2)}(x) + \varepsilon P_1\left(\frac{x}{\varepsilon}\right) U^{(2)}_{,x}(x) + \varepsilon^2 P_2\left(\frac{x}{\varepsilon}\right) U^{(2)}_{,xx}(x), \\ \tilde{\sigma}^{(2)}(x) &= \Sigma_1\left(\frac{x}{\varepsilon}\right) U^{(2)}_{,x} + \varepsilon \Sigma_2\left(\frac{x}{\varepsilon}\right) U^{(2)}_{,xx}(x) + \varepsilon^2 \Sigma_3\left(\frac{x}{\varepsilon}\right) U^{(2)}_{,xxx}(x), \end{aligned} \tag{4.52}$$

where the second-order mean field $U^{(2)}$ is defined using the "time" model (t) for the bulk equation as the solution of the problem:

$$\left| \begin{array}{ll} U^{(2)}_{,xx} + n_t(k)k^2 U^{(2)} = 0 & x \in [0, L] \\ \Big(1 - \varepsilon^2 n_t(k) k^2 P_2(0)\Big) U^{(2)} + \varepsilon P_1(0) U^{(2)}_{,x} = 0 & x = 0 \\ \Big(\Sigma_1(0) - \varepsilon^2 n_t(k) k^2 \Sigma_3(0)\Big) U^{(2)}_{,x} - \varepsilon n_t(k) k^2 \Sigma_2(0) U^{(2)} = E k u_L & x = L. \end{array} \right. \tag{4.53}$$

The effective index $n_t(k)$ in the field equation is given by (4.33) as:

$$n_t(k) = n\left(1 + nk^2\ell^2\beta\right) = n\left(1 + \varepsilon^2 nk^2 \left[\frac{\mathcal{E}_2}{\mathcal{E}_0} - \frac{\varrho_2}{\varrho_0}\right]\right). \tag{4.54}$$

We then consider the errors:

$$\begin{aligned} z^\varepsilon &= u^{\mathrm{p}} - \tilde{u}^{(2)}, \\ s^\varepsilon &= E_{\mathrm{p}} u^{\mathrm{p}}{}_{,x} - \tilde{\sigma}^{(2)}, \end{aligned} \tag{4.55}$$

and again remark that the boundary conditions on $U^{(2)}$ in problem (4.53) were chosen so that

$$z^\varepsilon(0) = 0 \qquad \text{and} \qquad s^\varepsilon(L) = 0. \tag{4.56}$$

Moreover, differentiating these terms yields the relations:

$$\begin{aligned} \hat{E} z^\varepsilon_{,x} &= s^\varepsilon - \varepsilon^2 s^{(2)} + o(\varepsilon^2) && \text{with } s^{(2)} = -\hat{E}\frac{\varrho_0}{\mathcal{E}_0}\omega^2 P_{3,y} U^{(2)}_{,x}, \\ s^\varepsilon_{,x} &= -\omega^2\left(\hat{\rho} z^\varepsilon - \varepsilon^2 z^{(2)}\right) + o(\varepsilon^2) && \text{with } z^{(2)} = \left(\frac{\varrho_0}{\mathcal{E}_0}\Sigma_3 - \hat{\rho} P_2 - \left[\frac{\mathcal{E}_2}{\mathcal{E}_0} - \frac{\varrho_2}{\varrho_0}\right]\right)\frac{\varrho_0}{\mathcal{E}_0} U^{(2)}. \end{aligned} \tag{4.57}$$

The $o(\varepsilon^2)$ terms, not specified here for brevity, come from the fact that we used $U^{(2)}_{,xx} = -nk^2 U^{(2)} + O(\varepsilon^2)$ to deal with higher-order derivatives of $U^{(2)}$ (while we had the strict equality $U^{(1)}_{,xx} = -nk^2 U^{(1)}$ for the first-order case). As expected, we gain one order of convergence in the following sense:

Lemma 4.3. *The second-order approximation $\tilde{u}^{(2)} := U^{(2)} + \varepsilon P_1 U^{(2)}_{,x} + \varepsilon^2 P_2 U^{(2)}_{,xx}$ defined in terms of the second-order mean field $U^{(2)}$ satisfying* (4.53) *is such that:*

$$\exists C > 0 \qquad \|z^\varepsilon\|_1 = \|u^{\mathrm{p}} - \tilde{u}^{(2)}\|_1 \leq C\varepsilon^2 \|U^{(2)}\|_1 \tag{4.58}$$

Proof. The proof is exactly the same as for Lemma 4.2, except that the remainders of the errors z^ε and s^ε are of order $O(\varepsilon^2)$ as shown by (4.55), hence the $O(\varepsilon^2)$ final estimate. ☐

Remark 4.7. *We chose to consider only the "time" model (t) for simplicity. However, all the models of the (mt) family* (4.34) *would behave exactly the same way, replacing $n_t(k)$ by $n_{mt}(k)$ and making some minor computational adjustments.*

As announced in Remark 4.6, we are now in position to show the final result of this part:

Theorem 4.4. *The first-order approximation $\tilde{u}^{(1)} := U^{(1)} + \varepsilon P_1 U^{(1)}_{,x}$ satisfies the H^1 estimate of Lemma 4.2 together with the inequality:*

$$\exists C > 0 \quad \|u^{\mathrm{p}} - \tilde{u}^{(1)}\|_0 \leq C\varepsilon^2 \|U^{(2)}\|_2. \tag{4.59}$$

Proof. The aim of the proof is to show that $\|\tilde{u}^{(1)} - \tilde{u}^{(2)}\|_0 \leq C\varepsilon^2\|U^{(2)}\|_2$, and then (4.59) follows directly from Lemma 4.3. To this end, let us just note that this difference is:

$$\tilde{z}(x) := \tilde{u}^{(2)}(x) - \tilde{u}^{(1)}(x) = \tilde{Z}(x) + \varepsilon P_1\left(\frac{x}{\varepsilon}\right)\tilde{Z}_{,x}(x) + \varepsilon^2 P_2\left(\frac{x}{\varepsilon}\right)U^{(2)}(x) \tag{4.60}$$

where $\tilde{Z} := U^{(2)} - U^{(1)}$ satisfies the difference between the problems (4.53) and (4.43). Therefore, $\tilde{Z}$ is the solution of a problem similar to the first-order BVP (4.43), except that the source terms depend on $U^{(2)}$:

$$\left|\begin{array}{ll} \tilde{Z}_{,xx} + nk^2\tilde{Z} = -\varepsilon^2(nk^2)^2\left[\dfrac{\mathcal{E}_2}{\mathcal{E}_0} - \dfrac{\varrho_2}{\varrho_0}\right]U^{(2)} & x \in [0, L] \\ \tilde{Z} + \varepsilon P_1(0)\tilde{Z}_{,x} = \varepsilon^2 n_t(k)k^2 P_2(0)U^{(2)} & x = 0 \\ \Sigma_1(0)\tilde{Z}_{,x} - \varepsilon nk^2\Sigma_2(0)\tilde{Z} = \varepsilon^2\left(n_t(k)k^2\Sigma_3(0)U^{(2)}_{,x} - (nk^2)^2\left[\dfrac{\mathcal{E}_2}{\mathcal{E}_0} - \dfrac{\varrho_2}{\varrho_0}\right]\Sigma_2(0)U^{(2)}\right) & x = L, \end{array}\right. \tag{4.61}$$

Still under the assumption that k is not an eigenvalue of this problem, noting that the boundary source terms feature the derivative $U^{(2)}_{,x}$, hence the bound in H^2-norm in inequality (4.59) and below, we have:

$$\exists C > 0, \qquad \|\tilde{Z}\|_1 \leq C\varepsilon^2\|U^{(2)}\|_2. \tag{4.62}$$

Then from definition (4.60),

$$\exists C > 0, \qquad \|\tilde{z}\|_0 \leq C\varepsilon^2\|U^{(2)}\|_2, \tag{4.63}$$

and finally, by Lemma 4.3

$$\|u^{\mathrm{p}} - \tilde{u}^{(1)}\|_0 \leq \|u^{\mathrm{p}} - \tilde{u}^{(2)}\|_0 + \|\tilde{z}\|_0 \leq C\varepsilon^2\|U^{(2)}\|_2. \tag{4.64}$$

$\square$

Remark 4.8. *With the help of the observations of Remark 4.6, one could show that the second-order boundary corrections for $U^{(2)}$ in (4.58) were not necessary to establish Lemma 4.3 and Theorem 4.4. However, there would undoubtedly be necessary to establish a result such that:*

$$\exists C > 0 \quad \|u^{\mathrm{p}} - \tilde{u}^{(2)}\|_0 \leq C\varepsilon^3\|U^{(3)}\|_2 \tag{4.65}$$

for some third-order mean field $U^{(3)}$ obtained by pursuing the homogenization procedure. While we do not prove this result, we firmly believe it holds, and we will indeed observe such $O(\varepsilon^3)$ behavior for $\|u^{\mathrm{p}} - \tilde{u}^{(2)}\|_0$ in the numerical experiments presented in the next section.

4.2 Two-phase layered medium

In this section, we consider the case of a *two-phase layered medium* that is characterized from reference properties (E, ρ) using four material parameters $(\alpha_E,\ \alpha_\rho,\ \gamma_E,\ \gamma_\rho)$ such that $\hat{E}$ and $\hat{\rho}$ are piecewise constant and defined within a periodicity cell $[0, \hat{\ell}]$ as:

$$\hat{E}(y) = \begin{cases} E_1 = \alpha_E E & y \in [0, \hat{\ell}/2] \\ E_2 = \gamma_E E_1 = \alpha_E\gamma_E E & y \in [\hat{\ell}/2, \hat{\ell}] \end{cases} \qquad \hat{\rho}(y) = \begin{cases} \rho_1 = \alpha_\rho\rho & y \in [0, \hat{\ell}/2] \\ \rho_2 = \gamma_\rho\rho_1 = \alpha_\rho\gamma_\rho\rho & y \in [\hat{\ell}/2, \hat{\ell}] \end{cases} \tag{4.66}$$

Remark 4.9. *We considered only rods with constant section for simplicity. However, since the coefficients of the longitudinal wave equation are in fact ES and ρS (with S the section of the rod), for $\gamma_E = gR$ such a rod is equaivalent to a homogeneous rod with piecewise-constant section, as showed by Figure 4.1.*

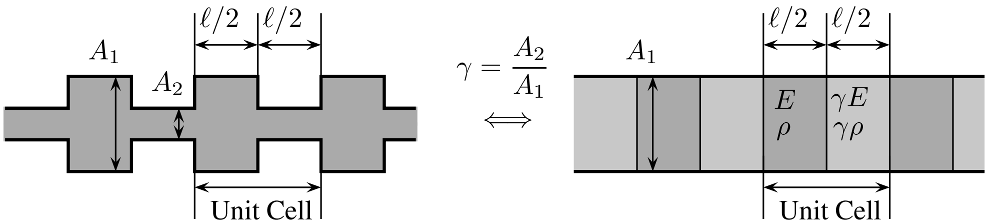

Figure 4.1: Rod with periodically variable section, and equivalent two-phase layered rod [Dontsov et al., 2013]

Despite some loss of generality, we choose to consider the simple case for which each material occupies half of the cell, rather than introducing an additional parameter $\alpha \in]0, 1[$ such that $[0, \hat{\ell}]$ is split into $[0, \alpha\hat{\ell}] \cup [\alpha\hat{\ell}, \hat{\ell}]$. The latter case is addressed in [Fish et al., 2002; Wautier & Guzina, 2015]. However, some of the results we need, in particular the exact expression of the cell functions, are not explicitly given in these references. For completeness, these results are therefore recalled thereafter.

4.2.1 Cell functions and homogenized coefficients

This part is dedicated to the computation of the cell functions for the two-phase layered material defined by (4.66). Similar cell functions are already given in [Andrianov et al., 2008] for symmetric cells $[-\hat{\ell}/2, \hat{\ell}/2]$, and we provide here their expressions with our notations from [Wautier & Guzina, 2015]. For later convenience, we introduce the additional material coefficients β_E, β_ρ and $\beta_{E\rho}$ as:

$$\beta_E = \frac{\gamma_E - 1}{4(\gamma_E + 1)}, \quad \beta_\rho = \frac{\gamma_\rho - 1}{4(\gamma_\rho + 1)} \quad \text{and} \quad \beta_{E\rho} = \frac{\beta_E + \beta_\rho}{2} = \frac{\gamma_E\gamma_\rho - 1}{4(\gamma_E + 1)(\gamma_\rho + 1)}. \tag{4.67}$$

and proceed with the cell problems definitions and notations.

First cell problem: P_1 satisfies the following problem on the cell $[0, \hat{\ell}]$:

$$\left| \begin{array}{l} [\hat{E}(1 + P_{1,y})]_{,y} = 0 \\ \langle P_1 \rangle = 0 \\ P_1 \text{ and } \hat{E}(1 + P_{1,y}) \text{ are } \hat{\ell}\text{-periodic} \\ \langle P_1 \rangle (\hat{\ell}/2) = 0, \quad \left\langle \hat{E}(1 + P_{1,y}) \right\rangle (\hat{\ell}/2) = 0. \end{array} \right. \tag{4.68}$$

The solution is given e.g. in [Fish et al., 2002, eq. (17)] by:

$$P_1(y) = \begin{cases} \beta_E \left(4y - \hat{\ell}\right) & y \in [0, \hat{\ell}/2], \\ \beta_E \left(3\hat{\ell} - 4y\right) & y \in [\hat{\ell}/2, \hat{\ell}]. \end{cases} \tag{4.69}$$

The associated stress $\Sigma_1 = \hat{E}(y)(1 + P_{1,y})$ is constant and therefore equal to the leading-order homogenized Young's modulus:

$$P_1(0 < y < \hat{\ell}/2) = P_1(\hat{\ell}/2 < y < \hat{\ell}) = \frac{2\gamma_E \alpha_E}{(1+\gamma_E)} E = \mathcal{E}_0. \tag{4.70}$$

Second cell problem: P_2 satisfies the following problem on the cell $[0, \hat{\ell}]$:

$$\left| \begin{array}{l} [\hat{E}(P_1 + P_{2,y})]_{,y} = -\hat{E}(1 + P_{1,y}) + \hat{\rho}\dfrac{\mathcal{E}_0}{\varrho_0} = \mathcal{E}_0 \left(\dfrac{\hat{\rho}}{\varrho_0} - 1 \right) \\ \langle P_2 \rangle = 0 \\ P_2 \text{ and } \hat{E}(P_1 + P_{2,y}) \text{ are } \hat{\ell}\text{-periodic} \\ \langle P_2 \rangle (\hat{\ell}/2) = 0, \quad \left\langle \hat{E}(P_1 + P_{2,y}) \right\rangle (\hat{\ell}/2) = 0 \end{array} \right. \tag{4.71}$$

Using the cell function P_1 determined previously, the solution is computed as:

$$P_2(y) = \begin{cases} A_1(2y - \hat{\ell})y + C\hat{\ell}^2 & y \in [0, \hat{\ell}/2], \\ A_2(3\hat{\ell} - 2y)y + (C - A_2)\hat{\ell}^2 & y \in [\hat{\ell}/2, \hat{\ell}], \end{cases} \tag{4.72}$$

with:

$$A_1 = -4\beta_E\beta_\rho - 2\beta_{E\rho}, \quad A_2 = 4\beta_E\beta_\rho - 2\beta_{E\rho} \quad \text{and} \quad C = -\frac{\beta_E\beta_\rho}{3}. \tag{4.73}$$

And the second cell stress Σ_2 is:

$$\Sigma_2(y) = \hat{E}(y)(P_1 + P_{2,y})(y) = \begin{cases} \mathcal{E}_0\beta_\rho \left(4y - \hat{\ell}\right) & y \in [0, \hat{\ell}/2], \\ \mathcal{E}_0\beta_\rho \left(3\hat{\ell} - 4y\right) & y \in [\hat{\ell}/2, \hat{\ell}]. \end{cases} \tag{4.74}$$

Third cell problem: P_3 satisfies the following problem on the cell $[0, \hat{\ell}]$:

$$\left| \begin{array}{l} [\hat{E}(P_2 + P_{3,y})]_{,y} = -\hat{E}(P_1 + P_{2,y}) + \hat{\rho}P_1\dfrac{\mathcal{E}_0}{\varrho_0} \\ \langle P_3 \rangle = 0 \\ P_3 \text{ and } \hat{E}(P_2 + P_{3,y}) \text{ are } \hat{\ell}\text{-periodic} \\ \langle P_3 \rangle (\hat{\ell}/2) = 0, \quad \left\langle \hat{E}(P_2 + P_{3,y}) \right\rangle (\hat{\ell}/2) = 0 \end{array} \right. \tag{4.75}$$

The solution is written:

$$P_3(y) = \begin{cases} \left(\dfrac{2\gamma_E A_2}{\gamma_E + 1} + A_1 \right) \left(\dfrac{\hat{\ell}}{2} - \dfrac{2y}{3} \right) y^2 + B_1\hat{\ell}^2 y + D_1\hat{\ell}^3 & y \in [0, \hat{\ell}/2] \\ \left(\dfrac{2A_1}{\gamma_E + 1} + A_2 \right) \left(\dfrac{2y}{3} - \dfrac{3\hat{\ell}}{2} \right) y^2 + B_2\hat{\ell}^2 y + D_2\hat{\ell}^3 & y \in [\hat{\ell}/2, \hat{\ell}], \end{cases} \tag{4.76}$$

$$
\text{with:}\quad B_1 = \frac{\beta_E}{3}\left(\frac{2\gamma_E\beta_E}{\gamma_E+1}+\beta_\rho\right), \qquad B_2 = \frac{2A_1}{\gamma_E+1}+A_2+\frac{\beta_E}{3}\left(\frac{2\beta_E}{\gamma_E+1}+\beta_\rho\right),
$$
$$
D_1 = \frac{\beta_{E\rho}}{24}\left(1+\left(\frac{2\gamma_E}{\gamma_E+1}\right)^2\right), \qquad D_2 = D_1+\frac{5}{6}\left(\frac{2A_1}{\gamma_E+1}+A_2\right)-B_2. \tag{4.77}
$$

The third cell stress Σ_3 is:

$$
\Sigma_3(y) = \hat{E}(y)(P_2+P_{3,y})(y) = \begin{cases} \mathcal{E}_0\left(-A_2(2y-\hat{\ell})y+\dfrac{\beta_E^2}{3}\hat{\ell}^2\right) & y\in[0,\hat{\ell}/2] \\ \mathcal{E}_0\left(-A_1(3\hat{\ell}-2y)y+\left(\dfrac{\beta_E^2}{3}+A_1\right)\hat{\ell}^2\right) & y\in[\hat{\ell}/2,\hat{\ell}]. \end{cases} \tag{4.78}
$$

These three cell functions P_1, P_2 and P_3 are plotted on Figure 4.2, along with Σ_2 and Σ_3.

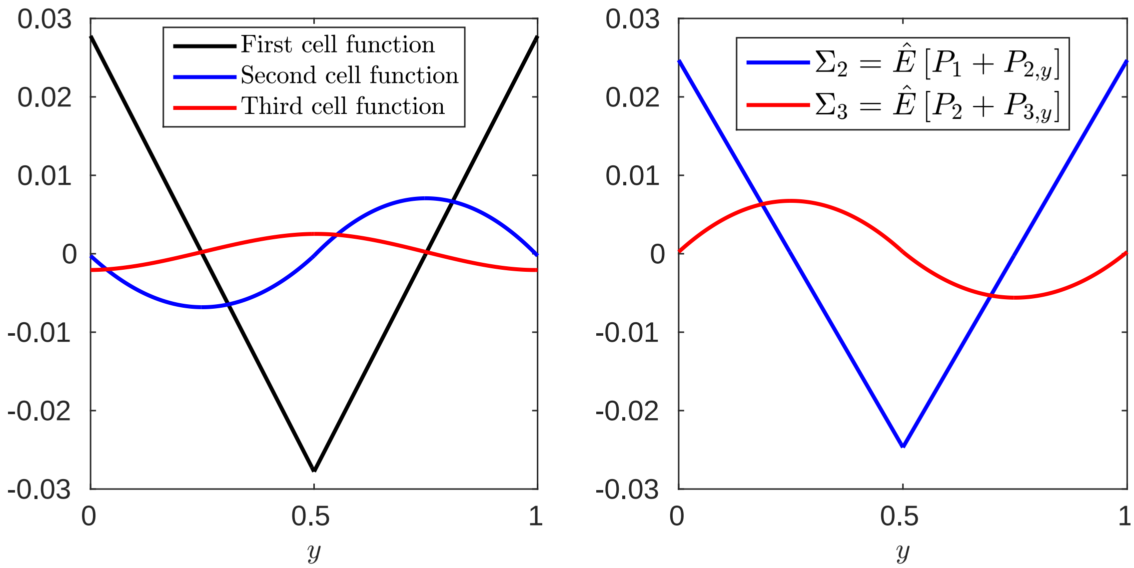

Figure 4.2: Cell functions and stresses for $E = 1$, $\rho = 1$, $\hat{\ell} = 1$ and $\gamma_E = \gamma_\rho = 0.8$. The first cell stress is constant with $\Sigma_1 = \mathcal{E}_0$ ($= 0.889$ in this case) and is not represented.

Boundary values: We saw in Section 4.1.2 that the boundary values of the cell functions and those of the corresponding cell stresses are required to build the high-order boundary conditions. For convenience, we recall here these values, which are obtained by setting $y = 0$ in the identities (4.69,4.70,4.72,4.74, 4.76,4.78):

$$\begin{aligned} P_1(0) &= -\beta_E \hat{\ell} & \Sigma_1(0) &= \mathcal{E}_0 \\ P_2(0) &= -\frac{\beta_E \beta_\rho}{3} \hat{\ell}^2 & \Sigma_2(0) &= \mathcal{E}_0 \beta_\rho \hat{\ell} \\ P_3(0) &= \frac{\beta_{E\rho}}{24} \left(1 + \left(\frac{2\gamma_E}{\gamma_E + 1} \right)^2 \right) \hat{\ell}^3 & \Sigma_3(0) &= \frac{1}{3} \mathcal{E}_0 \beta_E^2 \hat{\ell}^2 \end{aligned} \tag{4.79}$$

Homogenized coefficients: The homogenized coefficients defined by (4.14), and given in [Wautier & Guzina, 2015] for any material ratio within the cell, are as follow for the simpler configuration considered here:

$$\begin{aligned} \mathcal{E}_0 &= \frac{2\gamma_E}{1+\gamma_E} E_1 = \frac{2\gamma_E \alpha_E}{1+\gamma_E} E, & \mathcal{E}_1 &= 0, & \mathcal{E}_2 &= \frac{2}{3} \beta_E \beta_{E\rho} \hat{\ell}^2 \mathcal{E}_0, \\ \varrho_0 &= \frac{1+\gamma_\rho}{2} \rho_1 = \frac{(1+\gamma_\rho)\alpha_\rho}{2} \rho, & \varrho_1 &= 0, & \varrho_2 &= -\frac{2}{3} \beta_\rho \beta_{E\rho} \hat{\ell}^2 \varrho_0. \end{aligned} \tag{4.80}$$

The index n is:

$$n := \frac{E \varrho_0}{\rho \mathcal{E}_0} = \frac{\alpha_\rho}{\alpha_E} \frac{(1+\gamma_E)(1+\gamma_\rho)}{\gamma_E}, \tag{4.81}$$

and the second-order coefficient β (4.31) is:

$$\beta := \frac{1}{\hat{\ell}^2} \left[\frac{\mathcal{E}_2}{\mathcal{E}_0} - \frac{\varrho_2}{\varrho_0} \right] = \frac{4}{3} {\beta_{E\rho}}^2 = \frac{(1-\gamma_E \gamma_\rho)^2}{12(1+\gamma_E)^2(1+\gamma_\rho)^2}, \tag{4.82}$$

which corresponds to the result of [Fish et al., 2002; Andrianov et al., 2008].

4.2.2 Dispersive properties of real material and second-order homogenized models

To conclude this section, we briefly recall the dispersive properties of such layered medium. Upon noting κ_p the effective wavenumber of the microstructure, then the corresponding dispersion relation (given in terms of $k = \omega/c$) is given by [Wautier & Guzina, 2015] as:

$$\cos(\kappa_\mathrm{p} \ell) = (1+\chi) \cos\left(\frac{k\ell}{2} \sqrt{\frac{\alpha_\rho}{\alpha_E}} \left(1 + \frac{1}{\sqrt{\gamma_E \gamma_\rho}} \right) \right) - \chi \cos\left(\frac{k\ell}{2} \sqrt{\frac{\alpha_\rho}{\alpha_E}} \left(1 - \frac{1}{\sqrt{\gamma_E / \gamma_\rho}} \right) \right), \tag{4.83}$$

where χ is the parameter defined by:

$$\chi = \frac{1}{4} \left(\sqrt{\gamma_E \gamma_\rho} + \frac{1}{\sqrt{\gamma_E \gamma_\rho}} - 2 \right). \tag{4.84}$$

One of the remarkable feature of the layered material is the presence of *band gaps*, i.e. intervals of frequency ω for which the propagation within the structure is forbidden. Since we address mostly low-frequency behavior, we refer to [Dontsov et al., 2013] for more precise characterization of this phenomenon and numerical and experimental observations. In terms of the dispersion relation (4.83), these frequency values are the one for which only purely imaginary solutions κ_{p} can exist. We call the onset of the first band-gap the couple $(\omega_{\mathrm{BG}}, \kappa_{\mathrm{BG}})$ that corresponds to the beginning of this band and the corresponding wavenumber. In particular, one can show that κ_{BG} is given as:

$$\kappa_{\mathrm{BG}} = \frac{\pi}{\ell}. \tag{4.85}$$

Roughly speaking, we can show that for "reasonable" contrasts (γ_E and γ_ρ close to 1), one has $k_{\mathrm{BG}} = \omega_{\mathrm{BG}}/c = O(\kappa_{\mathrm{BG}})$, so that the corresponding homogenization parameter is $\varepsilon_{\mathrm{BG}} = k_{\mathrm{BG}}\ell/2\pi = O(1/2)$, which is out of the usual bounds for a "small parameter" assumption. This explains the difficulty for classical models to reach such band-gap. We therefore show how the second-order family of homogenized equations that was obtained in the first section can be calibrated so that the dispersion relation (4.83) is well approached.

Recall that the family of second order equations (4.32) is:

$$\beta_x \ell^2 U^{(2)}_{,xxxx} + \left(1 + \beta_m n k^2 \ell^2\right) U^{(2)}_{,xx} + n k^2 \left(1 - \beta_t n^2 k^2 \ell^2\right) U^{(2)} = 0, \tag{4.86}$$

with $\beta_x - \beta_m - \beta_t = \beta$. All these models capture the low-frequency dispersive behavior of the propagation within the periodic material. Indeed, the low-frequency dispersion relations for the models (4.86) are:

$$\sqrt{n} k\ell = \sqrt{\frac{1 - \beta_m(\kappa\ell)^2 - \sqrt{1 - 2(\beta_m + 2\beta_t)(\kappa\ell)^2 + (\beta_m^2 + 4\beta_x\beta_t)(\kappa\ell)^4}}{2\beta_t}} \tag{4.87}$$

and the obtained asymptotic expansion of $k\ell$ as $\kappa\ell \to 0$ coincides with that of (4.83) up to $O((\kappa\ell)^3)$ for any set of parameters $(\beta_x, \beta_m, \beta_t)$ satisfying condition (4.31). Additionally, one can take advantage of the degrees of freedom offered by models (4.86) to obtain better agreement.

Optimized two-parameter model (mt)**:** If $\beta_x = 0$, the relation $\beta = -\beta_m - \beta_t$ is prescribed, but then we still have a degree of freedom to fit the dispersion relation. The two-parameter dispersion relation is:

$$\sqrt{n} k\ell = \sqrt{\frac{1 - \beta_m(\kappa\ell)^2 - \sqrt{1 - 2(\beta_m + 2\beta_t)(\kappa\ell)^2 + \beta_m^2(\kappa\ell)^4}}{2\beta_t}}. \tag{4.88}$$

We have to choose the condition to impose:

- Predicting the onset of the first band gap (as done in [Wautier & Guzina, 2015, sect. 3.4.3], for $\beta_t = 0$) would be:

$$\left.\frac{\partial k}{\partial \kappa}\right|_{\kappa\ell=\pi} = 0. \tag{4.89}$$

  However, it cannot be achieved for $\beta_x = 0$ when (4.88) holds, since in this case the derivative cancels only for $\kappa \to \infty$.

- Predict the location of the band-gap as done in [Dontsov et al., 2013], i.e. impose $k(\kappa = \pi/\ell) = \omega_{\mathrm{BG}}/c = k_{\mathrm{BG}}$. This gives:

$$\begin{aligned} \beta_m &= -\frac{n(k_{\mathrm{BG}}\ell)^2(1 + n(k_{\mathrm{BG}}\ell)^2\beta) - \pi^2}{n(k_{\mathrm{BG}}\ell)^2(n(k_{\mathrm{BG}}\ell)^2 - \pi^2)}, \\ \beta_t &= -\beta - \beta_m. \end{aligned} \tag{4.90}$$

However, this condition was shown for a similar three-parameter model in [Wautier & Guzina, 2015, Sect. 3.4.3] to be less accurate at low-frequency (in terms of approaching the exact dispersion relation) than even one-parameter models.

- Approaching the Taylor's expansion of the exact dispersion relation (4.83) up to $O((\kappa\ell)^5)$ instead of $O((\kappa\ell)^3)$ as $\kappa\ell \to 0$. To simplify the computations, we address only the simplest case for which $\gamma_E = \gamma_\rho = \gamma$. The real dispersion relation is given as a particular case of (4.83) by [Dontsov et al., 2013] as:

$$k\ell = \cos^{-1}\left(\frac{\cos(\kappa_{\mathrm{p}}\ell) + \chi}{1+\chi}\right), \quad \chi = \frac{1}{4}\left(\gamma + \gamma^{-1} - 2\right), \tag{4.91}$$

and its Taylor expansion as $\kappa\ell \to 0$ is:

$$k\ell = \frac{1}{\sqrt{1+\chi}}\left(\kappa_{\mathrm{p}}\ell - \frac{1}{24}\frac{\chi}{1+\chi}(\kappa_{\mathrm{p}}\ell)^3 + \frac{1}{1920}\frac{\chi\,(-8+\chi)}{(1+\chi)^2}(\kappa_{\mathrm{p}}\ell)^5 + O((\kappa_{\mathrm{p}}\ell)^7)\right). \tag{4.92}$$

In this case, the index n and second-order coefficient β given by (4.81) and (4.82) become:

$$n = 1+\chi \qquad \text{and} \qquad \beta = \frac{1}{12}\frac{\chi}{1+\chi}, \tag{4.93}$$

and we therefore write the expansion (4.92) as:

$$\sqrt{n}k\ell = \kappa_{\mathrm{p}}\ell - \frac{\beta}{2}(\kappa_{\mathrm{p}}\ell)^3 + \frac{\beta(27\beta-2)}{40}(\kappa_{\mathrm{p}}\ell)^5 + O((\kappa_{\mathrm{p}}\ell)^7). \tag{4.94}$$

Similarly, we expand the homogenized dispersion relation (4.88) as:

$$\sqrt{n}k\ell = \kappa\ell + \frac{\beta_m+\beta_t}{2}(\kappa\ell)^3 + \frac{(\beta_m+\beta_t)(3\beta_m+7\beta_t)}{8}(\kappa\ell)^5 + O((\kappa\ell)^7). \tag{4.95}$$

Equating the coefficients of expansions (4.94) and (4.95) thus provides the additional condition:

$$3\beta_m + 7\beta_t = \frac{2-27\beta}{5}, \tag{4.96}$$

which, along with the already known relation $\beta_m + \beta_t = -\beta$, leads to:

$$\beta_m = \frac{-1-4\beta}{10} \quad \text{and} \quad \beta_t = \frac{1-6\beta}{10}. \tag{4.97}$$

Optimized three-parameter model The full (xmt) model presented in [Wautier & Guzina, 2015] is numerically optimized to respect both the slope condition $\partial\omega/\partial\kappa = 0$ at the beginning of the BG and the width of the BG.

Eventually, the Figure 4.3 plots the dispersion relations obtained for the models described above. Note that the latter one (optimized (xmt)) is the only one able to accurately fit the dispersion curve up to and even after the band-gap.

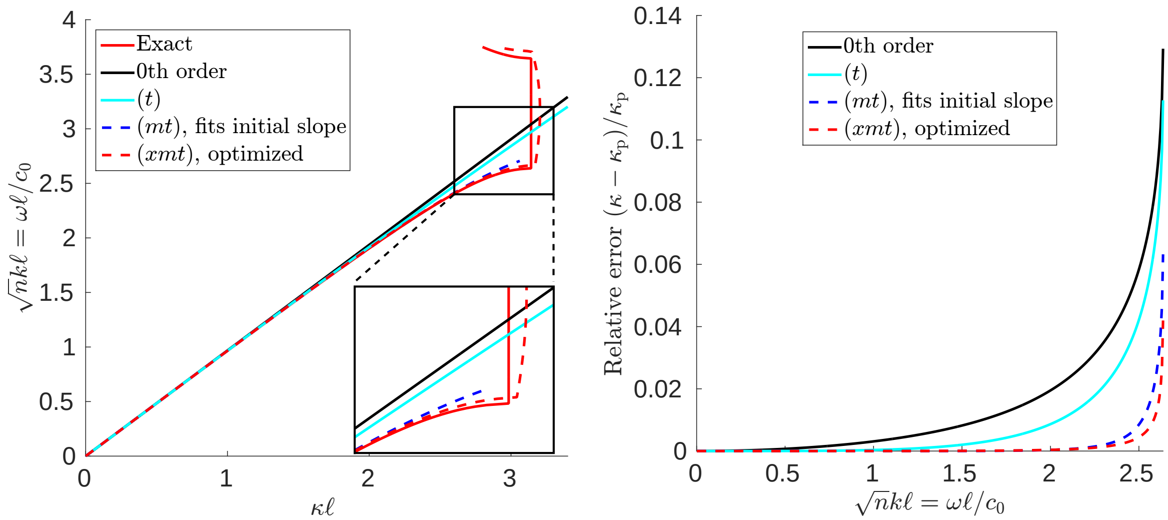

Figure 4.3: Dispersion relations: $\kappa\ell$ as a function of $\sqrt{n}k\ell$ (plotted as usual with shifted axes) for $\gamma_E = \gamma_\rho = 0.6$, up to the first band-gap. The error for the 2nd-order simplest model (t) is to be compared to these of optimized models (mt) and (xmt).

4.3 Analytical and numerical examples

This final section is dedicated to the illustration of the approximate high-order models proposed in Section 4.1.2 in the simple case of the bi-layered material. Consider the model problem of a clamped rod submitted to time-harmonic axial tractions:

$$\left| \begin{array}{ll} (E_{\mathrm{p}} u^{\mathrm{p}}{}_{,x})_{,x} + \rho_{\mathrm{p}}\omega^2 u^{\mathrm{p}} = 0 & x \in [0, L] \\ u = 0 & x = 0 \\ E_{\mathrm{p}} u^{\mathrm{p}}{}_{,x} = E k u_L & x = L, \end{array} \right. \tag{4.98}$$

for which an exact solution is available in the case of a bilayered material as presented now.

4.3.1 Exact solution

Let E_{p} and ρ_{p} in (4.98) be the piecewise-constant coefficients defined by (4.66). The number of cells in the rod, supposed to be an integer, is given by $N = L/\ell$. We note $x_n := n\ell$, $n = 0, \ldots, N$ the positions of the interfaces between cells, and $n_j = (E/\rho)/(E_j/\rho_j)$ the index in the half-cell j for $j \in \{1, 2\}$. Then u^{p} is piecewise and defined by the coefficients $(a_n^{(1)}, b_n^{(1)}, a_n^{(2)}, b_n^{(2)})$ corresponding to the cells $[x_n, x_{n+1}]$ according to:

$$u^{\mathrm{p}}(x) = \begin{cases} a_n^{(1)} \cos\left(\sqrt{n_1}k(x - x_n)\right) + b_n^{(1)} \sin\left(\sqrt{n_1}k(x - x_n)\right) & x \in [x_n, x_n + \ell/2], \\ a_n^{(2)} \cos\left(\sqrt{n_2}k(x - x_n - \ell/2)\right) + b_n^{(2)} \sin\left(\sqrt{n_2}k(x - x_n - \ell/2)\right) & x \in [x_n + \ell/2, x_{n+1}]. \end{cases} \tag{4.99}$$

We then write the boundary condition at $x = 0$ and at $x = L$, and the transmission conditions for each interface within the microstructure.

$$
\begin{aligned}
x = 0 \ &: a_0^{(1)} = 0 \\
x = x_n + \ell/2 \ &: \begin{bmatrix} a_n^{(2)} \\ b_n^{(2)} \end{bmatrix} = \boldsymbol{B}_1(k) \cdot \begin{bmatrix} a_n^{(1)} \\ b_n^{(1)} \end{bmatrix} \\
x = x_{n+1} \ &: \begin{bmatrix} a_{n+1}^{(1)} \\ b_{n+1}^{(1)} \end{bmatrix} = \boldsymbol{B}_2(k) \cdot \begin{bmatrix} a_n^{(2)} \\ b_n^{(2)} \end{bmatrix} = \boldsymbol{B}_2(k)\boldsymbol{B}_1(k) \cdot \begin{bmatrix} a_n^{(1)} \\ b_n^{(1)} \end{bmatrix} \\
x = L \ &: E_1\sqrt{n_1}k b_N^{(1)} = E k u_L
\end{aligned}
\tag{4.100}
$$

where we added a "virtual" half-cell with coefficients $(a_N^{(1)}, b_N^{(1)})$ at $x_N = L$ for a more compact expression. The transmission matrices $\boldsymbol{B}_1$ and $\boldsymbol{B}_2$ in (4.100) are defined by:

$$
\begin{aligned}
\boldsymbol{B}_1(k) &= \begin{bmatrix} \cos(\sqrt{n_1}k\ell/2) & \sin(\sqrt{n_1}k\ell/2) \\ -(\gamma_E\gamma_\rho)^{-1/2}\sin(\sqrt{n_1}k\ell/2) & (\gamma_E\gamma_\rho)^{-1/2}\cos(\sqrt{n_1}k\ell/2) \end{bmatrix} \\
\boldsymbol{B}_2(k) &= \begin{bmatrix} \cos(\sqrt{n_2}k\ell/2) & \sin(\sqrt{n_2}k\ell/2) \\ -(\gamma_E\gamma_\rho)^{1/2}\sin(\sqrt{n_2}k\ell/2) & (\gamma_E\gamma_\rho)^{1/2}\cos(\sqrt{n_2}k\ell/2) \end{bmatrix}
\end{aligned}
\tag{4.101}
$$

Combining all these equations, we finally rewrite the boundary condition at $x = L$ as:

$$
\left(\big[\boldsymbol{B}_2(k)\boldsymbol{B}_1(k)\big]^N \begin{bmatrix} 0 \\ b_0^{(1)} \end{bmatrix} \right) \cdot \begin{bmatrix} 0 \\ 1 \end{bmatrix} = \frac{E u_L}{E_1\sqrt{n_1}} \tag{4.102}
$$

Note that the eigenvalues of problem (4.98) are the wavenumbers k that cancel the left-hand-side of (4.102), i.e. those for which the homogeneous problem ($u_L = 0$) admits a non-trivial solution. We therefore define the characteristic function f_p as:

$$
f_\mathrm{p}(k) := \begin{bmatrix} 0 \\ 1 \end{bmatrix}^T \cdot \big[\boldsymbol{B}_2(k)\boldsymbol{B}_1(k)\big]^N \cdot \begin{bmatrix} 0 \\ 1 \end{bmatrix}. \tag{4.103}
$$

Provided that $f_\mathrm{p}(k) \neq 0$, the value of the first coefficient $b_0^{(1)}$, which uniquely defines the solution, is therefore given by:

$$
b_0^{(1)} = \frac{E u_L}{E_1\sqrt{n_1} f_\mathrm{p}(k)}, \tag{4.104}
$$

and it can easily be computed numerically. The coefficients $(a_n^{(1)}, b_n^{(1)}, a_n^{(2)}, b_n^{(2)})$ are then determined iteratively thanks to the transmission conditions (4.100), and the complete solution is defined by (4.99).

Remark 4.10. *We chose the boundary conditions for the problem* (4.98) *so that both displacement and stress boundary corrections introduced previously are used. However, considering other boundary conditions would result in very similar expression for the characteristic function f_p and the solution u. As an example, considering a prescribed displacement $u(L) = u_L$ instead of an applied force, the associated characteristic function $f_\mathrm{p}^{\mathrm{disp}}$ and the coefficient $b_0^{(1)\mathrm{disp}}$ would be:*

$$
f_\mathrm{p}^{\mathrm{disp}}(k) := \begin{bmatrix} 1 \\ 0 \end{bmatrix}^T \cdot \big[\boldsymbol{B}_2(k)\boldsymbol{B}_1(k)\big]^N \cdot \begin{bmatrix} 0 \\ 1 \end{bmatrix}. \tag{4.105}
$$

and, provided that $f_\mathrm{p}^{\mathrm{disp}}(k) \neq 0$:

$$
b_0^{(1)\mathrm{disp}} = \frac{u_L}{f_\mathrm{p}^{\mathrm{disp}}(k)}, \tag{4.106}
$$

4.3.2 Homogenized models

We now apply the homogenization procedure described in the previous sections to the problem (4.98).

Leading-order: The leading-order homogenized BVP reads:

$$\left| \begin{array}{ll} u_{0,xx} + nk^2 u_0 = 0 & x \in [0, L] \quad \text{with } n = \dfrac{E\varrho_0}{\rho\mathcal{E}_0} \\ u_0 = 0 & x = 0 \\ u_{0,x} = \dfrac{ku_L}{\alpha} & x = L, \quad \text{with } \alpha = \dfrac{\mathcal{E}_0}{E}. \end{array} \right. \tag{4.107}$$

This problem is well-posed provided k is not an eigenvalue for the homogeneous problem (given by $u_L = 0$), i.e.

$$f_0(k) := \cos(\sqrt{n}kL) \neq 0 \Longrightarrow k \notin \left\{ \frac{\pi}{2\sqrt{n}L} + \frac{m\pi}{\sqrt{n}L} \ ; \ m \in \mathbb{N} \right\}. \tag{4.108}$$

In this case, its solution is unique and given by:

$$u_0(x) = \frac{u_L}{\alpha\sqrt{n}} \frac{\sin(\sqrt{n}kx)}{\cos(\sqrt{n}kL)}. \tag{4.109}$$

It is natural to wonder whether the eigenvalues of the homogenized problem (i.e. the zeros of f_0) are related to those of the periodic problem (i.e. the zeros of f_p). A short discussion on this complex issue is delayed to Section 4.3.3.

First order As seen for the general case (4.43), the first-order homogenized BVP is written for the first-order mean field $U^{(1)}$ as:

$$\left| \begin{array}{ll} U^{(1)}_{,xx} + nk^2 U^{(1)} = 0 & x \in [0, L] \\ U^{(1)} - \beta_E \ell U^{(1)}_{,x} = 0 & x = 0 \\ U^{(1)}_{,x} - \beta_\rho nk^2 \ell U^{(1)} = \dfrac{ku_L}{\alpha} & x = L, \end{array} \right. \tag{4.110}$$

The characteristic function f_1 is defined by:

$$f_1(k) := (1 - \beta_E\beta_\rho n(k\ell)^2)\cos(\sqrt{n}kL) - (\beta_E + \beta_\rho)\sqrt{n}k\ell\sin(\sqrt{n}kL), \tag{4.111}$$

so that k is an eigenvalue of the homogeneous counterpart of (4.110) if and only if $f_1(k) = 0$. Assuming this is not the case, the solution of (4.110) is unique and given by:

$$U^{(1)}(x) = \frac{u_L}{\alpha\sqrt{n}f_1(k)} \left[\beta_E\sqrt{n}k\ell\cos(\sqrt{n}kx) + \sin(\sqrt{n}kx) \right]. \tag{4.112}$$

Second order "time" model: Similarly, up to the second order $u^{(2)}$, and using the "time" model as in (4.53) we obtain for the second-order mean displacement:

$$\left| \begin{array}{ll} U^{(2)}_{,xx} + n_t(k)k^2 U^{(2)} = 0 & x \in [0, L] \\ \left(1 + \dfrac{\beta_E \beta_\rho}{3} nk^2\ell^2\right) U^{(2)} - \beta_E \ell U^{(2)}_{,x} = 0 & x = 0 \\ \left(1 - \dfrac{{\beta_E}^2}{3} nk^2\ell^2\right) U^{(2)}_{,x} - \beta_\rho nk^2 \ell U^{(2)} = \dfrac{ku_L}{\alpha} & x = L \end{array} \right. \tag{4.113}$$

where the refraction index $n_t(k)$ is given by:

$$n_t(k) := n\left(1 + \beta nk^2\ell^2\right). \tag{4.114}$$

The characteristic function f_2 is:

$$\begin{aligned} f_2(k) :=& \sqrt{\frac{n_t}{n}} \left(1 - \frac{{\beta_E}^2}{3} nk^2\ell^2\right) \left[\left(1 + \frac{\beta_E\beta_\rho}{3} nk^2\ell^2\right) \cos(\sqrt{n_t}kL) - \beta_E \sqrt{n_t} k\ell \sin(\sqrt{n_t}kL)\right] \\ & - \beta_\rho \sqrt{n} k\ell \left[\left(1 + \frac{\beta_E\beta_\rho}{3} nk^2\ell^2\right) \sin(\sqrt{n_t}kL) - \beta_E \sqrt{n_t} k\ell \cos(\sqrt{n_t}kL)\right] \end{aligned} \tag{4.115}$$

where the dependency of n_t on k was omitted for compactness. Provided that $f_2(k) \neq 0$, the solution of (4.113) is:

$$U^{(2)}(x) = \frac{u_L}{\alpha\sqrt{n} f_2(k)} \left[\frac{\beta_E \sqrt{n} k\ell}{1 + (\beta_E\beta_\rho/3)nk^2\ell^2} \cos(\sqrt{n_t}kx) + \sin(\sqrt{n_t}kx)\right] \tag{4.116}$$

Numerical illustration The mean fields u_0, $U^{(1)}$ and $U^{(2)}$ (respectively given by (4.109), (4.112) and (4.116)) are first plotted on Figure 4.4 with the exact solution u^{p}. The first-order boundary corrections are seen to improve qualitatively the match between $U^{(1)}$, $U^{(2)}$ and u^{p}. From these solutions, we then reconstruct the approximations $\tilde{u}^{(1)}$ and $\tilde{u}^{(2)}$ as:

$$\begin{aligned} \tilde{u}^{(1)}(x) &= U^{(1)}(x) + \varepsilon P_1\left(\frac{x}{\varepsilon}\right) U^{(1)}_{,x}(x) \\ \tilde{u}^{(2)}(x) &= U^{(2)}(x) + \varepsilon P_1\left(\frac{x}{\varepsilon}\right) U^{(2)}_{,x}(x) + \varepsilon^2 P_2\left(\frac{x}{\varepsilon}\right) U^{(2)}_{,xx}(x) \\ &= \left(1 - \varepsilon^2 n_t(k)k^2 P_2\left(\frac{x}{\varepsilon}\right)\right) U^{(2)}(x) + \varepsilon P_1\left(\frac{x}{\varepsilon}\right) U^{(2)}_{,x}(x) \end{aligned} \tag{4.117}$$

while the cell functions are given for the bi-layered material by (4.69) for P_1 and by (4.72) for P_2. These approximations are plotted on Figure 4.5 and a very good qualitative agreement between u and $\tilde{u}^{(2)}$ is observed.

Figure 4.6 finally illustrates the convergence of these models as $\varepsilon \to 0$ (in this case, k is kept fixed while $N \to +\infty$ so that $\ell \to 0$). The first and second-order H^1-estimates provided by Lemmas 4.2 and 4.3 are clearly observed. Moreover, L^2-estimate stated by Theorem 4.4 for $\tilde{u}^{(1)}$ is seen, as well as its counterpart for $\tilde{u}^{(2)}$ predicted by Remark 4.8. The solutions obtained without boundary corrections (i.e. by replacing $U^{(1)}$ and $U^{(2)}$ by u_0 in (4.117)) are plotted in dashed lines, and they highlight the need for these corrections as discussed in Remarks 4.6 and 4.8.

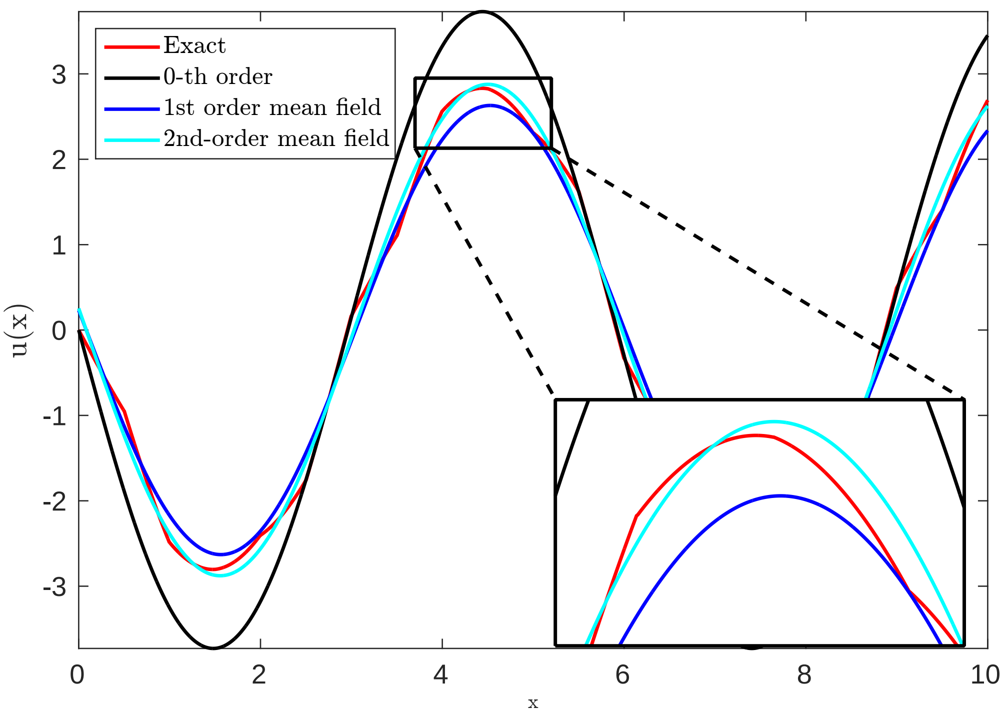

Figure 4.4: Exact displacement u^{p} and homogenized mean fields U_0, $U^{(1)}$ and $U^{(2)}$ for $k = 1$, $\ell = 1$ (so that $\varepsilon = 0.16$), $\gamma = 0.5$ and $u_L = 1$.

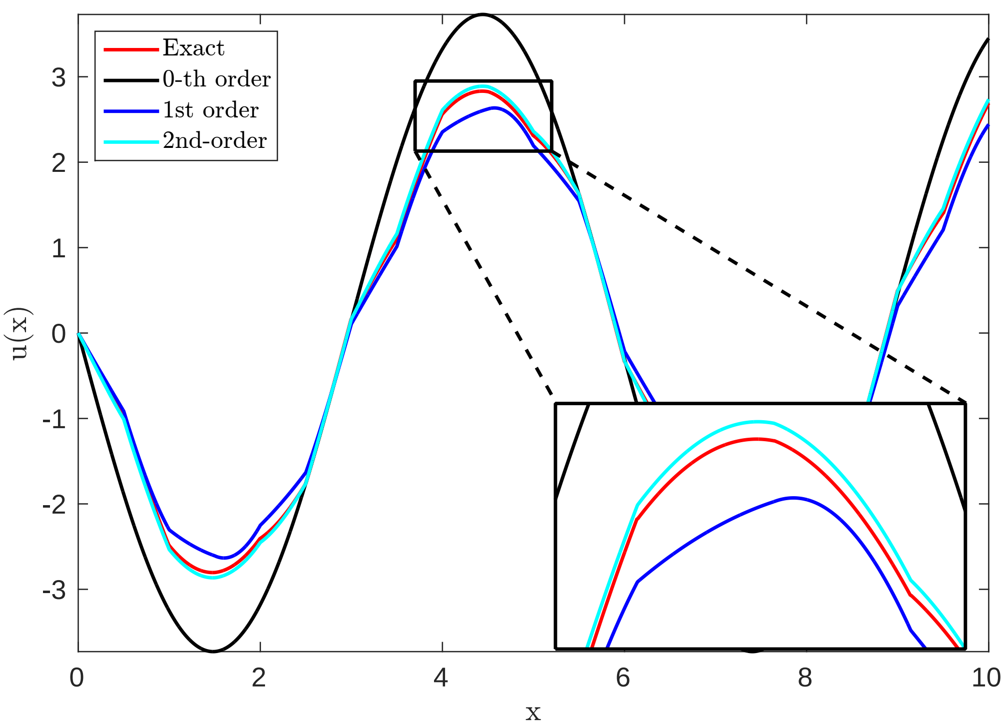

Figure 4.5: Exact displacement u^{p} and homogenized total fields U_0, $\tilde{u}^{(1)}$ and $\tilde{u}^{(2)}$ defined by (4.117) for $k = 1$, $\ell = 1$ (so that $\varepsilon = 0.16$), $\gamma = 0.5$ and $u_L = 1$.

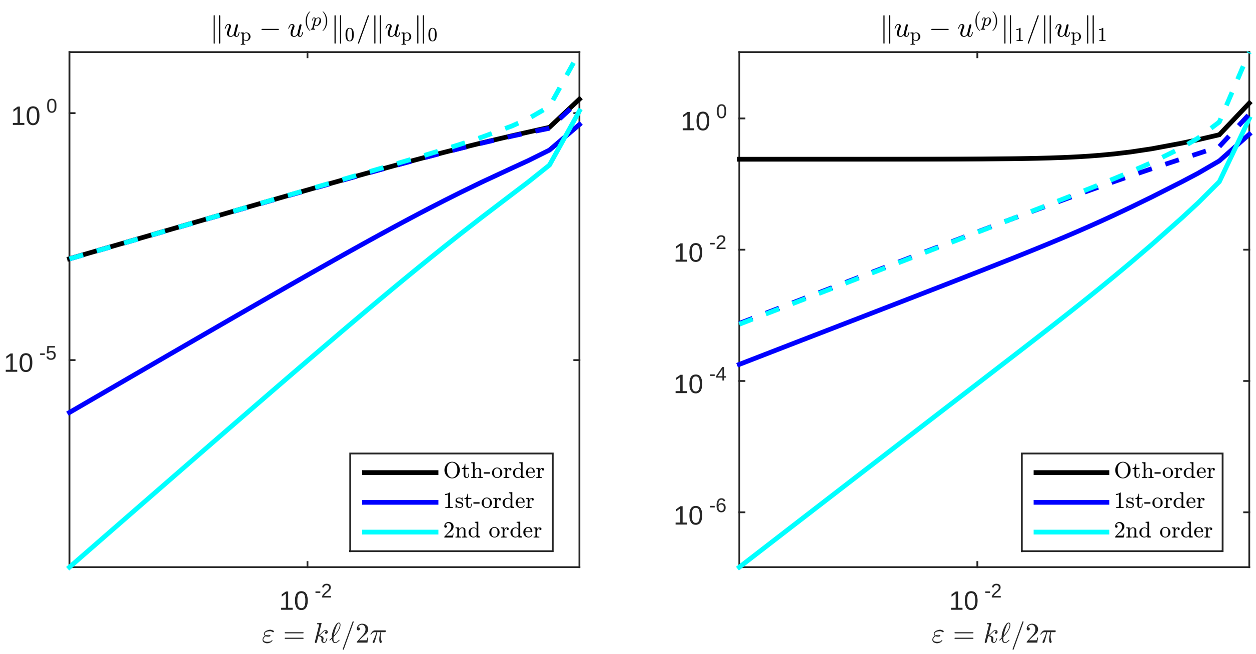

Figure 4.6: Errors on the L^2 and H^1-norms of the homogenized approximations $\tilde{u}^{(p)}$ defined by (4.117), in log-scale. The parameters are $\gamma = 0.5$, $k = 1$. Dashed lines correspond to the solutions computed with no corrections on the boundary conditions.

4.3.3 About the associated eigenvalue problems

Up to this point, we only have considered the sets of eigenvalues of the periodic problem (i.e. the zeros of the characteristic function f_{p}) and those of the homogenized mean field problems (i.e the zeros of f_0, f_1 and f_2), without specifying further the relationships between these sets. Indeed, the homogenization of eigenvalue problems is a complex issue addressed in [Santosa & Vogelius, 1993] [2] and completed later by [Moskow & Vogelius, 1997] for the Dirichlet eigenvalue problem, while [Moskow, 1997] addressed the Neumann eigenvalue problem. It is well-known that the eigenvalues of the exact problem (4.98) (the zeros of f_{p}) converge to those of the leading-order homogenized eigenvalue problem (4.107) (the zeros of f_0) as $\varepsilon \to 0$. However higher-order correction must be addressed carefully, by means of an analysis that involves the boundary correctors we invoked in Section 4.1.2 rather than the boundary corrections we introduced in problems (4.110) and (4.113).

As a consequence, we *do not* claim that the eigenvalues of these problems (i.e. the zeros of f_1 and f_2 defined resp. by (4.111) and (4.115)) are better approximations to those of f_{p}, but rather limit ourselves to empirical observations on a specific example. On Figure 4.7 are shown the errors on the first six eigenvalues associated with the homogenized models corresponding to a given microstructured rod. These eigenvalues were chosen so that all of them are smaller than the onset of the band-gap of the periodic structure k_{BG}. On the particular setting that is shown here, all models are very accurate: the associated eigenvalues have less than 1% misfit with those of the periodic model. However the second-order model provides a slightly better approximation, which could justify further investigations.

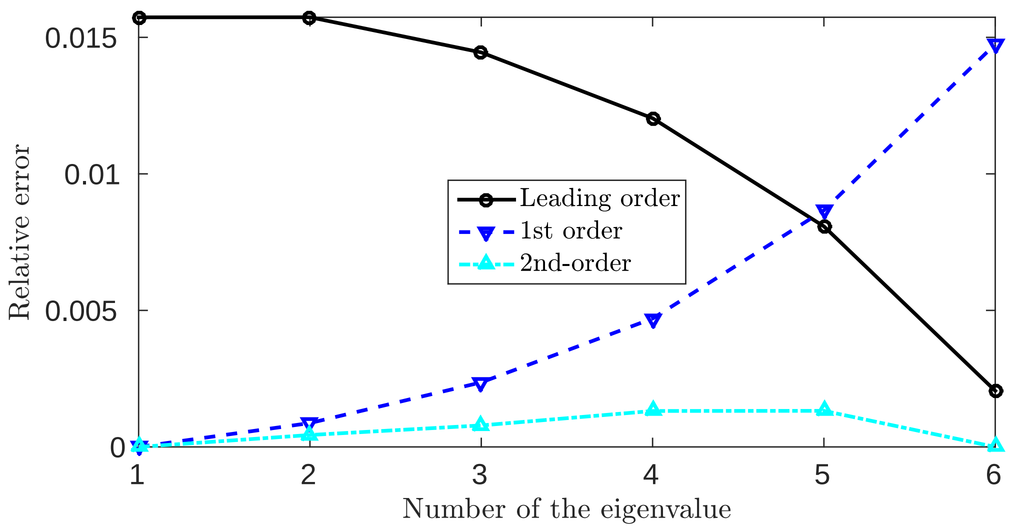

Figure 4.7: Relative errors on the eigenvalues for the problems (4.107), (4.110) and (4.113) (zeros of f_0, f_1 and f_2) with respect to those of problem (4.98) (zeros of f_{p}), $\ell = 1$, $\gamma = 0.5$ and $u_L = 1$.

[2] See also erratum [Santosa & Vogelius, 1995]

4.4 Conclusion and perspectives

The main addition of this chapter is the presentation and justification of simple boundary conditions for high-order homogenized one-dimensional problems. The idea promoted here is to enforce exact boundary condition for the two-scale expansion in the BVP satisfied by the mean fields. However it cannot be generalized to higher dimensions, as discussed in Section 4.1.2. Nonetheless, we think they can provide a simple framework for a better understanding of second-order homogenization in bounded domains.

Many follow-ups come to mind. The first one is to look into the models that feature fourth-order space derivatives, that we have discarded yet and for which deriving accurate BCs requires other mathematical and/or physical considerations. A very interesting perspective is also investigate into the relevance of the proposed local boundary conditions for eigenvalue problems, following the brief discussion and observations of Section 4.3.3. In particular, the relationships between these boundary conditions and the boundary correctors used in the analysis of such eigenvalue problem are to be explicated -if any- and understood further.

Chapter 5

Homogenized interior transmission problem and identification of a periodically-varying rod.

Contents

This chapter comes to the main purpose of the second part, which is to propose an identification procedure of a two-phase layered 1D inhomogeneity of length L. Typically, such an inhomogeneity may be the rod with piecewise constant cross section studied in the last chapter, this time prolongated on both sides by parts with fixed cross section. We suppose that the only knowledge available is the low-frequency spectrum of the associated transmission eigenvalues (TEs). As explained in the introduction, such eigenvalues are defined as the frequencies for which there exists an incident wave (the associated eigenfunction) that is transmitted through the inhomogeneity with no reflected wave. They can be seen e.g. as the "counterpart" of the band-gap frequencies for which no energy is transmitted through the inhomogeneity as discussed by [Dontsov et al., 2013] for such a one-dimensional microstructure.

Recall also that the TEs can be computed as the eigenvalues of an equivalent *interior* transmission problem (ITP) posed only on the support $[0, L]$ of the inhomogeneity. Thus we propose to study the ITP to propose a model suitable for identification. At our knowledge, the simple one-dimensional ITP we will focus on here has not yet been addressed, but close studies [Colton et al., 2010; Aktosun et al., 2011] address a spherically stratified acoustic medium.

To provide a convenient model, while accounting for microstructure effects, we aim at using homogenized approximations of the exact ITP for the periodic inhomogeneity, based on the results presented in the last chapter and leaning on the recent work [Cakoni et al., 2015] that shows that the

TEs of the leading-order homogenized ITP converge to these of the exact ITP. After some reminders and preliminary results on ITPs for homogeneous and periodic inhomogeneitys in Section 5.1, we investigate this leading-order homogenized ITP in Section 5.2. In the present case, it is shown to be accurate to approach low-frequency TEs and well suited for asymptotic expansions under low-contrast assumption. These asymptotics lead to remarkably simple formulas expressing the length L of the inhomogeneity and the section ratio γ as functions of the first two TEs. However, the leading-order homogenized ITP does not retain the period ℓ as a parameter, thus it cannot be inverted to recover this parameter. Preliminary qualitative results for higher-order homogenized ITP are then presented, yet without complete analysis.

5.1 Definitions and preliminary results

Consider (i) a homogeneous background material characterized by constant Young's modulus E and density ρ and (ii) an heterogeneous inhomogeneity characterized by the length L, and the space-varying Young's modulus $E_{\mathrm{p}}(x)$ and the density $\rho_{\mathrm{p}}(x)$. The 1D elastic interior problem consists in finding a couple of displacements (v, w) such that:

$$\left| \begin{array}{ll} Ev_{,xx} + \rho\omega^2 v = 0 & x \in [0, L] \\ \left(E_{\mathrm{p}} w_{,x}\right)_{,x} + \rho_{\mathrm{p}}\omega^2 w = 0 & x \in [0, L] \\ v = w & x = 0 \text{ and } x = L \\ Ev_{,x} = E_{\mathrm{p}} w_{,x} & x = 0 \text{ and } x = L \end{array} \right. \tag{5.1}$$

The displacement v is associated with the inhomogeneity geometry but with the background material properties, whereas w corresponds to the periodic inhomogeneity. We require that both the displacements and stresses associated to these fields match at the boundaries $x = 0$ and $x = L$. Defining the longitudinal wave speed c and wave number k for the background medium as:

$$c = \sqrt{\frac{E}{\rho}} \text{ and } k = \frac{\omega}{c} = \omega\sqrt{\frac{\rho}{E}}, \tag{5.2}$$

then the *transmission eigenvalues (TEs)* $k \in \mathbb{R}\backslash\{0\}$ are defined as the wavenumbers such that there exists a non-trivial solution $(v, w) \in (L^2([0, L]))^2$ to the problem (5.1).

Remark 5.1. *In this work, we will address only* real *transmission eigenvalues. However, as in [Colton et al., 2010] for spherically stratified inhomogeneities, we could observe that there exists complex TEs, at least for particular configurations such as the homogeneous inhomogeneity presented next.*

5.1.1 ITP for a homogeneous inhomogeneity

Focusing on the ITP for a *homogeneous* inhomogeneity permits to carry out analytical and asymptotic developments which will also be of use thereafter. We characterize such inhomogeneity by constant Young's modulus and density $(E^\star, \rho^\star)$. For convenience, we introduce the alternative set of parameters:

- Young's moduli ratio $\alpha = E^\star/E$

- refraction index $n = c^2/(c^\star)^2 = (E/\rho)/(E^\star/\rho^\star)$.

The ITP (5.1) then becomes:

$$\left| \begin{array}{ll} v_{,xx} + k^2 v = 0 & x \in [0, L] \\ w_{,xx} + nk^2 w = 0 & x \in [0, L] \\ v = w & x = 0 \text{ and } x = L \\ v_{,x} = \alpha w_{,x} & x = 0 \text{ and } x = L \end{array} \right. \tag{5.3}$$

The solutions v and w to the equilibrium equations can be given in terms of four real coefficients (A, B, a, b) as:

$$\begin{aligned} v(x) &= A\cos(kx) + B\sin(kx), \\ w(x) &= a\cos(\sqrt{n}kx) + b\sin(\sqrt{n}kx). \end{aligned} \tag{5.4}$$

Moreover, the boundary conditions at $x = 0$ impose $A = a$ and $B = \alpha\sqrt{n}b$ while those at $x = L$ result in the 2×2 system:

$$\boldsymbol{M}_0(k) \begin{bmatrix} a \\ b \end{bmatrix} = 0, \tag{5.5}$$

with:

$$\boldsymbol{M}_0(k) = \begin{bmatrix} \cos(kL) - \cos(\sqrt{n}kL) & \alpha\sqrt{n}\sin(kL) - \sin(\sqrt{n}kL) \\ -\sin(kL) + \alpha\sqrt{n}\sin(\sqrt{n}kL) & \alpha\sqrt{n}\left[\cos(kL) - \cos(\sqrt{n}kL)\right] \end{bmatrix}. \tag{5.6}$$

This linear system has non-trivial solutions if and only if the matrix $\boldsymbol{M}_0(k)$ is singular, i.e. if and only if $\det(\boldsymbol{M}_0(k)) = 0$. Therefore, we define the *characteristic function* f_0, such that $f_0(k) = 0$ if and only if k is a TE, as:

$$\begin{aligned} f_0(k) &= \det(\boldsymbol{M}_0(k)) \\ &= 2\alpha\sqrt{n}(1 - \cos(kL)\cos(\sqrt{n}kL)) - (1 + \alpha^2 n)\sin(kL)\sin(\sqrt{n}kL). \end{aligned} \tag{5.7}$$

For easier visualizations, we will also use the *indicator function* $I_0(k) := 1/|f_0(k)|$ whose peaks indicate the location of TEs. For a given TE $k^\star$, the corresponding eigenvector $(v^\star, w^\star)$ is (up to a multiplicative constant):

$$\left\{ \begin{array}{l} v^\star(x) = \cos(k^\star x) + \alpha\sqrt{n}\zeta\sin(k^\star x) \\ w^\star(x) = \cos(\sqrt{n}k^\star x) + \zeta\sin(\sqrt{n}k^\star x) \end{array} \right. \text{ with } \zeta = \frac{\cos(\sqrt{n}k^\star L) - \cos(k^\star L)}{\alpha\sqrt{n}\sin(k^\star L) - \sin(\sqrt{n}k^\star L)}. \tag{5.8}$$

Finally, we define r such that $\sqrt{n} = 1 + r$ and remark that the characteristic function f_0 (5.7) admits the alternative expressions:

$$\begin{aligned} f_0(k) &= 2\alpha(1+r) - \left[2\alpha(1+r) + (1 - \alpha(1+r))^2\sin^2(kL)\right]\cos(rkL) \\ &\quad - \left[(1 - \alpha(1+r))^2\sin(kL)\cos(kL)\right]\sin(rkL) \\ &= 2\alpha(1+r)\left[1 - \cos(rkL)\right] - (1 - \alpha(1+r))^2\sin(kL)\sin((1+r)kL) \end{aligned} \tag{5.9}$$

The expressions (5.9) emphasize the fact that f_0 features oscillatory functions with the two periods $2\pi/L$ and $2\pi/rL$, which can be very different, especially at the limit case $n \to 1$ i.e. $r \ll 1$. Figure 5.1 illustrates this observation for $(\alpha, n) = (2, 2)$. It also plots the characteristic and indicator functions for the limit cases $n = 1$ and $\alpha = 1$, that we address next.

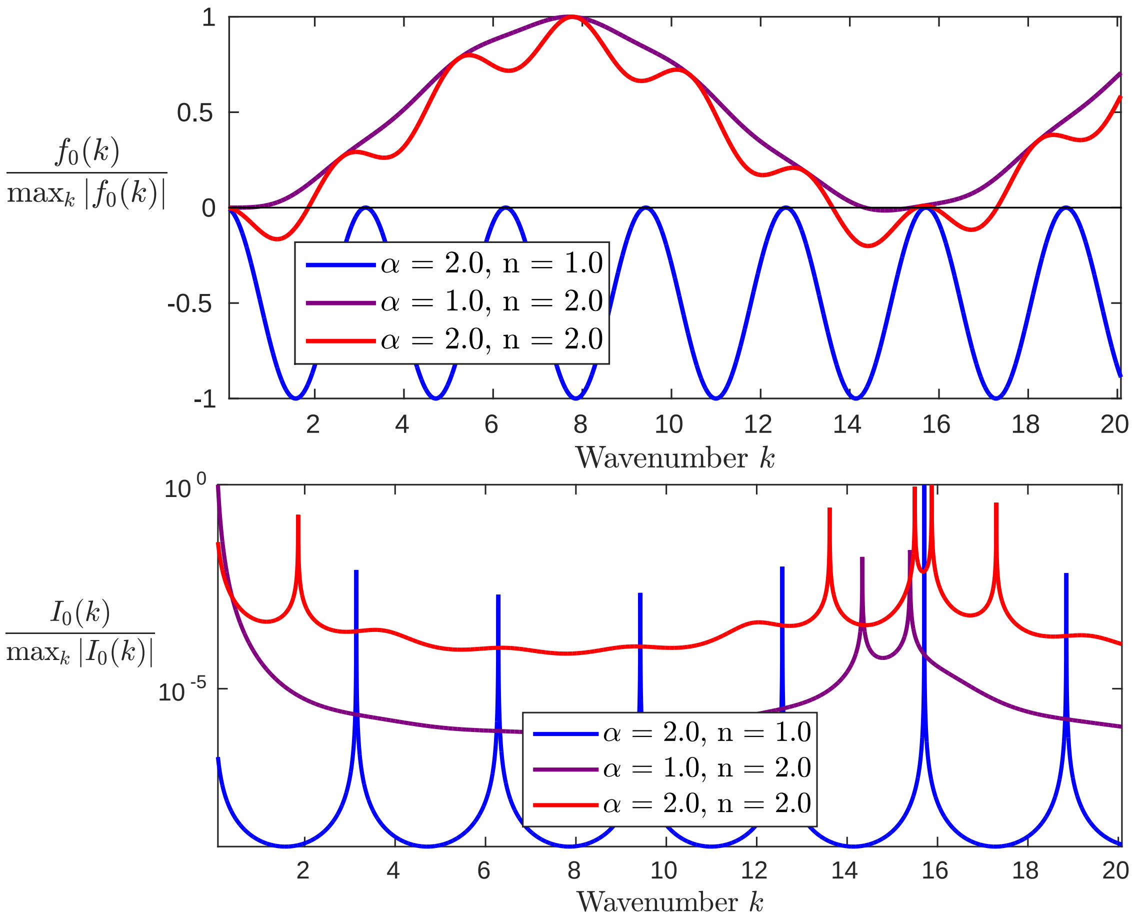

Figure 5.1: Normalized characteristic function f_0 (5.9) and indicator function $I_0 := 1/|f_0|$ for $L = 1$ and different values of material coefficients (α, n). The transmission eigenvalues are such that $f_0(k) = 0$ (and thus correspond to the peaks of I_0).

5.1.1.1 Refraction index $n = 1$

In the case $n = 1$, i.e. $E^\star/E = \rho^\star/\rho$, the inhomogeneity is completely characterized by the Young's moduli ratio α and its length L. In this case, the characteristic function f_0 (5.7) reduces to:

$$f_0(k) = -(1+\alpha)^2 \sin^2(kL), \tag{5.10}$$

and the two-period behavior discussed above vanishes as seen on Figure 5.1. The set of transmission eigenvalues is $\{k^\star_m = m\pi/L, \; m \in \mathbb{N}\}$. The length L of the inhomogeneity is therefore easily identifiable from the first TE, or any other TE provided we now its rank m:

$$L = \frac{\pi}{k^\star_1} = \frac{m\pi}{k^\star_m} \quad \forall m \in \mathbb{N}. \tag{5.11}$$

On the other hand, for such configuration, the TEs are independent of the contrast α, which thus cannot be recovered if these TEs are the only available information.

5.1.1.2 Young's moduli ratio $\alpha = 1$

If $\alpha = 1$, i.e. $E^\star = E$, then the index $n = \rho^\star/\rho$ is the only remaining material parameter, and the characteristic function (5.9) becomes

$$f_0(k) = 2(1+r)\left[1 - \cos(rkL)\right] - r^2 \sin(kL)\sin((1+r)kL), \tag{5.12}$$

in terms of $r = \sqrt{n} - 1$. Unlike the previous case, there is no simple way to determine the zeros of this function and thus to provide an inversion scheme. However, one can make further assumptions. In particular, a possibility is to investigate the low-contrast regime, i.e. to look for the zeros of f_0 when $r \to 0$, whichcorresponds to $n \to 1$.

In this case, since $r^2 = o(1+r)$, by looking at the two terms in formula (5.12) one can expect that the condition $|1 - \cos(rkL)| \ll 1$ is required for k to be a TE. This leads us to look for TEs around what we refer to as the "central zeros" k_m:

$$k_m = \frac{2m\pi}{rL}. \tag{5.13}$$

To this end, we compute the Taylor expansion of f_0 about these k_m values. Setting $k = k_m + \delta_m$, we look for the zeros of the second-order approximation f_m of f_0, given in term of the dimensionless variable $X := \delta_m L$ as:

$$f_m(X) := f_0(k_m) + \frac{f_0'(k_m)}{L}X + \frac{f_0''(k_m)}{2L^2}X^2 \quad \text{with} \quad X = \delta_m L = (k - k_m)L \tag{5.14}$$

and

$$\begin{aligned}
f_0(k_m) &= -r^2 s_m^2 && \text{with } s_m = \sin(k_m L) = \sin(2m\pi/r),\\
\frac{f_0'(k_m)}{L} &= -r^2(2+r)s_m c_m && \text{with } c_m = \cos(k_m L) = \cos(2m\pi/r),\\
\frac{f_0''(k_m)}{2L^2} &= \frac{1}{2}r^2(2+r)^2 s_m^2.
\end{aligned} \tag{5.15}$$

The discriminant of the polynomial equation $f_m(X) = 0$ is:

$$\Delta = r^4(2+r)^2 s_m^2\left(1 + s_m^2\right), \tag{5.16}$$

and the solutions $\delta_m^\pm$ of this equation are:

$$\delta_m^\pm = \frac{c_m \pm \sqrt{1+s_m^2}}{L(2+r)s_m}, \tag{5.17}$$

so that the two values $k_m + \delta_m^\pm$ are expected to provide a good approximation of the TEs.

Figure 5.2 shows an example of this approximation for two low-contrast values of the index n. The first couple of transmission eigenvalues is plotted. The first point to be noted is that they are indeed on either side of $k_1 = 2\pi/rL$. However, for the two values of n considered, only one of the corresponding couple of TEs is correctly approximated by $k_1 + \delta_1^\pm$. To provide another illustration, we represent on Figure 5.3 the three first couples of TEs for $n = 2$. Again, depending on how f_0 behave around a given central zero k_m, then the quality of the approximation varies.

Due to these variations, we cannot use the second-order approximation f_m of f_0 as a model suitable for straightforward inversion and identification. However, this pattern of coupled TEs around the central zeros k_m (5.13) is characteristic and provides itself some information: in the case $\alpha \neq 1$, it can be checked that there would be (at least) one low-frequency TE as seen on Figure 5.1. Moreover, the measure of these central zeros, which are reasonably well approximated as the mean of each couple of eigenvalues, could provide an accurate estimate of the product rL. Such an estimate could be used to e.g. initialize an iterative procedure to identify (r, L) from some of the available TEs.

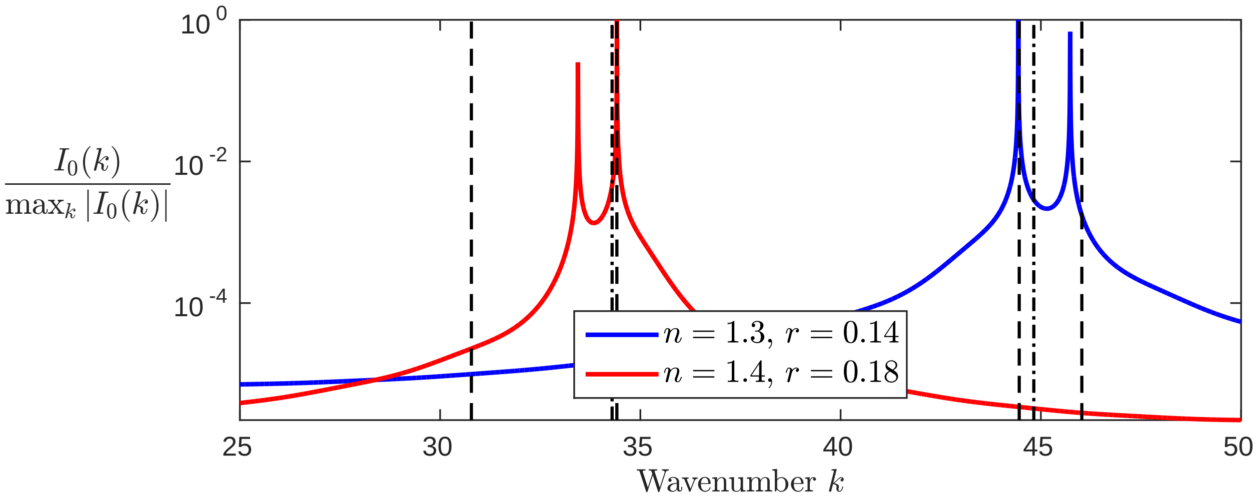

Figure 5.2: First couple of TEs for $L = 1$, $\alpha = 1$ and two low-contrast values of n. Dot-dashed vertical lines indicate the first fundamental zero $k_1 := 2\pi/rL$, and dashed lines the approximations $k_1 + \delta_1^{\pm}$.

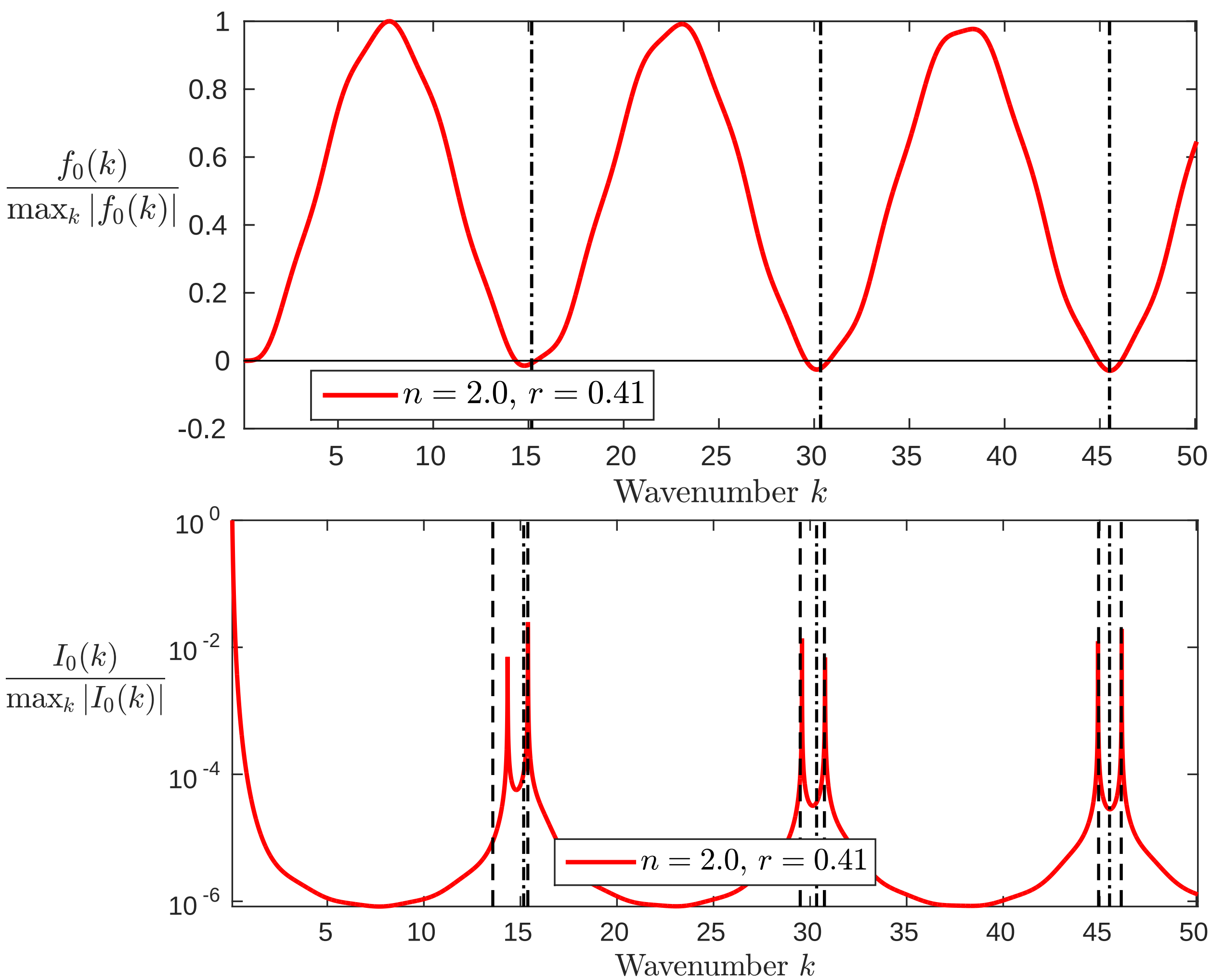

Figure 5.3: Normalized characteristic function f_0 and indicator function I_0 for $L = 1$, $\alpha = 1$ and $n = 2$. Dot-dashed vertical lines indicate the central zeros $k_m := 2m\pi/rL$, and dashed lines the approximations $k_m + \delta_m^{\pm}$.

To conclude this part, we would like to highlight the particular cases for which r takes rational values. Indeed, in such cases, the characteristic function f_0 (5.12) is periodic of period $2p\pi/rL$ for some $p \in \mathbb{N}$, which itself is a multiple of the two periods $2\pi/L$ and $2\pi/rL$. This could lead to shared zeros of the two oscillating contributions.

We do not provide further investigation, but we illustrate this remark with Figure 5.4. In particular, the couples of TEs around each central zero k_m in the general case can degenerate into a unique TE for some -but not necessarily all- of the k_m, see for example the case $r = 0.8$.

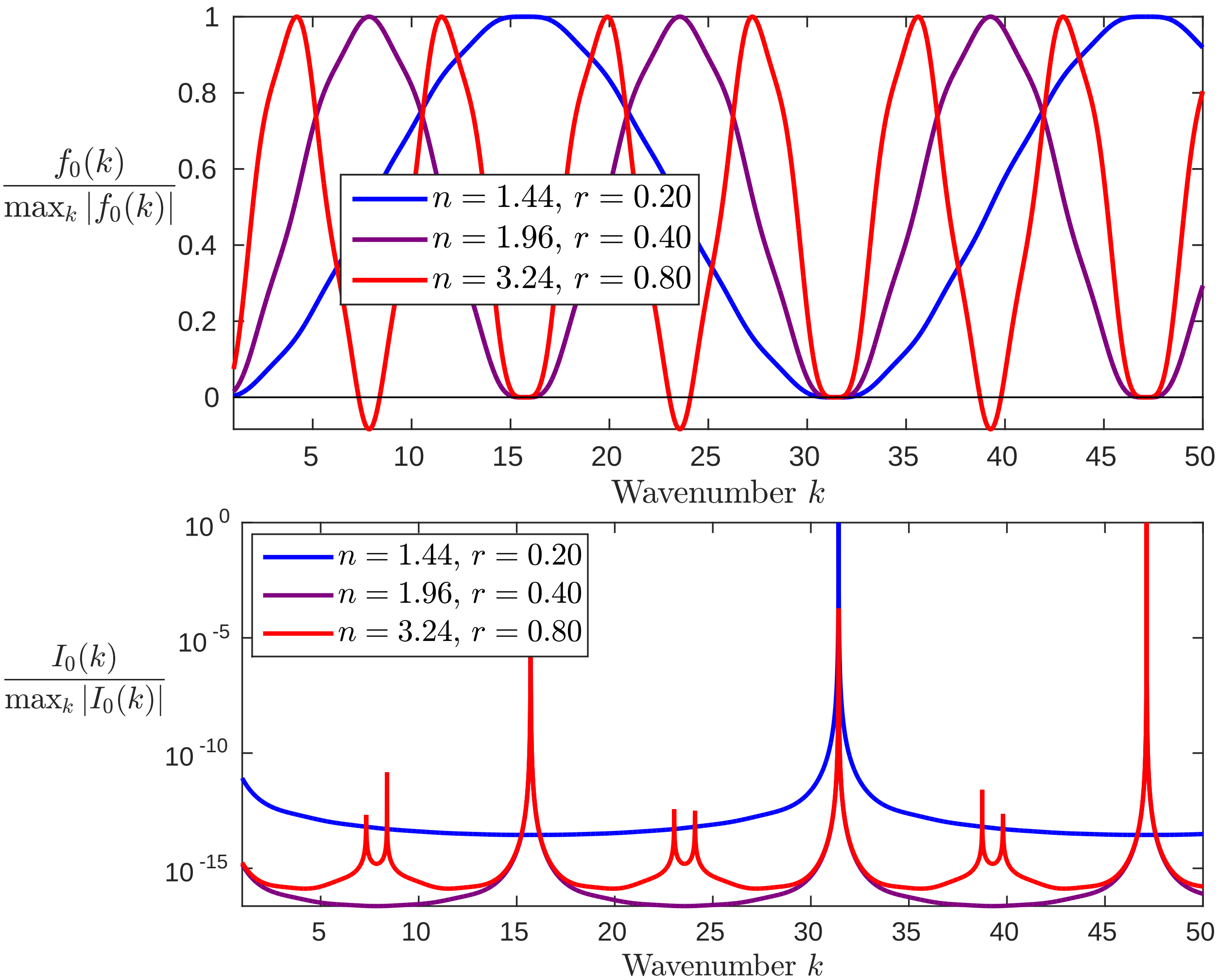

Figure 5.4: Normalized characteristic function f_0 and indicator function I_0 for $L = 1$, $\alpha = 1$ and rational values of $r = \sqrt{n} - 1$.

5.1.2 ITP for a microstructured inhomogeneity

In this section, the scatterer is considered to be made of the layered two-phase material that is described in the previous chapter and whose period or *cell length* is noted ℓ. The number of cells $N = L/\ell$ is supposed to be an integer, the small parameter to be considered is $\varepsilon = \ell/\lambda$, and $(E_{\rm p}, \rho_{\rm p})$ are defined by $E_{\rm p}(x) = \hat{E}(x/\varepsilon)$ and $\rho_{\rm p}(x) = \hat{\rho}(x/\varepsilon)$ with:

$$\hat{E}(y) = \begin{cases} E_1 = \alpha_E E & y \in [0, \hat{\ell}/2] \\ E_2 = \gamma_E E_1 = \alpha_E \gamma_E E & y \in [\hat{\ell}/2, \hat{\ell}] \end{cases} \qquad \hat{\rho}(y) = \begin{cases} \rho_1 = \alpha_\rho \rho & y \in [0, \hat{\ell}/2] \\ \rho_2 = \gamma_\rho \rho_1 = \alpha_\rho \gamma_\rho \rho & y \in [\hat{\ell}/2, \hat{\ell}] \end{cases} \tag{5.18}$$

where $\hat{\ell} = \ell/\varepsilon$ is the normalized cell length. Moreover, we note $x_n := n\ell$, $n = 0 \dots N$ the boundaries of the cells, and $n_i = (E/\rho)/(E_i/\rho_i)$, $i \in \{1, 2\}$ the two possible values for the refraction index in each of the half-cell.

Considering the resulting periodic ITP (5.1) and proceeding with the same steps than for the homogeneous inhomogeneity, we first remark that the solution v to the homogeneous "background" equilibrium equation can be defined by two coefficients (A, B) as:

$$v(x) = A\cos(kx) + B\sin(kx). \tag{5.19}$$

The solution w to the "periodic" equilibrium equation with piecewise-constant refraction index is accordingly defined piecewisely in each cell $[x_n, x_{n+1}]$ by the coefficients $(a_n^{(1)}, b_n^{(1)}, a_n^{(2)}, b_n^{(2)})$ as:

$$\left| \begin{array}{ll} w(x) = a_n^{(1)}\cos(\sqrt{n_1}k(x - x_n)) + b_n^{(1)}\sin(\sqrt{n_1}k(x - x_n)) & x \in [x_n, x_n + \ell/2], \\ w(x) = a_n^{(2)}\cos(\sqrt{n_2}k(x - x_n - \ell/2)) + b_n^{(2)}\sin(\sqrt{n_2}k(x - x_n - \ell/2)) & x \in [x_n + \ell/2, x_{n+1}]. \end{array} \right. \tag{5.20}$$

We then write the boundary conditions matching v, w and the corresponding stresses at $x = 0$ and $x = L$, and the transmission conditions for w at each interface between half-cells. Introducing for convenience an additional fictitious half-cell $[L, L+\ell/2]$ and corresponding coefficients $(a_N^{(1)}, b_N^{(1)})$, then these conditions can be expressed as the linear system:

$$\begin{aligned} x = 0 \ &: \begin{bmatrix} a_0^{(1)} \\ b_0^{(1)} \end{bmatrix} = \boldsymbol{B}_0(k) \begin{bmatrix} A \\ B \end{bmatrix}, \\ x = x_n + \ell/2 \ &: \begin{bmatrix} a_n^{(2)} \\ b_n^{(2)} \end{bmatrix} = \boldsymbol{B}_1(k) \begin{bmatrix} a_n^{(1)} \\ b_n^{(1)} \end{bmatrix}, \\ x = x_{n+1} \ &: \begin{bmatrix} a_{n+1}^{(1)} \\ b_{n+1}^{(1)} \end{bmatrix} = \boldsymbol{B}_2(k) \begin{bmatrix} a_n^{(2)} \\ b_n^{(2)} \end{bmatrix} = \boldsymbol{B}_2(k)\boldsymbol{B}_1(k) \begin{bmatrix} a_n^{(1)} \\ b_n^{(1)} \end{bmatrix}, \\ x = L \ &: \begin{bmatrix} a_N^{(1)} \\ b_N^{(1)} \end{bmatrix} = \boldsymbol{B}_L(k) \begin{bmatrix} A \\ B \end{bmatrix}. \end{aligned} \tag{5.21}$$

The "boundary" matrices $\boldsymbol{B}_0$ and $\boldsymbol{B}_L$ are defined by:

$$\boldsymbol{B}_0(k) = \begin{bmatrix} 1 & 0 \\ 0 & (\alpha_E\sqrt{n_1})^{-1} \end{bmatrix}, \quad \boldsymbol{B}_L(k) = \begin{bmatrix} \cos(kL) & \sin(kL) \\ -(\alpha_E\sqrt{n_1})^{-1}\sin(kL) & (\alpha_E\sqrt{n_1})^{-1}\cos(kL) \end{bmatrix}, \tag{5.22}$$

and the transmission matrices $\boldsymbol{B}_1$ and $\boldsymbol{B}_2$ by (4.101). Combining all these equations, we finally obtain the system:

$$(\boldsymbol{B}_2\boldsymbol{B}_1)^N\boldsymbol{B}_0 \begin{bmatrix} A \\ B \end{bmatrix} = \boldsymbol{B}_L \begin{bmatrix} A \\ B \end{bmatrix} \Longleftrightarrow \left[(\boldsymbol{B}_2\boldsymbol{B}_1)^N\boldsymbol{B}_0 - \boldsymbol{B}_L\right] \begin{bmatrix} A \\ B \end{bmatrix} = 0. \tag{5.23}$$

The characteristic function f_p that satisfies $f_\mathrm{p}(k) = 0$ if and only if k is a TE and its associated indicator function I_p are therefore given by:

$$f_\mathrm{p}(k) := \det\left(\left[(\boldsymbol{B}_2\boldsymbol{B}_1)^N\boldsymbol{B}_0 - \boldsymbol{B}_L\right](k)\right) \quad \text{and} \quad I_\mathrm{p}(k) := \frac{1}{|f_\mathrm{p}(k)|}. \tag{5.24}$$

This function, although easily computable numerically for any set of parameters defining the periodic inhomogeneity, does not have a convenient closed-form expression, and therefore is not well-suited for an analytical inversion procedure. It is why we rely on an homogenized version of this periodic ITP to obtain an identification procedure in closed forms.

Some examples of the characteristic and indicator functions are shown on Figure 5.5 and for $\alpha_E = \alpha_\rho = 1$. For the indicator functions, we plotted the whole first Brillouin zone, i.e. the range of frequencies before the first band-gap. It is observed that the characteristic functions present a fast oscillatory behavior around a slower "mean", as for the homogeneous ITP addressed in the previous section. Depending on the amplitude ratio of these two contributions, governed by the couple (γ_E, γ_ρ), they can have one or several zeros at low-frequency, where "low-frequency" is to be understood in the sense "in beginning of the first Brillouin zone".

On Figures 5.6, we impose an "initial" contrast by setting $\alpha_E = \alpha_\rho = 2$ so that $E_\mathrm{p}(x)$ (resp. $\rho_\mathrm{p}(x)$) varies between $E_1 = 2E$ and $E_2 = 2\gamma_E E$ (resp. $\rho_1 = 2\rho$ and $\rho_2 = 2\gamma_\rho\rho$). As a result, more low-frequency TEs are observed for the plotted configurations.

In both these examples, the most low-frequency TEs are observed for (i) $\gamma_E = \gamma_\rho$ and (ii) γ_E and γ_ρ close to 1, which corresponds to low contrast within the periodic structure. We therefore focus next on such configurations.

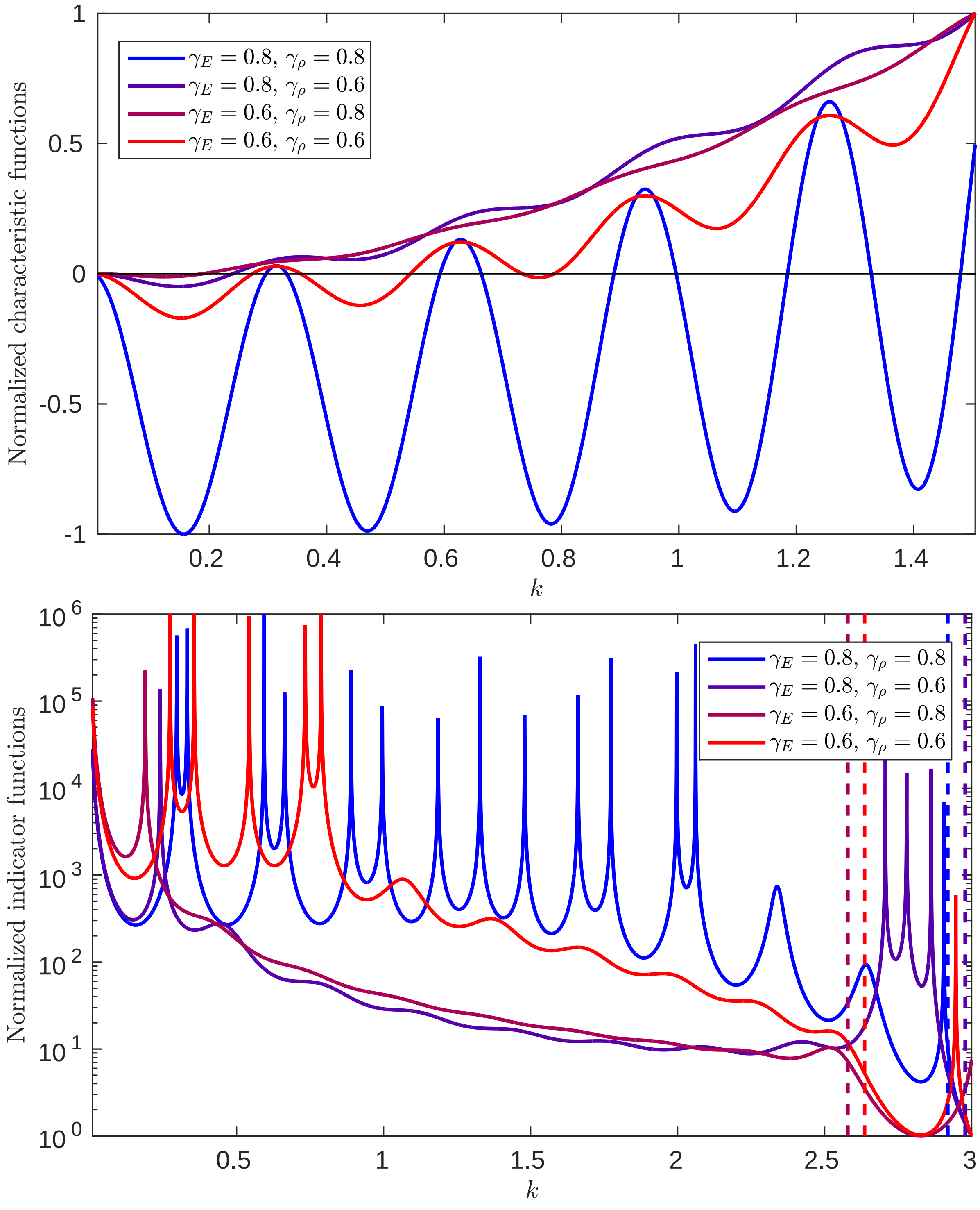

Figure 5.5: Characteristic function $f_{\mathrm{p}}(k)$ (top) and indicator function $I_{\mathrm{p}}(k) = 1/|f_{\mathrm{p}}(k)|$ (bottom) of the periodic ITP for $L = 10$, $\ell = 1$, $E = 1$, $\rho = 1$,$\alpha_E = \alpha_\rho = 1$ and various couples (γ_E, γ_ρ). The frequency spreads the range $[0, k_{\mathrm{BG}}/2]$ for f_{p}, with k_{BG} the onset of the first band-gap, and $[0, k_{\mathrm{BG}}]$ for I_{p}, with k_{BG} indicated by dashed vertical lines for each couple.

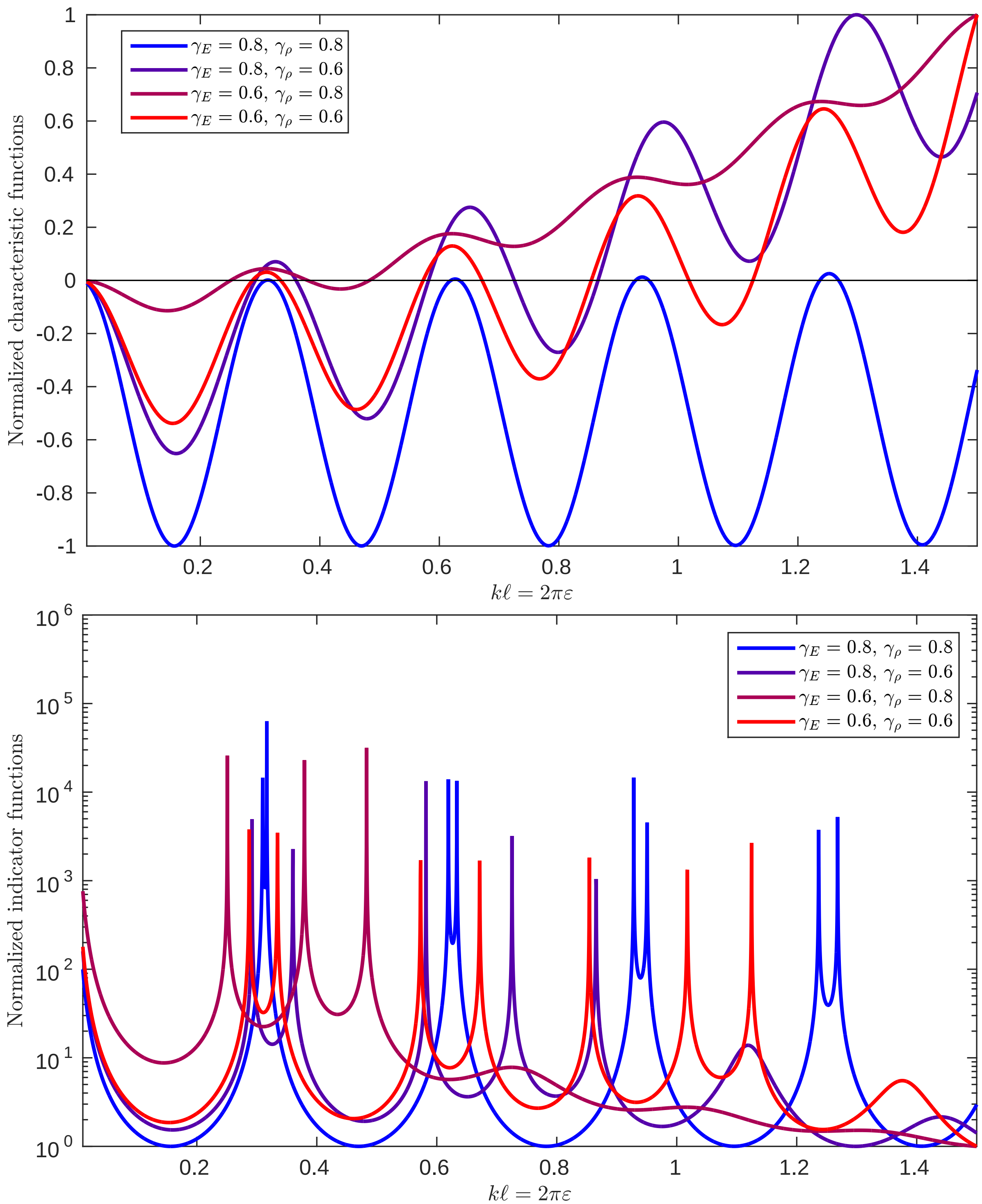

Figure 5.6: Characteristic and indicator functions of the periodic ITP for $L = 10$, $\ell = 1$, $E = 1$, $\rho = 1$, $\alpha_E = \alpha_\rho = 2$ and various couples (γ_E, γ_ρ).

5.2 Homogenized interior transmission problem

We present now the application of the homogenization process presented in the previous section to the interior transmission problem for the periodic inhomogeneity discussed in Section 5.1.2.

5.2.1 Leading-order homogenization

The leading-order homogenized ITP, is obtained by replacing (v, w) in the periodic ITP (5.1) by its homogenized approximation (v_0, w_0), which satisfies:

$$\left| \begin{array}{ll} v_{0,xx} + k^2 v_0 = 0 & x \in [0, L] \\ w_{0,xx} + nk^2 w_0 = 0 & x \in [0, L] \\ v_0 = w_0 & x = 0 \text{ and } x = L \\ v_{0,x} = \alpha w_{0,x}, & x = 0 \text{ and } x = L. \end{array} \right. \tag{5.25}$$

This is the ITP for a homogeneous inhomogeneity presented in Section 5.1.1, with $(E^\star, \rho^\star)$ replaced by the leading order homogenized coefficients $(\mathcal{E}_0, \varrho_0)$ defined by (4.80), so that α and n are given by:

$$\alpha = \frac{\mathcal{E}_0}{E} = \alpha_E \frac{2\gamma_E}{\gamma_E + 1} \quad \text{and} \quad n = \frac{c^2}{c_0^2} = \frac{E/\rho}{\mathcal{E}_0/\varrho_0} = \frac{\alpha_\rho}{\alpha_E} \frac{(\gamma_E + 1)(\gamma_\rho + 1)}{4\gamma_E}. \tag{5.26}$$

Recall that the characteristic function reads:

$$f_0(k) = 2\alpha\sqrt{n}(1 - \cos(kL)\cos(\sqrt{n}kL)) - (1 + \alpha^2 n)\sin(kL)\sin(\sqrt{n}kL). \tag{5.27}$$

The recent work [Cakoni et al., 2015, Thms. 3.1 and 3.2] justified the use of such homogenized model by proving the convergence (up to a subsequence) of the TEs and the associated eigenfunctions of the periodic ITP to those of the homogenized ITP as $\varepsilon \to 0$. It is to be noted that this is achieved under certain assumptions on the bounds of the parameters corresponding to the coefficients $(E_\text{p}, \rho_\text{p})$. In particular, permitting both E_p and ρ_p to reach the values of E and ρ somewhere within the inhomogeneity (which is the case for any two half-cell when we set $\alpha_E = \alpha_\rho = 1$) does not fulfill these assumptions. However, we choose to retain this setting in order to keep our empirical work as simple as possible. We will see thereafter that very good agreement between the TEs of both problems can be observed, even if not proven rigorously.

5.2.1.1 Approximation of the TEs for (not so) weak contrast

As we did for the homogeneous inhomogeneity, we restrain the number of involved parameters by setting $\alpha_E = \alpha_\rho = 1$ and $\gamma_E = \gamma_\rho = \gamma$. These assumptions furthermore correspond to the physically relevant case of a rod with periodically varying cross-section which is represented on Figure 4.1, for which experimental data is available [Dontsov et al., 2013]. They imply:

$$\alpha = \frac{2\gamma}{\gamma + 1} \quad \text{and} \quad n = \frac{(\gamma + 1)^2}{4\gamma}. \tag{5.28}$$

In this case, the characteristic function denoted f_h is:

$$f_h(k) = 2\sqrt{\gamma}(1 - \cos(kL)\cos(\sqrt{n}kL)) - (1 + \gamma)\sin(kL)\sin(\sqrt{n}kL). \tag{5.29}$$

While closed-form formulas for the zeros of f_h are not available, we attempt again to derive approximate expressions by investigating the asymptotic behavior of f_h for weak contrasts, i.e. for $\gamma \to 1$. To this end, let us introduce the index contrast $\chi := n - 1$, given by:

$$\chi = \frac{1}{4}(\gamma + \gamma^{-1} - 2) \Longleftrightarrow \gamma = 1 - 2\sqrt{\chi}\sqrt{1+\chi} + 2\chi. \tag{5.30}$$

Remark that $\chi \sim (\gamma - 1)^2/4$ as $\gamma \to 1$, so that χ is well-suited to be a small parameter even for "quite large" contrasts $\gamma - 1$. Letting $\chi \to 0$ and writing the asymptotic expansion of $f_h(k)$, we obtain:

$$f_h(k) = (-\chi + \chi^{3/2}) \sin^2(kL) + O(\chi^2). \tag{5.31}$$

We thus define the central zeros k_m such that $\sin^2(k_m L) = 0$ as

$$k_m = \frac{m\pi}{L} \text{ for } m \in \mathbb{N}\backslash\{0\}. \tag{5.32}$$

For a fixed value $\chi \neq 0$ such that $|\chi| \ll 1$, we seek the zeros of f_h around these central zeros as the zeros of the second-order Taylor expansion of f_h about k_m:

$$f_m(\delta_m) := f_h(k_m) + \delta_m f_h'(k_m) + \frac{\delta_m^2}{2} f_h''(k_m) \quad \text{with} \quad \delta_m = k - k_m. \tag{5.33}$$

For the values $k = k_m$, then f_h and its derivatives become:

$$\begin{aligned} f_h(k_m) &= 2\sqrt{\gamma}\left(1 - (-1)^m \cos\left(\sqrt{1+\chi}m\pi\right)\right), \\ f_h'(k_m) &= 0, \\ f_h''(k_m) &= -2L^2\chi\sqrt{\gamma}(-1)^m \cos\left(\sqrt{1+\chi}m\pi\right). \end{aligned} \tag{5.34}$$

We then expand $\gamma = 1 - \sqrt{\chi} + o(\sqrt{\chi})$, and $\sqrt{1+\chi} = 1 + \chi/2 + o(\chi)$. For the Taylor expansion of the cosines to be accurate, we have to make the additional assumption that *both* χ and m are small enough so that $\chi m\pi \ll 1$. The following equations are therefore valid only for the few first TEs:

$$\begin{aligned} f_h(k_m) &= \frac{\chi^2}{4}(m\pi)^2 + o(\chi^2), \\ f_h'(k_m) &= 0, \\ f_h''(k_m) &= -2L^2\chi + o(\chi). \end{aligned} \tag{5.35}$$

Inserting (5.34) into (5.33), then the location of the zeros of f_h around k_m is found to be symmetrical up to this approximation:

$$\delta_m = \pm k_m \frac{\sqrt{\chi}}{2} + o(\sqrt{\chi}). \tag{5.36}$$

Eventually, we expect the first TEs, i.e. the zeros of the original characteristic function, to be approached by:

$$k_m^\pm := k_m + \delta_m^\pm = \frac{m\pi}{L}\left(1 \pm \frac{\sqrt{\chi}}{2}\right). \tag{5.37}$$

Some examples are plotted on Figure 5.7. Even if we lie outside the necessary assumptions for the convergence results of [Cakoni et al., 2015] to hold, as discussed above, the low-frequency TEs, corresponding to small homogenization parameter$\varepsilon = k\ell/2\pi$, are very well approximated by those of the homogenized ITP.

Moreover, and unlike the homogeneous inhomogeneity, the second approximation (5.37) we make here for low contrasts also gives very satisfying results for the first two TEs $k_1^{\pm}$ (when they exist) and for γ significantly different from 1: up to $\gamma = 0.6$ in the chosen example.

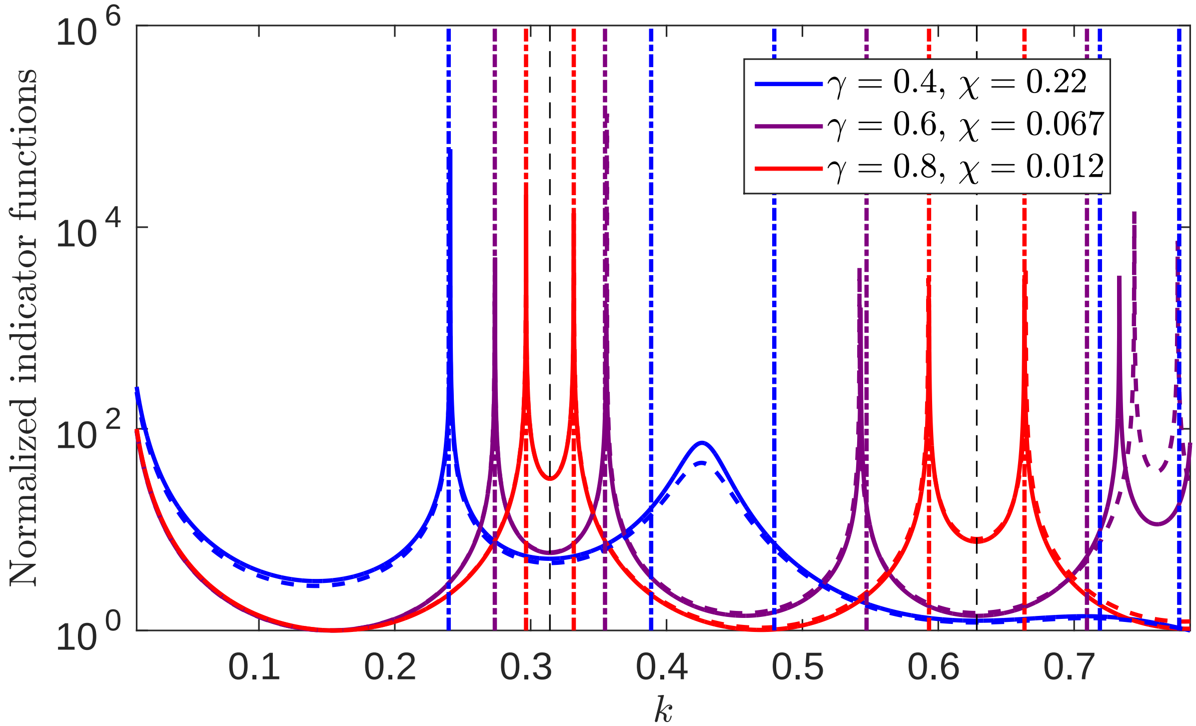

Figure 5.7: Exact indicator function $I_{\mathrm{p}} = 1/|f_{\mathrm{p}}|$ (solid lines), homogenized indicator function $I_h = 1/|f_h|$ (dashed lines) and low-contrast approximation of the TEs $k_m^{\pm}$ (dot-dashed vertical lines) for $L = 10$, $\ell = 1$, $E = 1$, $\rho = 1$ and several section ratio γ.

These approximations thus give a straightforward way to identify γ and L for a given inhomogeneity, provided we have an a priori knowledge that $\gamma \approx 1$. Indeed, suppose there exists at least two low-frequency TEs, k_1^- and k_1^+ that are measurable. Then inverting (5.37) leads to:

$$L \approx \frac{2\pi}{k_1^- + k_1^+}, \quad \text{and then:} \quad \chi \approx \left(\frac{L(k_1^+ - k_1^-)}{\pi}\right)^2 = \left(\frac{2(k_1^+ - k_1^-)}{k_1^- + k_1^+}\right)^2. \tag{5.38}$$

Theses expressions are the main result of this first section. They show how restrictive -but physically realistic- assumptions can lead to simple direct formulas for the identification of a periodic rod.

The last parameter we would need to completely characterize such inhomogeneity would then be the period ℓ. Obviously, that cannot be done using the leading-order homogenized ITP, since it the dependency on ℓ vanishes in the homogenization process. It is why it is necessary to push the homogenization to higher orders.

5.2.2 Higher-order homogenized interior transmission problem

First order. We consider the first-order approximation of (v, w), and note $(\tilde{v}, \tilde{w} = W^{(1)})$ the associated homogenized mean fields (note that since v is associated with a homogeneous medium, its homogenized approximation is equal to its mean field). Using the boundary corrections already specified for the first-order boundary-value problem (4.110), we obtain the following ITP for $(\tilde{v}, \tilde{w})$:

$$\left|\begin{array}{ll} \tilde{v}_{,xx} + k^2 \tilde{v} = 0 & x \in [0, L] \\ \tilde{w}_{,xx} + nk^2 \tilde{w} = 0 & x \in [0, L] \\ \tilde{v} = \tilde{w} - \beta_E \ell \tilde{w}_{,x} & x = 0 \text{ and } x = L \\ \tilde{v}_{,x} = \alpha \left(\tilde{w}_{,x} - \beta_\rho n k^2 \ell \tilde{w}\right) & x = 0 \text{ and } x = L. \end{array}\right. \tag{5.39}$$

As previously, we write:

$$\begin{aligned} \tilde{v}(x) &= \tilde{A} \cos(kx) + \tilde{B} \sin(kx) \\ \tilde{w}(x) &= \tilde{a} \cos(\sqrt{n} kx) + \tilde{b} \sin(\sqrt{n} kx), \end{aligned} \tag{5.40}$$

and injecting these expressions into the boundary conditions leads to for $x = 0$:

$$\begin{aligned} \tilde{A} &= \tilde{a} - \beta_E \sqrt{n} k \ell \tilde{b}, \\ \tilde{B} &= \alpha \sqrt{n} \left(\tilde{b} - \beta_\rho \sqrt{n} k \ell \tilde{a}\right). \end{aligned} \tag{5.41}$$

Then for $x = L$ one obtains the usual system

$$\boldsymbol{M}_1(k) \left[\begin{array}{c} \tilde{a} \\ \tilde{b} \end{array}\right] = 0 \qquad \text{with: } \boldsymbol{M}_1(k) = \boldsymbol{M}_0(k) - \sqrt{n} k \ell \, \boldsymbol{T}_1(k) \tag{5.42}$$

with $\boldsymbol{M}_0$ being defined by (5.6) for a homogeneous ITP with coefficients (n, α) and $\boldsymbol{T}_1$ is given by:

$$\boldsymbol{T}_1(k) = \left[\begin{array}{cc} \beta_E \sin(\sqrt{n} kL) + \alpha \sqrt{n} \beta_\rho \sin(kL) & \beta_E \left[\cos(kL) - \cos(\sqrt{n} kL)\right] \\ \alpha \sqrt{n} \beta_\rho \left[\cos(kL) - \cos(\sqrt{n} kL)\right] & -\beta_E \sin(kL) - \alpha \sqrt{n} \beta_\rho \sin(\sqrt{n} kL) \end{array}\right]. \tag{5.43}$$

The characteristic function is thus $f_1(k) := \det(\boldsymbol{M}_1(k))$.

Second order using the "time" model. We now consider the second-order approximation of (v, w), and note $(\tilde{v}, \tilde{w} = W^{(2)})$ the associated homogenized mean fields. Using the "time" model (t) for the equilibrium equation governing $\tilde{w}$, and using the same boundary corrections than for the second-order boundary-value problem (4.113), we obtain:

$$\left|\begin{array}{ll} \tilde{v}_{,xx} + k^2 \tilde{v} = 0 & x \in [0, L] \\ \tilde{w}_{,xx} + n_t(k) k^2 \tilde{w} = 0 & x \in [0, L] \\ \tilde{v} = \left(1 + \dfrac{\beta_E \beta_\rho}{3} n k^2 \ell^2\right) \tilde{w} - \beta_E \ell \tilde{w}_{,x} & x = 0 \text{ and } x = L \\ \tilde{v}_{,x} = \alpha \left\{\left(1 - \dfrac{{\beta_E}^2}{3} n k^2 \ell^2\right) \tilde{w}_{,x} - \beta_\rho n k^2 \ell \tilde{w}\right\} & x = 0 \text{ and } x = L \end{array}\right. \tag{5.44}$$

with:

$$n_t(k) = n(1 + \beta n k^2 \ell^2) \quad \text{and} \quad \beta = \frac{4}{3}{\beta_{E\rho}}^2 = \frac{(1-\gamma_E\gamma_\rho)^2}{12(1+\gamma_E)^2(1+\gamma_\rho)^2}. \tag{5.45}$$

Writing

$$\begin{aligned} \tilde{v}(x) &= \tilde{A}\cos(kx) + \tilde{B}\sin(kx) \\ \tilde{w}(x) &= \tilde{a}\cos(\sqrt{n_t}kx) + \tilde{b}\sin(\sqrt{n_t}kx), \end{aligned} \tag{5.46}$$

leads to the linear system

$$\boldsymbol{M}_{2t}(k)\begin{bmatrix} \tilde{a} \\ \tilde{b} \end{bmatrix} = 0 \qquad \text{with} \quad \boldsymbol{M}_{2t}(k) = \boldsymbol{M}_{0t}(k) - \sqrt{n}k\ell\, \boldsymbol{T}_{1t}(k) + \frac{\beta_E}{3}n(k\ell)^2\, \boldsymbol{T}_{2t}(k), \tag{5.47}$$

and

$$\begin{aligned}
\boldsymbol{M}_{0t}(k) &= \begin{bmatrix} \cos(kL) - \cos(\sqrt{n_t}kL) & \alpha\sqrt{n_t}\sin(kL) - \sin(\sqrt{n_t}kL) \\ -\sin(kL) + \alpha\sqrt{n_t}\sin(\sqrt{n_t}kL) & \alpha\sqrt{n_t}\left[\cos(kL) - \cos(\sqrt{n_t}kL)\right] \end{bmatrix} \\
\boldsymbol{T}_{1t}(k) &= \begin{bmatrix} \beta_E\sqrt{n_t/n}\sin(\sqrt{n_t}kL) + \alpha\sqrt{n}\beta_\rho\sin(kL) & \beta_E\sqrt{n_t/n}\left[\cos(kL) - \cos(\sqrt{n_t}kL)\right] \\ \alpha\sqrt{n}\beta_\rho\left[\cos(kL) - \cos(\sqrt{n_t}kL)\right] & -\beta_E\sqrt{n_t/n}\sin(kL) - \alpha\sqrt{n}\beta_\rho\sin(\sqrt{n_t}kL) \end{bmatrix} \\
\boldsymbol{T}_{2t}(k) &= \begin{bmatrix} \beta_\rho\left[\cos(kL) - \cos(\sqrt{n_t}kL)\right] & -\alpha\sqrt{n_t}\beta_E\sin(kL) + \beta_\rho\sin(\sqrt{n_t}kL) \\ -\beta_\rho\sin(kL) + \alpha\sqrt{n_t}\beta_E\sin(\sqrt{n_t}kL) & -\alpha\sqrt{n_t}\beta_E\left[\cos(kL) - \cos(\sqrt{n_t}kL)\right] \end{bmatrix}
\end{aligned} \tag{5.48}$$

The dependency $n_t(k)$ is omitted in the above expressions for readability. The associated characteristic function is therefore:

$$f_{2t}(k) := \det(\boldsymbol{M}_{2t}(k)). \tag{5.49}$$

First results. Figures 5.8 (for $\alpha_E = \alpha_\rho = 1$) and 5.9 (for $\alpha_E = \alpha_\rho = 2$, which is compatible with the theoretical framework of [Cakoni et al., 2015]) show the discrepancy on the first TEs between the periodic and homogenized ITPs. We consider the "canonical" setting $\gamma_E = \gamma_\rho = 0.8$ for which the ITPs feature numerous low-frequency TEs as shown by e.g. Figure 5.5. As seen before on Figure 5.7, the first TEs are very well approximated even by the leading-order homogenization, which is confirmed by the errors observed here: less that 1% misfit until the 10th TE.

The first-order model (5.39) is seen to perform no better than the leading-order model, and even worse from some TEs. This could mean that (i) there is no first-order correction for the TEs; that is the case for the Dirichlet eigenvalue problem for an integer number of cells [Santosa & Vogelius, 1993] or (ii) there is such correction but our choice of first-order correction is not adapted to capture them.

The second-order model (5.44), however, does clearly improve the approximation quality for the TEs in these two cases, which somehow motivates the need for a further mathematical investigation of this model.

Remark 5.2. *We have also tested the* (mt) *models described in Section 4.2 as well as the* (xmt) *models , using both the boundary conditions proposed in [Askes et al., 2008] and [Kaplunov & Pichugin, 2009]. In terms of approximation quality for the TEs, none of these performed better than the simplest* (t) *model presented here.*

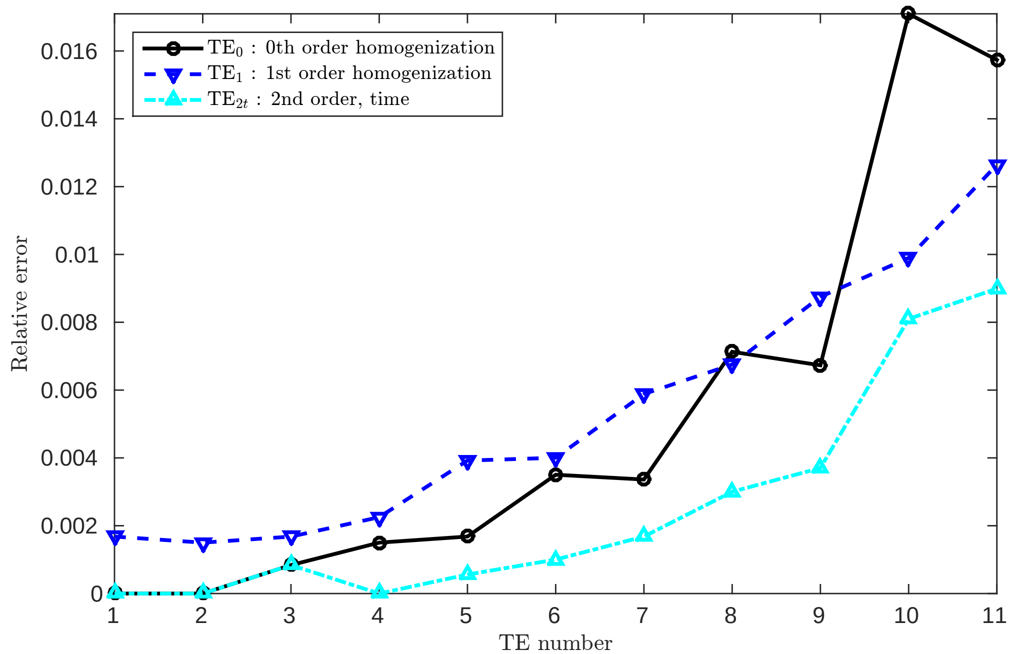

Figure 5.8: Errors on the first TEs given by homogenized ITPs for $\alpha_E = \alpha_\rho = 1$ and $\gamma_E = \gamma_\rho = 0.8$.

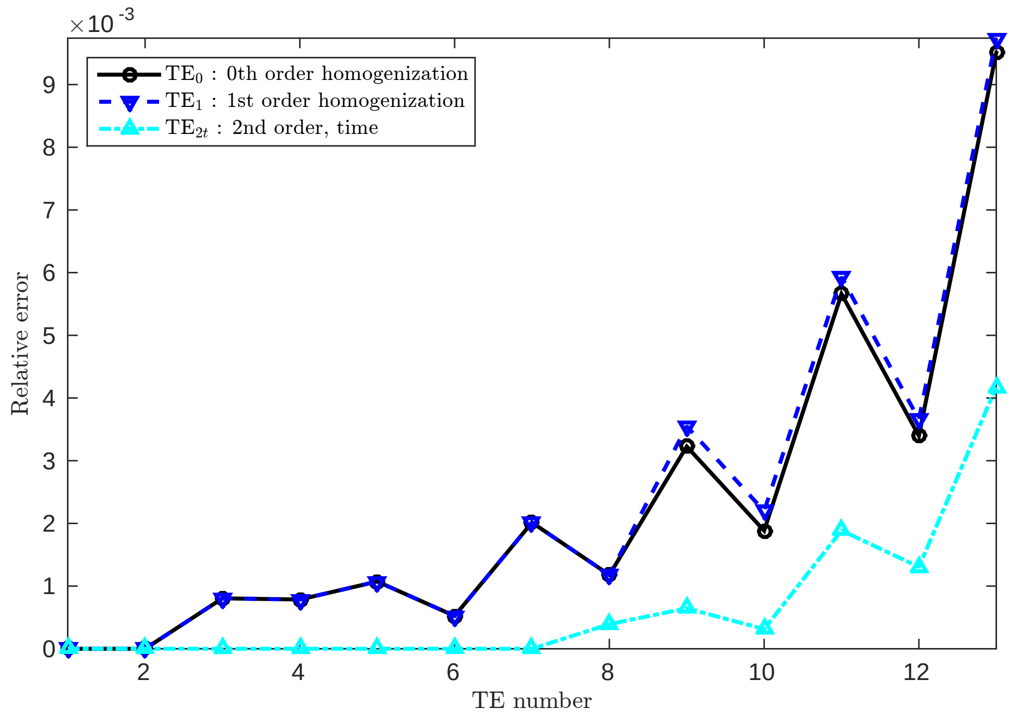

Figure 5.9: Errors on the first TEs given by homogenized ITPs for $\alpha_E = \alpha_\rho = 2$ and $\gamma_E = \gamma_\rho = 0.8$.

5.3 Conclusion and future work

An accurate - but incomplete - identification of a periodic inhomogeneity was provided by (5.38) under the assumption of "reasonably" low-contrast variations within the periodic structure. This is achieved using the leading-order homogenization of the corresponding interior transmission problem. To be able to recover the period ℓ to complete the reconstruction, some efforts have been made towards proposals of higher-order homogenized models.

However, our conclusions are limited to observation, lacking some time to push further (i) the understanding of higher-order models and their TEs and (ii) a thorough analysis of their properties possibly leading to a comprehensive identification procedure. In particular, an investigation of the boundary layer formalism introduced precisely for eigenvalue problems in [Santosa & Vogelius, 1993; Moskow & Vogelius, 1997] is under consideration, and should benefit of the latest study [Cakoni et al., 2016] which addresses the homogenization of a transmission problem using such boundary layers. First attempts have been made in this direction, but are not complete enough to be presented here. We expect that their completion will lead to an article on this problem.

Another natural continuation of this work is to investigate the accurately dispersive models proposed in [Wautier & Guzina, 2015] that feature fourth-order derivatives and are discussed briefly in Section 4.2. As underlined by Remarks 5.2 and discussion of Section 4.1.2, some unsuccessful attempts to use them (in the sense that they yield no better approximations of the TEs than the simpler models) convinced us that careful treatment of the chosen boundary conditions is required to take full advantage of such high-order models.

Conclusion

The purpose of the research presented in this dissertation is to propose new methods for the identification of elastic inhomogeneities. We focus on configurations that feature a small parameter, and we take advantage of this peculiarity by means of asymptotic analysis of the problems under considerations. More specifically, an effort is made to provide higher-order expansions of existing asymptotic models and to investigate the new possibilities brought by such expansions.

The work presented in the first part aims at providing a method to detect and identify a penetrable inhomogeneity embedded in a tridimensional elastic solid submitted to "probing" static or time-harmonic loads. To this end, we consider cost-functionals depending on a trial inhomogeneity and that quantify the misfit between the perturbations of the displacement fields in the solid due the real and trial inhomogeneities. By building up on the widely studied concept of *topological derivative*, we compute the expansion of such cost-functional with respect to the size of the trial inhomogeneity, up to order 6 which corresponds to the leading-order contribution of its second functional derivative. Such expansion is to be used as an approximation of the cost functional and to be minimized with respect to various characteristics of the trial inhomogeneity (typically, its position, size, mechanical properties ...) to find the best agreement with the unknown inhomogeneity.

The computations that we perform to derive such expansion lean on the integral formulations associated with the transmission or scattering problems featuring the small trial inhomogeneity embedded in the reference solid. The corresponding integral operators are therefore carefully specified and studied. In particular, it is found that the terms of the inner expansion of the displacement (i.e. inside the trial inhomogeneity) are solutions to *free-space transmission problems* for both elastostatics and time-harmonic elastodynamics (in the latter case, the frequency acts only as a parameter in the static problems solved by these terms). Eventually, the terms of the cost functional expansion, that we call the high-order topological derivatives, are expressed in terms of (i) the background and adjoint fields, which are both solution of elastic problems on the *homogeneous* reference domain, and their high-order derivatives, (ii) the so-called *elastic moment tensors* and their counterparts for time-harmonic expansions, and (iii) Green's tensor associated to the bounded domain and to the loads into consideration. Special attention is given to the remainder of this expansion, which is proven to be of higher (seventh) order as expected.

All the main results, including the expressions of the various expansions and the estimates of the remainders, are stated for general anisotropic materials, arbitrary shapes for the trial inhomogeneity, and possibly bounded domains. However, the practical evaluation of these expansions are performed only in the simple cases of isotropic materials, ellipsoidal shapes and unbounded domain. In particular, the explicit expressions we obtain are used to illustrate an identification method through a simple example featuring an unknown spherical scatterer illuminated by an incident plane wave in full-space. The position and size of this obstacle are estimated by minimizing the sixth-order approximation of a simple least-square misfit function depending on a spherical trial inhomogeneity. For the investigated configurations, this method improves the quality of the localization compared to the estimate provided by using only the first topological derivative.

The difficulties one has to address when considering more general settings are discussed; in particular we emphasize the need for an effective and numerically affordable way to compute the Green's tensor of a bounded domain. Moreover, some of the other possibilities provided by such polynomial approximation of a cost functional, including e.g. material identification, are briefly considered.

The purpose of the second part is to propose an identification procedure of a two-phases layered one-dimensional inclusion (which corresponds e.g. to a rod whose cross-section is periodically varying, in which longitudinal waves propagate). This time, the data which are supposedly known are the *transmission eigenvalues* of such inclusion. Such frequencies, for which there exists incident waves completely transmitted throughout the inclusion, are computed in practice as the eigenvalues of an *interior* transmission problem posed only on the domain that supports the inclusion. However, such problem is not easily analytically solvable, especially for the periodic inclusion under consideration. Therefore, we rely on *asymptotic homogenization*, valid in the low-frequency domain, to obtain a approximated model suitable for inversion.

A first chapter is dedicated to high-order asymptotic homogenization for one-dimensional problems. The main addition of this chapter is the presentation and justification of simple boundary conditions for such problems. Although the simple idea we proposed to derive such boundary conditions cannot be generalized to higher dimensions, this work is expected to provide a first basis for a more thorough understanding and use of second-order homogenization in bounded domains. Future work on this part includes notably the investigation on the links between our proposition and the so-called *boundary correctors* that provide a rigorous but not always explicit way to deal with homogenization of bounded domains.

Finally, in the last chapter, an accurate - but incomplete - identification of a periodic inhomogeneity is performed under the assumption of "reasonably" low-contrast variations within the periodic structure, using the first two transmission eigenvalues. This is achieved using the leading-order homogenization of the corresponding interior transmission problem. To be able to recover the period of the microstructure and thus to complete its identification, some efforts have been made towards proposals of higher-order homogenized models. So far, these attempts are limited to preliminary observations, showing some potential for a better approximation of the transmission eigenvalues by the second-order homogenized model. The completion of this work is expected to provide a better understanding on the relation between the transmission eigenvalues of the real structure and these of the high-order homogenized models, and to lead to an approximation of these eigenvalues explicit enough to be inverted and to complete the identification procedure.

Bibliography

Achenbach, J. D., Gautesen, A. K., & McMaken, H. (1982). *Ray methods for waves in elastic solids: with applications to scattering by cracks*, volume 14. Pitman.

Aktosun, T., Gintides, D., & Papanicolaou, V. G. (2011). The uniqueness in the inverse problem for transmission eigenvalues for the spherically symmetric variable-speed wave equation. *Inverse Problems*, *27*(11), 115004.

Allaire, G. & Amar, M. (1999). Boundary layer tails in periodic homogenization. *ESAIM: Control, Optimisation and Calculus of Variations*, *4*, 209–243.

Alouges, F. & Aussal, M. (2015). The sparse cardinal sine decomposition and its application for fast numerical convolution. *Numerical Algorithms*, *70*(2), 427–448.

Ammari, H., Garnier, J., Jugnon, V., & Kang, H. (2012). Stability and resolution analysis for a topological derivative based imaging functional. *SIAM Journal on Control and Optimization*, *50*(1), 48–76.

Ammari, H. & Kang, H. (2007). *Polarization and moment tensors: with applications to inverse problems and effective medium theory*, volume 162. Springer.

Ammari, H., Kang, H., Nakamura, G., & Tanuma, K. (2002). Complete asymptotic expansions of solutions of the system of elastostatics in the presence of an inclusion of small diameter and detection of an inclusion. *Journal of elasticity and the physical science of solids*, *67*, 97–129.

Andrianov, I. V., Bolshakov, V. I., Danishevs'kyy, V. V., & Weichert, D. (2008). Higher order asymptotic homogenization and wave propagation in periodic composite materials. *Proceedings of the Royal Society of London A: Mathematical, Physical and Engineering Sciences*, *464*(2093), 1181–1201.

Anger, G., Gorenflo, R., Jochmann, H., Moritz, H., & Webers, W. (1993). *Inverse problems: principles and applications in geophysics, technology, and medicine*. John Wiley & Sons.

Askes, H. & Aifantis, E. C. (2011). Gradient elasticity in statics and dynamics: An overview of formulations, length scale identification procedures, finite element implementations and new results. *International Journal of Solids and Structures*, *48*(13), 1962 – 1990.

Askes, H., Metrikine, A., Pichugin, A., & Bennett, T. (2008). Four simplified gradient elasticity models for the simulation of dispersive wave propagation. *Philosophical Magazine*, *88*(28-29), 3415–3443.

Bader, B. W., Kolda, T. G., et al. (2012). Matlab tensor toolbox version 2.5. Available online.

Bellis, C. & Bonnet, M. (2009). Crack identification by 3d time-domain elastic or acoustic topological sensitivity. *Comptes Rendus Mécanique*, *337*(3), 124 – 130.

Bellis, C., Bonnet, M., & Cakoni, F. (2013). Acoustic inverse scattering using topological derivative of far-field measurements-based l 2 cost functionals. *Inverse Problems*, *29*(7), 075012.

Bellis, C. & Guzina, B. (2010). On the existence and uniqueness of a solution totheinterior transmission problem forpiecewise-homogeneous solids. *Journal of Elasticity*, *101*, 29–57. 10.1007/s10659-010-9242-0.

Bensoussan, A., Lions, J. L., & Papanicolau, G. (1978). *Asymptotic Analysis for Periodic Structures*. Amsterdam: North-Holland.

Bonnet, M. (1999). *Boundary integral equations methods in solids and fluids*. John Wiley and sons.

Bonnet, M. (2006). Topological sensitivity for 3d elastodynamic and acoustic inverse scattering in the time domain. *Computer Methods in Applied Mechanics and Engineering*, *195*(37-40), 5239 – 5254. John H. Argyris Memorial Issue. Part I.

Bonnet, M. (2008). Inverse acoustic scattering by small-obstacle expansion of a misfit function. *Inverse Problems*, *24*(3), 035022.

Bonnet, M. (2009). Higher-order topological sensitivity for 2-d potential problems. application to fast identification of inclusions. *International Journal of Solids and Structures*, *46*(11?12), 2275 – 2292.

Bonnet, M. (2011). Fast identification of cracks using higher-order topological sensitivity for 2-d potential problems. *Engineering Analysis with Boundary Elements*, *35*(2), 223 – 235.

Bonnet, M. (2016a). Second-order homogenization of wave problems: properties of cell-based tensor functions. Private communication.

Bonnet, M. (2016b). Solvability of a volume integral equation formulation for anisotropic elastodynamic scattering. *Journal of Integral Equations and Applications, accepted for publication, to appear*.

Bonnet, M. & Constantinescu, A. (2005). Inverse problems in elasticity. *Inverse problems*.

Bonnet, M. & Cornaggia, R. (a). Higher order topological derivatives for three-dimensional anisotropic elasticity. submitted to ESAIM: Mathematical Modelling and Numerical Analysis.

Bonnet, M. & Cornaggia, R. (b). Higher-order expansion of misfit function for small defect identification in time-harmonic elasticity. In preparation.

Bonnet, M. & Delgado, G. (2013). The topological derivative in anisotropic elasticity. *Quarterly Journal of Mechanics and Applied Mathematics*, *66*, 557–586.

Bonnet, M. & Guzina, B. B. (2004). Sounding of finite solid bodies by way of topological derivative. *International Journal for Numerical Methods in Engineering*, *61*(13), 2344–2373.

Bonnet, M. & Guzina, B. B. (2009). Elastic-wave identification of penetrable obstacles using shape-material sensitivity framework. *Journal of Computational Physics*, *228*(2), 294 – 311.

Brezis, H. (2011). *Functional Analysis, Sobolev Spaces and Partial Differential Equations*. Number 1 in 0172-5939. Springer-Verlag New York.

Cakoni, F. & Colton, D. (2006). *Qualitative methods in inverse scattering theory: An introduction.* Springer-Verlag Berlin Heidelberg.

Cakoni, F., Colton, D., & Haddar, H. (2010). On the determination of dirichlet or transmission eigenvalues from far field data. *Comptes Rendus Mathematique*, *348*(7-8), 379 – 383.

Cakoni, F., Colton, D., & Monk, P. (2011). *The linear sampling method in inverse electromagnetic scattering.*

Cakoni, F., Guzina, B. B., & Moskow, S. (2016). On the homogenization of a scalar scattering problem for highly oscillating anisotropic media. *SIAM Journal on Mathematical Analysis*, *48*(4), 2532–2560.

Cakoni, F. & Haddar, H. (2013). Transmission eigenvalues in inverse scattering theory. *Inside Out: Inverse Problems and Applications II.*

Cakoni, F., Haddar, H., & Harris, I. (2015). Homogenization of the transmission eigenvalue problem for periodic media and application to the inverse problem. *Inverse Problems and Imaging*, *9*(4), 1025–1049.

Céa, J., Garreau, S., Guillaume, P., & Masmoudi, M. (2000). The shape and topological optimizations connection. *Computer Methods in Applied Mechanics and Engineering*, *188*(4), 713 – 726. {IVth} World Congress on Computational Mechanics. (II). Optimum.

Chaillat, S., Bonnet, M., & Semblat, J.-F. (2008). A multi-level fast multipole bem for 3-d elastodynamics in the frequency domain. *Computer Methods in Applied Mechanics and Engineering*, *197*(49-50), 4233 – 4249.

Cioranescu, D. & Donato, P. (1999). *An introduction to homogenization*, volume 17 of *Oxford Lecture Series in Mathematics and its Applications*. Oxford University Press.

Colton, D. & Kress, R. (1998). *Inverse acoustic and electromagnetic scattering theory*, volume 93. Springer.

Colton, D., Monk, P., & Sun, J. (2010). Analytical and computational methods for transmission eigenvalues. *Inverse Problems*, *26*(4), 045011.

Colton, D., Paivarinta, L., & Sylvester, J. (2007). The interior transmission problem. *Inverse Problems and Imaging (IPI)*, *1*, 13–28.

Cornaggia, R., Bellis, C., & Guzina, B. B. (a). On the homogenization of a 1d interior transmission problem for the identification of a microstructured rod. In preparation.

Dahlberg, B. E. J., Kenig, C. E., & Verchota, G. C. (1988). Boundary value problems for the systems of elastostatics in lipschitz domains. *Duke Math. J.*, *57*(3), 795–818.

Delgado, G. & Bonnet, M. (2015). The topological derivative of stress-based cost functionals in anisotropic elasticity. *Computers and Mathematics with Applications.*

Dontsov, E. V., Tokmashev, R. D., & Guzina, B. B. (2013). A physical perspective of the length scales in gradient elasticity through the prism of wave dispersion. *International Journal of Solids and Structures*, *50*(22-23), 3674 – 3684.

Eringen, A. C. & Suhubi, E. (1975). *Elastodynamics, vol 2 - Linear Theory.* Academic Press.

Eschenauer, H., Kobelev, V., & Schumacher, A. (1994). Bubble method for topology and shape optimization of structures. *Structural optimization*, *8*(1), 42–51.

Eshelby, J. (1957). The determination of the elastic field of an ellipsoidal inclusion, and related problems. *Proceedings of the Royal Society*, *241*, 376–396.

Eshelby, J. (1961). Elastic inclusions and inhomogeneities. *Progress in solid mechanics*, *2*(1), 89–140.

Fish, J., Chen, W., & Nagai, G. (2002). Non-local dispersive model for wave propagation in heterogeneous media: one-dimensional case. *International Journal for Numerical Methods in Engineering*, *54*(3), 331–346.

Freidin, A. B. & Kucher, V. A. (2016). Solvability of the equivalent inclusion problem for an ellipsoidal inhomogeneity. *Mathematics and Mechanics of Solids*, *21*(2), 255–262.

Fu, Y., Klimkowski, K. J., Rodin, G. J., Berger, E., Browne, J. C., Singer, J. K., Van De Geijn, R. A., & Vemaganti, K. S. (1998). A fast solution method for three-dimensional many-particle problems of linear elasticity. *International Journal for Numerical Methods in Engineering*, *42*(7), 1215–1229.

Furuhashi, R. & Mura, T. (1979). On the equivalent inclusion method and impotent eigenstrains. *Journal of Elasticity*, *9*, 263–270. 10.1007/BF00041098.

Garreau, S., Guillaume, P., & Masmoudi, M. (2001). The topological asymptotic for pde systems: The elasticity case. *SIAM Journal on Control and Optimization*, *39*(6), 1756–1778.

Gérard-Varet, D. & Masmoudi, N. (2012). Homogenization and boundary layers. *Acta Mathematica*, *209*(1), 133–178.

Gintides, D. & Kiriaki, K. (2015). Solvability of the integrodifferential equation of eshelby's equivalent inclusion method. *The Quarterly Journal of Mechanics and Applied Mathematics*, *68*(1), 85–96.

Giusti, S. M., Novotny, A. A., & de Souza Neto, E. A. (2010). Sensitivity of the macroscopic response of elastic microstructures to the insertion of inclusions. *Proceedings of the Royal Society of London A: Mathematical, Physical and Engineering Sciences.*

Gonzalez, O. & Stuart, A. M. (2008). *A first course in continuum mechanics.* Cambridge texts in applied mathematics. Cambridge: Cambridge University Press.

Gurtin, M. & Sternberg, E. (1961). Theorems in linear elastostatics for exterior domains. *Archive for Rational Mechanics and Analysis*, *8*(1), 99–119.

Guzina, B. B. & Bonnet, M. (2004). Topological derivative for the inverse scattering of elastic waves. *The Quarterly Journal of Mechanics and Applied Mathematics*, *57*(2), 161–179.

Guzina, B. B. & Chikichev, I. (2007). From imaging to material identification: A generalized concept of topological sensitivity. *Journal of the Mechanics and Physics of Solids*, *55*(2), 245 – 279.

Guzina, B. B. & Pourahmadian, F. (2015). Why the high-frequency inverse scattering by topological sensitivity may work. *Proceedings of the Royal Society of London A: Mathematical, Physical and Engineering Sciences*, *471*(2179).

Guzina, B. B. & Yuan, H. (2009). On the small-defect perturbation and sampling of heterogeneous solids. *Acta Mechanica*, *205*(1), 51–75.

Helnwein, P. (2001). Some remarks on the compressed matrix representation of symmetric second-order and fourth-order tensors. *Computer Methods in Applied Mechanics and Engineering*, *190*(22-23), 2753 – 2770.

Hintermüller, M., Laurain, A., & Novotny, A. (2012). Second-order topological expansion for electrical impedance tomography. *Advances in Computational Mathematics*, *36*(2), 235–265.

Holmes, M. (1995). *Introduction to perturbation methods*. Texts in applied mathematics. New York, NY: Springer.

Hsiao, G. & Wendland, W. L. (2008). *Boundary Integral Equations*, volume 164. Springer-Verlag Berlin Heidelberg.

Kang, H. & Milton, G. (2008). Solutions to the pòlya-szegö conjecture and the weak eshelby conjecture. *Archive for Rational Mechanics and Analysis*, *188*(1), 93–116.

Kaplunov, J. & Pichugin, A. (2009). On rational boundary conditions for higher-order long-wave models. In F. Borodich (Ed.), *IUTAM Symposium on Scaling in Solid Mechanics*, volume 10 of *Iutam Bookseries* (pp. 81–90). Springer Netherlands.

Kirsch, A. (1986). The denseness of the far field patterns for the transmission problem. *IMA Journal of Applied Mathematics*, *37*(3), 213–225.

Kirsch, A. (2011). *An introduction to the mathematical theory of inverse problems, 2nd ed.*, volume 120. Springer Science+ Business Media.

Knops, R. J. (1964). Further considerations of the elastic inclusion problem. *Proceedings of the Edinburgh Mathematical Society (Series 2)*, *14*, 61–70.

Knops, R. J. & Payne, L. E. (1971). *Uniqueness Theorems in Linear Elasticity*, volume 1 of *19*. Springer-Verlag Berlin Heidelberg.

Kress, R. (1989). *Linear integral equations*, volume 82. Springer.

Kupradze, V. (1979). *Three-dimensional problems of elasticity and thermoelasticity*. North-Holland Series in Applied Mathematics and Mechanics. Burlington, MA: Elsevier Science.

McLean, W. (2000). *Strongly Elliptic Systems and Boundary Integral Equations.* Cambridge University Press.

Mikhlin, S. G. & Prössdorf, S. (1986). *Singular integral operators*, volume 1986. Springer-Verlag Berlin.

Mindlin, R. & Eshel, N. (1968). On first strain-gradient theories in linear elasticity. *International Journal of Solids and Structures*, *4*(1), 109 – 124.

Moskow, S., . V. M. (1997). First-order corrections to the homogenized eigenvalues of a periodic composite medium: the case of neumann boundary conditions. *Preprint Rutgers University.*

Moskow, S. & Vogelius, M. (1997). First-order corrections to the homogenised eigenvalues of a periodic composite medium. a convergence proof. *Proceedings of the Royal Society of Edinburgh: Section A Mathematics*, *127*, 1263–1299.

Mura, T. (1982). *Micromechanics of defects in solids.* M. Nijhoff (The Hague and Boston and Higham, Mass.).

Novotny, A., Feijo, R., Taroco, E., & Padra, C. (2003). Topological sensitivity analysis. *Computer Methods in Applied Mechanics and Engineering*, *192*(7-8), 803 – 829.

Onofrei, D. & Vernescu, B. (2012). Asymptotic analysis of second-order boundary layer correctors. *Applicable Analysis*, *91*(6), 1097–1110.

Parnell, W. J. (2016). The eshelby, hill, moment and concentration tensors for ellipsoidal inhomogeneities in the newtonian potential problem and linear elastostatics. *Journal of Elasticity*, 1–64.

Parton, V. Z., Perlin, P. I., & Wadhwa, R. S. (1984). *Mathematical methods of the theory of elasticity*, volume 2. Mir Moscow.

Prange, C. (2013). Asymptotic analysis of boundary layer correctors in periodic homogenization. *SIAM Journal on Mathematical Analysis*, *45*(1), 345–387.

Ramm, A. G. (2001). A simple proof of the fredholm alternative and a characterization of the fredholm operators. *The American Mathematical Monthly*, *108*(9), pp. 855–860.

Rocha de Faria, J. & Novotny, A. (2009). On the second order topological asymptotic expansion. *Structural and Multidisciplinary Optimization*, *39*(6), 547–555.

Rudin, W. (1991). *Functional Analysis.*

Sanchez-Palencia, E. (Ed.). (1980). *Non-Homogeneous Media and Vibration Theory*, volume 127 of *Lecture Notes in Physics, Berlin Springer Verlag.*

Santosa, F. & Vogelius, M. (1993). First-order corrections to the homogenized eigenvalues of a periodic composite medium. *SIAM Journal on Applied Mathematics*, *53*(6), 1636–1668.

Santosa, F. & Vogelius, M. (1995). Erratum to the paper: First-order corrections to the homogenized eigenvalues of a periodic composite medium. *SIAM Journal on Applied Mathematics*, *55*(3), 864–864.

Schneider, M. & Andr, H. (2014). The topological gradient in anisotropic elasticity with an eye towards lightweight design. *Mathematical Methods in the Applied Sciences*, *37*(11), 1624–1641.

Schumacher, A. (1996). *Topologieoptimierung von Bauteilstrukturen unter Verwendung von Lochpositionierungskriterien.* PhD thesis, Forschungszentrum für Multidisziplinäre Analysen und Angewandte Strukturoptimierung. Institut für Mechanik und Regelungstechnik.

Silva, M., Matalon, M., & Tortorelli, D. A. (2010). Higher order topological derivatives in elasticity. *International Journal of Solids and Structures*, *47*(22?23), 3053 – 3066.

Sokolowski, J. & Zochowski, A. (1999). On the topological derivative in shape optimization. *SIAM Journal on Control and Optimization*, *37*(4), 1251–1272.

Toader, A.-M. (2011). The topological derivative of homogenized elastic coefficients of periodic microstructures. *SIAM Journal on Control and Optimization*, *49*(4), 1607–1628.

Tokmashev, R., Tixier, A., & Guzina, B. B. (2013). Experimental validation of the topological sensitivity approach to elastic-wave imaging. *Inverse Problems*, *29*(12), 125005.

Wang, C.-Y. & Achenbach, J. D. (1995). Three-dimensional time-harmonic elastodynamic green's functions for anisotropic solids. *Proceedings of the Royal Society of London A: Mathematical, Physical and Engineering Sciences*, *449*(1937), 441–458.

Wautier, A. & Guzina, B. B. (2015). On the second-order homogenization of wave motion in periodic media and the sound of a chessboard. *Journal of the Mechanics and Physics of Solids*, (0), –.

Yoshida, K.-i. (2001). *Applications of fast multipole method to boundary integral equation method.* PhD thesis, Kyoto University.

Yoshida, K.-i., Nishimura, N., & Kobayashi, S. (2001). Application of fast multipole galerkin boundary integral equation method to elastostatic crack problems in 3d. *International Journal for Numerical Methods in Engineering*, *50*(3), 525–547.

Université Paris-Saclay
Espace Technologique / Immeuble Discovery
Route de l'Orme aux Merisiers RD 128
91190 Saint-Aubin, France

École doctorale de mathématiques Hadamard (EDMH)

DEVELOPPEMENT ET UTILISATION DE MÉTHODES ASYMPTOTIQUES D'ORDRE ÉLEVÉ POUR LA RÉSOLUTION DE PROBLÈMES DE DIFFRACTION INVERSE

Résumé : L'objectif de ce travail fut le développement de nouvelles méthodes pour aborder certains problèmes inverses en élasticité, en tirant parti de la présence d'un petit paramètre dans ces problèmes pour construire des approximation asymptotiques d'ordre élevé.

La première partie est consacrée à l'identification de la taille et la position d'une inhomogénéité B^{true} enfouie dans un domaine élastique tridimensionnel. Nous nous concentrons sur l'étude de fonctions-coûts $\mathbb{J}(B_a)$ quantifiant l'écart entre B^{true} et une hétérogénéité "test" B_a. Une telle fonction-coût peut en effet être minimisée par rapport à tout ou partie des caractéristiques de l'inclusion "test" B_a (position, taille, propriétés mécaniques ...) pour établir la meilleure correspondance possible entre B_a et B^{true}. A cet effet, nous produisons un développement asymptotique de $\mathbb{J}$ en la taille a de B_a, qui en constitue une approximation polynomiale plus aisée à minimiser. Ce développement, établi jusqu'à l'ordre $O(a^6)$, est justifié par une estimation du résidu. Une méthode d'identification adaptée est ensuite présentée et illustrée par des exemples numériques portant sur des obstacles de formes simples dans l'espace libre $\mathbb{R}^3$.

L'objet de la seconde partie est de caractériser une inclusion microstructurée de longueur L, modélisée en une dimension, composée de couches de deux matériaux alternés périodiquement, en supposant que les plus basses de ses fréquences propres de transmission (TEs) sont connues. Ces fréquences sont les valeurs propres d'un problème dit de transmission intérieur (ITP). Afin de disposer d'un modèle propice à l'inversion, tout en prenant en compte les effets de la microstructure, nous nous reposons sur des approximations de l'ITP exact obtenues par homogénéisation. A partir du modèle homogénéisé d'ordre 0, nous établissons tout d'abord une méthode simple pour déterminer les paramètres macroscopiques (L et contrastes matériaux) d'une telle inclusion. Pour avoir accès à la période de la microstructure, nous nous intéressons ensuite à des modèles homogénéisés d'ordre élevé, pour lesquels nous soulignons le besoin de conditions aux limites adaptées.

Mots-clés: diffraction inverse, méthodes asymptotiques, élastodynamique, dérivées topologiques, valeurs propres de transmission, homogénéisation.

DEVELOPMENT AND USE OF HIGHER-ORDER ASYMPTOTICS TO SOLVE INVERSE SCATTERING PROBLEMS

Abstract: The purpose of this work was to develop new methods to address inverse problems in elasticity, taking advantage of the presence of a small parameter in the considered problems by means of higher-order asymptotic expansions.

The first part is dedicated to the localization and size identification of a buried inhomogeneity B^{true} in a 3D elastic domain. In this goal, we focus on the study of functionals $\mathbb{J}(B_a)$ quantifying the misfit between B^{true} and a trial homogeneity B_a. Such functionals are to be minimized w.r.t. some or all the characteristics of the trial inclusion B_a (location, size, mechanical properties ...) to find the best agreement with B^{true}. To this end, we produce an expansion of $\mathbb{J}$ with respect to the size a of B_a, providing a polynomial approximation easier to minimize. This expansion, established up to $O(a^6)$ in a volume integral equations framework, is justified by an estimate of the residual. A suited identification procedure is then given and supported by numerical illustrations for simple obstacles in full-space $\mathbb{R}^3$.

The main purpose of this second part is to characterize a microstructured two-phases layered 1D inclusion of length L, supposing we already know its low-frequency transmission eigenvalues (TEs). Those are computed as the eigenvalues of the so-called interior transmission problem (ITP). To provide a convenient invertible model, while accounting for the microstructure effects, we rely on homogenized approximations of the exact ITP for the periodic inclusion. Focusing on the leading-order homogenized ITP, we first provide a straightforward method to recover the macroscopic parameters (L and material contrast) of such inclusion. To access the key features of the microstructure, higher-order homogenization is finally addressed, with emphasis on the need for suitable boundary conditions.

Keywords: inverse scattering, asymptotic methods, elastodynamics, topological derivatives, transmission eigenvalues, homogenization.